OLLSCOIL NA GAILLIMHE
UNIVERSITY OF GALWAY

Computational Modelling Framework for Predicting the Evolution of Biodegradable Polymers During Degradation

A thesis submitted by

Aoife Hill, B.Sc.

to

Discipline of Biomedical Engineering,
College of Science and Engineering,
University of Galway

in fulfilment of the requirements of the degree of

Doctor of Philosophy

November 2022

Supervised by: Dr William Ronan

Table of Contents

Declaration

This thesis is presented in fulfilment of the requirements for the degree of Doctor of Philosophy. It is entirely my own work and has not been submitted to any other university or institute of higher education, or for any other academic award in this university. Where use has been made of the work of other people it has been fully acknowledged and referenced.

Aoife Hill

November 2022

Abstract

Biodegradable polymers are attractive alternatives for many permanent implants, potentially reducing long term risks. Designing optimal devices for their intended purpose, however, is costly and time consuming, with small changes to the sample significantly altering the behaviour. Computational models speed up the design process; however, these models require accurate descriptions of material behaviour and predicting changes in properties during degradation has proved challenging.

This thesis aims to develop a computational modelling framework for biodegradable polymers by considering how changes in the material at the microscale affect mechanical properties. First, a kinetic chain-scission model is introduced, predicting the molecular weight distribution evolution as a function of degradation time. A refined kinetic model is also developed which allows for faster solutions with acceptable accuracy. The autocatalytic effect of carboxylic acid ends created via chain scissions and also present in the manufactured polymer are considered. Our framework accounts for molecular weight reduction via the cleavage of monomers from chain ends and from scissions in the middle of the polymer chain. These developments allow for a more complete representation of the molecular weight distribution during degradation.

In the second phase of the thesis, the relationship between the molecular weight distribution and ductility of the material is explored. During degradation, biocompatible polymers exhibit a transition from ductile to brittle behaviour. Following a review of the literature, trends in this phenomenon are identified and failure criteria are considered. These predictions can offer insight into material failure, particularly at advanced stages of degradation.

Finally, the effect of finite chain extensibility on the mechanical behaviour is investigated. As degradation proceeds, short chains build up in the system and may fully extend at moderate strains. We investigate how this contributes to elasticity changes during degradation and, thus, predict the evolving stress-strain behaviour. Results indicated that molecular weight distributions and proper treatment of fully extended chains should be considered for more accurate predictions of the mechanical properties in degrading samples.

The models introduced in this thesis are investigated alongside existing experimental data, with predictions strongly supported by experimental observations of degrading biocompatible polymers. Ultimately, the framework presented offers predictions for evolving molecular weight distributions and evolving stress-strain behaviour, including the point of failure, throughout degradation.

Acknowledgements

First and foremost, thank you, Will, for all your guidance and support, and for immersing me into the world of biomedical engineering. I hope my mathematical traits weren't too tiresome to deal with!

Thank you, Michel, for your insight and, in particular, your help with funding and career opportunities.

Thank you to members of my graduate research committee for your advice and support throughout the years.

It's been a pleasure being part of the Ronan research group – thank you to everyone who made it an enjoyable experience; a special mention to my desk neighbour, Ruth.

Thank you to the staff of both the School of Biomedical Engineering and the School of Mathematical and Statistical Sciences for your abundance of support throughout the years in too many ways to mention. Special thanks to both Niall and Andrew for very willingly providing their expertise on coding and statistics, respectively.

Thank you, also, to the postgraduate students of both Schools for the tea breaks, lunchtime chats, and conference fun.

Thank you to everyone that provided me with opportunities to present my research throughout the years, from the local groups to those further afield. I'm grateful to both the organisers and the audiences.

Finally, thank you to my funding sources, without who this research would not be possible: Irish Research Council (GOIPG/2018/2697); College of Engineering and Informatics; and Higher Education Authority.

For my parents, Róisín and Henry,

My sister, Eimear,

And my fiancé, Michael

You have enriched and supported this experience in countless ways

Thank you for everything

Abbreviations and nomenclature

C_a, C_{a0} – (initial) concentration of carboxylic acid ends
C_{c0} – initial molar concentration of chains
$C_e, C_{e0}, C_{e,mid}, C_{e,end}$ – (initial) concentration of overall, mid, and end ester bonds
C_m, C_{m0} – (initial) concentration of monomers
C_n, C_∞ – characteristic ratios
C_{ol}, C_{ol0} – (initial) concentration of oligomers
C_w – concentration of water molecules
$Đ_M$ – molar mass dispersity
E – Young's modulus
GPC – gel permeation chromatography
k – Boltzmann constant
k_a, k_{am}, k_{ae} – overall, mid-, and end-chain rate of autocatalysis
k_h, k_{hm}, k_{he} – overall, mid-, and end-chain rate of hydrolysis
KOM – kinetic ODE model
KSM – kinetic scission model
l – length of bond
l_K – Kuhn length
L_0, L_{def}, L_f – initial, deformed and final length
M_0 – molar mass
M_e – average molecular weight related to C_e
M_n, M_{n0} – (initial) number average molecular weight
M_n^{crit}, M_w^{crit} – critical molecular weight threshold parameters
M_w, M_{w0} – (initial) weight average molecular weight
MW – unspecified average molecular weight
MWD – molecular weight distribution
n – number of units in a chain
n – acid dissociation constant
n_b – number of backbone bonds in a monomer
n_K – Kuhn length
N – number of polymer chains per unit volume
N_c, N_{c0} – (initial) number of chains
$N_{c>M_w^{crit}}$ – number of chains above M_w^{crit}
NKOM – new kinetic ODE model
ODE – ordinary differential equation
$p(r)$ – probability density distribution
$P(r)$ – volumetric end-to-end distance distribution
PBS – phosphate buffer solution
PCL – polycaprolactone
PDLA – poly(D-lactic acid)
PDLLA – poly(D,L-lactic acid)
PGA – poly(glycolic acid)
PLA – poly(lactic acid)

PLGA – poly(lactic-co-glycolic acid)
PLLA – poly(L-lactic acid)
PL/GA – poly(lactic/glycolic acid)
r, r_0, r_{def} – end-to-end length of chain (initial, deformed)
$\langle r^2 \rangle_0$ – undeformed mean square end-to-end distance of chain
r_{max} – maximum end-to-end length of chain
r_{rms} – root mean square end-to-end distance of chain
$S_{tot}, S_{mid}, S_{end}$ – molar number of total, mid-, and end-chain scissions
S, s – entropy of network and single chain
SC – semi-crystalline
SEC – size exclusion chromatography
T – absolute temperature
T_g – glass transition temperature
X_c – crystalline fraction
ε – (nominal) strain
$\varepsilon_f, \varepsilon_{f0}$ – (initial) failure strain
ε_f^{exp} – exponential empirical failure criterion
ε_f^{MW} – failure criterion related to average molecular weight
ε_f^{N} – failure criterion related to chains above a critical molecular weight
σ – (nominal) stress
σ_y – yield stress
σ_{max} – maximum tensile stress
σ_∞ – fracture strength at infinite molecular weight
θ – backbone bond angle
ϕ – torsional bond angle
φ – size of the system
λ – principal stretch ratios
τ – shear stress
γ – shear strain

1 Introduction

Bioresorbable polymers offer temporary implants that degrade fully after healing is complete, an attractive characteristic in the medical device industry. They are used in clinical applications such as orthopaedic fixation devices, vessel scaffolds, tissue engineering, and controlled drug delivery (Allen and Cullis, 2004; McGinty et al., 2011; Nasajpour et al., 2018; O'Brien, 2011; Ramakrishna et al., 2001; Vert, 2009; Vo et al., 2017). Their optimisation is often hindered by many underlying complex degradation mechanisms and the uncertainty in how they affect the material properties. For example, polymeric bioresorbable stents are considered attractive alternatives to permanent metal stents for the treatment of coronary artery disease (Cheng et al., 2019; Durand et al., 2012; Ormiston et al., 2008; Serruys et al., 2016; Wykrzykowska et al., 2009). However, obtaining biomechanical properties to match that offered by a metal stent has proved a difficult task (Im et al., 2017). Understanding the complex behaviour of these materials is crucial for ensuring sufficient mechanical integrity and a suitable degradation rate for the intended purpose (Fig. 1.1). As the mechanical behaviour is related to the polymer microstructure (Farrar, 2008; Hertzberg et al., 2013), an understanding of how the latter changes as degradation takes place is essential.

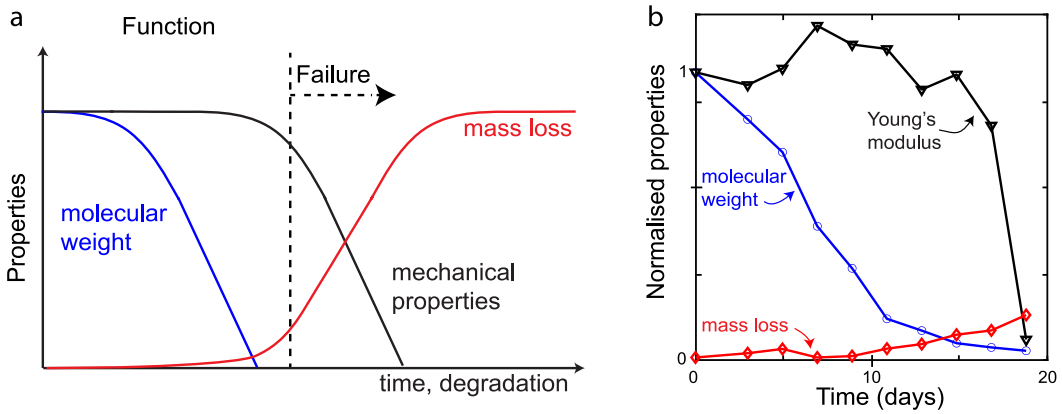

Fig. 1.1. (a) Generic curves detailing general sequence of molecular weight, mechanical properties and mass reduction. Adapted from Pietrzak et al. (1997) and Li et al. (2020). (b) Experimentally observed evolution of these properties for poly(lactic-co-glycolic) acid as reported by Shirazi et al. (2014).

Experimental studies often take years to complete, with small changes to the material significantly altering the behaviour (Grizzi et al., 1995; Mainil-Varlet et al., 1997; Tsuji, 2002). Computational studies can provide important insight into the evolution of material and mechanical properties during degradation. However, many of the existing models are phenomenological in nature and while they have been calibrated to capture the evolution of properties including molecular weight (Wang et al., 2008), crystallinity (Zhang et al., 2019),

and Young's modulus (Shirazi et al., 2016b), determining what model parameters should be for a newly designed, untested material remains a challenge. An in-depth understanding of the polymer at microscopic and molecular levels and the underlying degradation mechanisms is essential towards designing devices with optimal, tuneable properties.

The primary focus of this thesis is on developing predictive tools for the evolution of polymer properties during degradation that take microscopic degradation mechanisms and deformation into account. Some key observations from literature that have motivated the work include the following:

- The findings of Tracy et al. (1999) indicate that the polymer end group plays an important role in degradation, with uncapped PLGA degrading faster than ester capped. This suggests that all carboxylic acid ends should be considered catalysts when modelling degradation, and not only those of short chains as has been widely used in the literature (Gleadall et al., 2014a; Shirazi et al., 2016b; Wang et al., 2008).
- While many models focus on predictions for average molecular weight (Lyu et al., 2007; Wang et al., 2008), some experimental reports have stated that it is the molecular weight distribution controlling the properties, suggesting that a broader distribution may reduce the mechanical performance (Merz et al., 1951; Thomas and Hagan, 1969). Thus, a more complete representation of the evolving molecular weight distribution may be necessary for a robust modelling framework.
- Polymer chain scission models that simulate bond cleavages on a representative polymer network can provide predictions for evolving molecular weight distributions (Gleadall and Pan, 2013; Shirazi et al., 2016b), offering an in-depth description of the polymer throughout degradation. However, the rate of the simulated scissions has not been considered, making it a challenge to relate results to time.
- A ductile-brittle transition has been noted as degradation proceeds (Fig. 1.2a,b). The failure mechanism of the polymer changes drastically as this occurs (Polak-Kraśna et al., 2021). Understanding what contributes to this and when it occurs is crucial to ensure sufficient mechanical integrity throughout the functional time. Although relationships between evolving molecular weight and failure strain have been observed (Deng et al., 2005; Weir et al., 2004b), this does not appear to have been translated into a predictive tool.
- On simulating stretching on a polymer network, Stepto and Taylor (1995a) noted increasing departures from affine, Gaussian behaviour for lower molecular weight chains (Fig. 1.2c). This departure was due to shorter chains fully extending more

readily and, thus, causing a reduction in the rate of free energy change as the simulation progressed. Their work was restricted to uniform polymer systems, i.e., chains with an average molecular weight. It is expected that the finite extensibility of polymer chains becomes increasingly relevant as degradation proceeds due to short chains building up in the system; however, this has not been considered when modelling biodegradable polymers.

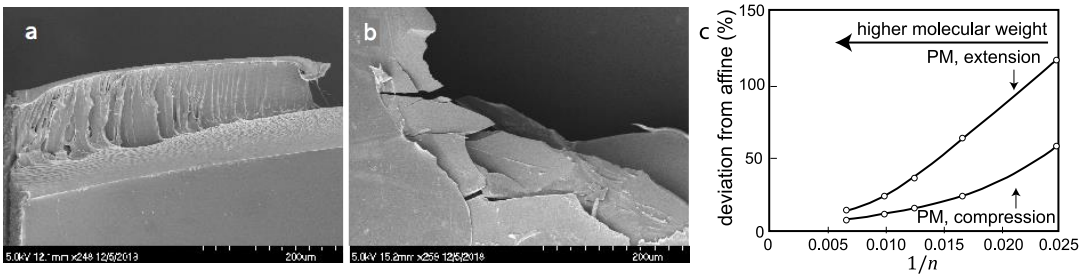

Fig. 1.2. Microscopic images of PLA samples (approximately ×250 magnification) (a) before degradation, exhibiting ductile failure on tensile testing, and (b) after 112 days degradation, showing brittle fracture on gentle handling. Reproduced from Polak-Kraśna et al. (2021), licensed under CC BY 4.0. (c) Simulated stretching indicated shorter chains deviated further from affine Gaussian behaviour, accredited to an increased number of fully extended chains in those networks. Adapted from Stepto and Taylor (1995a).

Several good textbooks include those by Ward (1971), Buchanan (2008), Mark (2007), Hertzberg et al. (2013), and Callister and Rethwisch (2018). Terms such as biodegradable, bioabsorbable and bioresorbable are often used interchangeably to describe synthetic polymers that degrade over time (Buchanan, 2008). More precise definitions exist, with bioresorbable polymers defined as those whose degradation products can “resorb” in the body and include poly(α-hydroxy) acids such as poly(lactic acid), poly(glycolic acid) and their copolymers. Throughout this thesis, while these terms may be used interchangeably, it is poly(α-hydroxy) acids that are the primary focus, with these polymers having FDA approval.

1.1 Aims and objectives

The primary aim of this thesis is to develop a computational modelling framework for biodegradable polymers. A microscopic approach is taken to aid in the understanding of the effect of degradation on the polymer properties. The core focus is restricted to amorphous aliphatic polyesters. Many of the techniques introduced could be extended to consider amorphous phases in semi-crystalline polymers or alternative synthetic biodegradable polymers provided appropriate consideration of the polymer structure and specific degradation mechanism is given.

The main objectives are as follows:

- Understand the degradation mechanism controlling polymer chain scissions and develop a model that simulates this process on a representative polymer chain distribution to provide evolving molecular weight distributions as a function of degradation duration.
- Investigate the effect of polymer chain ends on the degradation behaviour.
- Determine how failure strain is affected by degradation and seek a relationship between molecular weight and failure strain that can be used to predict the simultaneous evolution of these properties.
- Understand how the mechanics of deformation varies for polymer networks with different degrees of degradation and predict changes in the evolving stress-strain curves for these materials, giving appropriate consideration to the finite extensibility of polymer chains.

1.2 Thesis structure

Chapter 2 presents an overview of biodegradable polymers, considering aspects such as structure, degradation mechanism, and applications. Details on the macroscopic deformation of an elastic solid are given, prior to presenting a molecular level approach that offers a more detailed understanding of the underlying behaviour. Information on the numerical methods used in this thesis is also stated. In Chapter 3, a literature review detailing both experimental observations and modelling techniques is provided.

In Chapter 4, the model of Shirazi et al. (2016b) and previous studies (Wang et al., 2010, 2008) motivates the development of a kinetic scission model (KSM) to predict the evolution of molecular weight distribution and Young's modulus as a function of degradation time for bioresorbable polymers. A refined kinetic model is developed to capture the autocatalytic effect of carboxylic acid ends. The results obtained are quantitatively compared to and calibrated with existing experimental data for PLGA films (Shirazi et al., 2014).

Chapter 5 concentrates on the relationship between molecular weight, MW, and failure strain, ε_f, in poly(lactic acid) (PLA). Two main regimes were identified from a literature review with a final collection of 27 datasets from 9 publications. Several failure criteria are proposed and investigated. The predictions obtained can offer insight into the end-of-use time of such polymers during the design process.

In Chapter 6, the physical mechanisms behind the evolution of mechanical properties are explored following an approach similar to Stepto and Taylor (1995a). A simulated stretch is applied to representative polymer chain distributions, where the finite extensibility of chains

is accounted for. When combined with the models introduced in Chapters 4 and 5, evolving stress-strain curves, including the point of failure, for various degradation durations are simulated. A qualitative comparison of predicted stress-strain curves with experimental trends is presented (Vieira et al., 2011).

Finally, the overall thesis findings are discussed in Chapter 7, providing an overview of the novel contributions.

Some of the contents of Chapters 2 and 3 are summarised or expanded on in subsequent chapters to allow each chapter to standalone. Bibliographies and, where relevant, appendices are included at the end of each chapter.

References

Allen, T.M., Cullis, P.R., 2004. Drug Delivery Systems: Entering the Mainstream. Science 303, 1818–1822. https://doi.org/10.1126/science.1095833

Buchanan, F.J. (Ed.), 2008. Degradation rate of bioresorbable materials: prediction and evaluation. Woodhead Publishing Limited/CRC Press LLC, Cambridge, England/Boca Raton, FL.

Callister Jr, W.D., Rethwisch, D.G., 2018. Materials Science and Engineering - An Introduction, 10th ed. John Wiley & Sons.

Cheng, Y., Gasior, P., Ramzipoor, K., Lee, C., McGregor, J.C., Conditt, G.B., McAndrew, T., Kaluza, G.L., Granada, J.F., 2019. In vitro mechanical behavior and in vivo healing response of a novel thin-strut ultrahigh molecular weight poly-L-lactic acid sirolimus-eluting bioresorbable coronary scaffold in normal swine. Int. J. Cardiol. 286, 21–28. https://doi.org/10.1016/j.ijcard.2019.04.012

Deng, M., Zhou, J., Chen, G., Burkley, D., Xu, Y., Jamiolkowski, D., Barbolt, T., 2005. Effect of load and temperature on in vitro degradation of poly(glycolide-co-L-lactide) multifilament braids. Biomaterials 26, 4327–4336. https://doi.org/10.1016/j.biomaterials.2004.09.067

Durand, E., Lemitre, M., Couty, L., Sharkawi, T., Brasselet, C., Vert, M., Lafont, A., 2012. Adjusting a polymer formulation for an optimal bioresorbable stent: a 6-month follow-up study. EuroIntervention 8, 242–249. https://doi.org/10.4244/EIJV8I2A38

Farrar, D.F., 2008. Modelling of the degradation process for bioresorbable polymers, in: Degradation Rate of Bioresorbable Materials - Prediction and Evalutaion. pp. 183–206.

Gleadall, A., Pan, J., 2013. Computer Simulation of Polymer Chain Scission in Biodegradable Polymers. J. Biotechnol. Biomater. 3, 154. https://doi.org/10.4172/2155-952X.1000154

Gleadall, A., Pan, J., Kruft, M.A., Kellomäki, M., 2014. Degradation mechanisms of bioresorbable polyesters. Part 2. Effects of initial molecular weight and residual monomer. Acta Biomater. 10, 2233–2240. https://doi.org/10.1016/j.actbio.2014.01.017

Grizzi, I., Garreau, H., Li, S., Vert, M., 1995. Hydrolytic degradation of devices based on poly(DL-lactic acid) size-dependence. Biomaterials 16, 305–311. https://doi.org/10.1016/0142-9612(95)93258-F

Hertzberg, R.W., Vinci, R.P., Hertzberg, J.L., 2013. Deformation and Fracture Mechanics of Engineering Materials, 5th ed, Fatigue Design. John Wiley & Sons. https://doi.org/10.1016/b978-0-08-026167-6.50013-8

Im, S.H., Jung, Y., Kim, S.H., 2017. Current status and future direction of biodegradable metallic and polymeric vascular scaffolds for next-generation stents. Acta Biomater. 60, 3–22. https://doi.org/10.1016/J.ACTBIO.2017.07.019

Li, C., Guo, C., Fitzpatrick, V., Ibrahim, A., Zwierstra, M.J., Hanna, P., Lechtig, A., Nazarian, A., Lin, S.J., Kaplan, D.L., 2020. Design of biodegradable, implantable devices towards clinical translation. Nat. Rev. Mater. 5, 61–81. https://doi.org/10.1038/s41578-019-0150-z

Lyu, S.P., Schley, J., Loy, B., Lind, D., Hobot, C., Sparer, R., Untereker, D., 2007. Kinetics and time-temperature equivalence of polymer degradation. Biomacromolecules 8, 2301–2310.

https://doi.org/10.1021/bm070313n

Mainil-Varlet, P., Curtis, R., Gogolewski, S., 1997. Effect of in vivo and in vitro degradation on molecular and mechanical properties of various low-molecular-weight polylactides. J. Biomed. Mater. Res. 36, 360–380. https://doi.org/10.1002/(SICI)1097-4636(19970905)36:3<360::AID-JBM11>3.0.CO;2-I

Mark, J.E. (Ed.), 2007. Physical Properties of Polymers Handbook, Second. ed. Springer. https://doi.org/10.1016/s0039-9140(97)80037-9

McGinty, S., McKee, S., Wadsworth, R.M., McCormick, C., 2011. Modelling drug-eluting stents. Math. Med. Biol. 28, 1–29. https://doi.org/10.1093/imammb/dqq003

Merz, E.J., Nielsen, L.E., Buchdahl, R., 1951. Influence of Molecular Weight on the Properties of Polystyrene. Ind. Eng. Chem. 43, 1396–1401. https://doi.org/10.1021/ie50498a036

Nasajpour, A., Ansari, S., Rinoldi, C., Rad, A.S., Aghaloo, T., Shin, S.R., Mishra, Y.K., Adelung, R., Swieszkowski, W., Annabi, N., Khademhosseini, A., Moshaverinia, A., Tamayol, A., 2018. A Multifunctional Polymeric Periodontal Membrane with Osteogenic and Antibacterial Characteristics. Adv. Funct. Mater. 28. https://doi.org/10.1002/adfm.201703437

O'Brien, F.J., 2011. Biomaterials & scaffolds for tissue engineering. Mater. Today 14, 88–95. https://doi.org/10.1016/S1369-7021(11)70058-X

Ormiston, J.A., Serruys, P.W., Regar, E., Dudek, D., Thuesen, L., Webster, M.W.I., Onuma, Y., Garcia-Garcia, H.M., McGreevy, R., Veldhof, S., 2008. A bioabsorbable everolimus-eluting coronary stent system for patients with single de-novo coronary artery lesions (ABSORB): a prospective open-label trial. Lancet 371, 899–907. https://doi.org/10.1016/s0735-1097(12)60320-9

Pietrzak, W.S., Sarver, D.R., Verstynen, M.L., 1997. Bioabsorbable polymer science for the practicing surgeon. J. Craniofac. Surg. 8, 87–91. https://doi.org/10.1097/00001665-199703000-00004

Polak-Kraśna, K., Abaei, A.R., Shirazi, R.N., Parle, E., Carroll, O., Ronan, W., Vaughan, T.J., 2021. Physical and mechanical degradation behaviour of semi-crystalline PLLA for bioresorbable stent applications. J. Mech. Behav. Biomed. Mater. 118, 1–11. https://doi.org/10.1016/j.jmbbm.2021.104409

Ramakrishna, S., Mayer, J., Wintermantel, E., Leong, K.W., 2001. Biomedical applications of polymer-composite materials: a review. Compos. Sci. Technol. 61, 1189–1224. https://doi.org/10.1109/isemc.2002.1032709

Serruys, P.W., Chevalier, B., Sotomi, Y., Cequier, A., Carrié, D., Piek, J.J., Van Boven, A.J., Dominici, M., Dudek, D., McClean, D., Helqvist, S., Haude, M., Reith, S., de Sousa Almeida, M., Campo, G., Iñiguez, A., Sabaté, M., Windecker, S., Onuma, Y., 2016. Comparison of an everolimus-eluting bioresorbable scaffold with an everolimus-eluting metallic stent for the treatment of coronary artery stenosis (ABSORB II): a 3 year, randomised, controlled, single-blind, multicentre clinical trial. Lancet 388, 2479–2491. https://doi.org/10.1016/S0140-6736(16)32050-5

Shirazi, R.N., Aldabbagh, F., Erxleben, A., Rochev, Y., McHugh, P., 2014. Nanomechanical properties of poly(lactic-co-glycolic) acid film during degradation. Acta Biomater. 10, 4695–4703. https://doi.org/10.1016/j.actbio.2014.08.004

Shirazi, R.N., Ronan, W., Rochev, Y., McHugh, P., 2016. Modelling the degradation and elastic properties of poly(lactic-co-glycolic acid) films and regular open-cell tissue engineering scaffolds. J. Mech. Behav. Biomed. Mater. 54, 48–59. https://doi.org/10.1016/j.jmbbm.2015.08.030

Stepto, R.F.T., Taylor, D.J.R., 1995. Molecular Modelling of the Elastic Behaviour of Polymer Chains in Networks: Comparison of Polymethylene and Poly(dimethylsiloxane). J. Chem. Soc. Faraday Trans. 91, 2639–2647. https://doi.org/10.1039/FT9959102639

Thomas, D.P., Hagan, R.S., 1969. The Influence of Molecular Weight Distribution on Melt Viscosity, Melt Elasticity, Processing Behaviour and Properties of Polystyrene. Polym. Eng. Sci. 9, 164–171. https://doi.org/10.1002/pen.760090304

Tracy, M.A., Ward, K.L., Firouzabadian, L., Wang, Y., Dong, N., Qian, R., Zhang, Y., 1999. Factors affecting the degradation rate of poly(lactide-co-glycolide) microspheres in vivo and in vitro. Biomaterials 20, 1057–1062. https://doi.org/10.1016/S0142-9612(99)00002-2

Tsuji, H., 2002. Autocatalytic hydrolysis of amorphous-made polylactides: effects of L-lactide content, tacticity, and enantiomeric polymer blending. Polymer 43, 1789–1796. https://doi.org/10.1016/S0032-3861(01)00752-2

Vert, M., 2009. Degradable and bioresorbable polymers in surgery and in pharmacology: beliefs and facts. J. Mater. Sci. Mater. Med. 20, 437–446. https://doi.org/10.1007/s10856-008-3581-4

Vieira, A.C., Vieira, J.C., Ferra, J.M., Magalhães, F.D., Guedes, R.M., Marques, A.T., 2011. Mechanical

study of PLA–PCL fibers during in vitro degradation. J. Mech. Behav. Biomed. Mater. 451–460. https://doi.org/10.1016/j.jmbbm.2010.12.006

Vo, T., Lee, W., Peddle, A., Meere, M., 2017. Modelling chemistry and biology after implantation of a drug-eluting stent. Part I: Drug transport. Math. Biosci. Eng. 14, 491–509. https://doi.org/10.3934/mbe.2017030

Wang, Y., Han, X., Pan, J., Sinka, C., 2010. An entropy spring model for the Young's modulus change of biodegradable polymers during biodegradation. J. Mech. Behav. Biomed. Mater. 3, 14–21. https://doi.org/10.1016/j.jmbbm.2009.02.003

Wang, Y., Pan, J., Han, X., Sinka, C., Ding, L., 2008. A phenomenological model for the degradation of biodegradable polymers. Biomaterials 29, 3393–3401. https://doi.org/10.1016/j.biomaterials.2008.04.042

Ward, I.M., 1971. Mechanical properties of solid polymers. Wiley-Interscience.

Weir, N.A., Buchanan, F.J., Orr, J.F., Farrar, D.F., Dickson, G.R., 2004. Degradation of poly-L-lactide. Part 2: Increased temperature accelerated degradation. Proc. Inst. Mech. Eng. Part H J. Eng. Med. 218, 321–330. https://doi.org/10.1243/0954411041932809

Wykrzykowska, J.J., Onuma, Y., Serruys, P.W., 2009. Advances in stent drug delivery: the future is in bioabsorbable stents. Expert Opin. Drug Deliv. 6, 113–126. https://doi.org/10.1517/17425240802668495

Zhang, T., Jin, G., Han, X., Gao, Y., Zeng, Q., Hou, B., Zhang, D., 2019. Multiscale modelling for the heterogeneous strength of biodegradable polyesters. J. Mech. Behav. Biomed. Mater. 90, 337–349. https://doi.org/10.1016/j.jmbbm.2018.10.018

2 Background and theory

The present chapter presents an overview of biodegradable polymers and modelling techniques that have motivated the work in this thesis. Initially, background information about the polymer (i) structure, (ii) molecular weights, (iii) degradation mechanism, (iv) mechanical properties and (v) applications is outlined in Section 2.1. Section 2.2 describes the deformation of an elastic solid, where a macroscopic scale has been considered, prior to considering a molecular level approach in Section 2.3 to understand the behaviour mechanisms, where rubber-like elasticity is assumed. Finally, numerical methods used throughout the thesis are presented in Section 2.4.

2.1 Biodegradable polymers

Biodegradable polymers readily experience degradation, typically either hydrolytically or enzymatically. They can be classified as natural or synthetic. The primary focus of this thesis is given to synthetic aliphatic polyesters due to their popularity in the medical device industry; however, much of the work presented is either relevant as is or extendable to additional synthetic biodegradable polymers provided appropriate consideration of the specific degradation mechanism is given.

To begin, the polymer structure is outlined, with consideration given to chain arrangements and chemical structure (Section 2.1.1). Following this, an overview of molecular weight is presented, with details of average values and methods of experimental determination provided (Section 2.1.2). Next, details of the degradation mechanism of polymers of interest are described (Section 2.1.3), prior to an overview of their mechanical properties (Section 2.1.4). Finally, a brief history of these materials is presented in relation to applications and some of the challenges present during the development of new designs are discussed (Section 2.1.5). More detailed descriptions may be found in textbooks such as those by Callister and Rethwisch (2018) and Ward and Sweeney (2013).

2.1.1 Polymer structure

Polymer materials are composed of many long macromolecular, interconnected chains of varying lengths (Fig. 2.1). Each chain contains small repeat units or ‘mers’ bonded together chemically. An individual molecular building block or isolated unit is called a monomer, while a very short, water-soluble chain is termed an oligomer. Polymer properties are not only determined by the underlying chemical structure, but also depend on chain arrangement and length.

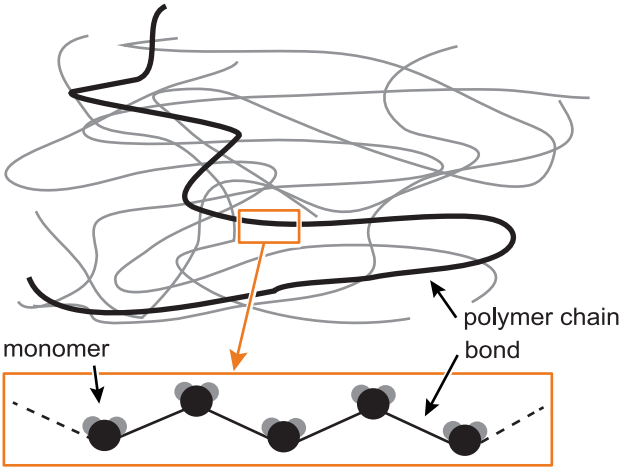

Fig. 2.1. Schematic diagram of sample polymer structure, which contains many polymer chains composed of single monomer units bonded together chemically.

Polymers can exist in one of three states – amorphous, semi-crystalline, or crystalline (Fig. 2.2). In an amorphous state, an ensemble of polymer chains is similar to a plate of well-cooked spaghetti, with flexible, intertwined and disordered strands. In contrast, a crystalline polymer has a more definite, rigid structure, more like a bunch of uncooked spaghetti. Semi-crystalline polymers fall between these two extremes, containing both amorphous and crystalline regions. An increase in the crystalline fraction typically corresponds to an increase in material stiffness, strength, and brittleness. The increased density of crystalline regions makes them effectively impermeable to water and other transport processes, leading to slower degradation in these regions (Laycock et al., 2017).

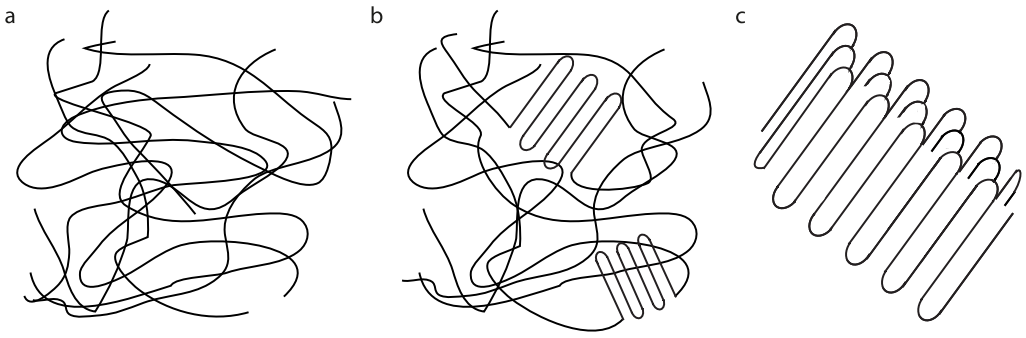

Fig. 2.2. Schematic diagrams of (a) amorphous, (b) semi-crystalline, and (c) crystalline polymer chain structures.

Other factors of importance when considering polymer structure include chain conformation, packing, orientation and configuration (for example, side group size, shape, and location); these are discussed in detail in the book by Hertzberg et al. (2013). The primary focus in this thesis is on the backbones of randomly orientated amorphous polymers.

2.1.1.1 PLA, PGA, PCL, and their copolymers

Biocompatible polymers such as poly(lactic acid) (PLA), poly(glycolic acid) (PGA) and polycaprolactone (PCL) are popular choices for bioresorbable devices, all having FDA approval, with degradation by-products removed from the body through physiological processes via the lungs and kidneys (Buchanan, 2008). Their molecular structures are given in Fig. 2.3, in which x, y and z indicate the number of repeat units in the polymer chain. Poly(L-lactide) (PLLA) and poly(D-lactide) (PDLA) are both forms of PLA; their structure differs with the CH_3 and H side-groups swapping sides.

A copolymer includes repeating combinations of two or more monomers in each individual chain; for example, a copolymer of PLA and PGA consists of chains containing both units, and is named poly(lactic-co-glycolic acid) (PLGA) (Fig. 2.3d). A polymer blend contains a mixture of chains, with each chain containing one type of unit; for example, a polymer blend of PLA and PGA includes individual chains of both and is denoted PL/GA (Fig. 2.3e). Polymer composition plays a significant role in the degradation behaviour observed (Durand et al., 2012; Karjalainen et al., 1996; Middleton and Tipton, 2000); in theory, this enables the optimisation of polymer properties for specific applications to be obtained through tailoring of the copolymer ratios.

2.1.1.2 Why focus on amorphous polymers?

Amorphous regions are typically the weak link in semi-crystalline polymers, degrading more quickly than crystalline regions (Buchanan, 2008). Polymers such as poly(DL-lactic-glycolic acid) 50:50 (50% PLA, 50% PGA), poly(DL-lactic-glycolic acid) 75:25 (37.5% PLLA, 37.5% PDLA, 25% PGA) and poly(DL-lactic acid) (50% PLLA, 50% PDLA) have been found to remain amorphous throughout degradation (Li et al., 1990a, 1990b; Shirazi et al., 2016a, 2014). This can be advantageous, resulting in a more predictable degradation profile than that seen with semi-crystalline polymers (Buchanan, 2008). The focus of this thesis is primarily on accurately modelling amorphous polymers. By focusing on amorphous polymers, we aim to obtain a thorough understanding of degradation pathways in these polymers. Once this is obtained, this understanding can be translated to amorphous regions within semi-crystalline polymers and further extended to consider the entire polymer in a larger modelling framework.

2.1.2 Molecular weight

Polymer samples contain many chains of varying lengths or, equivalently, varying molecular mass. Each monomer has a fixed molar mass; the number of these in a chain determines its

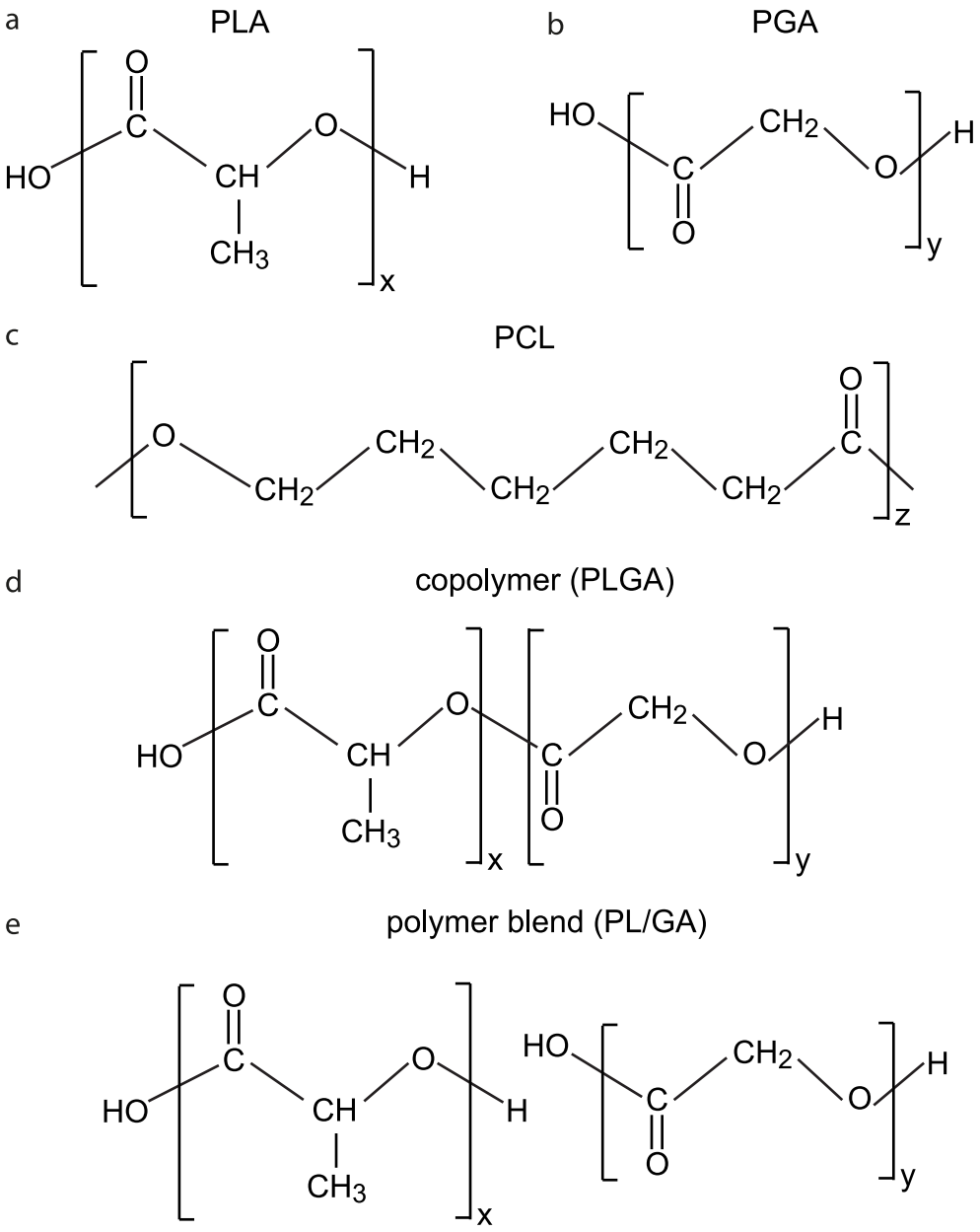

Fig. 2.3. Chemical structure of (a) poly(lactic acid) (PLA), (b) poly(glycolic acid) (PGA), (c) polycaprolactone (PCL), (d) poly(lactic-co-glycolic acid) (PLGA), a copolymer of PLA and PGA, and (e) poly(lactic/glycolic acid) (PL/GA), a polymer blend of PLA and PGA, where x is the number of units of lactic acid, y is the number of units of glycolic acid, and z is the number of units of caprolactone.

molecular mass. This mass distribution is typically referred to as the molecular weight distribution (MWD). As chains break during degradation, the material transitions from having a high molecular weight to a low molecular weight, with the MWD shifting to the left (Fig. 2.4). The MWD influences the mechanical properties of the polymer (Ward and Sweeney, 2004), and therefore knowledge of its evolution during degradation is important.

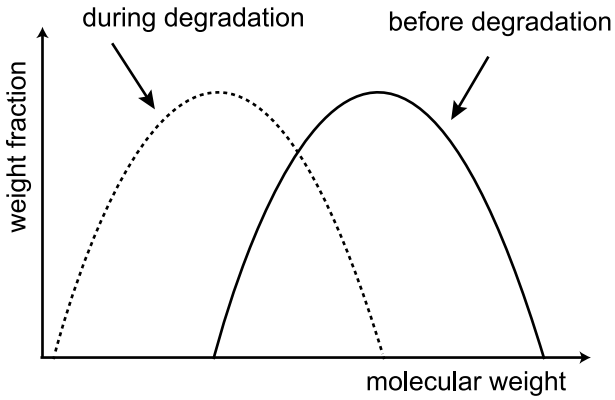

Fig. 2.4. Schematic diagram of molecular weight distribution and its evolution during degradation, moving from a high towards a reduced molecular weight.

2.1.2.1 Average molecular weights

Frequently, the evolution of an average molecular weight is reported in experimental studies of biodegradable polymers. Most often, this is in the form of either the number average or weight average molecular weight. The number average molecular weight, M_n, which emphasizes relatively short chains, is calculated as

$$M_n = \frac{\sum_{i=1}^{N_c} N_i M_i}{\sum_{i=1}^{N_c} N_i} \tag{2.1}$$

where N_c is the total number of chains and N_i is the number of polymer chains of weight M_i. The weight average molecular weight, M_w, can be calculated as

$$M_w = \frac{\sum_{i=1}^{N_c} N_i M_i^2}{\sum_{i=1}^{N_c} N_i M_i} \tag{2.2}$$

and this emphasizes relatively long chains in the distribution. A measure of the distribution, known as the molar mass dispersity, $Đ_M$, provides insight into the width of the MWD and is calculated as

$$Đ_M = \frac{M_w}{M_n} \tag{2.3}$$

Values of $Đ_M$ approaching unity indicate a polymer with almost uniform chain lengths. Less common averages considered include viscosity average, M_v, and Z average, M_z, with the following relationship typically holding: $M_n < M_v < M_w < M_z$.

Fig. 2.5 shows three sample molecular weight distributions displayed as a function of the number of polymer chains (a-c) and their corresponding weight fraction (d-f). Indicative values of M_n and M_w are shown, with the weight average molecular weight always greater as it is heavily impacted by very long chains. While the distributions and averages in Fig. 2.5a and c appear similar, their corresponding weight fraction distributions (Fig. 2.5d and f, respectively) differ substantially, highlighting the importance of knowledge of MWDs rather than averages alone. Experimental MWDs are typically presented with the weight fraction of polymer chains as a function of molecular weight plotted on a logarithmic scale. Monomodal distributions have a single peak (Fig. 2.5a-e), while Fig. 2.5f shows an extreme example of a bimodal distribution. During degradation, monomodal distributions have occasionally been seen to develop multiple peaks during degradation, typically accredited to crystalline residues (Tsuji and Del Carpio, 2003) or heterogenous degradation in larger samples (Grizzi et al., 1995); this is discussed further in Section 3.1.1.

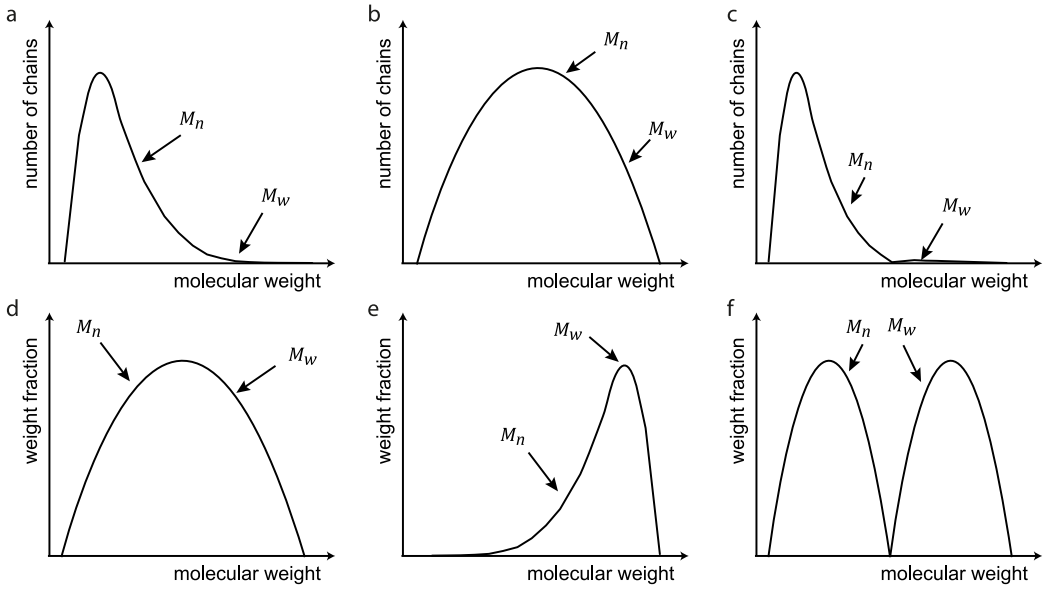

Fig. 2.5. Sample molecular weight distributions displaying the number average molecular weight, M_n, and the weight average molecular weight, M_w. The y-axes for (a)-(c) indicate the number of chains, while (d)-(f) are their corresponding weight fractions.

2.1.2.2 Experimental measurement of molecular weights

Gel permeation chromatography (GPC) (Moore, 1964), a type of size-exclusion chromatography, is the method regularly employed when experimentally determining the molecular weight of a polymer material, separating the polymer chains based on hydrodynamic volume using a column packed with porous beads. The chains are characterized based on the time they spend travelling through the column: smaller chains

can enter the pores more readily, increasing their retention time; larger chains, unable to fit into many of the pores, have a more direct path to follow through the column, allowing them to leave more quickly (Fig. 2.6). It is possible for some chains to be completely retained, while others may not be retained at all; GPC is unable to separate these chains. The detection range is determined both by the column packings used and their pore diameters (Skoog et al., 2017), and the sensitivity of the equipment used (for example, a Viscotek SEC-MALS 20 (Malvern, 2019), which couples GPC with multi-angle light scattering technology, claims a molecular weight detection range of $1000\,\mathrm{Da} - 10\,\mathrm{MDa}$ or $1.66 \times 10^{-21}\mathrm{g} - 1.66 \times 10^{-17}\mathrm{g}$, which is equivalent to approximately 14 – 140000 units of PLA). Polystyrene standards are often used to calibrate GPC, meaning the molecular weight of the sample is measured with respect to polystyrene; it has been reported that in doing so, lower molecular weights of PLA may not be accurately captured (Alex et al., 2018). Experimental determination of the chain lengths that this becomes relevant for will allow this to be factored into theoretical calculations, with chains below some critical length excluded from calculations using Eqs. (2.1)-(2.2). It is possible that these chains may significantly influence the mechanical properties, as is investigated in Chapter 6.

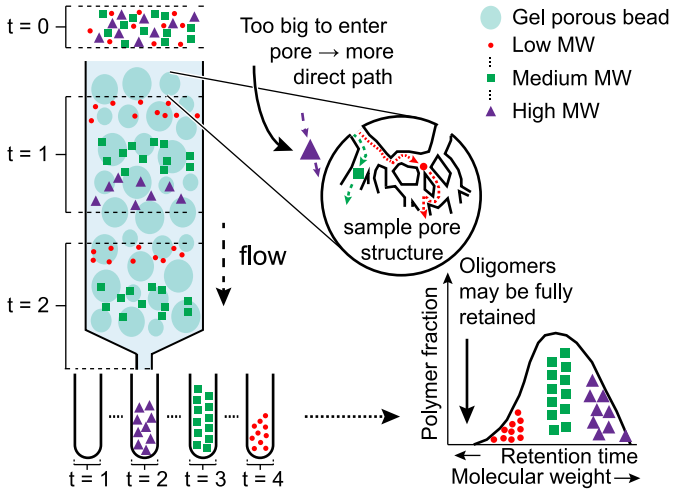

Fig. 2.6. Schematic diagram of gel permeation chromatography. At time zero (t = 0), a polymer sample is prepared and enters the column. The sample gradually progresses, with chains characterized based on the time they spend travelling through the column. For example, the high MW chains are too big to enter the narrow pore structures and have exited at t = 2, while the medium and low MW chains follow less direct paths and are still permeating through the column. Based on their retention time, a molecular weight distribution is obtained from which various averages can be determined.

An alternative method of determination is light scattering experiments. For this technique, light is passed through a liquid polymer-solvent solution and is scattered by the individual molecules suspended in the solution, with the degree of scattering arising from the molecule

size. From this, a molecular weight distribution can be determined from the total scattering created by the sample (Skoog et al., 2017). Analysis of polymer viscosity, osmotic pressure, and end groups each yield an average molecular weight and consequently are less insightful than methods such as GPC and multi-angle light scattering techniques that provide the overall distribution. Further details, including a comparison of different methods, are provided in the review by Oberlerchner et al. (2015).

2.1.3 Degradation mechanism

Biocompatible polyesters, such as poly(lactic acid) (PLA), poly(glycolic acid) (PGA) and their copolymers, experience degradation due to a hydrolytic reaction when placed in an aqueous medium (Buchanan, 2008), chemically described as follows:

$$-\mathrm{RCOOR'}- \; + \mathrm{H_2O} \xrightarrow{\mathrm{H^+ \; or \; OH^-}} -\mathrm{RCOOH} + \mathrm{HOR'}- \tag{2.4}$$

Ester bonds, the bonds that link one unit to the next, are hydrolysed throughout polymer chains, primarily in amorphous regions of the polymer, causing chains to split. Each chain scission results in two new end groups – an alcohol end, $\mathrm{HOR'}-$, and a carboxylic acid end group, $-\mathrm{RCOOH}$ (Ginjupalli et al., 2017; Laycock et al., 2017) (Fig. 2.7a). Both end and mid-chain scissions can occur, as outlined in Fig. 2.7b, and it is unclear which is the dominant mechanism (de Jong et al., 2001; Schliecker et al., 2003; Shih, 1995).

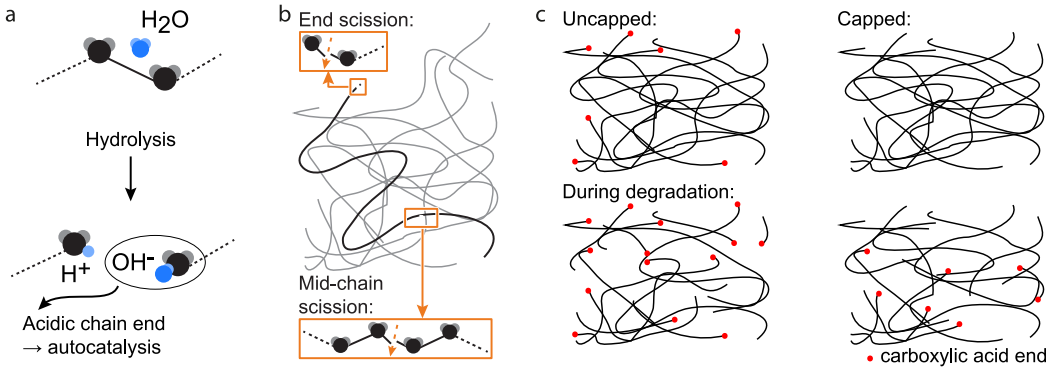

Fig. 2.7. Schematic diagram of degradation mechanism showing (a) the formation of carboxylic acid end groups during polymer hydrolysis, which can subsequently accelerate the reaction; (b) end and mid-chain scission processes; and (c) an initially uncapped and capped polymer chain ensemble before and during degradation with the carboxylic acid ends highlighted in red. Carboxylic acid ends are initially present in uncapped systems, in contrast to capped polymers. Chain scissions result in the formation of additional carboxylic acid ends irrespective of the initial configuration.

As reported by Batycky et al. (1997), the increased acid concentration at the end of each chain may be the driver behind different mid- and end-chain scission rates. Shih (1995)

reported a faster rate of end-chain scission ($k' = 0.13\mathrm{h}^{-1}$) than mid-chain scission ($k' = 0.01\mathrm{h}^{-1}$) for PLA, while reporting a completely random process for PCL, attributing this difference to the larger functional groups in PCL. Acidic degradation products can build up in the material due to limited diffusion, which can further accelerate the hydrolytic degradation (i.e., autocatalysis) and lead to heterogeneous bulk degradation (Grizzi et al., 1995; Vey et al., 2008). In the natural or uncapped state, each polymer chain has a carboxylic acid end and these can contribute to an increased rate of degradation; to overcome this, the polymer chains may be processed to "cap" the acid end, thus making them less reactive initially (Tracy et al., 1999) (Fig. 2.7c).

Depending on the size and type of polymer, degradation may proceed as surface erosion or bulk degradation (Fig. 2.8), either homogenously or heterogeneously. Surface erosion gradually degrades the polymer from the outside inwards with the core remaining intact and may be caused by (i) hydrophobicity of the bulk polymer, with a higher rate of hydrolysis than diffusion or a slow rate of water diffusion due to a high glass transition temperature (detailed in Section 2.1.4), (ii) or high crystallinity. This results in the retention of average molecular weight and mechanical properties for the core, while the load bearing capability of the material steadily declines. In contrast, bulk degradation proceeds throughout the polymer due to an abundance of water molecules and their ability to quickly diffuse throughout the material, exceeding the rate of hydrolysis. Consequently, a reduction in mass, molecular weight and mechanical properties occurs throughout the material. Homogenous degradation may occur in very thin samples, with most acidic degradation products able to diffuse from the surface and the core. In thicker samples, acidic degradation products can diffuse from the surface more readily than the core, resulting in heterogenous degradation with accelerated degradation in the core. Shirazi et al. (2016a) predicted heterogenous degradation occurs in PLGA samples provided the characteristic diffusion length, calculated from material parameters, exceeds 3 µm. It is expected that the above mentioned poly(α-hydroxy acids) will degrade via bulk erosion, with a switch to surface erosion expected above a critical dimension estimated to be 7.4 cm by von Burkersroda et al. (2002).

Variations are expected in the degradation of samples in vivo and in vitro (Buchanan, 2008). Factors controlling this include additional fluid flow, mechanical loading, and biological interactions, such as enzymatic activity or inflammatory reactions, present in in vivo studies(Agrawal et al., 2000; Beslikas et al., 2011; Thompson et al., 1996). PLGA scaffolds tested under static conditions lost mass, molecular weight, and stiffness more rapidly than under flow conditions (Agrawal et al., 2000), while dynamically loaded PLGA implants

showed slower declines in molecular weight than unloaded samples (Thompson et al., 1996). The degradation medium is often replaced at set intervals in in vitro studies, effectively resetting the pH (Deng et al., 2005; Polak-Kraśna et al., 2021); while this may somewhat mimic fluid flow and diffusion in in vivo settings, it may impact the effect of autocatalysis.

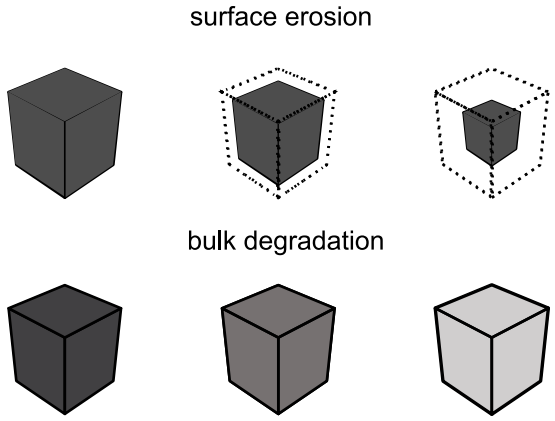

Fig. 2.8. In contrast to surface erosion, which gradually degrades the material from the outside inwards, bulk degradation results in a degraded core due to a rapid ingress of water molecules available to hydrolyse throughout the sample. The materials of interest in this thesis primarily undergo bulk degradation

2.1.4 Mechanical properties

In addition to molecular weight, the mechanical properties of polymers provide important characterisations of the materials. The three basic mechanical responses to an applied load are elasticity, plasticity, and fracture: elasticity is defined by a fully recoverable response, i.e., there is no permanent change to the material on loading and unloading; plasticity evokes a permanent shape change without cracking; and fracture involves the creation or propagation of a crack, separating portions of the material from one another. Further to these, viscoelasticity is particularly relevant for polymer materials and is defined as time-dependent elasticity, where the relationship between stress and strain changes with time. Material failure may coincide with any of these phases depending on the material requirements; for example, a polymeric stent may suddenly buckle elastically under certain conditions, failing to support and perhaps damaging the local tissue, without undergoing plasticity or fracture. This thesis is primarily concerned with the elastic response of amorphous biodegradable polymer materials; ultimately, the understanding obtained should be considered alongside other mechanical responses and extended to semi-crystalline materials. Further details are provided by Hertzberg et al. (2013) and Ward and Sweeney (2013).

Materials are often characterised based on measured stress-strain curves, which describe the relationship between stress and strain as a load is applied to a material. For polymer

materials, these curves are typically dependent on temperature and strain rate. Fig. 2.9a shows some typical forms of these curves, with a transition from brittle (i) to progressively ductile (iv) behaviour; each curve could correspond to different materials or the same material at different testing conditions. Furthermore, biodegradable polymers appear to transition during degradation, becoming increasingly brittle (Fig. 2.9b). It is common to categorize brittle and tough polymer fractures as those with low strain at failure (e.g., less than 4% in tension) and those with greater strain at failure, respectively. A linear (or nearly linear) elastic response is typically observed initially, followed by a nonlinear response controlled either by plasticity or viscoelasticity (i-iii) or hyperelasticity (iv).

The linear phase may be described by Hooke's law, where stress, σ, and strain, ε, are directly proportional:

$$\sigma = E\varepsilon \tag{2.5}$$

and E is Young's modulus or the modulus of elasticity and is a measure of stiffness. Materials with large values of E are stiff and show significant resistance to elastic behaviour, while low values of E correspond to compliant materials and their resistance to elastic behaviour is low. This property is temperature dependent in polymers and decreases with increasing temperature.

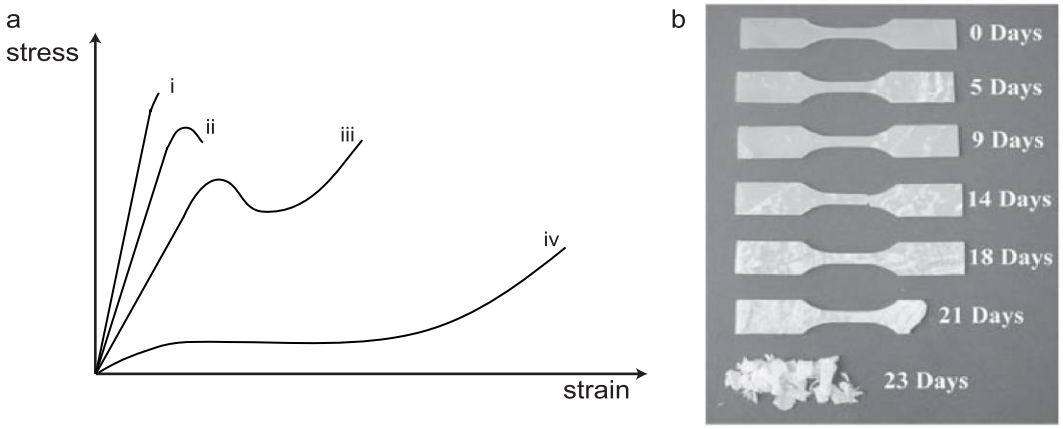

Fig. 2.9. (a) Schematic depiction of typical engineering stress-strain curve for polymers ranging from brittle (i) to progressively more ductile (iv). Adapted from Hertzberg et al. (2013). (b) PLLA specimens degraded at 70°C, showing an increasing decline of mechanical properties. Reproduced from Weir et al. (2004b) with permission, Copyright © 2004, SAGE Publications.

Each polymer has a glass-transition temperature, denoted T_g, exhibiting different behaviour above and below this threshold (Fig. 2.10). When polymers exist below T_g, the amorphous regions are relatively brittle or glass-like, with a relatively high modulus of elasticity that is

only mildly temperature dependent. As the test temperature rises, a large transition in stiffness occurs over a narrow temperature range; the midpoint in this range is termed T_g. Towards and above T_g, the energy within the polymer increases, which allows for additional chain mobility. As a result, amorphous regions gradually transition into a more viscous, rubber-like state. Loadbearing amorphous polymers must be used below T_g to avoid rapid changes in stiffness with temperature. In contrast, the magnitude of the change in stiffness for semi-crystalline polymers is more modest, allowing use at any temperature (Hertzberg et al., 2013).

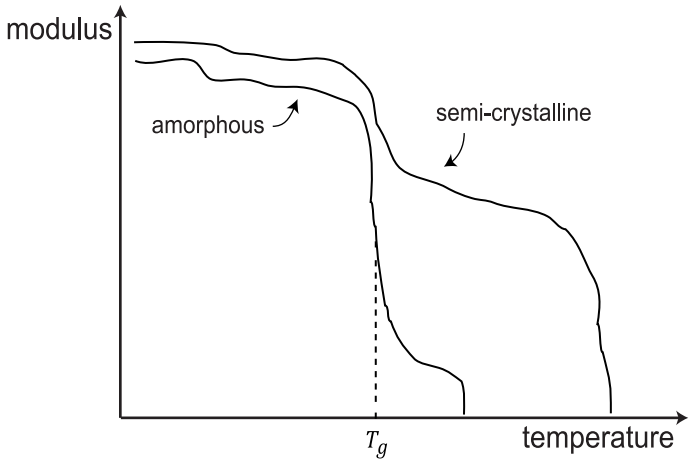

Fig. 2.10. Schematic depiction of the temperature dependence of the modulus of elasticity for polymer materials. At relatively low temperatures, a lack of chain mobility contributes towards stiff materials with large modulus. As the temperature increases so too does the energy, allowing for greater chain mobility and a more compliant material. The glass transition temperature, T_g, marks the midway point of the largest change in modulus, denoted here for the amorphous case. Adapted from Hertzberg et al. (2013).

Table 2.1 outlines the glass transition temperature of both biocompatible polymers and some used in alternative applications for comparison purposes. These values suggest that PLA, PGA and PLGA are likely to have $T < T_g$ at operable temperatures. Nevertheless, both PLLA (Venkatraman et al., 2003) and PLGA (Duval et al., 2018) have shown ductile failure modes in such scenarios. A number of studies observed variations in T_g during degradation (Malin et al., 1996; Vey et al., 2008; Weir et al., 2004b). A change from T_g above to below the testing temperature could cause a sudden increase in material property loss, as outlined by Laycock et al. (2017).

The backbones of polymer chains consist of strong covalent bonds that contribute to the strength of the material. Strength may be defined as a measure of resistance to plastic deformation or fracture. For ductile polymers, the yield strength is usually described as the first maximum in the stress-strain curve, while the ultimate tensile strength is the overall

maximum measured under tensile loading. The strength of brittle materials is measured by fracture strength, again the maximum of the curve, which often has a relatively large uncertainty due to the strong influence of the size and character of surface flaws.

Table 2.1. Typical glass transition temperatures, T_g, of a range of polymers as determined experimentally.

Polymer	T_g (°C)	Ref.
Poly(lactic acid)	49 – 69	(Hiljanen-Vainio et al., 1996; Weir et al., 2004a)
Poly(glycolic acid)	35 – 45	(Buchanan, 2008; Reed and Gilding, 1981)
Poly(lactic-co-glycolic acid)	30 – 45	(Duval et al., 2018; Nakafuku and Takehisa, 2004)
Polycaprolactone	-64 – -62	(Buchanan, 2008; Wang et al., 2005)
Poly(lactic-co-caprolactone)	-54 – 56	(Hiljanen-Vainio et al., 1996; Vieira et al., 2011)
Polystyrene	97 – 98	(Mark, 2007)
Polypropylene	-39 – -17	(Mark, 2007)

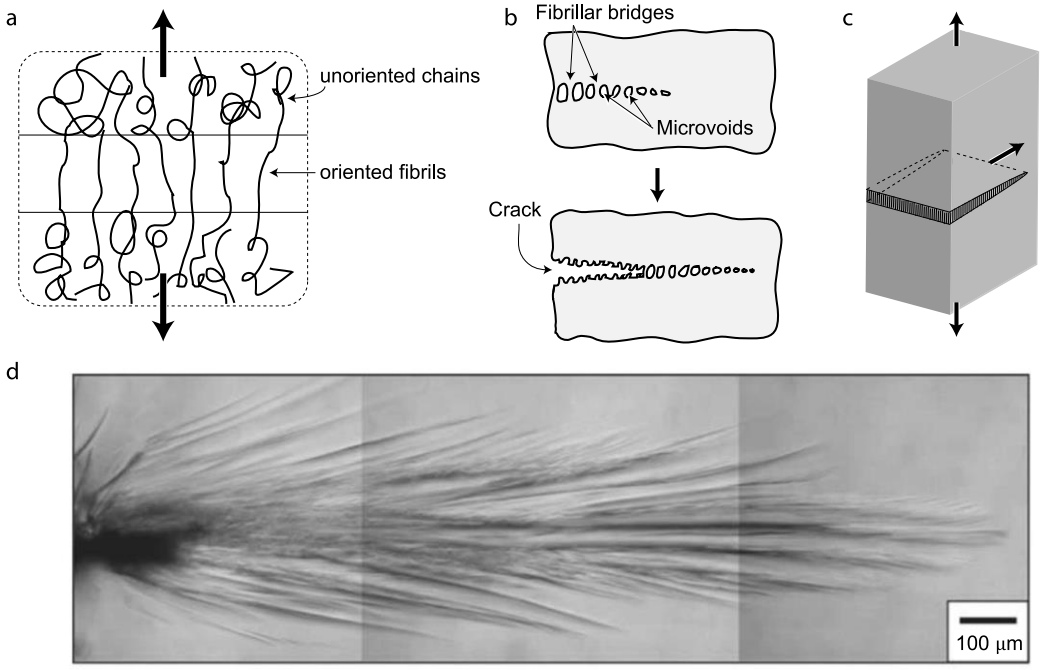

Fig. 2.11. (a) Schematic diagram of crazing caused by tensile stresses. The fibrils bridge the craze, preventing the microvoids from immediately linking up to form a true crack. Adapted from Hertzberg et al. (2013). (b) The craze will continue to propagate and the bridges will eventually break, leading to macroscale fracture in the form of a crack. Adapted from Callister and Rethwisch (2018). (c) Crazes form within the material along an axis perpendicular to the principal tensile stress direction and tend to grow along planes normal to the principal tensile stress direction. Adapted from Hertzberg et al. (2013). (d) Polarized micrograph of crack growth behaviour in low-crystalline PLA in the region of a notch under static loading conditions. Reproduced from Park et al. (2006) with permission from Elsevier.

In the presence of tensile stresses, crazing may occur. Crazes or microcracks that form in amorphous polymers are likely to underlie the brittle fracture process. They typically occur in regions of high stress concentration due to structural imperfections. Crazes are

micrometre-scale crack-like features that consist of expanded material containing oriented fibrils interspersed with small (10 to 20 nm) interconnected voids (Fig. 2.11a). These fibrils bridge the craze, preventing the microvoids from immediately linking up to form a true crack. Because of its intrinsic weakness, the craze is an ideal path for crack propagation; if the applied load is sufficient, the fibrils will eventually break, leading to macroscale fracture (Fig. 2.11b). Crazes form within the material along an axis perpendicular to the principal tensile stress direction and tend to grow along planes normal to the principal tensile stress direction (Fig. 2.11c). The initiation of a craze depends simultaneously on factors associated with the macroscopic state of stress and strain, the nature and distribution of heterogeneities within the solid, and the molecular behaviour of the polymer for a given set of thermal and environmental conditions. The typical craze thickness in glassy polymers is on the order of 5µm or less and remains relatively constant as the craze propagates. Several crazes can emanate from one region of weakness, as shown in the case of notched PLA in Fig. 2.11d. Although crazes contribute toward an overall weakening of the material, the craze may support some level of stress unlike a true crack. A more in-depth consideration of the fatigue and fracture behaviour of polymers is provided by Lesser (2002).

A link between mechanical properties and molecular weight has been observed, often suggesting a critical molecular weight coincident with a ductile to brittle transition (Fayolle et al., 2007, 2004; Gardner and Martin, 1979; Golden et al., 1964). For example, Golden et al. (1964) studied the effect of molecular weight (by using irradiation to induce scissions and decrease molecular weight) on flexural modulus, strength and strain for polycarbonate, reproduced in Fig. 2.12a. Below a critical molecular weight, rapid declines in flexural strength and strain were detected, while above this, mechanical properties were less sensitive to molecular weight. Fayolle et al. (2004) also found a critical molecular weight separating the ductile-brittle transition for thermally oxidised polypropylene (Fig. 2.12b). Merz et al. (1951) determined that below a critical molecular weight the shape of the MWD is important, observing an increase in tensile strength by keeping M_w constant and narrowing the MWD in polystyrene films. Thomas and Hagan (1969) also reported MWD affecting mechanical properties, with a polystyrene sample with $Đ_M$ = 1.06 having improved tensile strength, elongation at break and tensile creep properties compared with a sample with equal M_w and $Đ_M$ = 2.6, suggesting that a greater presence of short chains in the system reduces the mechanical performance. Venkatraman et al. (2003) observed a transition from ductile to brittle failure for PLLA with reducing molecular weight (Fig. 2.12c). An in-depth review of the influence of molecular weight and molecular weight distribution on mechanical properties

in both amorphous and semi-crystalline polymers above and below T_g is provided by Martin et al. (1972). While most of the above-mentioned studies focused on different degradation mechanisms than outlined in Section 2.1.3, it is likely that the overall effect of molecular weight on mechanical properties is similar for the materials of interest in this thesis.

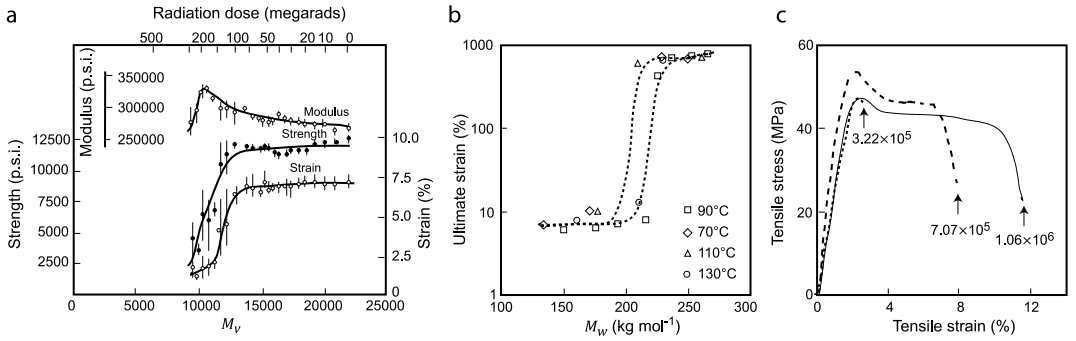

Fig. 2.12. (a) Flexural properties vs viscometric-average molecular weight for polycarbonate bars undergoing irradiation. (b) Ultimate strain vs weight average molecular weight for thermally oxidised polypropylene. (c) PLLA stress-strain curves showing a transition from ductile when $MW = 1.06 \times 10^6$ g mol^{-1} to brittle when $MW = 3.22 \times 10^5$ g mol^{-1} (average molecular weight measured not specified). Adapted from: (a) (Golden et al., 1964), (b) (Fayolle et al., 2004), (c) (Venkatraman et al., 2003).

The amorphous regions of semi-crystalline polymers have similar chain mobility and properties to fully amorphous materials. However, the surrounding crystallites impose restrictions that limit the movement of amorphous regions in semi-crystalline polymers. The crystalline regions typically contribute greater strength, stiffness, and thermal stability than fully amorphous polymers, with higher levels of crystallinity further emphasising this, while elongation and toughness are simultaneously reduced (Hertzberg et al., 2013). The mixed regions in semi-crystalline materials further complicate the mechanical behaviour.

2.1.5 Applications

Several industries have benefitted from the introduction of synthetic biodegradable polymers, most notably in the fields of packaging and medicine. The temporary nature of these materials offers an excellent alternative to conventional plastic packaging that is not readily biodegradable, such as polyethylene and polypropylene, helping to reduce the volume of plastic waste accumulating in landfills, provided they are disposed of correctly. An additional environmental benefit lies in the departure from the reliance on the production of plastics using petrochemicals and towards renewable resources while remaining economically viable. For example, glucose can be extracted from milled corn and fermented to produce lactic acid monomers, providing the building blocks of PLA (Vink et al., 2003).

Their short-term lifespan has also offered numerous benefits in the medical industry. During the 1960s, biodegradable polymers began replacing more traditional materials with the advent of synthetic bioabsorbable sutures (Herrmann et al., 1970). Providing an alternative to catgut, an animal protein that was the previous standard for dissolvable stitches with reports of its use in wound closure dating back to 130 AD, it proved an ideal suture material in terms of tensile strength, knot security and handling characteristics, while evoking minimal inflammatory reaction and being resistant to infection (Herrmann et al., 1970). The reduced inflammatory reaction observed has been attributed to the hydrolytic degradation it experiences in contrast to the enzymatic degradation experienced by catgut (Deveney and Way, 1977). With the potential of these materials for this industry made clear due to their success in dissolvable sutures, they have been utilised in many more settings, ranging from orthopaedic fixation devices to drug delivery devices to temporary scaffolds and beyond (Allen and Cullis, 2004; McGinty et al., 2011; O'Brien, 2011; Vert, 2009; Vo et al., 2017). One of the primary benefits in each of these scenarios is the lack of need for a repeat surgery, with the device initially carrying out its function and aiding with healing, before gradually absorbing as its work is complete; for example, a dissolvable suture initially seals a wound and proceeds to dissolve over time as the skin heals (Fig. 2.13). The eliminated second surgery for implant removal reduces pain, recovery time, and cost.

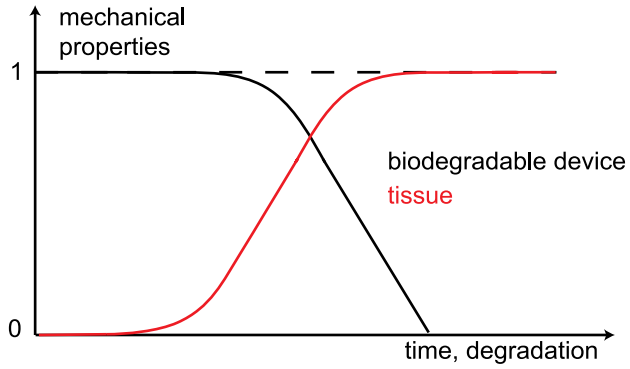

Fig. 2.13. The tuneable properties of the polymer implant must be designed to ensure sufficient initial mechanical properties for the intended purpose, with a suitable degradation rate aligned with the developing tissue.

In 2018, an estimated 2.1 million women were diagnosed with breast cancer worldwide (Sopik, 2021), over 34000 patients received organ transplants in Europe, with more than 150000 patients on the waitlist (Scholz, 2020), and more than four million people died of coronary heart disease (Wang, 2020). The need for alternative therapies remains huge, with biodegradable polymers being promising materials for reconstruction and treatment

purposes. Correct alignment of the degrading implant with the developing tissue is imperative. The initial product or device must have both adequate initial strength and a suitable, controlled rate of strength loss. Simultaneously optimising both for the intended application can prove challenging due to the complex behaviours these materials exhibit during degradation, which are further complicated by the incorporation of additional materials such as drugs or growth factors. Degradation studies often take years to complete, and small changes to the design can significantly alter the behaviour. Computational studies can provide important insight into the evolution of material and mechanical properties during degradation. An in-depth understanding of the polymer at microscopic and molecular levels and the underlying degradation mechanisms is essential towards designing devices with optimal, tuneable properties.

2.2 The deformation of an elastic solid

In general terms, mechanical behaviour is concerned with the deformations which occur under loading. This section focuses on a macroscopic or phenomenological description. Constitutive relations, which relate stress and strain for a particular type of material, that give an adequate description of the mechanical behaviour are defined. The following section (Section 2.3) then takes a molecular level approach to better understand the behaviour.

The scope of this thesis is limited to isotropic finite elasticity and rubber-like behaviour of incompressible materials. A more generalised approach should also consider (i) viscoelasticity, where constitutive relations also contain time or frequency as a variable, (ii) compressibility, (iii) orientation, and (iv) non-recoverable behaviour. Ward and Sweeney (2013) cover each of these topics in detail. Nevertheless, the work presented in this thesis is valuable in providing an improved understanding of the behaviour considered.

This section provides an overview of concepts such as stress (Section 2.2.1), strain and deformation (Section 2.2.2), work (Section 2.2.3), strain energy functions (Section 2.2.4), and stress-strain relationships (Section 2.2.5), that are all referred to throughout the thesis. This follows the format of Ward and Sweeney (2004). A more thorough description of continuum mechanics and deformation is provided by Belytschko et al. (2014).

2.2.1 Stress

On application of a load to a body, the resulting stress can be divided into components that describe the direction. The components of stress in a body are defined by considering the forces acting on an infinitesimal cubic volume element whose edges lie parallel with the coordinate axes x, y and z (Fig. 2.14). In equilibrium, the forces per unit area acting on the

cube faces are P_1 on the yz plane, P_2 on the zx plane and P_3 on the xy plane, with similar forces acting on the directly opposite faces of the cube.

The forces are resolved into nine components in the x, y and z directions as follows:

$$P_1: \sigma_{xx}, \sigma_{xy}, \sigma_{xz}$$

$$P_2: \sigma_{yx}, \sigma_{yy}, \sigma_{yz}$$

$$P_3: \sigma_{zx}, \sigma_{zy}, \sigma_{zz}$$

where the first subscript refers to the direction of the normal to the plane on which the stress acts, and the second subscript to the direction of the stress. For a cube in equilibrium, the net torque is zero, implying $\sigma_{xy} = \sigma_{yx}, \sigma_{xz} = \sigma_{zx}, \sigma_{yz} = \sigma_{zy}$.

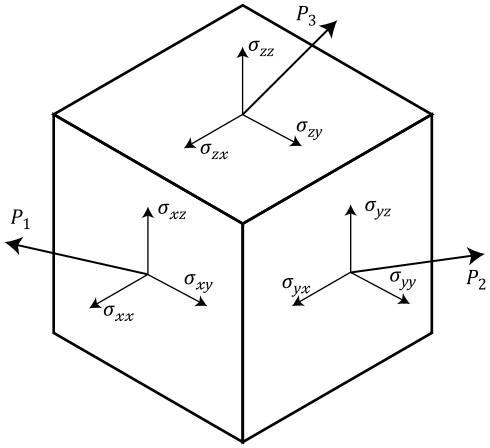

Fig. 2.14. The components of stress, as detailed in the text.

The components of stress are defined by six independent quantities: the normal stresses, $\sigma_{xx}, \sigma_{yy}, \sigma_{zz}$, and the shear stresses, $\sigma_{xy}, \sigma_{yz}, \sigma_{zx}$. These components describe the complete stress state, which is described by the stress tensor, σ_{ij}:

$$\sigma_{ij} = \begin{pmatrix} \sigma_{xx} & \sigma_{xy} & \sigma_{xz} \\ \sigma_{xy} & \sigma_{yy} & \sigma_{yz} \\ \sigma_{xz} & \sigma_{yz} & \sigma_{zz} \end{pmatrix} \tag{2.6}$$

Note that shear stresses are often denoted by τ in place of σ. The Lagrangian approach is taken in this thesis unless otherwise stated, wherein the reference state is the undeformed state of material. Nominal stresses are considered, which are defined as the force per unit of unstrained cross-section; this is analogous to the transpose of the first Piola-Kirchhoff stress. Although true stresses would be more informative for the large stretches considered in this thesis, nominal stresses are chosen to enable direct comparison with experimental data, which typically report nominal stress versus strain. A transformation, where the

reference state is the deformed state of material, could be facilitated as described by, for example, Belytschko et al. (2014).

2.2.2 Strain and deformation

Extensional strain is defined as the fractional change in length in the stretching direction, while simple shear strain is defined by the displacement of parallel planes (Fig. 2.15). To describe the deformation of a body, components of extensional ($\varepsilon_{xx}, \varepsilon_{yy}, \varepsilon_{zz}$) and shear ($\varepsilon_{xy}, \varepsilon_{yz}, \varepsilon_{zx}$, often denoted by γ in place of ε) strain are considered, comparable with the components of tensile and shear stress. While the strain tensor also contains information on rigid body rotations, these do not correspond to deformation and are not considered here.

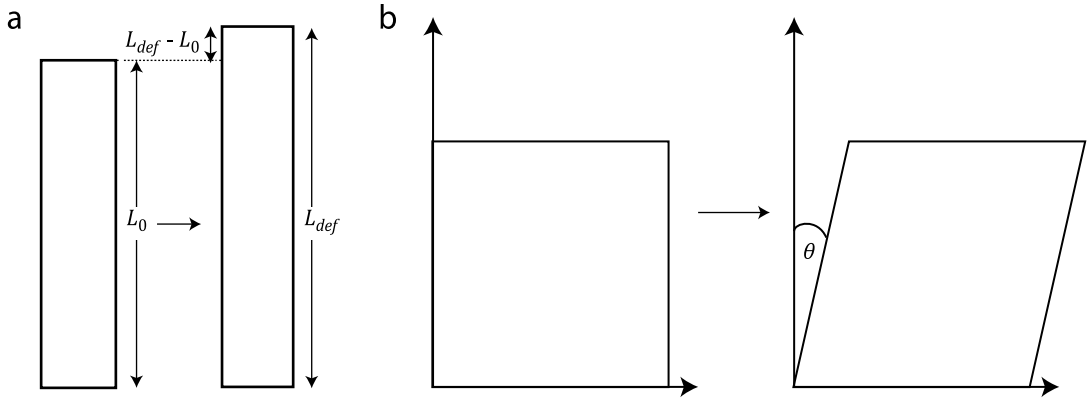

Fig. 2.15. (a) Extensional strain is the fractional change in length in the stretching direction, measured as the change in length, $L_{def} - L_0$, divided by original length, L_0. (b) Simple shear strain is defined by the displacement by angle θ of parallel planes.

A deformation in which lines of material along the three coordinate axes x, y and z in the undeformed state remain mutually perpendicular is called normal strain because the shear strain components are zero. A deformation can always be defined in terms of normal strain provided careful choice of axes by reference to the deformed state. Without loss of generality, this simplification will be used throughout this thesis, unless otherwise stated.

Such axes are referred to as principal axes and allow the deformation to be defined in terms of extensional strain components defined by principal stretches or deformation ratios, $\lambda_x, \lambda_y, \lambda_z$. The deformation ratios are so titled because they define the ratio of the length of lines in x, y, z directions in the deformed body to their length in the undeformed body. For example, the deformation of a unit cube to a parallelepiped may be defined in terms of the deformation ratios, as shown in Fig. 2.16.

A point Q in the body with coordinates (x, y, z) moves to a point Q′ with coordinates (x', y', z') defined as

$$x' = \frac{L_{def,x}}{L_{0,x}} x = \lambda_x x, \qquad y' = \lambda_y y, \qquad z' = \lambda_z z \tag{2.7}$$

where $L_{0,x}$ and $L_{def,x}$ are the length in the undeformed and deformed body. The deformation ratios may be translated into engineering strains as follows (Fig. 2.15):

$$\varepsilon_{xx} = \frac{L_{def,x} - L_{0,x}}{L_{0,x}} = \frac{L_{def,x}}{L_{0,x}} - 1 = \lambda_x - 1 \tag{2.8}$$

and similarly for ε_{yy} and ε_{zz}.

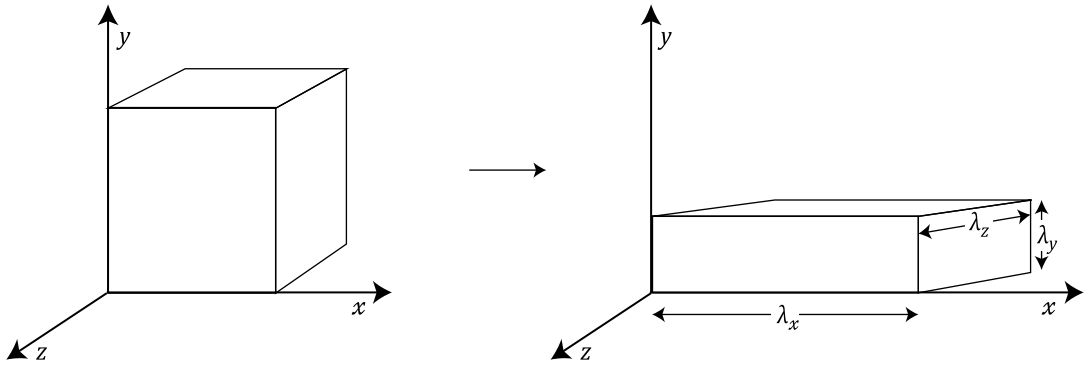

Fig. 2.16. A unit cube is deformed into a parallelepiped with sides of length λ_x, λ_y and λ_z, thus defining the deformation ratios.

2.2.3 Work

The work done per unit of initial undeformed volume in an infinitesimal displacement from the deformation state in principal directions where $\lambda_x, \lambda_y, \lambda_z$ change to $\lambda_x + \mathrm{d}\lambda_x, \lambda_y + \mathrm{d}\lambda_y, \lambda_z + \mathrm{d}\lambda_z$ is

$$\mathrm{d}W = \sigma_{xx}\mathrm{d}\lambda_x + \sigma_{yy}\mathrm{d}\lambda_y + \sigma_{zz}\mathrm{d}\lambda_z \tag{2.9}$$

where the stresses are the normal nominal stresses.

The first law of thermodynamics relates the work done on the body, $\mathrm{d}W$, to the increase in internal energy, $\mathrm{d}U$, and the mechanical value of the heat supplied, $\mathrm{d}Q$:

$$\mathrm{d}W = \mathrm{d}U - \mathrm{d}Q \tag{2.10}$$

For an adiabatic change of state, $\mathrm{d}Q = 0$, the work done can be equated to a change in the stored elastic energy: $\mathrm{d}W = \mathrm{d}U$. Assuming the deformation is produced by independent changes in each of the components of stretch, Eq. (2.9) gives

$$\sigma_{xx} = \frac{\partial U}{\partial \lambda_x}, \qquad \sigma_{yy} = \frac{\partial U}{\partial \lambda_y}, \qquad \sigma_{zz} = \frac{\partial U}{\partial \lambda_z} \tag{2.11}$$

In the case of rubbers, it is usual to consider a reversible isothermal change of state at constant volume, with the work done equated to the change in the Helmholtz free energy A, i.e.,

$$\mathrm{d}W = \mathrm{d}A \tag{2.12}$$

Free energies are used to analyse non-adiabatic cases, where the heat exchanged is subtracted from the internal energies. The Helmholtz free energy is associated with constant volume conditions. While this can be challenging to replicate experimentally, the molecular theories are typically derived using this assumption.

To ensure energy balance, it is important to carefully select pairs of stress and strain rate measures that are conjugate in work or power (Belytschko et al., 2014). Examples of these include nominal stress and rate of the deformation gradient; Cauchy (true) stress and rate-of-deformation; and second Piola-Kirchhoff stress and rate of Green strain, with definitions provided by Belytschko et al. (2014). For deformations in the principal directions, Eq. (2.11) is balanced and corresponds to the conjugate pair of nominal stress and rate of the deformation gradient.

2.2.4 Strain energy function

Eq. (2.11) may be used to obtain constitutive relations between stress and strain with knowledge of U. Termed the strain energy function, U defines the energy stored as a result of the strain and is often presented as a function of the components of a measure of strain such as the deformation ratios. Restrictions are applied to the function to ensure (i) the energy is not dependent on the choice of axes (e.g., a symmetric function of $\lambda_x, \lambda_y, \lambda_z$ is chosen), (ii) it is zero for zero strain and (iii) it simplifies to Hooke's law for small strains.

The most elementary form of U is often presented for incompressible materials as

$$U = C_1(\lambda_x^2 + \lambda_y^2 + \lambda_z^2 - 3) \tag{2.13}$$

for material constant C_1, satisfying each of the restrictions just mentioned. This form is known as the neo-Hookean or Gaussian model, first proposed by Rivlin (1948). The same relationship is obtained as a consequence of the molecular theories of a rubber network, as

detailed in Section 2.3.5. An alternative form of the neo-Hookean model exists for compressible materials; see, for example, Belytschko et al. (2014).

More complex phenomenological models are detailed by Ward and Sweeney (2013) and Belytschko et al. (2014) and include the Mooney-Rivlin and Ogden models.

2.2.5 Stress-strain relationships

Once the form of U has been decided, Eq. (2.11) may be used to obtain a stress-strain relationship. For example, for an incompressible material, i.e., there is no change in volume on deformation ($\lambda_x\lambda_y\lambda_z = 1$), consideration of uniaxial tension in the x direction gives

$$\lambda_x = \lambda, \qquad \lambda_y = \lambda_z = \frac{1}{\sqrt{\lambda}}, \qquad \sigma_{yy} = \sigma_{zz} = 0 \tag{2.14}$$

Combining Eqs. (2.11) and (2.13) gives the stress as a function of the stretch:

$$\sigma_{xx} = \frac{\partial U}{\partial \lambda} = 2C_1\left(\lambda - \frac{1}{\lambda^2}\right) \tag{2.15}$$

which may be related to strain using Eq. (2.8).

Alternative forms of mechanical testing can be considered in a similar way. For example, for equibiaxial tension ($\sigma_{yy} = \sigma_{zz} = \sigma, \sigma_{xx} = 0$), the extension ratios in the y- and z-directions are $\lambda_y = \lambda_z = \lambda$. Continuing the assumption of incompressibility, $\lambda_x = \frac{1}{\lambda^2}$. Using Eq. (2.9) and $dW = dU$, σ is found as follows:

$$\mathrm{d}U = 2\sigma\mathrm{d}\lambda \implies \sigma = \frac{1}{2}\frac{\partial U}{\partial \lambda} \tag{2.16}$$

Combining Eq. (2.13) with Eq. (2.16) gives

$$\sigma = 2C_1\left(\lambda - \frac{1}{\lambda^5}\right) \tag{2.17}$$

Similarly, simple shear may be considered by setting $\lambda_z = \lambda$, $\lambda_y = 1$ and $\lambda_x = 1/\lambda$, which gives a purely deviatoric stretch, i.e., with no volume change ($\lambda_x\lambda_y\lambda_z = 1$) (Treloar, 1975a). Assuming the work done on the body is due entirely to the shear stress $\tau = \tau_{yz}$, Eq. (2.9) is rewritten as

$$\mathrm{d}U = \tau\mathrm{d}\gamma \tag{2.18}$$

where $\gamma = \gamma_{yz}$ is the shear strain and here γ may be related to the principal extension ratios as follows (Love, 1944):

$$\gamma = \lambda - \frac{1}{\lambda} \tag{2.19}$$

The neo-Hookean (Eq. (2.13)) form for simple shear is then given by

$$U = C_1\left(\lambda^2 + \frac{1}{\lambda^2} - 2\right) = C_1\gamma^2 \tag{2.20}$$

and from Eq. (2.18),

$$\tau = 2C_1\gamma \tag{2.21}$$

with the shear stress proportional to the shear strain.

Some additional classic modes of deformation are considered in this way by Treloar (1975a), where an outline of the principal extension ratios and the corresponding general stress relationships are provided.

2.3 Statistical mechanics of polymeric chains (rubber-like elasticity)

The statistical mechanics theory for rubber-like deformation of materials is presented in this section. Further details are provided by Ward and co-workers (1971; 1993; 2013) and Mark and co-workers (Mark, 2007; Mark and Erman, 2007). While the previous section focused on a macroscopic description of deformation, a molecular level approach is now described, which provides a better understanding of the underlying behaviour.

Although polymers such as PLA ($T_g = 49 - 69°\mathrm{C}$) (Hiljanen-Vainio et al., 1996; Weir et al., 2004a) and PGA ($T_g = 35 - 45°\mathrm{C}$) (Buchanan, 2008; Reed and Gilding, 1981) are not elastomers and are typically below T_g initially, models that assume rubber-like behaviour have previously sufficiently captured their behaviour (Shirazi et al., 2016b; Wang et al., 2010), with many such polymers initially exhibiting ductile behaviour (Tsuji, 2002; Vieira et al., 2011; Weir et al., 2004a). Throughout degradation, variations in T_g exist, often declining below the testing temperature (Malin et al., 1996; Vey et al., 2008). Additionally, the deformation of glassy, thermoplastic polymers is not well understood. Although molecular dynamics can capture the behaviour at and below T_g, this is not currently a feasible approach with computational restrictions limiting this technique to short time periods (Ding et al., 2012). Consequently, the generally accepted rubber-like idealisation is used in this work for

simplicity. In theory, this may assume greater elasticity than would be present in these materials. However, all models presented are considered in parallel with experimental data to ensure the behaviour is suitably captured.

In this work, incompressibility is also assumed, with no changes in volume accounted for. Incompressibility is appropriate for densely packed polymer materials, where any volume changes are negligible. The density of the polymer will depend on the manufacturing technique. Incompressible materials have a Poisson's ratio, ν, (a measure of the deformation of the material in directions perpendicular to the loading direction) of 0.5, while compressible materials typically have $0 \leq \nu < 0.5$. PLA has a reported Poisson's ratio of 0.36 (Jamshidian et al., 2010), meaning some level of compressibility is expected. Thus, for a more rigorous consideration of mechanical properties, the incompressibility assumption should be removed in the future.

2.3.1 "Entropy springs"

In contrast to materials known as "energy springs", where extension causes an increase in internal energy, the terms "probability or entropy springs" are sometimes used to refer to rubber-like materials. This is because all chain configurations have approximately the same internal energy and it is instead the entropy controlling the deformation. When subjected to an external force, chains, forced from their state of maximum entropy, extend in the direction of the force, reducing the entropy and resulting in a state of strain (Fig. 2.17); on the removal of an external stress, an extended chain returns to its most probable state (assuming no irreversible deformation has taken place). By first calculating the entropy of a single chain in the polymer network and then relating this to the change in entropy of a network of chains as a function of strain, one can gain insight into the stress-strain characteristics of the material; subsequent sections describe how to approach this.

Chains that have slid past one another, preventing full recovery, are not considered here, nor are entanglements, consistent with simple theories of rubber-like elasticity. It is assumed that chains change from a coiled to an extended configuration instantaneously on application of stress, and similarly on removal of stress. Equilibrium thermodynamics can be used to determine how the stress is related to changes in both internal energy and entropy. Complementary to this, molecular theories of a statistical nature offer an equation of state relating the force causing extension to molecular parameters.

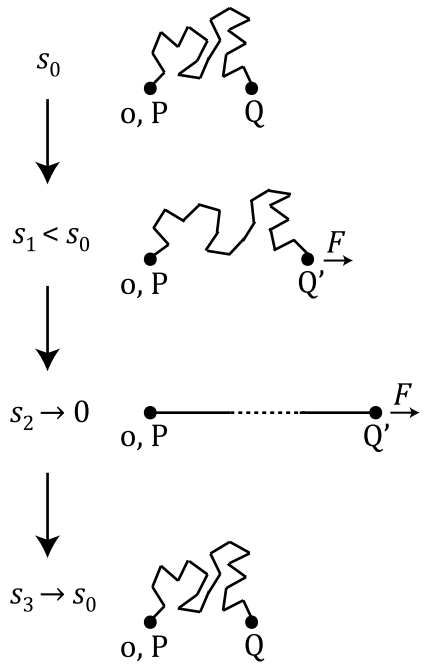

Fig. 2.17. Prior to deformation, a chain is attracted to a maximum state of entropy, s_0. On deformation, F, the entropy reduces ($s_1 < s_0$), with fewer possible configurations, gradually reaching its fully extended state ($s_2 \to 0$), for which only one configuration exists. On removal of the external force, the chain is once again attracted to a maximum state of entropy ($s_3 \to s_0$), provided no irreversible deformation has taken place.

2.3.2 Polymer chain models

As well detailed by Fetters et al. (2007), aliphatic backbone polymers have n monomers, each with n_b backbone bonds, with a well-defined average backbone bond length l, and known average backbone bond angle θ;an example is shown in Fig. 2.18 for PLLA. Restrictions on torsional rotation (ϕ) and local interactions are also present. Several polymer chain models exist, which consider these aspects to varying extents.

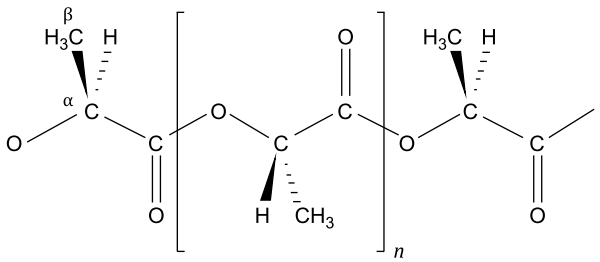

Bond Length [$\times 10^{-12}$ m]	Valence angle [°]
O–C^{α} : 144	O–C^{α}–C : 110
C^{α}–C : 152	C^{α}–C–O : 114
C–O : 134	C–O–C^{α} : 113
C=O : 122	C^{α}–C=O : 121
C^{α}–C^{β} : 154	O–C^{α}–C^{β} : 110
C^{α}–H : 107	O–C^{α}–H : 110

Fig. 2.18. Chemical structure of PLLA detailing the bond lengths and valence angles. Adapted from Rehahn et al. (1997). Each of the n monomers contain n_b backbone bonds, average backbone bond length l and average backbone bond angle θ.

The simplest polymer chain model, first proposed by Kuhn (1934; 1946), assumes a freely jointed chain, where chains contain n links, each of length l, jointed together in succession. It is assumed that there is no restriction on the angle between adjacent links, with all

directions ($\theta = [0, \pi], \phi = [0,2\pi]$) equally possible and the direction of neighbouring bonds uncorrelated. This model is equivalent to a random flight in three dimensions.

An advancement on this takes valence bond angles into account and is typically referred to as the freely rotating chain (Fig. 2.19a). Again, chains contain n links of length l, and now the backbone bond angle between neighbouring bonds at the ith backbone atom, $\pi - \theta_i$, remains fixed based on the chemical structure of the polymer. Torsional rotation about the ith bond remains possible and is denoted as ϕ_i.

Kuhn (1934) introduced an alternative approach, titled the equivalent freely jointed chain model. Chains are idealised as containing n_K equivalent Kuhn links of length l_K, referred to as the Kuhn length, where l_K holds information on short scale interactions and stiffness. The advantage of the equivalent freely jointed chain over the freely rotating chain lies with the characteristic ratio, C_n, introduced in the former. Defined as the ratio of the mean-square end-to-end vectors of a real chain, $\langle r^2 \rangle_0$, with that of a freely jointed chain (i.e., with no restriction on bond angles) containing the same number of bonds, nl^2, $C_n = \langle r_0^2 \rangle / nl^2$, it is a measure of chain flexibility and contains information on both θ and other short scale interactions. For flexible chains, $C_n \approx 1$, while this increases for more rigid polymers. For large n, $C_n \to C_\infty$, a polymer specific constant. In practice, C_∞ is first determined using experimental techniques. Parameters for a chain idealisation for a given value of n are then determined as

$$n_K = \frac{n \cos^2\left(\frac{\theta}{2}\right)}{C_\infty}, l_K = \frac{C_\infty l}{\cos\left(\frac{\theta}{2}\right)} \tag{2.22}$$

where C_∞, θ and l are all polymer specific constants based on their chemical structure.

While the freely jointed and freely rotating chains both consider each individual “mer” or link, with the latter restricting the position of the adjacent link according to the backbone bond angle, the equivalent freely jointed chain reconsiders the links in equally sized groups, with this reformulation better accounting for bond angle and local interaction restrictions. Fig. 2.19 shows an example of this reformulation solely for visualisation purposes, where each of the n_K links in the equivalent freely jointed chain represents three links or monomers; more generally, each of the n_K links contains n/n_K physical links.

In the case of freely jointed chains, where valence bond angles are ignored, i.e., there is no restriction on θ, the maximum end-to-end length of a chain, r_{max}, is a completely

straightened chain: $r_{max} = nl$ (Fig. 2.19c). In contrast, r_{max} is limited for freely rotating and equivalent freely jointed chains by θ, giving $r_{max} = nl\cos(\theta/2)$ in the all-trans conformation (Fig. 2.19c).

The rotational isomeric state statistics model goes a step further and considers more realistic chain conformations, building possible conformations bond by bond using the following structural details obtained from experimental structural analyses: bond lengths, l_i, bond angles, θ_i, torsion angles, ϕ_i, and differences in energy for conformations produced by rotation about a bond or pair of bonds. While some of the earliest reports of this technique date back to the 1960s (Brant et al., 1969), Helfer and Mattice (2007) outline the technique and advancements in detail.

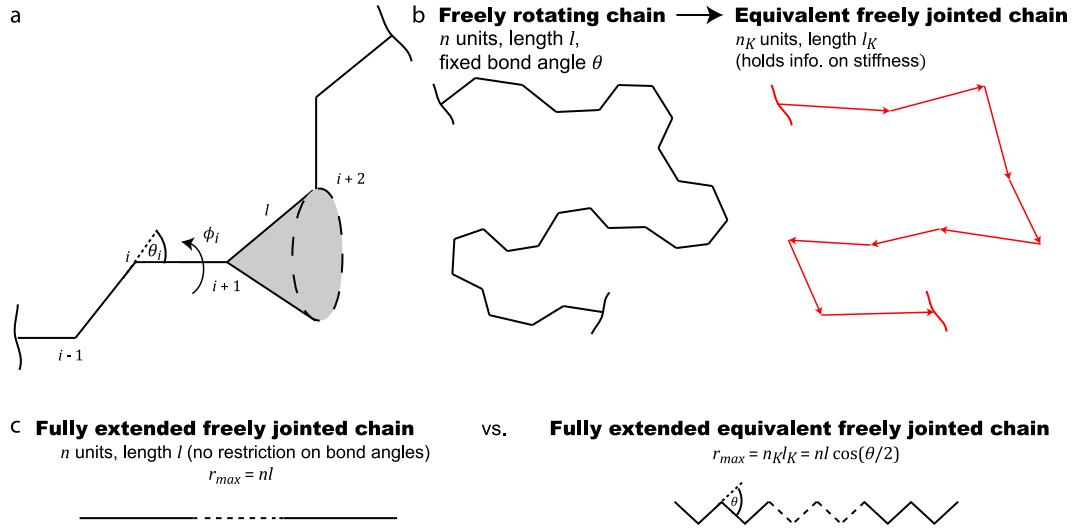

Fig. 2.19. (a) In the freely rotating polymer chain model, a chain contains bonds of average length l, while the valence bond angle between two neighbouring bonds at the ith backbone atom is $\pi - \theta_i$, where θ_i is the angle between consecutive bond vectors. The torsional rotation about bonds i and $i+1$ is denoted as ϕ_i. If the positions of $i-1, i$ and $i+1$ are fixed, and rotation is allowed about the bonds i and $i+1$, then the position of backbone atom $i+2$ is shown by the dashed circle. Adapted from Mark and Erman (2007). (b) The chain is reconsidered as having equivalent links of length l_K, referred to as the Kuhn length, where l_K holds information on short scale interactions and stiffness (i.e., more than just fixed θ_i). The number of links scales with this to give n_K Kuhn links, where each of these contains n/n_K physical links. (c) The maximum end-to-end length $r_{max} = nl$ for a freely jointed chain (where there is no restriction on bond angles), while for an equivalent freely jointed chain this is limited by the enforced bond angle θ, with $r_{max} = nl\cos(\theta/2)$.

A comparison between the three polymer chain idealisations mentioned is given in Table 2.2. The focus here is primarily restricted to the equivalent freely jointed chain model, with it offering the most detailed description of the three idealisations. Although the rotational

isomeric state statistics model provides a more realistic approach, it is more computationally demanding.

Table 2.2. Comparison between the freely jointed, freely rotating, and equivalent freely jointed chain models in terms of their (undeformed) mean square end-to-end distance, $\langle r^2 \rangle_0$, and their maximum physical extension, r_{max}. Where a link contains multiple backbone bonds, n_b, average bond lengths and bond angles may be taken, with $n = nn_b$ below.

	Number of links	Bond length	$\langle r^2 \rangle_0$	r_{max}
Freely jointed chain	n	l	nl^2	nl
Freely rotating chain	n	l	$nl^2 \frac{1+\cos\theta}{1-\cos\theta}$	$nl\cos\left(\frac{\theta}{2}\right)$
Equivalent freely jointed chain	$n_K = \frac{n\cos^2\left(\frac{\theta}{2}\right)}{C_\infty}$	$l_K = \frac{C_\infty l}{\cos\left(\frac{\theta}{2}\right)}$	$n_K l_K^2 = nl^2 C_\infty$	$n_K l_K = nl\cos\left(\frac{\theta}{2}\right)$

2.3.3 End-to-end distribution of chains

Much like a polymer has a molecular weight distribution, chains of equal weight are expected to have an end-to-end distance distribution. As detailed in Fig. 2.17, chains are typically attracted to a coiled state, with this controlled by entropy. For chains of increasing weight, i.e., containing more monomeric units, an increasing number of configurations or end-to-end distances are possible. Distributions such as the Gaussian and Langevin distributions describe these end-to-end distances well, with the latter favoured for greater accuracy when considering shorter chains.

To describe the end-to-end distance distribution, first consider an isolated idealised equivalent freely jointed polymer chain containing n_K links of length l_K. Any such chain has an end-to-end length, r, and its length at maximum physically possible extension is denoted r_{max} (Fig. 2.20a). A spherical distribution of chains is assumed, giving a surface area of $4\pi r^2$, with one end of each chain fixed at the origin, as is standard practice (Ward, 1971) (Fig. 2.20b). For a chain containing n_K links, the probability of a corresponding end-to-end length can be described using a Langevin distribution approximation, as detailed by Kuhn and Grün (1946). Thus, the probability of a chain having a particular end-to-end distance, r, is as follows:

$$\begin{aligned} P(r)\,\mathrm{d}r &= p(r)4\pi r^2\,\mathrm{d}r \\ &= \left(\frac{3}{2n_K l_K^2 \pi}\right)^{3/2} 4\pi r^2 \exp\left(-n_K\left(\frac{3}{2}\left(\frac{r}{n_K l_K}\right)^2\right.\right. \\ &\quad \left.\left. + \frac{9}{20}\left(\frac{r}{n_K l_K}\right)^4 + \frac{99}{350}\left(\frac{r}{n_K l_K}\right)^6 + \frac{1539}{9000}\left(\frac{r}{n_K l_K}\right)^8 + \cdots\right)\right)\mathrm{d}r \end{aligned} \tag{2.23}$$

with additional terms corresponding to more accurate approximations of the Langevin distribution. The end-to-end distance distribution, $P(r)$, is thus dependent on the chain parameters (n_K, l_K). Note that $P(r)$ is a volumetric end-to-end distribution which accounts for a spherical distribution of chains via the factor of $4\pi r^2$, while $p(r)$ is the more general probability density distribution (Treloar, 1975b; Ward, 1971). Fig. 2.20c illustrates Eq. (2.23), which describes the probability that end Q (Fig. 2.20b) lies within a volumetric element between r and $r + \mathrm{d}r$ from the origin, highlighting the concentric shells considered with this approach, to produce a spherical distribution of chains with different end-to-end distances.

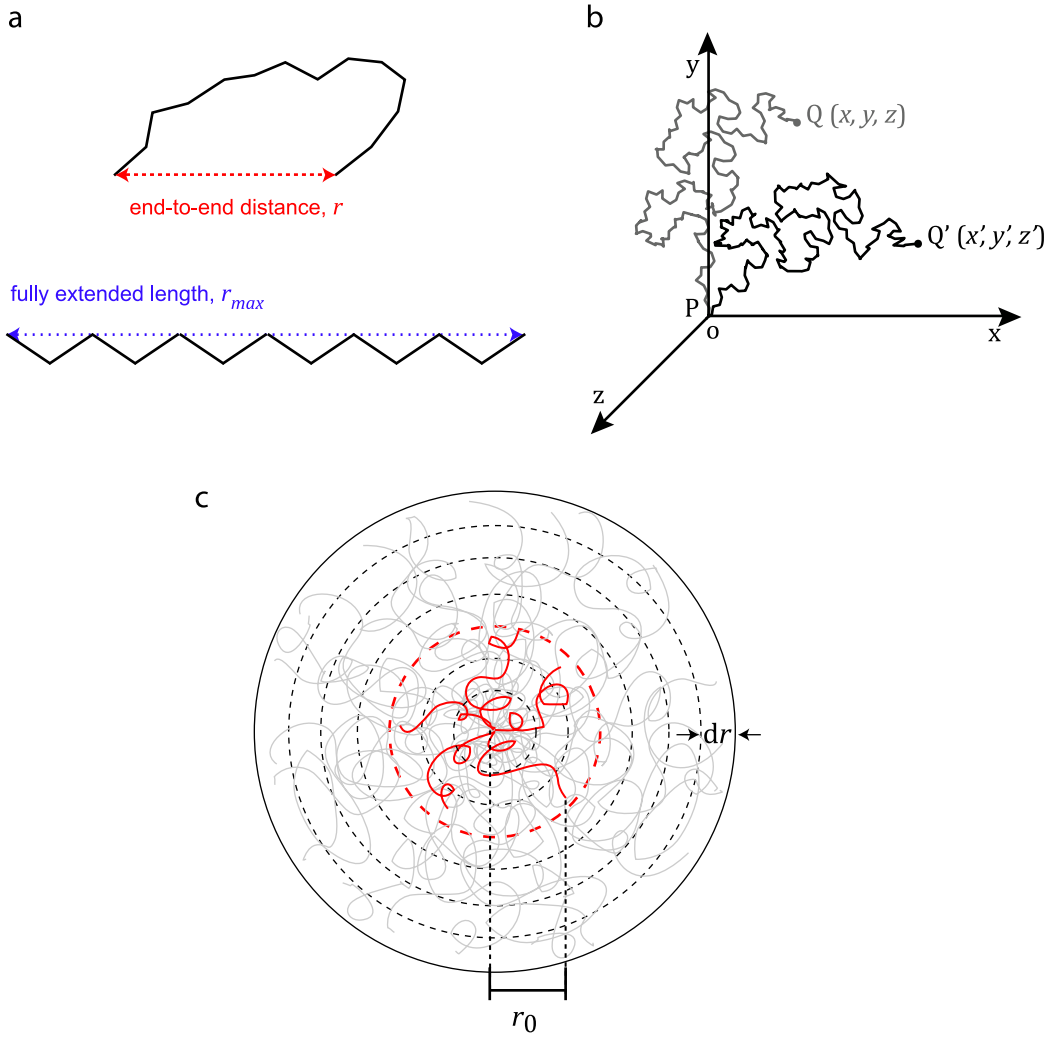

Fig. 2.20. (a) Each chain has both an end-to-end length, r, and a fully extended length, r_{max}. (b) Chains are assumed to have one end, P, fixed at the origin, o, with the other end Q displaced to Q′ during deformation. (c) A spherical distribution of polymer chains is considered, with the probability that end Q is situated within a volumetric element between r and $r + \mathrm{d}r$ from the origin described by Eq. (2.23). Infinitely small volumetric concentric shells can be considered, with each shell containing polymer chain ends to give an initial end-to-end length corresponding to that shell; the red shell and corresponding chains illustrate this concept.

The Gaussian distribution corresponds to the first term in Eq. (2.23) and is typically deemed sufficient provided n is large enough (typically $n > 100$) and $r \ll nl$. However, additional terms are needed for improved approximations, particularly in the case of short chains or for chains close to their limit of extensibility. Morovati et al. (2019) describe a method to obtain more refined approximations for the Langevin distribution. Nevertheless, the approximation given by Eq. (2.23) is deemed appropriate for this work, as investigated in Section 6.2.3.1.

An important property is the mean-square end-to-end distance of chains; this describes the most probable end-to-end distance for a polymer chain with parameters n_K and l_K and coincides with the peak of the end-to-end distance distribution. It may be calculated as follows:

$$\langle r^2 \rangle_0 = \int_0^\infty r^2 P(r) \mathrm{d}r \tag{2.24}$$

which approximates to $n_K l_K^2$ for long chains. Thus, for a chain containing $n_K = 100$ segments of unit length, the root-mean-square length is

$$r_{rms} \approx l_K \sqrt{n_K} = 10 \tag{2.25}$$

while $r_{max} = 100$, assuming no restriction on bond angles.

2.3.4 Change in entropy of the system

As mentioned, polymer chains are often described as “probability or entropy springs” because all chain configurations have approximately the same internal energy and it is instead the entropy primarily controlling the deformation. When subjected to an external force, chains, forced from their state of maximum entropy, extend in the direction of the force, reducing the entropy and resulting in a state of strain (Fig. 2.17). Here, the change in entropy on deformation is derived as detailed by Ward and Sweeney (2013).

The entropy of a single chain, s, is proportional to the logarithm of the number of configurations, Ω:

$$s = k \ln \Omega \tag{2.26}$$

where k is the Boltzmann constant. Provided $\mathrm{d}r$ is constant and in the case of a Gaussian distribution of freely jointed chains, which the Langevin distribution (Eq. (2.23)) reduces to for large n, the number of configurations available to a chain is proportional to the probability per unit volume, $p(r)$, giving

$$s = c - k\beta^2 r^2 = c - k\beta^2(x^2 + y^2 + z^2) \tag{2.27}$$

where $\beta^2 = 3/2nl^2$, $r^2 = x^2 + y^2 + z^2$ and c is a constant.

As stress is applied to the network, the entropy of a single freely jointed chain becomes

$$s' = c - k\beta^2(\lambda_x^2 x^2 + \lambda_y^2 y^2 + \lambda_z^2 z^2) \tag{2.28}$$

assuming affine deformation, i.e., components of the vector length of each chain are changed in the same ratio as the corresponding dimensions of the bulk material. The updated coordinates of $\mathrm{Q} \rightarrow \mathrm{Q}'$ (Fig. 2.20b) are given by $x' = \lambda_x x, y' = \lambda_y y, z' = \lambda_z z$, where $\lambda_x, \lambda_y, \lambda_z$ are the principal extension ratios chosen parallel to the x, y, z axes, respectively, without loss of generality (Section 2.2.2). Thus, the change in entropy for that chain is found to be

$$\Delta s = s' - s = -k\beta^2\left((\lambda_x^2 - 1)x^2 + \left(\lambda_y^2 - 1\right)y^2 + (\lambda_z^2 - 1)z^2\right) \tag{2.29}$$

For a network with N chains per unit volume with m having a given value of β, β_p, the entropy change for this group of chains is found by summing over the change in entropy for the m chains:

$$\Delta s_b = \sum_1^m \Delta s = -k\beta_p^2\left((\lambda_x^2 - 1)\sum_1^m x^2 + \left(\lambda_y^2 - 1\right)\sum_1^m y^2 + (\lambda_z^2 - 1)\sum_1^m z^2\right) \tag{2.30}$$

Assuming isotropy, with no preference for the x, y or z directions in the undeformed state, and using Eq. (2.25),

$$\sum_1^m x^2 = \sum_1^m y^2 = \sum_1^m z^2 = \frac{1}{3}\sum_1^m r^2 = \frac{1}{3}\,mr^2 = \frac{1}{3}m\left(\frac{3}{2\beta_p^2}\right) \tag{2.31}$$

Substituting Eq. (2.31) into (2.30) gives

$$\Delta s_b = -\frac{1}{2}mk\left(\lambda_x^2 + \lambda_y^2 + \lambda_z^2 - 3\right) \tag{2.32}$$

Adding the entropy contribution of all chains in the network in a similar way provides the change in entropy for the entire network, given by

$$\Delta S = \sum_{1}^{N} \Delta s = -\frac{1}{2} Nk\left(\lambda_x^2 + \lambda_y^2 + \lambda_z^2 - 3\right) \tag{2.33}$$

2.3.5 Resulting strain-energy potential

Following on from the previous section, the resulting strain energy potential of a Gaussian system is calculated following the techniques outlined by Ward and Sweeney (2013).

From the thermodynamic considerations detailed in Section 2.2.3, Eq. (2.12) related the change in work to the change in Helmholtz free energy, where an isothermal change of state was assumed: $\Delta W = \Delta A$. Returning to the first law of thermodynamics, $\Delta W = \Delta U - \Delta Q$, where U is internal energy and Q is the heat absorbed, and assuming no change in internal energy on deformation gives $\Delta A = -\Delta Q$. For a reversible process, the second law of thermodynamics relates ΔQ to the change in entropy: $\Delta Q = T\Delta S$, where T is temperature. Combining this with Eq. (2.33) offers a relationship between the change in entropy and the Helmholtz free energy as

$$\Delta A = -T\Delta S = \frac{1}{2} NkT\left(\lambda_x^2 + \lambda_y^2 + \lambda_z^2 - 3\right) \tag{2.34}$$

As mentioned previously, the Helmholtz free energy is associated with constant volume conditions. While this can be challenging to replicate experimentally, the molecular theories are typically derived using this assumption, and thus is the free energy considered throughout this work.

Provided the strain-energy function, U, is zero in the undeformed state,

$$U = \Delta A = \frac{1}{2} NkT\left(\lambda_x^2 + \lambda_y^2 + \lambda_z^2 - 3\right) \tag{2.35}$$

which is equivalent to the neo-Hookean relationship proposed by Rivlin (1948). This is the same relationship found in Eq. (2.13) when macroscopic deformations were considered, where $C_1 = \frac{1}{2} NkT$. While this captures the initial response to stress, polymer chains have a finite extensibility (which the affine assumption in this model fails to consider) and is typically accurate for strains less than 20%; see further details in Section 3.2.7.

For simple elongation λ in the x direction, where incompressibility is assumed ($\lambda_x\lambda_y\lambda_z = 1$), $\lambda_y = \lambda_z = \lambda^{-1/2}$. Substituting this into Eq. (2.35) gives

$$U = \frac{1}{2}NkT\left(\lambda^2 + \frac{2}{\lambda} - 3\right) \tag{2.36}$$

The resulting stress is again obtained using Eq. (2.11), with

$$\sigma_{xx} = \frac{\partial U}{\partial \lambda} = NkT\left(\lambda - \frac{1}{\lambda^2}\right) \tag{2.37}$$

as before.

Relating this to strain, $\lambda = 1 + \varepsilon_{xx}$ and in the case of small strain $\varepsilon_{xx}^2 \to 0$. Taking a Taylor series expansion

$$f(x) = f(a) + f'(a)(x-a) + \frac{f''(a)}{2!}(x-a)^2 + \cdots \tag{2.38}$$

where $f(x) = f(\varepsilon_{xx}) = \left(1 + \varepsilon_{xx} - \frac{1}{(1+\varepsilon_{xx})^2}\right)$ about the point $a = 0$ gives

$$\left(1 + \varepsilon_{xx} - \frac{1}{(1+\varepsilon_{xx})^2}\right) = 0 + 3(\varepsilon_{xx}) - 3(\varepsilon_{xx}^2) + \cdots \approx 3\varepsilon_{xx} \tag{2.39}$$

Combining Eq. (2.37) and Eq. (2.39),

$$\sigma_{xx} = 3NkT\varepsilon_{xx} = E\varepsilon_{xx} \tag{2.40}$$

giving the well-known Hooke's law for small strains, where stress and strain are directly proportional and where E is Young's modulus.

2.3.6 Modifications of the simple theory

A number of modifications to the above theory have been described, addressing some of the simplifying assumptions. Ward and Sweeney (2013) provide a discussion on some of the main theories, with a brief overview provided here. Much of the above (Eqs. (2.27)-(2.40)) assumed a Gaussian distribution of chain end-to-end distances; the Langevin distribution is considered more appropriate when $r \ll nl$ (James and Guth, 1943). Flory (1944) explored the effect of physical entanglements and chemical cross-links on the network behaviour. Chain approximations of various complexities exist, as discussed in Section 2.3.2, with those that consider effects from factors such as fixed bond angles or local interactions offering greater accuracy than the freely jointed chain idealisation (Mark, 2007). Consideration has

also been given to internal-energy contributions and strain-induced crystallisation and found to be increasingly relevant at large stretches (Ward and Sweeney, 2013). The theory has also been extended to consider the finite extensibility of chains within the system; further details of this are outlined in Section 3.2.7.

2.4 Numerical methods

2.4.1 Coefficient of determination

The coefficient of determination, typically denoted r^2, is used to compare predicted values, (x', y'), with experimentally reported values, (x, y), throughout this thesis. A description is provided by Devore (2016) and outlined here. A total least squares or orthogonal regression approach is taken rather than a linear least squares regression, with the former accounting for uncertainty in time points. Values of r^2 close to 1 indicate a good fit between both values. A perpendicular regression is considered with r^2 calculated as follows:

$$r^2 = 1 - \frac{SSE}{SST} \tag{2.41}$$

where SSE is the error of the sum of squares:

$$SSE = \sum_i \min((x' - x_i)^2 + (y' - y_i)^2) \tag{2.42}$$

and SST is the total sum of squares:

$$SST = \sum_i \left| y_i - \frac{1}{N} \sum_{i=1}^{N} y_i \right|^2 \tag{2.43}$$

SSE may be interpreted as a measure of how much variation in the data is left unexplained by the model, while SST describes deviations about the sample mean of the observed y values. The ratio SSE/SST is the proportion of total variation that cannot be explained by the model, and, finally, r^2 is the proportion of observed y variation explained by the model.

2.4.2 Runge-Kutta solver for ordinary differential equations

The ode45 solver in MATLAB® (R2019a, The MathWorks, Inc., MA, USA) is used to solve initial value problems for ordinary differential equations in Chapter 4. This in-built solver is based on an explicit Runge-Kutta (4,5) Dormand-Prince method and provides numerical solutions to such systems. Runge-Kutta methods are high-order methods that rely on evaluating $f(t, y)$ multiple times at each step, improving accuracy, resulting in a robust solution

method; alternative approaches are detailed by Chapra (2012). The Dormand-Prince method (Dormand and Prince, 1980) is outlined here.

The Dormand-Prince method is an adaptive Runge-Kutta method. Firstly, the fifth-order accurate solution is calculated; next, the fourth-order accurate solution is calculated; finally, the difference between these two solutions is determined and taken to be the error of the fourth-order solution. If the error is too high, a step is repeated with a lower step size; if the error is much smaller, the step size is increased to save time.

To begin, an initial value problem is defined, for example

$$\frac{dy}{dt} = f(t, y), \qquad y(t_0) = y_0 \tag{2.44}$$

where y is an unknown function of time t. For a step-size $\Delta t > 0$, the fifth-order approximation of y is defined by

$$y_{n+1} = y_n + \frac{35}{384}k_1 + \frac{500}{1113}k_3 + \frac{125}{192}k_4 - \frac{2187}{6784}k_5 + \frac{11}{84}k_6 \tag{2.45}$$

where

$$\begin{aligned}
k_1 &= \Delta t\, f(t_n, y_n) \\
k_2 &= \Delta t\, f\left(t_n + \frac{1}{5}\Delta t, y_n + \frac{1}{5}k_1\right) \\
k_3 &= \Delta t\, f\left(t_n + \frac{3}{10}\Delta t, y_n + \frac{3}{40}k_1 + \frac{9}{40}k_2\right) \\
k_4 &= \Delta t\, f\left(t_n + \frac{4}{5}\Delta t, y_n + \frac{44}{45}k_1 - \frac{56}{15}k_2 + \frac{32}{9}k_3\right) \\
k_5 &= \Delta t\, f\left(t_n + \frac{8}{9}\Delta t, y_n + \frac{19372}{6561}k_1 - \frac{25360}{2187}k_2 + \frac{64448}{6561}k_3 - \frac{212}{729}k_4\right) \\
k_6 &= \Delta t\, f\left(t_n + \Delta t, y_n + \frac{9017}{3168}k_1 - \frac{355}{33}k_2 + \frac{46732}{5247}k_3 + \frac{49}{176}k_4 \right. \\
&\qquad \left. - \frac{5103}{18656}k_5\right) \\
k_7 &= \Delta t\, f\left(t_n + \Delta t, y_n + \frac{35}{384}k_1 + \frac{500}{1113}k_3 + \frac{125}{192}k_4 - \frac{2187}{6784}k_5 + \frac{11}{84}k_6\right)
\end{aligned} \tag{2.46}$$

Here, y_{n+1} is the prediction of $y(t_{n+1} = t_n + \Delta t)$ and is estimated incrementally using y_n from the previous step. The fourth-order approximation is found using Eq. (2.46) as follows:

$$z_{n+1} = y_n + \frac{5179}{57600}k_1 + \frac{7571}{16695}k_3 + \frac{393}{640}k_4 - \frac{92097}{339200}k_5 + \frac{187}{2100}k_6 + \frac{1}{40}k_7 \tag{2.47}$$

The local error in the fourth-order formula is calculated as

$$e_{n+1} = |y_{n+1} - z_{n+1}| \tag{2.48}$$

which is $\mathcal{O}(\Delta t^5)$. If this error is too high (or much smaller than necessary), a new, optimal time-step is calculated as

$$\Delta t_{opt} = \left(\frac{\epsilon \Delta t}{2|y_{n+1} - z_{n+1}|}\right)^{1/5} \Delta t \tag{2.49}$$

where ϵ is the tolerance level.

2.4.3 Central difference operator for determining derivatives

The gradient function in MATLAB® (R2020b, The MathWorks, Inc., MA, USA) is used to calculate approximations of derivatives in Chapter 6. It is a central difference operator that calculates the central difference for interior data points. The central difference method is an explicit method that determines the value of the derivative at the centre of a time interval using the values at the ends of the interval (Belytschko et al., 2014).

To determine the gradient c of a vector a, for example, the gradient function is called as follows:

```
c=gradient(a,b)
```
(2.50)

where b is a uniform spacing between points. For a vector a, the interior gradient values are calculated as

$$c(i) = \frac{1}{2b}\big(a(i+1) - a(i-1)\big) \tag{2.51}$$

with $2 \leq i \leq N_a - 1$, where N_a is the length of a, while the exterior values are calculated as

$$c(1) = \frac{1}{b}\big(a(2) - a(1)\big) \tag{2.52}$$

$$c(N_a) = \frac{1}{b}\big(a(N_a) - a(N_a - 1)\big) \tag{2.53}$$

Calculating the numerical gradient in this way gives a good approximation of the derivative provided a suitable value of b is chosen.

2.5 Conclusion

This chapter provides an overview of theory for biodegradable polymers. The deformation of an elastic solid is summarised for the macroscopic level, while rubber-like elasticity theory is presented for the molecular level. Additionally, the numerical methods used are outlined. Overall, this chapter provides a broad overview of background and theory for the following chapters. Note that Chapters 3-6 contain additional background information that are directly relevant to the specific work presented therein.

The theory presented in Section 2.1, detailing polymer structure and degradation mechanism is particularly relevant for the model set-up in Chapter 4. To summarise the key points, biodegradable polymers contain many long macromolecular chains of varying lengths, resulting in a molecular weight distribution of chains. For the polymers considered in this thesis, when placed in an aqueous medium, hydrolysis causes chains to break; this may lead to a build-up of acid products that subsequently accelerate the degradation reaction.

As detailed in Section 2.1.2.2, experimental determination of the molecular weight distribution of polymer chains may have a degree of inaccuracy, particularly for very short chains; that is, very short polymer chains may be excluded from experimental molecular weight distributions, despite being present in the material. This is factored into the models presented in this thesis, both by (i) excluding short chains of varying lengths from the calculation of molecular weight in Chapter 4 and (ii) discussing how the presence of additional short chains that have not been experimentally reported may affect mechanical properties in Chapter 6.

Methods for modelling the statistical mechanics of polymeric chains, detailed in Section 2.3, are important when considering the evolution of mechanical properties and are relied on in Chapters 5 and 6.

References

Agrawal, C.M., McKinney, J.S., Lanctot, D.R., Athanasiou, K.A., 2000. Effects of fluid flow on the in vitro degradation kinetics of biodegradable scaffolds for tissue engineering. Biomaterials 21, 2443–2452. https://doi.org/10.1016/S0142-9612(00)00112-5

Alex, A., Ilango, N.K., Ghosh, P., 2018. Comparative Role of Chain Scission and Solvation in the Biodegradation of Polylactic Acid (PLA). J. Phys. Chem. B 122, 9516–9526.

https://doi.org/10.1021/acs.jpcb.8b07930
Allen, T.M., Cullis, P.R., 2004. Drug Delivery Systems: Entering the Mainstream. Science 303, 1818–1822. https://doi.org/10.1126/science.1095833
Batycky, R.P., Hanes, J., Langer, R., Edwards, D.A., 1997. A Theoretical Model of Erosion and Macromolecular Drug Release from Biodegrading Microspheres. J. Pharm. Sci. 86, 1464–1477. https://doi.org/10.1021/js9604117
Belytschko, T., Liu, W.K., Moran, B., Elkhodary, K.I., 2014. Nonlinear Finite Elements for Continua and Structures, 2nd ed. John Wiley & Sons Ltd.
Beslikas, T., Gigis, I., Goulios, V., Christoforides, J., Papageorgiou, G.Z., Bikiaris, D.N., 2011. Crystallization study and comparative in vitro-in vivo hydrolysis of PLA reinforcement ligament. Int. J. Mol. Sci. 12, 6597–6618. https://doi.org/10.3390/ijms12106597
Brant, D.A., Tonelli, A.E., Flory, P.J., 1969. The Configurational Statistics of Random Poly(lactic acid) Chains. II. Theory. Macromolecules 2, 228–235. https://doi.org/10.1021/ma60009a003
Buchanan, F.J. (Ed.), 2008. Degradation rate of bioresorbable materials: prediction and evaluation. Woodhead Publishing Limited/CRC Press LLC, Cambridge, England/Boca Raton, FL.
Callister Jr, W.D., Rethwisch, D.G., 2018. Materials Science and Engineering - An Introduction, 10th ed. John Wiley & Sons.
Chapra, S.C., 2012. Applied Numerical Methods with MATLAB for Engineers and Scientists, 3rd ed. McGraw-Hill, New York.
de Jong, S.J., Arias, E.R., Rijkers, D.T.S., van Nostrum, C.F., Kettenes-van den Bosch, J.J., Hennink, W.E., 2001. New insights into the hydrolytic degradation of poly(lactic acid): participation of the alcohol terminus. Polymer 42, 2795–2802. https://doi.org/10.1016/S0032-3861(00)00646-7
Deng, M., Zhou, J., Chen, G., Burkley, D., Xu, Y., Jamiolkowski, D., Barbolt, T., 2005. Effect of load and temperature on in vitro degradation of poly(glycolide-co-L-lactide) multifilament braids. Biomaterials 26, 4327–4336. https://doi.org/10.1016/j.biomaterials.2004.09.067
Deveney, K.E., Way, L.W., 1977. Effect of different absorbable sutures on healing of gastrointestinal anastomoses. Am. J. Surg. 133, 86–94. https://doi.org/10.1016/0002-9610(77)90199-4
Devore, J.L., 2016. Probability and Statistics for Engineering and the Sciences, 9th ed. Cengage Learning.
Ding, L., Davidchack, R.L., Pan, J., 2012. A molecular dynamics study of Young's modulus change of semi-crystalline polymers during degradation by chain scissions. J. Mech. Behav. Biomed. Mater. 5, 224–230. https://doi.org/10.1016/j.jmbbm.2011.09.002
Dormand, J.R., Prince, P.J., 1980. A family of embedded Runge-Kutta formulae. J. Comput. Appl. Math. 6, 19–26. https://doi.org/10.1016/0377-0427(86)90027-0
Durand, E., Lemitre, M., Couty, L., Sharkawi, T., Brasselet, C., Vert, M., Lafont, A., 2012. Adjusting a polymer formulation for an optimal bioresorbable stent: a 6-month follow-up study. EuroIntervention 8, 242–249. https://doi.org/10.4244/EIJV8I2A38
Duval, C., Rahouadj, R., Nouvel, C., Six, J.L., 2018. PLGA with less than 1 month of half-life time: Tensile properties in dry and wet states and hydrolytic degradation. Int. J. Polym. Mater. Polym. Biomater. 67, 509–516. https://doi.org/10.1080/00914037.2017.1354197
Fayolle, B., Audouin, L., Verdu, J., 2004. A critical molar mass separating the ductile and brittle regimes as revealed by thermal oxidation in polypropylene. Polymer 45, 4324–4330. https://doi.org/10.1016/j.polymer.2004.03.069
Fayolle, B., Colin, X., Audouin, L., Verdu, J., 2007. Mechanism of degradation induced embrittlement in polyethylene. Polym. Degrad. Stab. 92, 231–238. https://doi.org/10.1016/j.polymdegradstab.2006.11.012
Fetters, L.J., Lohse, D.J., Colby, R.H., 2007. Chain Dimensions and Entanglement Spacings, in: Mark, J.E. (Ed.), Physical Properties of Polymers Handbook. Springer, pp. 447–454.
Flory, P.J., 1944. Network structure and the elastic properties of vulcanized rubber. Chem. Rev. 35, 51–75. https://doi.org/10.1021/cr60110a002
Gardner, R.J., Martin, J.R., 1979. Humid aging of plastics: Effect of molecular weight on mechanical properties and fracture morphology of polycarbonate. J. Appl. Polym. Sci. 24, 1269–1280. https://doi.org/10.1002/app.1979.070240512
Ginjupalli, K., Shavi, G.V., Averineni, R.K., Bhat, M., Udupa, N., Nagaraja Upadhya, P., 2017. Poly(α-hydroxy acid) based polymers: A review on material and degradation aspects. Polym. Degrad. Stab. 144, 520–535. https://doi.org/10.1016/j.polymdegradstab.2017.08.024
Golden, J.H., Hammant, B.L., Hazell, E.A., 1964. Degradation of polycarbonates. IV. Effect of molecular

weight on flexural properties. J. Polym. Sci. Part A Gen. Pap. 2, 4787–4794. https://doi.org/10.1002/pol.1964.100021109

Grizzi, I., Garreau, H., Li, S., Vert, M., 1995. Hydrolytic degradation of devices based on poly(DL-lactic acid) size-dependence. Biomaterials 16, 305–311. https://doi.org/10.1016/0142-9612(95)93258-F

Helfer, C., Mattice, W., 2007. The Rotational Isomeric State Model, in: Mark, J.E. (Ed.), Physical Properties of Polymers Handbook. Springer, pp. 43–57.

Herrmann, J.B., Kelly, R.J., Higgins, G.A., 1970. Polyglycolic Acid Sutures: Laboratory and Clinical Evaluation of a New Absorbable Suture Material. Arch. Surg. 100, 486–490. https://doi.org/10.1001/archsurg.1970.01340220162027

Hertzberg, R.W., Vinci, R.P., Hertzberg, J.L., 2013. Deformation and Fracture Mechanics of Engineering Materials, 5th ed, Fatigue Design. John Wiley & Sons. https://doi.org/10.1016/b978-0-08-026167-6.50013-8

Hiljanen-Vainio, M., Karjalainen, T., Seppälä, J., 1996. Biodegradable Lactone Copolymers. I. Characterization and Mechanical Behavior of ε-Caprolactone and Lactide Copolymers. J. Appl. Polym. Sci. 59, 1281–1288. https://doi.org/10.1002/(sici)1097-4628(19960222)59:8<1281::aid-app11>3.3.co;2-e

James, H.M., Guth, E., 1943. Theory of the elastic properties of rubber. J. Chem. Phys. 11, 455–481. https://doi.org/10.1063/1.1723785

Jamshidian, M., Tehrany, E.A., Imran, M., Jacquot, M., Desobry, S., 2010. Poly-Lactic Acid: Production, applications, nanocomposites, and release studies. Compr. Rev. Food Sci. Food Saf. 9, 552–571. https://doi.org/10.1111/j.1541-4337.2010.00126.x

Karjalainen, T., Hiljanen-Vainio, M., Malin, M., Seppälä, J., 1996. Biodegradable Lactone Copolymers. III. Mechanical Properties of ε-Caprolactone and Lactide Copolymers After Hydrolysis in Vitro. J. Appl. Polym. Sci. 59, 1299–1304. https://doi.org/10.1002/(SICI)1097-4628(19960222)59:8<1299::AID-APP13>3.0.CO;2-1

Kuhn, W., 1934. Über die Gestalt fadenförmiger Moleküle in Lösungen. Kolloid-Zeitschrift 68, 2–15. https://doi.org/10.1007/BF01451681

Kuhn, W., Grün, F., 1946. Statistical behavior of the single chain molecule and its relation to the statistical behavior of assemblies consisting of many chain molecules. J. Polym. Sci. 1, 183–199. https://doi.org/10.1002/pol.1946.120010306

Laycock, B., Nikolić, M., Colwell, J.M., Gauthier, E., Halley, P., Bottle, S., George, G., 2017. Lifetime prediction of biodegradable polymers. Prog. Polym. Sci. 71, 144–189. https://doi.org/10.1016/j.progpolymsci.2017.02.004

Lesser, A.J., 2002. Fatigue behaviour of polymers. Encycl. Polym. Sci. Technol. https://doi.org/10.1002/0471440264.pst127

Li, S.M., Garreau, H., Vert, M., 1990a. Structure-property relationships in the case of the degradation of massive aliphatic poly-(α-hydroxy acids) in aqueous media - Part 1: Poly(DL-lactic acid). J. Mater. Sci. Mater. Med. 1, 123–130. https://doi.org/10.1007/BF00700871

Li, S.M., Garreau, H., Vert, M., 1990b. Structure-property relationships in the case of the degradation of massive poly(α-hydroxy acids) in aqueous media, Part 2: Degradation of lactide-glycolide copolymers: PLA37.5GA25 and PLA75GA25. J. Mater. Sci. Mater. Med. 1, 131–139. https://doi.org/10.1007/bf00700872

Love, A.E.H., 1944. A Treatise on the Mathematical Theory of Elasticity, 4th ed. Dover Publications, New York.

Malin, M., Hiljanen-Vainio, M., Karjalainen, T., Seppala, J., 1996. Biodegradable Lactone Copolymers. II. Hydrolytic Study of ε-Caprolactone and Lactide Copolymers. J. Appl. Polym. Sci. 59, 1289–1298. https://doi.org/10.1002/(SICI)1097-4628(19960222)59:8<1289::AID-APP12>3.0.CO;2-1

Malvern, 2019. Viscotek SEC-MALS 20 MRK1920-04-EN-00 [WWW Document]. URL https://www.malvernpanalytical.com/en/assets/MRK1920-04_tcm50-17235.pdf (accessed 2.23.21).

Mark, J.E. (Ed.), 2007. Physical Properties of Polymers Handbook, Second. ed. Springer. https://doi.org/10.1016/s0039-9140(97)80037-9

Mark, J.E., Erman, B., 2007. Rubberlike Elasticity: A Molecular Primer, 2nd ed. Cambridge University Press.

Martin, J.R., Johnson, J.F., Cooper, A.R., 1972. Mechanical Properties of Polymers: The Influence of Molecular Weight and Molecular Weight Distribution. J. Macromol. Sci. Part C 8, 57–199.

https://doi.org/10.1080/15321797208068169
McGinty, S., McKee, S., Wadsworth, R.M., McCormick, C., 2011. Modelling drug-eluting stents. Math. Med. Biol. 28, 1–29. https://doi.org/10.1093/imammb/dqq003
Merz, E.J., Nielsen, L.E., Buchdahl, R., 1951. Influence of Molecular Weight on the Properties of Polystyrene. Ind. Eng. Chem. 43, 1396–1401. https://doi.org/10.1021/ie50498a036
Middleton, J.C., Tipton, A.J., 2000. Synthetic biodegradable polymers as orthopedic devices. Biomaterials 21, 2335–2346. https://doi.org/10.1016/S0142-9612(00)00101-0
Moore, J.C., 1964. Gel Permeation Chromatography. I. A New Method for Molecular Weight Distribution of High Polymers. J. Polym. Sci. Part A 2, 835–843. https://doi.org/10.1002/pola.1996.842
Morovati, V., Mohammadi, H., Dargazany, R., 2019. A generalized approach to generate optimized approximations of the inverse Langevin function. Math. Mech. Solids 24, 2047–2059. https://doi.org/10.1177/1081286518811876
Nakafuku, C., Takehisa, S.Y., 2004. Glass transition and mechanical properties of PLLA and PDLLA-PGA copolymer blends. J. Appl. Polym. Sci. 93, 2164–2173. https://doi.org/10.1002/app.20687
O'Brien, F.J., 2011. Biomaterials & scaffolds for tissue engineering. Mater. Today 14, 88–95. https://doi.org/10.1016/S1369-7021(11)70058-X
Oberlerchner, J.T., Rosenau, T., Potthast, A., 2015. Overview of methods for the direct molar mass determination of cellulose. Molecules 20, 10313–10341. https://doi.org/10.3390/molecules200610313
Park, S.D., Todo, M., Arakawa, K., Koganemaru, M., 2006. Effect of crystallinity and loading-rate on mode I fracture behavior of poly(lactic acid). Polymer 47, 1357–1363. https://doi.org/10.1016/j.polymer.2005.12.046
Polak-Kraśna, K., Abaei, A.R., Shirazi, R.N., Parle, E., Carroll, O., Ronan, W., Vaughan, T.J., 2021. Physical and mechanical degradation behaviour of semi-crystalline PLLA for bioresorbable stent applications. J. Mech. Behav. Biomed. Mater. 118, 1–11. https://doi.org/10.1016/j.jmbbm.2021.104409
Reed, A.M., Gilding, D.K., 1981. Biodegradable polymers for use in surgery - poly(glycolic)/poly(lactic acid) homo and copolymers: 2. In vitro degradation. Polymer 22, 494–498. https://doi.org/10.1016/0032-3861(81)90168-3
Rehahn, M., Mattice, W., Suter, U., 1997. Rotational Isomeric State Models in Macromolecular Systems. Adv. Polym. Sci. 131-132/1, 485. https://doi.org/10.1007/BFb0050955
Rivlin, R.S., 1948. Large elastic deformations of isotropic materials. I. Fundamental concepts. Philos. Trans. R. Soc. London Ser. a-Mathematical Phys. Sci. 240, 459–508.
Schliecker, G., Schmidt, C., Fuchs, S., Kissel, T., 2003. Characterization of a homologous series of D,L-lactic acid oligomers; a mechanistic study on the degradation kinetics in vitro. Biomaterials 24, 3835–3844. https://doi.org/10.1016/S0142-9612(03)00243-6
Scholz, N., 2020. Organ donation and transplantation. Facts, figures and European Union action.
Shih, C., 1995. Chain-end scission in acid catalyzed hydrolysis of poly(D,L- lactide) in solution. J. Control. Release 34, 9–15. https://doi.org/10.1016/0168-3659(94)00100-9
Shirazi, R.N., Aldabbagh, F., Erxleben, A., Rochev, Y., McHugh, P., 2014. Nanomechanical properties of poly(lactic-co-glycolic) acid film during degradation. Acta Biomater. 10, 4695–4703. https://doi.org/10.1016/j.actbio.2014.08.004
Shirazi, R.N., Aldabbagh, F., Ronan, W., Erxleben, A., Rochev, Y., McHugh, P., 2016a. Effects of material thickness and processing method on poly(lactic-co-glycolic acid) degradation and mechanical performance. J. Mater. Sci. Mater. Med. 27, 1–12. https://doi.org/10.1007/s10856-016-5760-z
Shirazi, R.N., Ronan, W., Rochev, Y., McHugh, P., 2016b. Modelling the degradation and elastic properties of poly(lactic-co-glycolic acid) films and regular open-cell tissue engineering scaffolds. J. Mech. Behav. Biomed. Mater. 54, 48–59. https://doi.org/10.1016/j.jmbbm.2015.08.030
Skoog, D.A., Holler, F.J., Crouch, S.R., 2017. Separation Methods, in: Principles of Instrumental Analysis. Cengage Learning, pp. 746–781.
Sopik, V., 2021. International variation in breast cancer incidence and mortality in young women. Breast Cancer Res. Treat. 186, 497–507. https://doi.org/10.1007/s10549-020-06003-8
Thomas, D.P., Hagan, R.S., 1969. The Influence of Molecular Weight Distribution on Melt Viscosity, Melt Elasticity, Processing Behaviour and Properties of Polystyrene. Polym. Eng. Sci. 9, 164–171. https://doi.org/10.1002/pen.760090304
Thompson, D.E., Agrawal, C.M., Athanasiou, K.A., 1996. The Effects of Dynamic Compressive Loading

on Biodegradable Implants of 50-50% Polylactic Acid-Polyglycolic Acid. Tissue Eng. 2, 61–74. https://doi.org/10.1089/ten.1996.2.61

Tracy, M.A., Ward, K.L., Firouzabadian, L., Wang, Y., Dong, N., Qian, R., Zhang, Y., 1999. Factors affecting the degradation rate of poly(lactide-co-glycolide) microspheres in vivo and in vitro. Biomaterials 20, 1057–1062. https://doi.org/10.1016/S0142-9612(99)00002-2

Treloar, L.R.G., 1975a. Experimental examination of the statistical theory, in: The Physics of Rubber Elasticity. Clarendon Press, Oxford, pp. 80–100.

Treloar, L.R.G., 1975b. The Physics of Rubber Elasticity, 3rd ed. Clarendon Press, Oxford.

Tsuji, H., 2002. Autocatalytic hydrolysis of amorphous-made polylactides: effects of L-lactide content, tacticity, and enantiomeric polymer blending. Polymer 43, 1789–1796. https://doi.org/10.1016/S0032-3861(01)00752-2

Tsuji, H., Del Carpio, C.A., 2003. In vitro hydrolysis of blends from enantiomeric poly(lactide)s. 3. Homocrystallized and amorphous blend films. Biomacromolecules 4, 7–11. https://doi.org/10.1021/bm020090v

Venkatraman, S.S., Poh, T.L., Vinalia, T., Mak, K.H., Boey, F., 2003. Collapse pressures of biodegradable stents. Biomaterials 24, 2105–2111. https://doi.org/10.1016/S0142-9612(02)00640-3

Vert, M., 2009. Degradable and bioresorbable polymers in surgery and in pharmacology: beliefs and facts. J. Mater. Sci. Mater. Med. 20, 437–446. https://doi.org/10.1007/s10856-008-3581-4

Vey, E., Roger, C., Meehan, L., Booth, J., Claybourn, M., Miller, A.F., Saiani, A., 2008. Degradation mechanism of poly(lactic-co-glycolic) acid block copolymer cast films in phosphate buffer solution. Polym. Degrad. Stab. 93, 1869–1876. https://doi.org/10.1016/j.polymdegradstab.2008.07.018

Vieira, A.C., Vieira, J.C., Ferra, J.M., Magalhães, F.D., Guedes, R.M., Marques, A.T., 2011. Mechanical study of PLA–PCL fibers during in vitro degradation. J. Mech. Behav. Biomed. Mater. 451–460. https://doi.org/10.1016/j.jmbbm.2010.12.006

Vink, E.T.H., Rábago, K.R., Glassner, D.A., Gruber, P.R., 2003. Applications of life cycle assessment to NatureWorks™ polylactide (PLA) production. Polym. Degrad. Stab. 80, 403–419. https://doi.org/10.1016/S0141-3910(02)00372-5

Vo, T., Lee, W., Peddle, A., Meere, M., 2017. Modelling chemistry and biology after implantation of a drug-eluting stent. Part I: Drug transport. Math. Biosci. Eng. 14, 491–509. https://doi.org/10.3934/mbe.2017030

von Burkersroda, F., Schedl, L., Göpferich, A., 2002. Why degradable polymers undergo surface erosion or bulk erosion. Biomaterials 23, 4221–4231. https://doi.org/10.1016/S0142-9612(02)00170-9

Wang, M. (Ed.), 2020. Coronary Artery Disease: Therapeutics and Drug Discovery. Springer.

Wang, Y., Han, X., Pan, J., Sinka, C., 2010. An entropy spring model for the Young's modulus change of biodegradable polymers during biodegradation. J. Mech. Behav. Biomed. Mater. 3, 14–21. https://doi.org/10.1016/j.jmbbm.2009.02.003

Wang, Y., Rodriguez-Perez, M.A., Reis, R.L., Mano, J.F., 2005. Thermal and thermomechanical behaviour of polycaprolactone and starch/polycaprolactone blends for biomedical applications. Macromol. Mater. Eng. 290, 792–801. https://doi.org/10.1002/mame.200500003

Ward, I.M., 1971. Mechanical properties of solid polymers. Wiley-Interscience.

Ward, I.M., Hadley, D.W., 1993. An Introduction to the Mechanical Properties of Solid Polymers. John Wiley & Sons Ltd.

Ward, I.M., Sweeney, J., 2013. Mechanical properties of solid polymers, 3rd ed. John Wiley & Sons.

Ward, I.M., Sweeney, J., 2004. An Introduction to the Mechanical Properties of Solid Polymers, 2nd ed. John Wiley & Sons Ltd.

Weir, N.A., Buchanan, F.J., Orr, J.F., Dickson, G.R., 2004a. Degradation of poly-L-lactide. Part 1: In vitro and in vivo physiological temperature degradation. Proc. Inst. Mech. Eng. Part H J. Eng. Med. 218, 307–319. https://doi.org/10.1243/0954411041932782

Weir, N.A., Buchanan, F.J., Orr, J.F., Farrar, D.F., Dickson, G.R., 2004b. Degradation of poly-L-lactide. Part 2: Increased temperature accelerated degradation. Proc. Inst. Mech. Eng. Part H J. Eng. Med. 218, 321–330. https://doi.org/10.1243/0954411041932809

3 Literature review

To begin, the experimentally observed evolution of biodegradable polymers during degradation is reviewed in terms of (i) molecular weight, (ii) mechanical properties, and (iii) some limitations in sourcing suitable data for quantitative analysis with the models introduced in this thesis (Section 3.1). This is mainly restricted to amorphous polymers, as previously detailed; nevertheless, understanding of the amorphous phase of semi-crystalline polymers may also be obtained. The relationship between molecular weight and failure strain is explored, with 27 datasets across 9 publications considered as detailed in Table 3.1, which is central to Chapter 5. Table 3.2 provides an overview of various material and mechanical properties reported in a selection of studies. The inclusion criteria for experimental data considered in this thesis was hydrolytic experimental studies carried out on PLA, PGA, PCL, or their copolymers, in phosphate buffer solution.

A literature review of existing models for biodegradable polymers is presented in Section 3.2. Those that consider the evolution of molecular weight and mechanical properties are discussed separately before a chronology of many of the recent developments is offered (Table 3.4). This leads to an outline of a recent integrated model by Shirazi et al. (2016b), which couples a molecular weight model with a mechanical properties model and provides the starting point for Chapter 4 (Section 3.2.6). Section 3.2.7 considers the finite extensibility of polymer chains and gives attention to Stepto and Taylor's (1995a) implementation of such, which is the motivation for Chapter 6.

3.1 Experimentally observed evolution of polymer properties during degradation

As chains break due to the hydrolytic reaction, the polymer material transitions from having a high molecular weight to a low molecular weight (Li et al., 1990b; Tsuji, 2002). The evolution of mechanical properties has been seen to be largely dependent on this molecular weight degradation. Here, we discuss some of the typical changes observed in both molecular weight and mechanical properties during degradation.

3.1.1 Evolving molecular weight

Several experimental degradation studies on PLA and PLGA include the evolution of the molecular weight distributions (MWD), while others simply report an average molecular weight. An example of a typical evolving monomodal distribution is presented in Fig. 3.1a, showing the evolving MWD obtained by Vey et al. (2008) for amorphous PLGA 50:50 films (0.3 mm thickness, degraded in phosphate buffer solution at 37°C). A shift to the left was

observed, with distributions initially broadening and a gradual reduction in peak height before the opposite trend (taller and narrower distributions) was captured at later stages. The truncated tails in curves for Day 8.8 and onwards, denoted by the vertical dashed line, indicate that low molecular weight chains have either been removed through diffusion or that they are not accurately captured by the experimental technique used, size-exclusion chromatography. The initially monomodal distribution remained as such throughout degradation, indicative of bulk degradation.

Grizzi et al. (1995) demonstrated that the evolution of MWDs is dependent on the size of the sample, with polymer plates of thickness 2 mm producing bimodal MWDs as they underwent degradation (Fig. 3.1b), in contrast to the monomodal MWDs observed for films, microspheres and beads (with thicknesses of 0.3 mm, 0.125 – 0.250 mm, 0.5 – 1.0 mm, respectively). After 11 weeks degradation, the outer layer of the film appeared as a thin shell, about 0.2 mm thick, which surrounded a more degraded interior. Such heterogenous degradation is accredited to the build-up of degradation products within the medium, which further accelerate local degradation, i.e., autocatalysis. Most accelerative products may readily diffuse from the outer layer into the surrounding medium, reducing autocatalysis in that region.

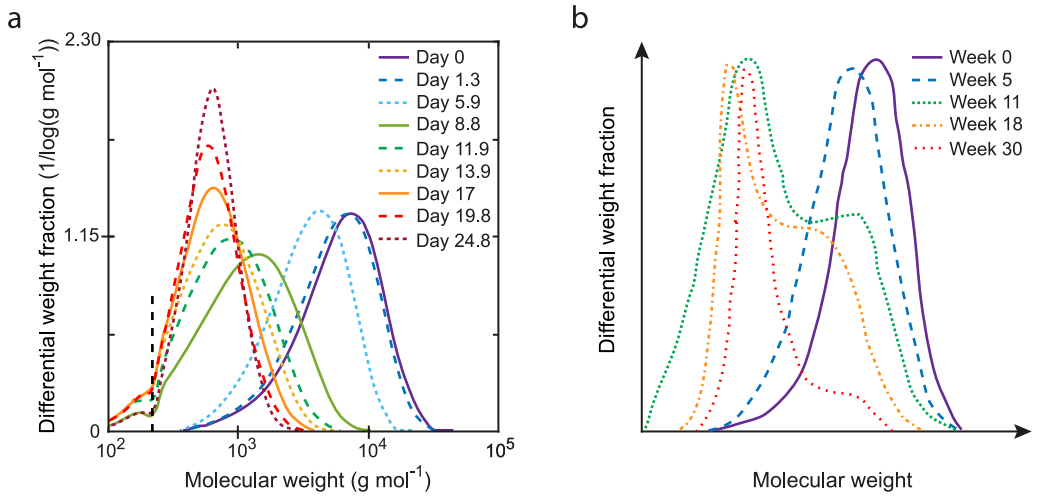

Fig. 3.1. Examples of evolving molecular weight distributions. (a) PLGA50:50 films (0.3 mm thickness) as degradation takes place. Adapted from Vey et al. (2008). The vertical dashed line draws attention to the truncated tails at low molecular weights. (b) PDLA plates (2 mm thickness) showing the formation of additional peaks during degradation, which are accredited to a more degraded inner due to a build-up of accelerative degradation products in that region. Adapted from Grizzi et al. (1995).

Tsuji and co-workers (2002; 2000; 2003) have carried out a number of experimental degradation studies on PLA with molecular weight characterization obtained using GPC,

providing evolving MWD. Initially amorphous films (thicknesses ranging from 0.025 – 0.15 mm) were found to remain monomodal throughout degradation, with similar trends observed to that of Vey et al. (2008) (Fig. 3.1a). In contrast, additional peaks were often seen in semi-crystalline polymers, similar to Fig. 3.1b, with low molecular weight peaks forming due to crystalline residues.

The reported evolution of the molar mass dispersity or width ($Đ_M = M_w/M_n$) of the distributions of these polymers has varied, as shown in Fig. 3.2 for amorphous polymers that all underwent hydrolysis under the same conditions (pH 7.4, 37°C). Shirazi et al. (2016a) reported no significant change in $Đ_M$ over the first 10 days of degradation for a solvent-cast PLGA film with thickness 0.25 mm (denoted SC250 in Fig. 3.2), with a gradual increase after that until it had doubled after 19 days. They found both size and processing technique affected this, with thinner (SC120, 0.12 mm thickness) and compression moulded (CM1000, 1 mm thickness) samples showing a more rapid increase in $Đ_M$. Although Ramchandani et al. (1997) observed an almost five-fold increase in $Đ_M$ during degradation for PLGA 85:15, it returned to its initial value at the end of the study (26 weeks). Tsuji (2002) reported no change in $Đ_M$ for PL/DLA after 24 months degradation, while the value tripled for PDLA after 16 months degradation. A constant $Đ_M$ indicates an equivalent decline in M_n and M_w, suggesting no preferential degradation of chains based on their length, with all bonds equally likely to experience scission. In contrast, an increase in $Đ_M$ is caused by an increased decline in M_n compared with M_w, suggesting a possible build-up of short chains in the material. Thus, knowledge of $Đ_M$ and its evolution can provide insight into the degradation pathways and indicate the presence of any preferential degradation at different stages.

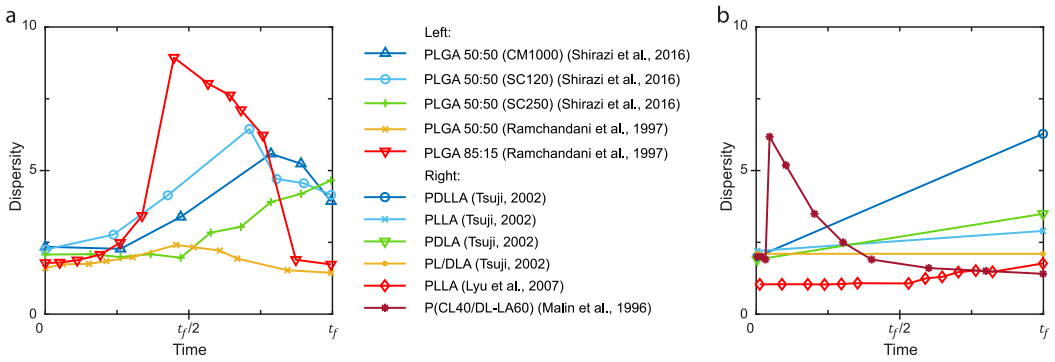

Fig. 3.2. Experimentally observed evolution of polymer molar mass dispersity, $Đ_M = M_w/M_n$, for polymers undergoing hydrolysis (pH 7.4, 37°C) for (a) PLGA (Ramchandani et al., 1997; Shirazi et al., 2016a) and (b) PLA (Lyu et al., 2007; Malin et al., 1996; Tsuji, 2002) with different copolymer ratios, processing techniques and thicknesses. The data are normalised on the x-axes, with the final time-point of degradation in each study taken as t_f.

On analysis of 31 sets of experimental data, Gleadall et al. (2014b) explored the various trends for the evolution of M_n and mass loss curves as a function of time. They interpreted the evolution of these curves by determining the degradation mechanisms necessary to produce such trends. While a deceleration on the molecular weight versus time curve indicates random scission with all bonds equally likely to undergo scission irrespective of their location in a chain, the absence of such suggests end scission. Additionally, an S-shaped curve, where there is an initial delay in the reduction of M_n, indicates autocatalytic behaviour, while a linear decrease in molecular weight with time suggests noncatalytic end scission. The shape of the M_n versus time curve is also influenced by the initial carboxylic acid end concentration, with an S-shaped curve for M_n indicative of a low value of the initial carboxylic acid end concentration and a more abrupt initial decline suggestive of an increased number of carboxylic acid ends available to catalyse the reaction (Antheunis et al., 2009; Göpferich, 1997). Fig. 3.3 shows some typical curves for M_n and suggests the degradation mechanisms behind them.

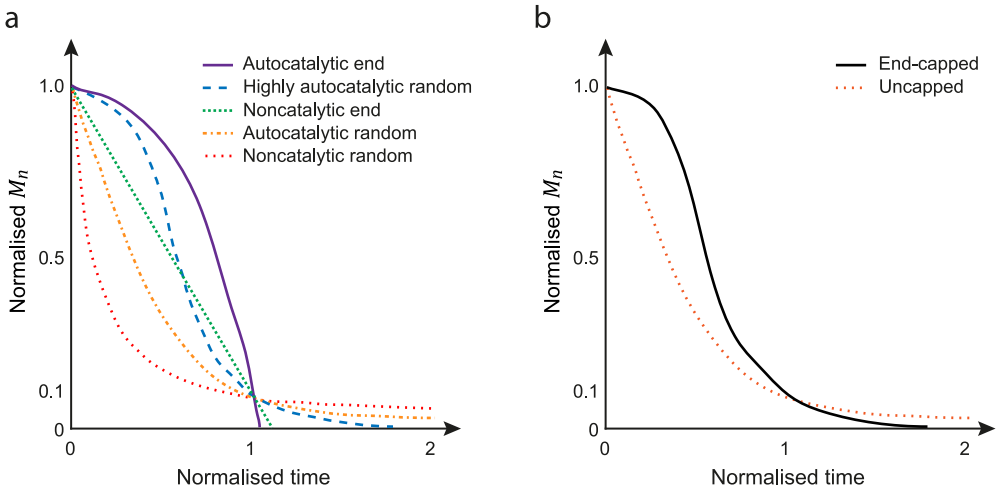

Fig. 3.3. (a) Typical forms of degradation, namely autocatalysis and noncatalytic hydrolysis via end and/or random scission, and their effect on the evolution of number average molecular weight, M_n, versus time. More abrupt declines are associated with random scission, while a linear decline suggests noncatalytic end scission. Adapted from Gleadall et al. (2014b). Time is normalised by the time taken for M_n to reach 10% of its initial value, while M_n is normalised by its initial value (as in the original figure). (b) A polymer with carboxylic acid end groups initially present (uncapped) produces a more abrupt decline in M_n compared with a system where the end groups are initially capped. Trends are adapted from Antheunis et al. (2009). Quantities are normalised as in (a).

3.1.2 Evolving mechanical properties of amorphous polymers

The evolution of mechanical properties of polymers during degradation has been seen to be largely dependent on the molecular weight degradation, as detailed in Section 2.1.4.

Extensive experimental studies have found that changes in the mechanical behaviour of the polymer as degradation proceeds can vary substantially between different polymer compositions. As mentioned above, we primarily consider amorphous polymers here; ultimately, the understanding obtained may be linked to the amorphous phase of semi-crystalline polymers.

3.1.2.1 Young's modulus

Tsuji (2002) carried out a degradation study on multiple forms of PLA created using the same processing techniques, which resulted in films with the same dimensions. Although the reduction in molecular weight followed similar trends for each of the samples, the resulting changes in mechanical properties did not follow a clear pathway (Fig. 3.4). The reduction in Young's modulus lags behind the decline in molecular weight, often losing less than 20% of the initial stiffness after 80% reduction in molecular weight. An increase in stiffness has previously typically been accredited to an increase in crystallinity during degradation; however, it was reported that all films were initially amorphous and remained so throughout that study. Tsuji and Suzuyoshi (2002) suggested that such an increase in stiffness for an amorphous polymer may be due to a more stable chain packing with the introduction of water molecules.

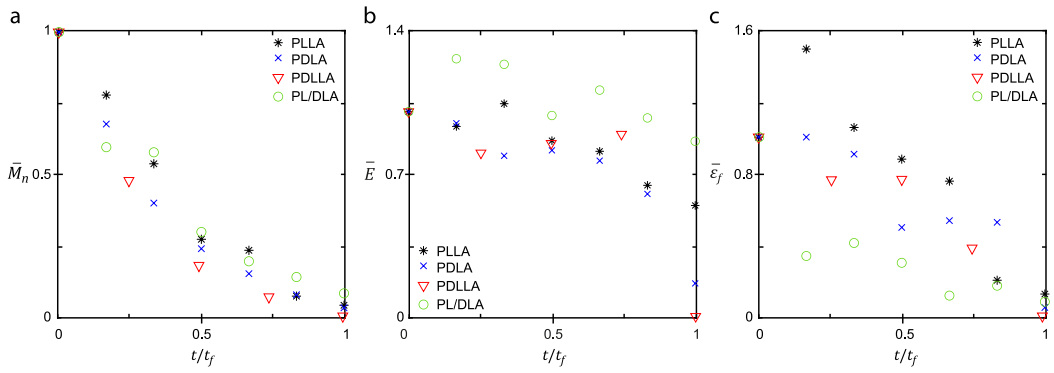

Fig. 3.4. Evolving (a) number average molecular weight, M_n, (b) Young's modulus, E, and (c) elongation at break, ε_f, for various PLA copolymers as reported by Tsuji (2002). M_n, E and ε_f are normalised by their initial values, while time is normalised by its final value.

Shirazi et al. (2016a, 2014) reported that although the molecular weight of degrading amorphous PLGA declines rapidly, the Young's modulus remained relatively constant until a significant number of polymer chains had been removed from the system, in agreement with the lag observed by Tsuji (2002).

Gleadall (2015) analysed 21 sets of experimental data for the degradation of PLA in the context of the relationship between average molecular weight and Young's modulus. The

data used corresponds to a wide range of experimental conditions, encompassing various sample sizes, temperatures, measurement techniques, and processing conditions, with both amorphous and semi-crystalline polymers considered. Although erratic behaviour was typically seen, with increases, decreases and abrupt declines to zero observed, it was found that they demonstrated a similar gradient for a linear relationship between the reduction in Young's modulus, E (GPa), and logarithm of number average molecular weight, M_n (g mol^{-1}). The following general trend was extracted:

$$E = E_0 + k_m \log_{10} \frac{M_n}{M_{n0}} \tag{3.1}$$

where E_0 (GPa) and M_{n0} (g mol^{-1}) are the initial Young's modulus and number average molecular weight, respectively, and k_m (GPa) is the degradation rate constant for Young's modulus, determined to be 1.4 GPa. Eq. (3.1) provides insight into the general relationship typically observed experimentally between Young's modulus and molecular weight, suggesting that a reduction in M_n by a factor of ten results in Young's modulus reducing by 1.4 GPa. However, a physical understanding of this relationship was not obtained.

3.1.2.2 Ductility

As degradation proceeds, large declines in ductility have been observed. As detailed in Section 2.1.4, a reduction in molecular weight may be responsible for the transition from ductile to brittle behaviour (Fig. 2.12c, (Venkatraman et al., 2003)). On inspection of PLA-PCL (90:10) suture fibres during degradation (pH 8, 37°C), Vieira et al. (2011) obtained evolving stress-strain curves over the first 16 weeks, reproduced in Fig. 3.5. Despite a glass transition temperature of $T_g = 56$°C, the material became brittle only after 16 weeks. Both the axial stress and failure strain exhibited changes over this degradation period, while the slope in the linear elastic region remained almost constant, again indicating a delay in the decline of Young's modulus. The abrupt change between Week 8 and 16 coincides with a reduction in number average molecular weight, M_n, from approximately 45% to 25% of the initial value and a change in mass loss from approximately 4% to 10%. Despite the increased mass loss, likely caused by the removal of short oligomeric chains, a substantial decline in M_n was still observed, suggesting a larger number of short chains were introduced via chain scission, indicative of accelerated degradation. The increased presence of short chains may explain the rapid decline in ε_f, with those chains quickly reaching full extension as the material is strained and resisting further deformation.

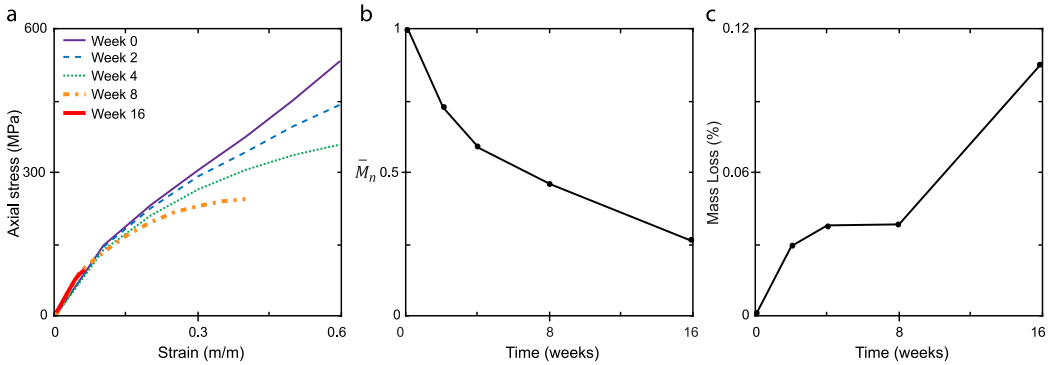

Fig. 3.5. Experimentally observed evolution of (a) stress-strain curves, (b) number average molecular weight (normalised by initial value), $\overline{M_n}$, and (c) mass loss for PLA-PCL (90:10) suture fibres. Adapted from Vieira et al. (2011).

In the study carried out by Tsuji (2002) on amorphous polymers (see overview in Section 3.1.2.1), PLLA saw a substantial increase in ductility as degradation proceeded, while the elongation at break of PL/DLA declined rapidly (Fig. 3.4). Both the copolymer (PDLLA, $\varepsilon_{f0} = 21.0\%$) and the polymer blend (PL/DLA, $\varepsilon_{f0} = 14.5\%$) demonstrated larger initial values of elongation at break compared with the homopolymers (PLLA, $\varepsilon_{f0} = 6.5\%$ and PDLA, $\varepsilon_{f0} = 5.3\%$) (Fig. 3.6a). At the next observation point, the elongation at break of both the copolymer and polymer blend had decreased, while both homopolymers showed increases, although to a lesser extent for PDLA. Nevertheless, this may suggest that different mechanisms are at play for homopolymers and heteropolymers. It should also be noted that large error margins were reported in this study, most remarkably for elongation at break, with error margins of >50% reported in some instances.

With minimal variances in the study of Tsuji (2002) between the four polymer types, the relationship between evolving ε_f and M_n is explored (Fig. 3.6b-c). When absolute values are considered (Fig. 3.6b), PLLA, PDLA and PL/DLA appear to follow a similar pathway after variances in initial values of ε_f and M_n. In contrast, when both properties are normalised by their respective initial values, different relationships are evident (Fig. 3.6c). In that case, two trends emerge: (i) PLLA, PDLA and PDLLA experience a lagged reduction in ε_f, with minimal decline until M_n has reduced by >50%; and (ii) the polymer blend, PL/DLA, experiences a more rapid decline, no longer appearing to exhibit similar behaviour to the homopolymers. The factors contributing to these two trends should be further explored in the context of a wider set of experimental data to investigate the underlying causes.

To further explore the relationship between ε_f and M_n, a larger dataset is examined. Focusing solely on PLA and copolymers, 27 datasets from 9 publications that measured the

evolution of molecular weight and mechanical properties during degradation are considered, restricted to those carried out in PBS (Deng et al., 2005; Duek et al., 1999; Kranz et al., 2000; Polak-Kraśna et al., 2021; Tsuji, 2002; Tsuji et al., 2000; Tsuji and Del Carpio, 2003; Weir et al., 2004a, 2004b). This restriction was imposed due to PBS regularly being used as a hydrolytic control that helps maintain pH during testing (Woodard and Grunlan, 2018). The ASTM standard (F1635) for in vitro degradation for surgical implants recommends a solution-to-specimen mass ratio of greater than 30:1 to provide adequate buffer capacity ("ASTM F1635-16, Standard Test Method for in vitro Degradation Testing of Hydrolytically Degradable Polymer Resins and Fabricated Forms for Surgical Implants," 2016). Most studies considered here do not report following a particular standard; this limits the strength of the comparison between different studies, with experimental procedures possibly impacting the behaviour observed. For example, frequency of medium replacement or stirring the samples would impact fluid flow, and static testing has previously shown increased rates of degradation compared with samples tested under fluid flow (Agrawal et al., 2000).

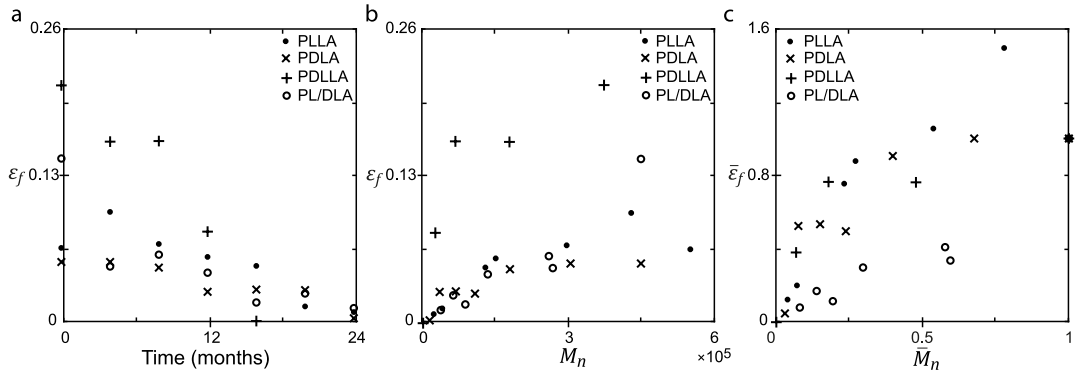

Fig. 3.6. Experimental degradation data adapted from Tsuji (2002) for amorphous PLA. (a) Evolving elongation at break, ε_f ($\varepsilon_f = \frac{L_f - L_0}{L_0}$, where L_f is the final length and L_0 is the initial length of the sample tested). Various trends emerge, ranging from an initial increase (PLLA) to a rapid decline (PL/DLA). For PDLLA, $\varepsilon_f = 0$ after 16 months degradation, while for the other three polymers, $\varepsilon_f \to 0$ after 24 months degradation. (b) Relationship between ε_f and number average molecular weight, M_n (g/mol). PLLA, PDLA and PL/DLA appear to follow a similar pathway after variances in initial values of ε_f and M_n. (c) Alternative version of (b), where both properties are normalised by their respective initial values. Two trends emerge: (i) PLLA, PDLA and PDLLA experience a lagged reduction in ε_f, with minimal decline until M_n has reduced by >50%; (ii) the polymer blend, PL/DLA, experiences a more rapid decline.

Several variances exist in the studies considered, encompassing polymers which are either amorphous or crystalline, prepared using different techniques, having varying geometries, and tested with different equipment, with details outlined in Table 3.1. While some of these studies reported both M_n and M_w, others restricted their focus to one of those. Absolute

data is presented in Fig. 3.7a, while both properties have been normalised by their respective initial values in Fig. 3.7b. Focusing first on the absolute data, it is challenging to determine a unique relationship between these properties due to the large variance in initial values. The normalised data also spans a wide range; while often a lag in the decline in ε_f was evident, other data suggested an immediate exponential decline. Separating the data based on these two observations, two trends emerge: (i) Trend 1 typically experiences no decline in ductility initially (or even increases), with a lagged decline compared with the reduction in MW (Fig. 3.7c); while (ii) for Trend 2, ε_f has declined by >50% with a 20% reduction in average molecular weight, MW, and no initial increase in ε_f was observed (Fig. 3.7d).

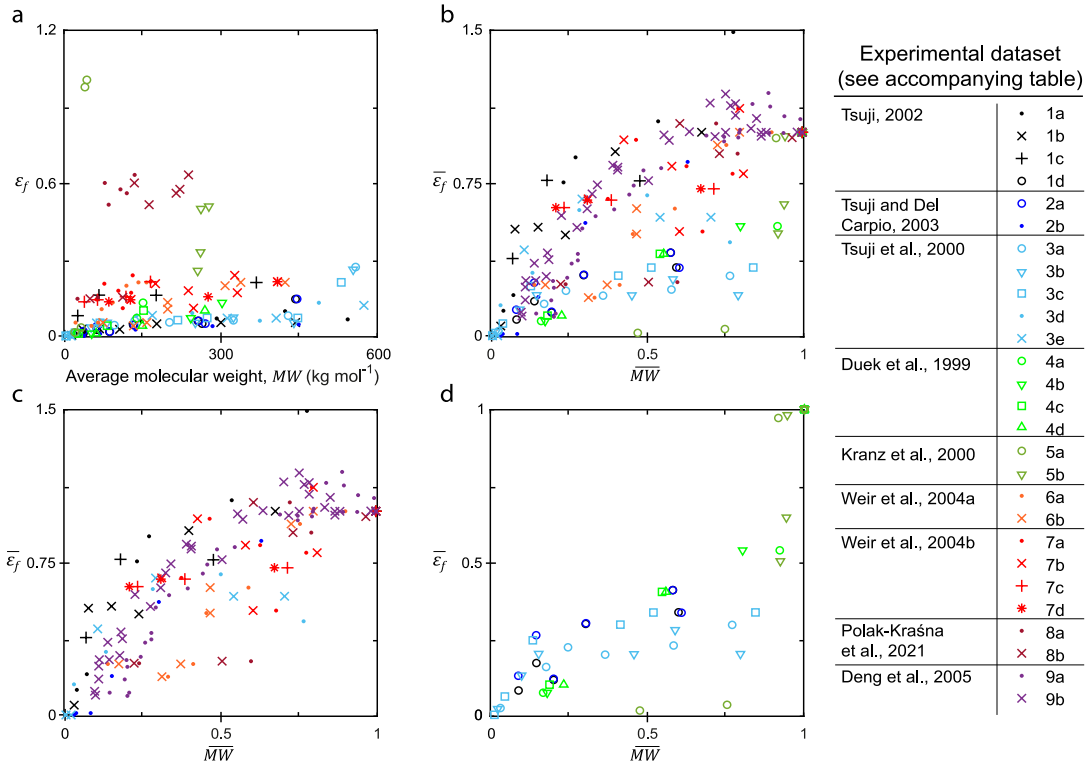

Fig. 3.7. Experimental datasets reproduced from literature (Deng et al., 2005; Duek et al., 1999; Kranz et al., 2000; Polak-Kraśna et al., 2021; Tsuji, 2002; Tsuji et al., 2000; Tsuji and Del Carpio, 2003; Weir et al., 2004a, 2004b) showing the relationship between elongation at break, ε_f, and average molecular weight, MW. Details on each dataset are given in Table 3.1. Each unique colour corresponds to a different publication. (a) Absolute data for publications 1 – 8 covers a wide range, with large variances in initial values of both properties. Differences between M_n and M_w data are not evident. (b) Normalised data for all 9 publications, where both properties are normalised by their initial values. No single trend emerges. (c) Normalised data for a subset of the overall datasets where a lag in the decline of ε_f is observed, subsequently referred to as Trend 1. (d) The remaining normalised datasets not shown in (c), where ε_f has declined by >50% with a 20% reduction in MW (Trend 2). Closed symbols correspond to Trend 1, while open symbols represent datasets following Trend 2.

To understand what may contribute to these differing trends, Table 3.1 indicates many features of the polymers considered. Interestingly, many of the features present spanned both trends. Most surprisingly may be the lack of distinction between amorphous and semi-crystalline materials. It has typically been accepted that when the polymer undergoes loading, chains in amorphous regions unwind and adopt extended configurations, allowing for relatively large, typically reversible deformations, while in contrast, the rigid structure exhibited by crystalline regions prevents those regions from responding in the same way. Despite this, instances of both polymer types were seen to follow both identified trends. While glass transition temperature also plays a role in the loading response, little variance is expected for the polymers considered here. Based on the data provided in each of the experimental studies considered, no distinction could be made between trends.

3.1.3 Limitations of experimental data for amorphous polymers

A single comprehensive set of experimental data is desirable for each unique polymer studied for validation of models to limit the effect of experimental conditions on the results. For example, Shirazi et al. (2014) performed a degradation study on amorphous PLGA (50:50), providing important insight into the evolution of the molecular weight distributions and associated averages, weight loss, and Young's modulus. However, additional mechanical properties, such as yield stress and failure strain, were not reported. In contrast, Renouf-Glauser et al. (2005) provide tensile test results for amorphous PLLA in the form of load-displacement curves. However, only two time points were considered, and molecular weight distributions were not provided, with only average values reported. Table 3.2 outlines relevant quantities reported in a sample of 25 experimental studies where the effect of hydrolytic degradation on biodegradable materials was explored in phosphate buffer solution at 37°C.

To calibrate a model for a specific polymer, not only is knowledge of the evolution of material and mechanical properties via experimental studies relevant, but information on initial properties is also important. For example, polymer materials can be supplied with different end group functionalities, often either carboxylic acid end groups (uncapped) or ester terminated groups (capped). This can impact degradation behaviour, with uncapped PLGA degrading at an increased rate due to carboxylic acid end groups causing the polymer to be more hydrophilic while also allowing for increased autocatalysis (Houchin and Topp, 2008). Residual monomers as degradation initiates can also affect the degradation rate due to their increased mobility and contribution to autocatalysis (Gleadall et al., 2014a). Reports of

Table 3.1. Datasets used to explore the relationship between MW and ε_f. Details on each dataset are given based on that provided in literature, indicating the corresponding publication (Ref.), identification number and symbol assigned in this thesis (ID), polymer type, trend observed in the relationship between ε_f and MW (Fig. 3.7), polymer structure (homopolymer (H), copolymer (C), or polymer blend (B), and amorphous (Am.) or semi-crystalline (SC)), average molecular weight, MW, provided in experimental study (number, M_n, or weight average, M_w) and the corresponding initial value ($\times 10^5$ g/mol), testing temperature, sample geometry, and methods of preparation, degradation protocol, molecular weight determination and mechanical properties testing. Where information is unknown, the cell is unfilled.

Ref.	ID	Polymer	Trend	Structure		MW	MW_0	Temp.	Geometry	Preparation	Degradation protocol	MW det.	Mechanical properties test method
(Tsuji, 2002)	• 1a	PLLA	1	H	Am.	M_n	3.7	37°C	Films – 3 mm x 30 mm x 50-150 μm	Solvent-cast – evaporation at room temperature for ~1 day. Films dried in vacuum for 1 week.	10mL PBS (pH 7.4±0.1) containing 0.02 wt% sodium azide exchanging buffered solution once a month.	GPC	Washed and dried under reduced pressure for >2 weeks. Measured at 25°C using a tensile tester at a crosshead speed of 100%/min (20 mm/min). Gauge length: 20 mm.
	× 1b	PDLA	1	H			4.4						
	+ 1c	PDLLA	1	C			5.4						
	o 1d	PL/DLA	2	B			4.4						
(Tsuji and Del Carpio, 2003)	o 2a	PL/DLA	2	B	Am.	M_n	4.4	37°C	As above	As above.	As above.	GPC	As above.
	• 2b		1		SC		4.5						
(Tsuji et al., 2000)	o 3a	PLLA	2	H	SC	M_n	5.4	37°C	Films – 18 mm x 30 mm x 50 μm	PLLA films melted at 200°C for 3 min and annealed at 140°C for (3a) 0, (3b) 15, (3c) 30, (3d) 45, (3e) 60 min prior to being quenched at 0°C.	As above; 0.15M PBS.	GPC	As above.
	▽ 3b		2				5.5						
	□ 3c		2				5.1						
	• 3d		1				5.0						
	× 3e		1				5.8						
(Duek et al., 1999)	o 4a	PLLA	2	H	Am.	M_n	1.5	38°C	Rods – 30mm x 3mm	Injection-moulded (190°C) and quenched (20°C).	Samples sterilized with ethylene oxide and immersed in tubes containing PBS (pH 7.4) in a thermally- controlled bath.	GPC	Three-point bending of a 19 mm segment were made at 15°C using an MTS-810.
	▽ 4b		2		→ SC	M_w	3.0						
	□ 4c		2		SC	M_n	1.5		Rods – 30mm x 2mm	Injection-moulded (190°C); cooled at room temperature for 30 min.			
	△ 4d		2			M_w	2.7						
(Kranz et al., 2000)	o 5a	PDLLGA	2	C	-	M_w	2.7	37°C	Films – 40 mm x 40 mm x 100 μm	Solvent-cast – dried for 12h at room temperature and for 12h at 40°C.	200 mL of PBS (pH 7.4).	SEC	Instron 4466, 500 N load, 10 mm/min, wet condition.
	▽ 5b	PDLLA	2				0.57						
(Weir et al., 2004a)	• 6a	PLLA	1	H	SC	M_n	1.6	37°C	Plates (0.8mm thick) – type V tensile samples	Compression moulded and annealed at 120°C for 4 hours.	28 ml screw-top glass bottles, fully immersed in PBS (pH 7.4 – monitored throughout) (ISO 15814:1999). Placed in air circulating oven. PBS (mm):polymer mass (g) > 30:1.	GPC	JJ Lloyd EZ 50 tensile testing machine equipped with a 1 kN load cell and tested at 10 mm/min while wet. Gauge length: 7.62 mm.
	× 6b		1			M_w	4.2						
(Weir et al., 2004b)	• 7a	PLLA	1	H	SC	M_n	1.7	50°C	As above	As above.		GPC	
	× 7b		1			M_w	4.1						
	+ 7c		1			M_n	1.7	70°C					
	* 7d		1			M_w	4.1						
(Polak-Kraśna et al., 2021)	• 8a	PLLA	1	H	SC	M_n	0.98	50°C	1.5 mm diameter tubes cut into curved dog-bones for mechanical testing	Pre-processed.	PBS (pH 7.4±0.2) changed every 3-4 weeks to maintain pH.	GPC	Zwick mechanical test machine with 100 N load cell tested at 10 mm/min while wet. Gauge length: 5mm.
	× 8b		1			M_w	2.2						
(Deng et al., 2005)	• 9a	PLLGA	1	C	SC	M_n	0.19	27.5 – 47.5°C	Multifilament braids, diameter: 0.304 mm	Pre-processed.	0.1M PBS (pH 7.4) changed at least once a week.	GPC	Instron 4501, 500-N load at 127 mm/min. Room temperature, wet. Gauge length: 80mm.
	× 9b		1			M_w	0.57						

Table 3.2. Details of various material and mechanical properties reported in a selection of hydrolytic experimental studies carried out in phosphate buffer solution at 37°C.

Ref.	Material	MWD	M_n, M_w v. t	E v. t	σ v. ε	σ_y v. t	σ_{max} v. t	ε_f v. t	Mass loss v. t	Water uptake v t	Amorphous
(Shirazi et al., 2014)	PLGA (50:50)	Y	Y – M_n	Y	N	N	N	N	Y	Y	Y
(Shirazi et al., 2016a)	PLGA (50:50)	N	Y	Y	N	N	N	N	Y	Y	Y
(Grizzi et al., 1995)	PDLA	Y	Y – M_w	N	N	N	N	N	Y	Y	Y
(Vey et al., 2008)	PLGA (50:50)	Y	Y – M_n	N	N	N	N	N	Y	Y	Y
(Lyu et al., 2007)	PLA	N	Y	N	N	N	N	N	Y	Y	Y
(Li et al., 1990b, 1990a)	PLGA, PLA	Y	Y	N	N	N	N	N	Y	Y	Y
(Ramchandani et al., 1997)	PLGA	Y	Y	N	N	N	N	N	Y	N	Y
(Renouf-Glauser et al., 2005)	PLLA	N	Y	Y	Y	Y	Y	Y	N	N	Y
(Hiljanen-Vainio et al., 1996; Karjalainen et al., 1996; Malin et al., 1996)	P(CL40/DL-LA60)	Y	Y	Initial	Initial	Initial	Initial	N	Y	Y	Y
	P(CL40/L-LA60)	N	Y	Y	Initial	Y	Initial	Initial	Y	Y	Initially
	PL(CL60/L-LA40)	N	Y – M_w	Y	Y	Y	Y	Y	Y	Y	Initially
(Tsuji and Del Carpio, 2003)	PLLA, PDLA	Y	Y – M_n	N	N	N	Y	Y	Y	N	Y
(Tsuji, 2002)	PLA	Y	Y – M_n	Y	N	N	Y	Y	Y	N	Y
(Duval et al., 2018)	PLGA (50:50)	N	N	N	Y	Y	N	Y	Y	N	Y
(Phong et al., 2010)	PLGA (80:20)	N	N	Y	N	Y	N	N	Y	Y	Y
(Breche et al., 2016)	PLA-b-PEG-b-PLA	N	Y	N	Y	N	Y	N	Y	N	Y
(Kranz et al., 2000)	PDLA, PLGA	N	Y – M_w	N	N	N	Y	Y	Y	Y	?
(Luo et al., 2014)	PLLA stent	N	Y	Y	Y	N	N	Y	N	N	?
(Mainil-Varlet et al., 1997)	PLA	Y	Y	Y	N	N	Y	N	N	N	N
(Weir et al., 2004a)	PLLA	Y	Y	Y	N	N	Y	Y	Y	N	N
(Vieira et al., 2011)	PLA-PCL	N	Y – M_n	N	Y	N	Y	N	Y	N	N
(Limbert et al., 2016)	DegraPol® DP30	N	Y – M_w	Y	Y	N	Y	Y	N	N	N
(Farrar and Gillson, 2002)	Polyglyconate B	N	Y	N	N	Y	Y	Y	Y	N	N
(Venkatraman et al., 2003)	PLLA stent	N	Y – M_w	Y	Initial	N	Y	N	N	N	N

oligomer length varies from 3-34 units (Kasperczyk et al., 2008; Vey et al., 2008), while the sensitivity of the equipment used to measure the molecular weight can impact the level of oligomers experimentally observed, influencing the reported molecular weight distribution (see Section 2.1.2.2). With the number average molecular weight emphasizing shorter chains, experimental determination of the chain lengths that this becomes relevant for will allow this to be factored into theoretical calculations. Typically, information on the polymer end group, residual monomer concentration, and oligomer length are not reported in experimental studies. Without these, determining reaction rates or the impact of these on degradation is more challenging and may result in less optimal parameter calibrations.

3.2 Modelling techniques for biodegradable polymers

Farrar (2008) outlined four stages of degradation as follows:

1. Diffusion of water into the polymer
2. Hydrolysis of the polymer chains and reduction in molecular weight
3. Reduction in mechanical properties and changes in other physical properties such as crystallinity and glass transition temperature
4. Production of water-soluble oligomers and mass loss

Although these processes can all occur simultaneously, they typically proceed in the order listed and at increasing timescales. Fig. 3.8 indicates the processes involved in hydrolytic degradation and the relationships between them. Because of the complex overlap that they can exhibit, it is unsurprising that many existing models primarily focus on one stage in isolation. While this assists in providing an understanding of the specific stage studied, it is ultimately necessary to consider the processes simultaneously to fully understand the behaviour.

Numerous modelling techniques have been employed to predict the evolution of polymer properties during degradation. The scale of interest often dictates the techniques used. For example, molecular dynamics models have been used to study the polymer at the nanoscale, while finite element modelling can predict the degradation of polymers in specific applications, taking geometry into account. Both phenomenological and physicochemical models have been utilised, with the former describing an empirical relationship between phenomena and the latter focusing on the physical and chemical behaviour that takes place. While some models predict changes in material properties such as molecular weight or weight loss, others are concerned with changes in mechanical properties. For a more

rigorous model that predicts a multitude of polymer behaviour at different scales, various modelling techniques are often used in conjunction with each other. Table 3.3 provides an overview of some existing models, which are expanded on in the following subsections.

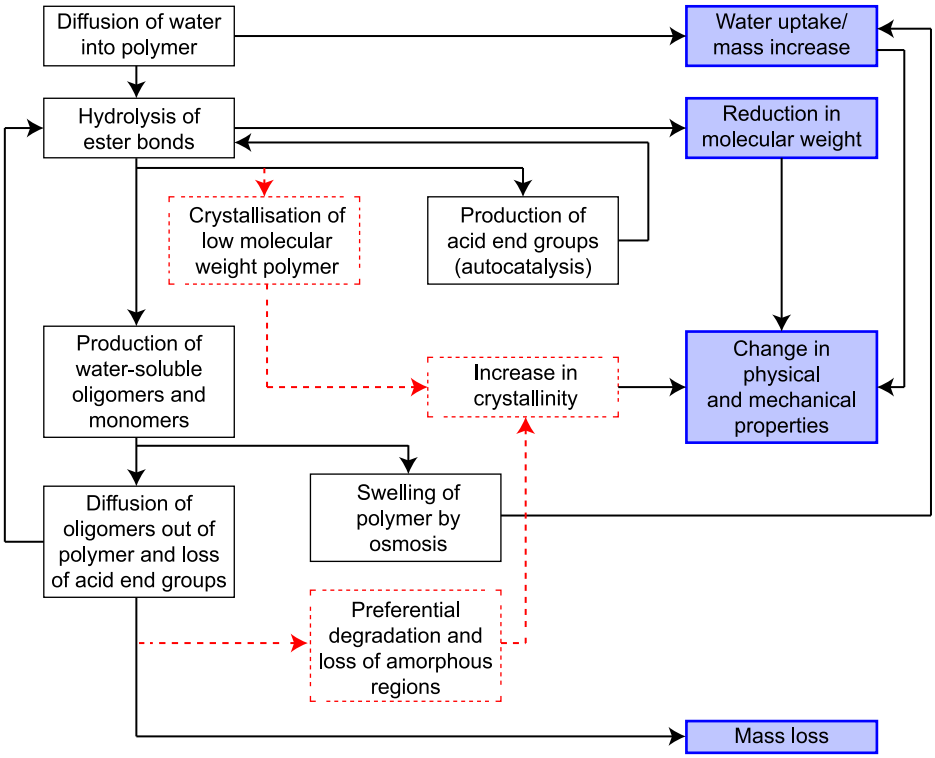

Fig. 3.8. Processes involved in hydrolytic degradation and the relationships between them. Shaded boxes refer to the most frequently measured properties. Dotted lines/boxes indicate processes applicable only to semi-crystalline polymers. Adapted from Buchanan (2008).

The techniques outlined here focus on modelling biodegradable polymers solely. In the case of biomedical applications, interactions between the polymer material and the local surroundings are of great importance. Furthermore, when used as drug delivery devices, understanding how the polymer and drug interact is necessary to ensure correct drug transport into the surrounding tissue. This has been given a lot of attention in recent years, particularly in the context of drug-eluting stents (McGinty et al., 2011; Vo et al., 2017), and further details are presented in the review by McGinty (2014).

3.2.1 Modelling water uptake

As mentioned in Section 2.1.3, degradation of polymers can proceed as surface erosion or bulk degradation, and this largely impacts the observed evolution of properties. The first stage of polymer hydrolysis is diffusion of water molecules into the material. When this occurs slowly, surface erosion begins prior to the complete saturation of the material.

Table 3.3. Brief overview of various models used to describe degradation behaviour of polymers.

Model type	Brief description	Properties modelled	Comments	Ref.
Kinetic equations	Several kinetic models have been described with various levels of complexity. Early models considered isolated noncatalytic or autocatalytic degradation. Extensions include those that consider both mechanisms simultaneously, and separate end- and mid-chain scissions.	M_n, mass loss, X_c	Easy to implement. Further clarity required on properties that impact reaction rates and how to implement this to obtain consistent values for materials.	(Antheunis et al., 2009; Busatto et al., 2017; Gleadall et al., 2014b; Lyu et al., 2007; Pitt and Gu, 1987; Siparsky et al., 1998; Wang et al., 2008)
Scission	Stochastic model that randomly simulates bond scission on a representative ensemble of polymer chains.	MWD, M_n, M_w	Advantageous in its production of an evolving MWD. Kinetics are not considered, making it difficult to relate to time.	(Gleadall and Pan, 2013; Shirazi et al., 2016b; Simha, 1941)
Monte Carlo	Polymer matrix considered, containing pixels with a defined state (amorphous, crystalline, degraded, etc.). The lifetime of individual sections of the polymer is determined using random numbers.	Mass loss, porosity	As individual chain lengths are not considered, and instead are represented by a pixel, insight into the evolving molecular weight is limited, with the primary focus on polymer erosion.	(Göpferich, 1997; Göpferich and Langer, 1993)
Kinetic Monte Carlo	An expansion on standard Monte Carlo methods, a multiscale approach is used. Polymer chain scission and oligomer production are modelled at the molecular scale using a kinetic Monte Carlo scheme, while oligomer diffusion is modelled using a diffusion equation at the device scale.	MWD, M_n, M_w, mass loss, X_c	Many properties can be modelled using this multiscale approach. Autocatalysis not fully accounted for. Discrepancies between the scission pathway were noted: random chain scission process where (i) all bonds are equally likely to break (Han and Pan, 2011); (ii) all chains are equally likely to break (Zhang et al., 2017).	(Han and Pan, 2011; Zhang et al., 2017)
Empirical relationship	Links have been made between molecular weight and mechanical properties and described using an empirical relationship.	σ, E	Such models have shown promise for accelerated testing methods, with relationships between M_n and both σ and E found to be temperature independent.	(Deng et al., 2005; Farrar and Gillson, 2002; A. Gleadall, 2015)
Constitutive	Hyperelastic models are typically combined with some measure of degradation to provide evolving stress-strain curves.	σ vs ε	This approach has successfully captured deformation induced degradation. Material parameters are a function of deformation.	(Hayman et al., 2014; Soares et al., 2010; Vieira et al., 2014, 2011)
Statistical mechanics	An ensemble of chains is typically considered alongside its evolving strain-energy potential. Extensions allow finite chain extensibility to be studied.	E, σ, ε	While the underlying theory is decades old, its application in bioresorbable polymers has only been utilized quite recently. Finite chain extensibility has been given limited consideration in this field to date.	(Arruda and Boyce, 1993; Edwards and Vilgis, 1986; Shirazi et al., 2016b; Stepto and Taylor, 1995a; Wang et al., 2010; Ward, 1971)
Molecular dynamics	Simulations consider detailed interactions within the polymer at an atomic scale.	σ, ε, E, MWD	Computational intensity limits this approach to tiny time scales or well-structured materials.	(Ding et al., 2012; Messmer et al., 2019; Monnier et al., 2015)
Multiscale approach	Various methods outlined above have been used in combination to obtain greater insight into the polymer evolution. Additionally, finite element techniques have been used in conjunction with kinetic models to explore the effect of device geometry.	See above.	Properties modelled depend on multiscale approach used. These offer an important step towards a complete modelling framework. Distinct components are typically the limiting factor; for example, if simplified degradation kinetics are considered, they will affect model reliability.	(Shine et al., 2017; Shirazi et al., 2016b; Soares et al., 2010; Wang et al., 2010; Zhang et al., 2019)

In contrast, quick diffusion of water into the material results in bulk degradation. Farrar (2008) describes how to incorporate this first stage of degradation into their modelling approach, where Fick's law was solved using Finite Element Analysis. In that approach, the diffusion coefficient was assumed to remain constant, and ignored any effects of density and degradation. Measuring what the diffusion coefficient should be remains a challenge. In many modelling approaches, it is assumed that amorphous regions of hydrophilic aliphatic polymers become instantly saturated and any changes in the water concentration are assumed to be negligible. That approach has proved to be successful, possibly due to only the bound water being reactive, with bulk water not contributing to the hydrolysis reaction. This idea is supported by the experimental work of Schmitt et al. (1994) who found that hydrolysis rates of PLGA were not impacted by water content.

3.2.2 Modelling hydrolysis kinetics

The degradation of aliphatic polyesters typically proceeds as the hydrolysis of ester bonds throughout the chains, chemically described as follows:

$$-\mathrm{RCOOR'}- \ +\mathrm{H_2O} \xrightarrow{\mathrm{H^+ \ or \ OH^-}} -\mathrm{RCOOH} + \mathrm{HOR'}- \tag{3.2}$$

with every ester bond broken resulting in the formation of a carboxylic acid end group. The simplest kinetic equation describing the (total) rate of chain scissions, S_{tot}, is thus (Pitt and Gu, 1987)

$$\frac{dS_{tot}}{dt} = -\frac{dC_e}{dt} = k_h C_e C_w = \frac{dC_a}{dt} \tag{3.3}$$

with each scission reducing the ester bond concentration, C_e, and simultaneously increasing the concentration of carboxylic acid end groups, C_a. The reaction rate of hydrolysis is controlled by k_h, and C_w is the concentration of water molecules. As discussed in Section 3.2.1, C_w can typically be taken to be constant in the case of hydrophilic polyesters where bulk degradation proceeds. Eq. (3.3) accounts for simple noncatalytic hydrolysis in the absence of diffusion of degradation products from the material.

For a polymer experiencing autocatalytic hydrolysis (in the absence of diffusion and with constant water concentration), the kinetics can be described as (Pitt and Gu, 1987)

$$\frac{dS_{tot}}{dt} = -\frac{dC_e}{dt} = kC_e C_a = \frac{dC_a}{dt} \tag{3.4}$$

with the rate of chain scissions now dependent on the concentration of carboxylic acid ends, C_a, available to catalyse the reaction, controlled by a reaction rate k. A modification to Eq. (3.4) was proposed (Lyu et al., 2007; Siparsky et al., 1998), where a distinction was made between the acid product concentration, C_a, and the acid catalyst concentration, $(C_a K_a)^{0.5}$. The autocatalysis rate is considered to be proportional to the concentration of dissociated hydrogen ions, $[\mathrm{H}^+]$, with

$$K_a[\mathrm{COOH}] = [\mathrm{H}^+][\mathrm{COO}^-] = [\mathrm{H}^+]^2 \tag{3.5}$$

at equilibrium, where K_a is the dissociation rate constant for acid end groups and $[\mathrm{COOH}]$ is the concentration of carboxylic acid ends (molality rather than molarity as above). Incorporating this into Eq. (3.4) results in

$$\frac{dS_{tot}}{dt} = -\frac{dC_e}{dt} = k_a C_e C_a^{0.5} = \frac{dC_a}{dt} \tag{3.6}$$

where k_a is the reaction rate for autocatalysis.

While studies have found that Eq. (3.3), Eq. (3.4) or Eq. (3.6) could successfully describe the degradation behaviour of different forms of PLA (Helder et al., 1990; Siparsky et al., 1998), Lyu et al. (2007) found that PLA underwent two distinct kinetic processes, requiring more than one reaction rate to obtain a fit to their experimental data (Fig. 3.9).

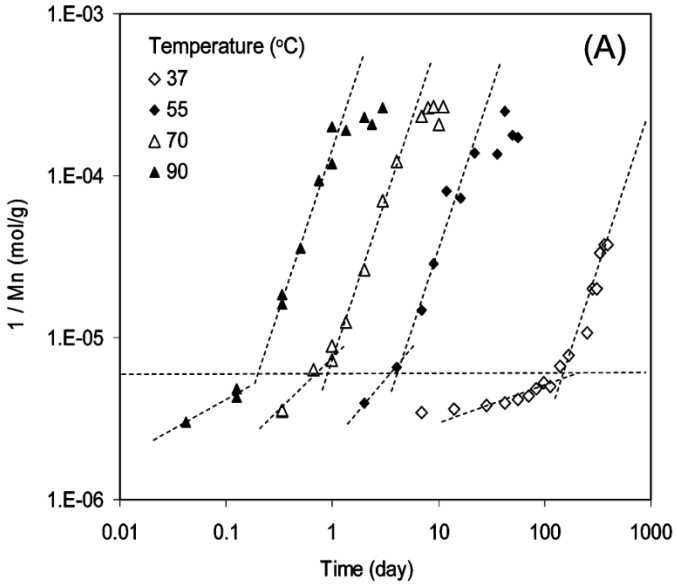

Fig. 3.9. Degradation of solid PLA samples at various temperatures, reprinted with permission from Lyu et al. (2007). Copyright © 2007 American Chemical Society. Fitting equations of the form of Eqs. (3.4) or (3.6) indicated two distinct stages that required a second reaction constant to capture the accelerated behaviour at later stages.

In practice, rather than determining multiple reaction rates for the same kinetic equation and establishing when this switch should occur, a single kinetic equation which captures all the behaviour is preferential. This may be achieved by introducing an equation that considers both hydrolysis and autocatalysis, each with unique reaction rates. Wang et al. (2008) considered this as follows:

$$\frac{dS_{tot}}{dt} = -\frac{dC_e}{dt} = k_h C_e + k_a C_e C_m^n \tag{3.7}$$

where they assumed only the monomer concentration, C_m, controlled autocatalysis. The index n is an acid dissociation constant representing the availability of the acid catalyst in the reaction and can be varied to capture the behaviour of Eq. (3.4), Eq. (3.6), or some intermediate behaviour. Pan and co-workers have introduced several additional extensions to Eq. (3.7), including considering diffusion of degradation products from the material, changes in crystallinity and mass loss, and the effect of end- and mid-chain scissions on the degradation behaviour; further details are provided in Section 3.2.5.

While the kinetic equations described above are typically used to predict changes in average molecular weight, more complex models have considered a set of coupled differential equations that describe changes in the length of polymer chains caused by autocatalysis (Antheunis et al., 2009; Busatto et al., 2017). Mai et al. (2018) followed a similar approach when modelling the degradation of hyaluronan, tracking the evolution of polymer chains of given lengths as scissions occur according to kinetic equations. In doing so, predictions for the evolving molecular weight distribution, average molecular weights, and mass loss were obtained as a function of degradation time.

The common thread of kinetic models are the reaction rates, which are chosen to best fit experimental data for a specific polymer. In theory, unique reaction rates would exist for each unique homopolymer, and ultimately these could be combined to predict the behaviour of different copolymers without the need for lengthy degradation experiments. However, a variability typically exists in reported reaction rates; for example, Zhang et al. (1994) found reaction rates for PDLLA varied from 0.0183–0.0447, attributing the differences to different processing techniques, initial conditions, and sample dimensions. This highlights the need for further clarity about how the reaction rates are affected by variabilities in studies and how this can be accounted for.

3.2.3 Alternative molecular weight models

While kinetic models have received much interest when it comes to predicting changes in molecular weight of polymers due to the relative ease of their implementation, various other approaches have previously been explored. An overview is presented here, while further details can be found in the comprehensive review of many of the modelling approaches to date by Laycock et al. (2017).

Many of the earliest models for polymer degradation were stochastic in nature, with properties described using a random probability distribution. Simha (1941) developed a random chain scission theory to predict changes in the distribution of polymer chains as degradation occurs using first order degradation kinetics. Three case studies were considered: (i) all bonds are equally likely to break; (ii) preferential scission of end bonds; and (iii) all chains are equally likely to break, independent of their size. Such an approach allows changes in the molecular weight distribution to be explored in the context of how any preferential degradation impacts its evolving shape. However, autocatalytic degradation was not considered, resulting in relatively abrupt declines in average molecular weight, similar to that associated with noncatalytic random scission (Fig. 3.3). Alternative scission models have been proposed (Gleadall and Pan, 2013; Shirazi et al., 2016b) where a representative molecular weight distribution is input and subjected to randomly simulated scissions, resulting in evolving molecular weight distributions. While these are useful in determining the effects of end and mid-chain scissions, they require iterative fitting to experimental data as kinetics are not considered.

An alternative approach is Monte Carlo methods, which have been used to randomly simulate degradation on a representative material. In contrast to scission models that typically consider a polymer chain ensemble and the individual chains within it, the Monte Carlo approach takes a polymer matrix containing pixels, each with a defined state (for example, amorphous, crystalline, degraded, etc.). Göpferich and co-workers used this method to describe the erosion of the polymer, with the lifetime of individual sections of the polymer determined using random numbers (Fig. 3.10) (Göpferich, 1997; Göpferich and Langer, 1993). The kinetics of the degradation were not considered, nor was a distribution of chain lengths.

Zhang et al. (2017) later introduced a multi-scale approach by considering both chemical and physical events such as polymer chain scission, oligomer production and diffusion, and microstructure evolution due to erosion of the small chains. A kinetic Monte Carlo method

was used to simulate chain scission, where each pixel in the matrix corresponds to a polymer chain, and this was coupled with Fick's laws to model the oligomer diffusion. Predictions for mass loss, average molecular weight and crystallinity were in good agreement with experimental results for PLGA. The temporal evolution of the molecular weight distribution was also obtained and indicated a random chain scission process where all chains are equally likely to break, irrespective of chain length. This approach results in a peak forming towards the lower end of the distribution, while the higher end of the distribution (corresponding to high molecular weight chains) is impacted minimally. This is typically not seen experimentally, with experimental distributions usually indicative of a scission process where all bonds are equally likely to break (perhaps with some preferential end-chain scissions). Han and Pan (2011) addressed this in their two-scale model, where polymer chain scission and oligomer production are modelled at the molecular scale using a kinetic Monte Carlo scheme, while oligomer diffusion is modelled using a diffusion equation at the device scale (Fig. 3.11). By introducing different reaction rates for end and mid-chain scissions, they obtained predictions for evolving MWDs of PLA that were in reasonable agreement with experimental data (Grizzi et al., 1995). When considering the autocatalytic reaction, it was assumed that only oligomers contributed to this, despite experimental evidence suggesting all chain ends can contribute to this mechanism (Tracy et al., 1999).

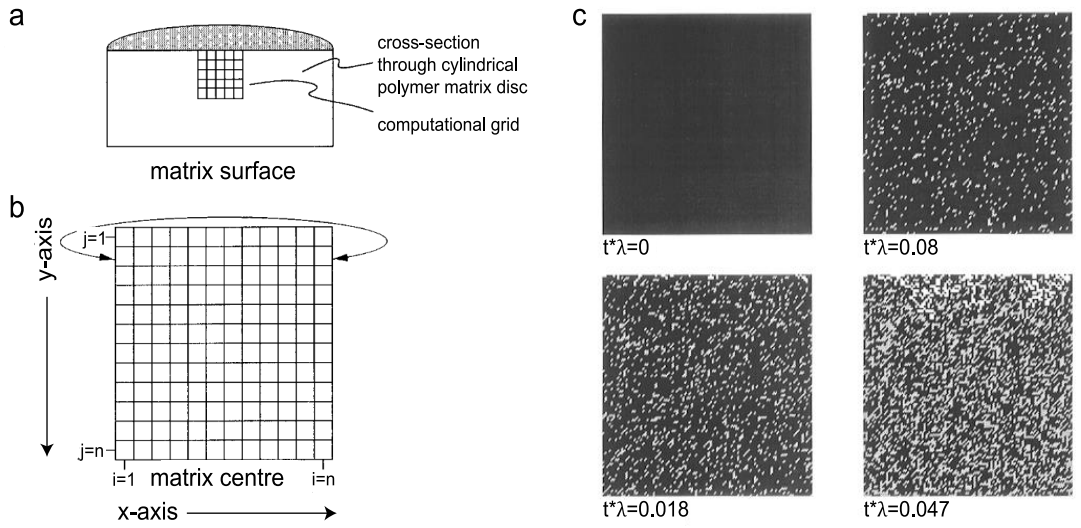

Fig. 3.10. Example of a Monte Carlo approach. Schematic representation of a polymer matrix cross section by a rectangular grid: (a) location of the grid on the cross section of a cylindric matrix disk; (b) computational grid in detail. (c) Simulation of erosion: (black) nondegraded polymer; (grey) degraded polymer; (white) eroded polymer (pores). Adapted from Göpferich (1997).

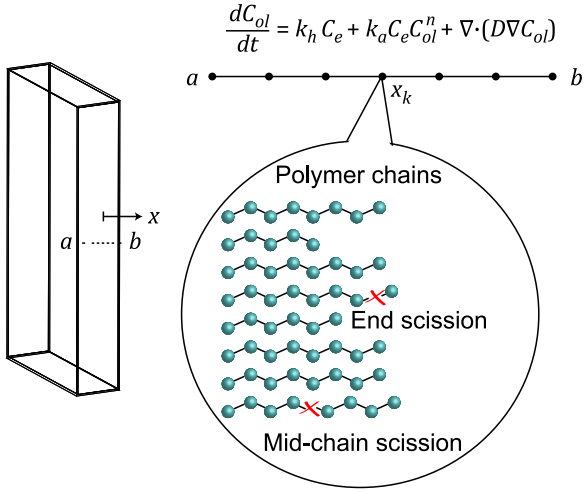

Fig. 3.11. Schematic diagram of the two-scale model for the biodegradation of a plate in which the diffusion of oligomers occurs only in the thickness direction (a–b) of the plate. The equation describes the change in the concentration of oligomers, C_{ol}, due to the rate of hydrolysis (k_h), autocatalysis (k_a), and diffusion (D), where C_e is the concentration of ester bonds and n is the acid dissociation constant. Adapted from Han and Pan (2011).

3.2.4 Modelling mechanical properties

Despite the importance of the evolving mechanical properties in the context of material performance, there have been fewer studies focusing on the time taken for the mechanical properties of a biodegradable polymer to break down. With various models proving successful in providing good predictions for the evolution of molecular weight (Section 3.2.2-3.2.3), particularly in terms of average values, attempts have been made to link these changes with changes in mechanical properties.

One of the earliest such models is that proposed by Flory (1945), albeit not in relation to biodegradable polymers specifically. Tensile strength, σ, was related to number average molecular weight, M_n, as follows:

$$\sigma = \sigma_\infty - \frac{B_F}{M_n} \tag{3.8}$$

where σ_∞ is the fracture strength at infinite molecular weight and B_F is a constant. As Eq. (3.8) is an empirical relationship, both σ_∞ and B_F must be determined using experimental calibration. While Farrar and Gillson (2002) demonstrated that Eq. (3.8) was only appropriate in the brittle failure regime, Weir et al. (2004b) showed that it was unable to capture the behaviour displayed by PLLA, where they found an almost linear relationship existed between the two properties (Fig. 3.12a). Different trends were observed by Deng et al. (2005) for the degradation of PLGA braids (Fig. 3.12b), where they found the following

relationship between breaking strength retention, BSR, i.e., ultimate tensile strength as a percentage of its original value, and average molecular weight, MW:

$$BSR = a + b \ln MW \tag{3.9}$$

where MW was taken to be either M_n or M_w and a and b are constants. Eq. (3.9) was also found to successfully capture the behaviour of PLGA at various increased temperatures, suggesting its practicality in accelerated degradation studies. The different trends observed by Weir et al. (2004b) and Deng et al. (2005) may be due to the large difference in initial molecular weight ($M_{n0} \approx 160,000$ and $19,000$ g/mol respectively). Both studies did determine a clear relationship between M_n and σ over a range of testing conditions; however, this relationship must be further explored using a wider range of experimental data. Interestingly, Farrar and Gillson (2002) found that such a relationship did not exist between M_w and σ, in contrast to the findings of Deng et al. (2005). It has also been noted that a different relationship exists between M_n and true stress (Farrar and Gillson, 2002) (as opposed to nominal stress, which is typically reported in experimental studies), and so care should be taken to distinguish between these during further investigations.

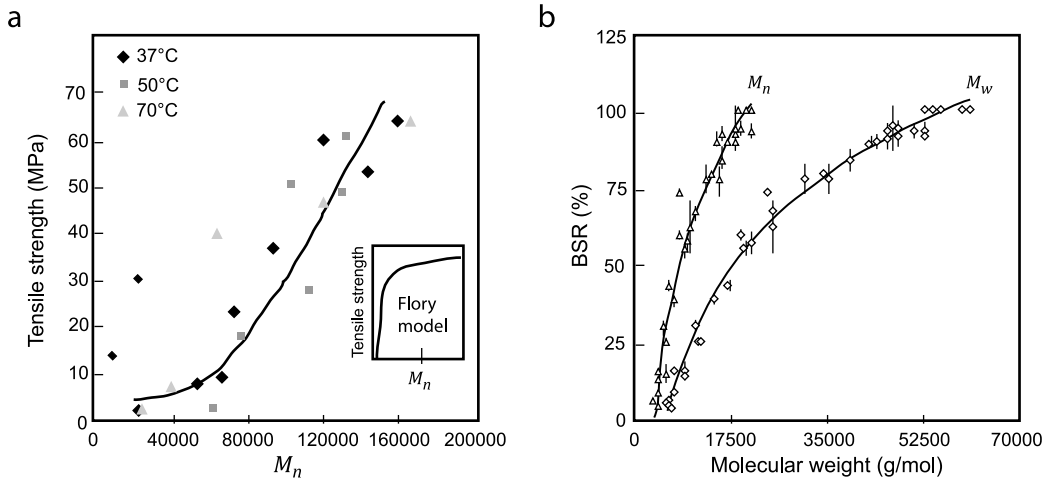

Fig. 3.12. (a) Adapted from Weir et al. (2004b), where an almost linear relationship between tensile strength and M_n was observed in contrast to Flory's relationship (Eq. (3.8)). (b) The relationship between breaking strength retention, BSR, i.e., ultimate tensile strength as a percentage of its original value, and average molecular weight, MW, described by Eq. (3.9). Adapted from Deng et al. (2005).

Although it is unlikely for any property to depend solely on molecular weight, it has been shown that when most properties are held constant and degradation conditions are minorly varied (for example, increased temperature leading to accelerated testing), relationships can be found between M_n and properties ranging from tensile strength to Young's modulus to

strain retention (Deng et al., 2005; Weir et al., 2004b). While these are typically empirical relationships, they can still prove hugely insightful for designing improved devices, with accelerated testing used to determine any parameters, reducing development time.

Models concerned with relating polymer stiffness to average molecular weight have also been introduced. Wang et al. (2010) developed a theory for amorphous bioresorbable polymers based on the relationship between Young's modulus and the number of polymer chains per unit volume based on rubber-like elasticity theories (Section 2.3, (Ward and Sweeney, 2013)). The change in entropy of the polymer system due to chain scissions was considered as a binary count of chain groups above a threshold molecular weight. They found the reduction in Young's modulus lagged behind the reduction in M_n, successfully capturing PLLA degradation data (Tsuji, 2002). Shirazi et al. (2016b) expanded on that approach, implementing the theory just described into a scission model to capture the relationship between stiffness and M_n and then coupling that with a kinetic model (Wang et al., 2008) to predict changes in M_n as a function of degradation duration (for further details, see Section 3.2.6). The basis of these models is derived using statistical mechanics of polymeric chains theory, which is further detailed in Section 2.3. As mentioned in that section, extensions have also considered the effect of finite chain extensibility on the mechanical behaviour (Arruda and Boyce, 1993; Edwards and Vilgis, 1986; Stepto and Taylor, 1995a); however, this approach does not yet appear to have been extended to bioresorbable polymer models.

Several studies have developed material damage and constitutive models to describe the evolution of mechanical properties in degrading polymers. Towards this, Vieira et al. (2014, 2011) presented a model that combined a relationship between fracture strength and molecular weight with hyperelastic material models to obtain evolving stress-strain curves for PLA–PCL fibres during degradation. Soares et al. (2010) took a thermodynamic approach and considered the effect of deformation on degradation behaviour. They considered PLLA stent fibres under tensile loading conditions with a deformation-dependent rate of degradation and obtained evolving stress-strain curves. However, these were qualitative in nature due to a lack of experimental data. Hayman et al. (2014) proceeded by expanding on this model in conjunction with an experimental study investigating the effect of different loads at different stages of degradation on PLLA fibres. Their model captured the increased reduction in mechanical properties with increased loading observed experimentally. As the material parameters are material functions of degradation damage instead of material constants in these constitutive models, extensive experimental data is needed for this

approach. Further understanding of the physicochemical response during deformation may allow for an improved modelling framework that requires less experimental calibration.

Molecular dynamics simulations consider detailed interactions within the polymer at an atomic scale and have been utilised in several studies. The resulting force that chemical bonds and other non-bonded interactions, such as van der Waals forces, Coulomb attraction, and Pauli repulsion, have on atoms provides information on their acceleration, which in turn offers their speed and position. A detailed description of this method can be found in the book by Rapport (2004). Ding et al. (2012) used molecular dynamics simulations to consider the effect of temperature and chain scissions on Young's modulus of semi-crystalline polyethylene. They found a delayed reduction in Young's modulus for polymers above the glass transition temperature, which was less apparent for polymers below the glass transition temperature. It has been suggested that this delay may in part be due to isolated scissions having minimal impact on entropy, with large chain degradation required to cause a significant reduction in entropy (Wang et al., 2010). Molecular dynamics techniques have also been used in exploring the effects of processing conditions (Messmer et al., 2019; Monnier et al., 2015). The complex molecular structures of polymers, particularly in amorphous regions, limit the applications of this method due to the computational intensity, capable only of simulating tiny time scales or well-structured materials. Where molecular dynamics tracks changes in the positions of atoms based on the forces applied by surrounding atoms, statistical mechanics (Section 2.3) can update the positions of atoms based on a probability distribution according to the possible configurations of chains. Consequently, statistical mechanics methods are typically less computationally intense than molecular dynamics and are capable of tracking polymer evolution at a larger time scale.

As computational resources become more powerful, several models have been developed that take advantage of this. Amongst these, Gleadall et al. (2015) explored the effect of chain scissions on Young's modulus, suggesting localised reduced stiffness. They used an atomic finite element model, essentially a crossover between molecular dynamics and finite element modelling, where interactions between atoms were considered using finite elements. To prevent it from being overly computationally intense, the model restricted its focus to very small displacements. Zhang et al. (2019) further developed the Kinetic Monte Carlo approach (Han and Pan, 2011; Zhang et al., 2017) to consider the evolution of polymer tensile strength during degradation (Fig. 3.13). Three strength phases were considered – amorphous, crystalline, and strength vacancy phases – using a modified version of Flory's relationship (Eq. (3.8)) with different parameters for each phase. Their multiscale approach

provided predictions for M_n, crystalline fraction, X_c, and σ that agreed reasonably well with experimental data. Several studies have utilised finite element techniques to determine the mechanical responses to degradation, allowing for devices of any shape to be considered (Shine et al., 2017; Shirazi et al., 2016b; Wang et al., 2010). Such studies are typically multiscale in nature and rely on a description of the degradation kinetics (Section 3.2.2); therefore, any advancements in the understanding of the kinetics should impact these models favourably.

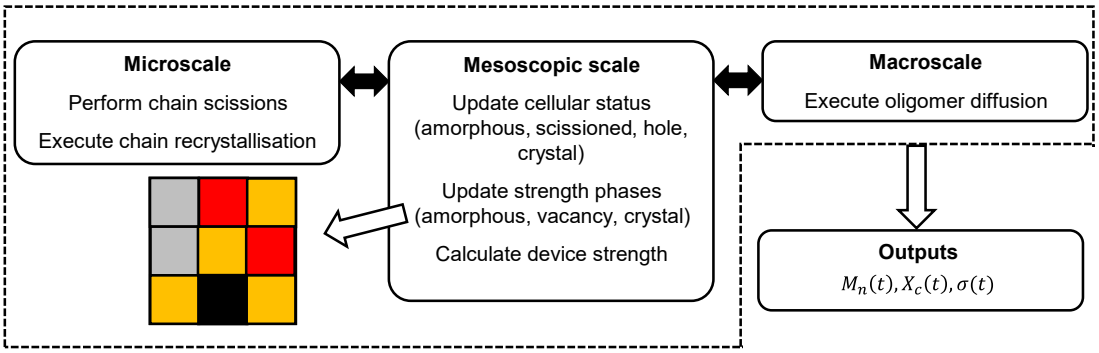

Fig. 3.13. Outline of a multiscale approach, adapted from Zhang et al. (2019). The microscale simulates scissions on chains and allows chain recrystallisation, the mesoscopic scale assigns and updates the strength phase (amorphous, crystalline, or strength vacancy) of pixelated regions, and the macroscale tracks oligomer diffusion, with information shared between each phase. This provides temporal predictions for number average molecular weight, M_n, crystalline fraction, X_c, and strength, σ.

Despite the multiple efforts that have been given to modelling these materials, little attention has focused on predicting the evolution of the failure strain. Although experimental data has suggested a relationship exists between failure strain and molecular weight independent of temperature (Deng et al., 2005; Weir et al., 2004b), this does not appear to have been translated into a predictive tool. Deroiné et al. (2014) suggested as little as 20% reduction in failure strain could correspond to end-of-use, with abrupt declines often seen after an induction period, while mechanical failure of polymers is often assessed by a 95% reduction in elongation at break (Laycock et al., 2017). Pickett and Coyle (2013) measured the time to embrittlement via bending tests on films and used this to develop a predictive tool for the lifetime of the polymer, described as follows:

$$t_{fail} = \frac{\exp\left(\frac{E_a}{RT}\right)}{A[\mathrm{RH}]^n} \tag{3.10}$$

where t_{fail} is the failure time, E_a is the activation energy, R is the gas constant, T is the temperature, A is a constant, $[\mathrm{RH}]$ is the relative humidity, and n is the kinetic order of $[\mathrm{RH}]$.

That study focused on the degradation of polycarbonate, poly(ethylene terephthalate) and resorcinol polyarylate and found that Eq. (3.10) accurately captured the failure time. A similar predictive tool for aliphatic polymer embrittlement or lifetime could be invaluable for future developments.

While many important developments have been outlined above, an all-inclusive framework that captures changes in material and mechanical properties simultaneously has huge potential for further optimising bioresorbable polymers for their intended application. Towards this, a multiscale approach provides the most promise. However, each scale modelled requires a rigorous understanding of the degradation behaviour at that level and its impact on other scales. Although links between M_n and various properties have been made, it is expected that the entire molecular weight distribution is important, while other parameters are likely also at play. Thus, while many models focus on predictions for M_n, knowledge of the entire molecular weight distribution and its evolution during degradation should offer greater insight into the overall degradation behaviour. The remaining parts of this section expand on some of the more subtle advantages and limitations of some existing kinetic models (Section 3.2.5) and provides a more detailed outline of an integrated molecular weight-mechanical properties model (Section 3.2.6).

3.2.5 Phenomenological degradation kinetics

Following the original kinetic phenomenological model of Wang et al. (2008), a variety of developments have been proposed; a summary is provided in Table 3.4. In the initial work, a reaction-diffusion model was developed to describe the degradation of amorphous biodegradable polymers; this was extended by Han and Pan (2009) to consider crystalline regions using a modified version of Avrami's theory to account for degradation-induced crystallisation. A further extension accounted for the production and diffusion of oligomers (Han et al., 2010). Gleadall et al. (2014b) updated the kinetic model by differentiating between mid-chain and end-chain scissions in new rate equations; although, comprehensive experimental data to separate the kinetics of these processes is lacking.

Despite the success of this family of models in capturing experimental trends, some key issues persist in the model assumptions and formulation. First, it is assumed that only monomers (and oligomers in later publications) could catalyse the hydrolysis reaction. The polymer end group plays an important role in degradation, with uncapped PLGA degrading faster than ester capped (Tracy et al., 1999) suggesting all carboxylic acid ends should be considered catalysts and not only those of short chains. Second, simplified molecular weight

distributions were assumed, characterised by the ester bond concentration, C_e, and the oligomer (or monomer, C_m) concentration, C_{ol}. This assumed distribution is unable to consider the effect of the overall molecular weight distribution on mechanical properties; this may be important, with reports that a narrow distribution of polystyrene had improved tensile strength, elongation at break and tensile creep properties compared to broader samples with the same value of weight average molecular weight, M_w (Thomas and Hagan, 1969). Third, although Han et al. (2010) improved the equations of Wang et al. (2008) to more correctly account for mid-chain scissions and thus prevent all scissions from affecting C_{ol} (i.e., not all scissions create oligomers), the effect of mid-chain scissions on C_e has not been accounted for (i.e., the rate equations do not account for the reduction of ester bonds due to mid-chain scissions). Fourth, it was assumed in earlier studies that average molecular weight was proportional to C_e and while later studies (Gleadall et al., 2014b; Han et al., 2010) calculated an average molecular weight based on C_e and other parameters, this quantity was not computed from a chain distribution and thus limited the understanding of consequential changes in molar mass dispersity (M_w/M_n).

In parallel to these models of degradation kinetics, Wang et al. (2010) introduced an entropy spring model to predict the mechanical behaviour, relating Young's modulus to the average molecular weight, again focusing on amorphous polymers. That work was motivated by the rubber-like elasticity theory detailed by Ward and co-workers (1971; 2013) and further details are provided in Section 2.3. They proposed that the entropic elasticity of the system is not significantly altered by isolated chain scissions; rather, it is suggested that a critical molecular weight exists for a chain, below which the chain has deteriorated to the point of no longer contributing to the entropy and, thus, Young's modulus of the material. An initial MWD was prescribed and subjected to numerically simulated mid-chain and end-chain scissions; however, the reaction kinetics were not considered within that scission model. Instead, the formulation was combined with the original kinetic model (Wang et al., 2008), where the reaction-diffusion equations were solved to describe the evolution of C_e, and it was assumed that this was equivalent to M_n of the simulated MWD, thus neglecting the effect of the formation and removal of chains from the system and not accounting for changes in molar mass dispersity. Although the entropy spring model was derived using the theory of rubber-like elasticity, degradation data for both amorphous PLA and PLGA below their glass transition temperature have been captured (Shirazi et al., 2016b; Wang et al., 2010). While further developments to these models have been proposed (Han and Pan, 2011), the key issues identified above persist and form the motivation for Chapter 4.

Table 3.4. Outline of several models proposed by Jingzhe Pan and colleagues, highlighting some advancements and limitations. C_e (C_{e0}), C_m, C_{ol}, C_{COOH} – (initial) molar concentrations of ester bonds, monomers, oligomers, and carboxylic acid ends, respectively; X_c – crystalline fraction; $R, \bar{R}, R_{ol}$ – production rate of monomers, monomers per unit volume of semi-crystalline polymer, and oligomers, respectively; R_s, R_{rs}, R_{es}; molar concentration of scission, random scission, and end scission, respectively; k_1 (k_{r1}, k_{e1}), k_2 (k_{r2}, k_{e2}) – reaction rate constants for simple hydrolysis and autocatalysis, respectively (via random, end scission); D – coefficient of diffusion; n – acid dissociation constant; m – average degree of polymerisation of oligomer; ω – molar number of the repeating units of the crystalline phase per unit volume; M_e (M_{e0}) – (initial) average molecular weight, related to the ester bond concentration; M_n – number average molecular weight; E – Young's modulus; N_{c0} – initial molar concentration of chains; $N_{c>M^{crit}}$ – molar concentration of chains above a critical molecular weight.

Ref.	Brief overview	Properties	Key equations	Comments
(Wang et al., 2008)	Reaction-diffusion model – hydrolysis (noncatalytic and acid-catalysed) and monomer diffusion in amorphous biodegradable polymers.	C_e, M_e vs time	$\frac{dR}{dt} = k_1 C_e + k_2 C_e C_m^n = -\frac{dC_e}{dt}$ $\frac{dC_m}{dt} = \frac{dR}{dt} + \mathrm{div}_{x_i}[D\ \mathrm{grad}_{x_i}(C_m)]$ $\frac{M_e}{M_{e0}} = \frac{C_e}{C_{e0}}$	The initial work in this series, resulting in biodegradation maps indicating when different mechanisms control the reaction. For every ester bond broken, a monomer is produced; this suggests a degradation mechanism consisting only of end scissions. The calculation of average molecular weight does not account for the number of chains.
(Han and Pan, 2009)	Updated to consider crystalline regions and mass loss.	C_e, M_e, X_c, mass loss vs time	$\frac{d\bar{R}}{dt} = (1 - X_c)\frac{dR}{dt}$ $\frac{dC_e}{dt} = -\frac{d\bar{R}}{dt} - \frac{C_e}{1 - X_c}\frac{dX_c}{dt}$ $\frac{dC_m}{dt} = \frac{d\bar{R}}{dt} + \mathrm{div}_{x_i}\left(D\ \mathrm{grad}_{x_i}(C_m)\right)$	Developments allow for additional properties to be tracked; however, the limitations mentioned above still apply. Ester bonds in amorphous regions can hydrolyse, while amorphous regions can also become crystalline.
(Han et al., 2010)	The production and diffusion of oligomers (rather than monomers alone) is integrated into an updated model.	M_n, X_c, mass loss vs time	$\frac{dC_{\mathrm{COOH}}}{dt} = k_1 C_e + k_2 C_e C_{ol}^{0.5}$ $\frac{\mathrm{d}C_e}{\mathrm{d}t} = -\frac{\mathrm{d}R_{ol}}{\mathrm{d}t} - \frac{C_e}{1 - X_c}\frac{\mathrm{d}X_c}{\mathrm{d}t}$ $\frac{\mathrm{d}C_{ol}}{\mathrm{d}t} = \frac{\mathrm{d}R_{ol}}{\mathrm{d}t} + \mathrm{div}_{x_i}[D\ \mathrm{grad}_{x_i}(C_{ol})]$ $M_n = \frac{(C_e + \omega X_c)M_0}{N_{c0} + R_s - \frac{R_{ol}}{m}}$	The change in acid concentration, rather than just the monomer concentration, is considered. However, only the acid ends of oligomers are considered to catalyse the reaction. Improved calculation of average molecular weight but still provides no information on molar mass dispersity. Random scissions are considered to not affect C_e, with $\mathrm{d}R_{ol}/\mathrm{d}t$ controlling the decline of C_e.
(Gleadall et al., 2014b)	The effect of mid-chain and end-chain scissions are now considered independently in new rate equations.	M_n, X_c, mass loss vs time	$\frac{dR_{rs}}{dt} = k_{r1} C_e + k_{r2} C_e \left(\frac{C_{\mathrm{COOH}}}{1 - X_c}\right)^n$ $\frac{dR_{es}}{dt} = k_{e1} C_{end} + k_{e2} C_{end} \left(\frac{C_{\mathrm{COOH}}}{1 - X_c}\right)^n$ $C_{\mathrm{COOH}} = C_m + \left(\frac{C_{ol}}{m}\right)$	New reaction rates are introduced, allowing the rates of end- and mid-chain scissions to be tailored to explore their individual effects on different properties. Contributions of acid ends to autocatalysis and the reduction in C_e are still not accurately accounted for.
(Wang et al., 2010)	Young's modulus is related to the average molecular weight, again focusing on amorphous polymers.	E vs M_n	$\frac{E}{E_0} = \frac{N_{c>M^{crit}}}{N_{c0}}$	A scission model was implemented, taking an initial molecular weight distribution and gradually performing scissions at random on the chain distribution. Reaction kinetics were not considered.

3.2.6 Integrated modelling framework for molecular weight and mechanical properties

Shirazi et al. (2016b) presented a modelling framework based on the kinetic model of Wang et al. (2008), which described changes in the polymer molecular weight, and the entropy-spring model of Wang et al. (2010), describing a relationship between the polymer molecular weight and Young's modulus. That framework, outlined in Fig. 3.14 and detailed below, provides the initial motivation for the model presented in Chapter 4.

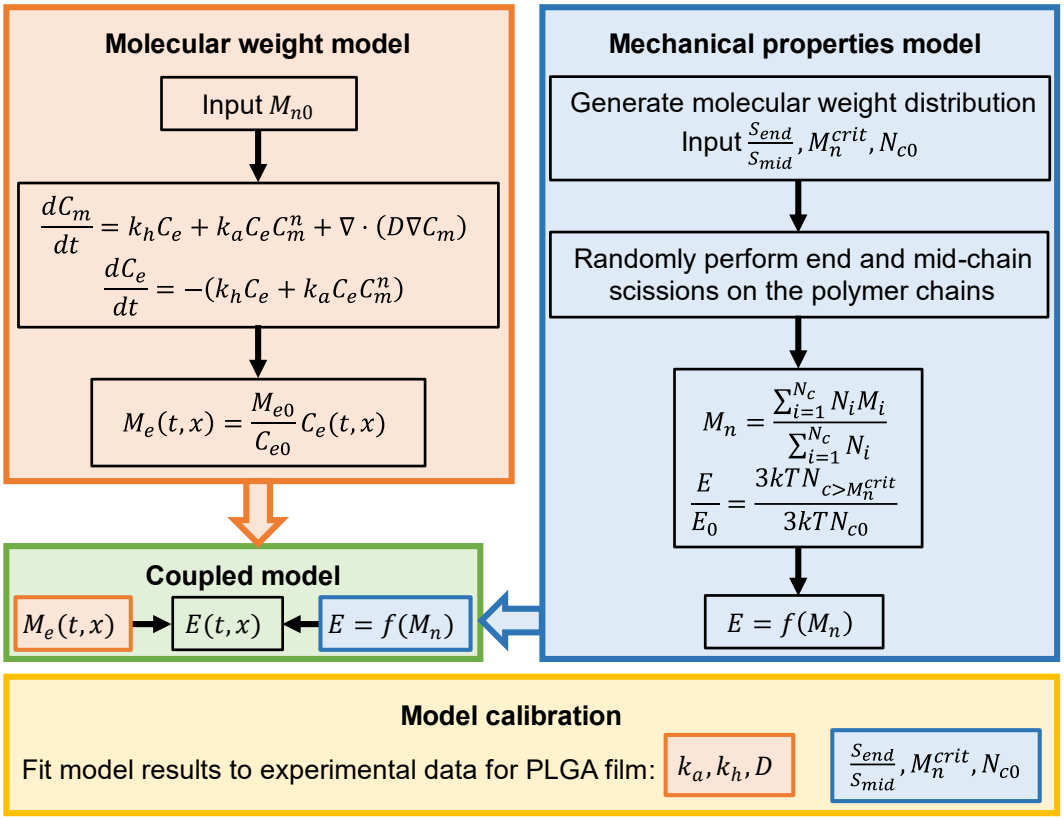

Fig. 3.14. Flowchart adapted from Shirazi et al. (2016b) outlining the simulation framework they used to model the degradation and elastic properties of PLGA films. The reaction-diffusion model of Wang et al. (2008) was first used to determine the evolution of C_e during degradation (molecular weight model). Next, a random scission process was implemented on an ensemble of theoretical polymer chains representative of a molecular weight distribution, with chain scissions gradually simulated on the chains according to the ratio of end to mid-chain scissions, S_{end}/S_{mid}. The evolution of Young's modulus was then determined using the entropy-spring theory of Wang et al. (2010), where it was assumed that isolated chain scissions and highly degraded chains ($M_n < M_n^{crit}$, a molecular weight threshold) do not contribute to the change in entropy and therefore stiffness of the system (mechanical properties model). Finally, both models were coupled and variables were calibrated to obtain the evolving stiffness as a function of degradation duration and location in the sample ($E(t,x)$).

3.2.6.1 Molecular weight model

To begin, the kinetic or molecular weight model (Wang et al., 2008) was used to predict the evolution of the molecular weight of (PLGA) polymers undergoing degradation. This was done using the following reaction-diffusion equations:

$$\frac{dC_e}{dt} = -(k_h C_e + k_a C_e C_m^n) \tag{3.11}$$

$$\frac{dC_m}{dt} = k_h C_e + k_a C_e C_m^n + \nabla \cdot (D \nabla C_m) \tag{3.12}$$

where C_e $(\mathrm{mol\ m^{-3}})$ is the concentration of ester bonds, C_m $(\mathrm{mol\ m^{-3}})$ is the concentration of monomers, and k_h $(\mathrm{day^{-1}})$ and k_a $((\mathrm{m^3 mol^{-1}})^n\ \mathrm{day^{-1}})$ are reaction rate constants for simple hydrolysis and autocatalysis respectively. The index n is an acid dissociation constant often taken to be 0.5, as detailed in Section 3.2.2. The last term in Eq. (3.12) takes the diffusion of monomers in the system into account. Eqs. (3.11)-(3.12) are representative of a system where each ester bond cleavage increases the monomer concentration in the system, i.e., all scissions are, in effect, end scissions. As water was assumed to be abundant, its concentration does not appear in Eqs. (3.11)-(3.12). The average molecular weight was calculated as

$$\frac{M_e}{M_{e0}} = \frac{C_e}{C_{e0}} \tag{3.13}$$

where M_{e0} and C_{e0} are the initial values of average molecular weight and ester bond concentration, respectively. Here, we refer to this average value as M_e to avoid confusion between alternative average values. Monomers are too small to be detected experimentally using standard measuring methods and, as such, are excluded from the calculation in Eq. (3.13). Average molecular weights are hugely dependent on the number of chains in the system, which this relationship fails to capture; consequently, Eq. (3.13) and M_e should be used with caution. In fact, M_e is a measure of the ester bond concentration, a feature that is hard to capture experimentally. In contrast, both M_n and M_w are more insightful measures of the molecular weight distribution, with the former placing an emphasis on short chains and the latter more sensitive to long chains. While average molecular weights are useful material characterisations, the complete molecular weight distribution is most insightful, providing a complete overview of the polymer chain lengths; it may be that this distribution is what controls many of the polymer properties (Thomas and Hagan, 1969).

Shirazi et al. (2016b) implemented Eqs. (3.11)-(3.13) in a finite element formulation using Comsol Multiphysics (v4.3b), providing predictions for the evolution of the average molecular weight, M_e, during degradation.

3.2.6.2 Mechanical properties model

Separately, predictions for the mechanical properties were explored. To begin, the entropy spring theory was considered (Section 2.3), which relates Young's modulus, E, of a polymer network to the number of polymer chains per unit volume N as follows:

$$E = 3NkT \tag{3.14}$$

where k is the Boltzmann constant and T is the absolute temperature. This relationship was described by Ward (1971) and its derivation is shown in Eq. (2.40). Wang et al. (2010) proposed two modifications to this theory to account for changes in N during polymer degradation (Fig. 3.15). The first assumption was that isolated scissions of very long chains do not significantly affect the entropy change and, hence, N does not increase. A molecular weight threshold was also introduced; it was assumed that once a parent chain and its resulting sub-chains created via scissions fell below this critical molecular weight, they no longer contributed to the polymer stiffness and, hence, were excluded from N. The model as proposed captures the reduction in Young's modulus during degradation; however, it is unable to predict any increase in E.

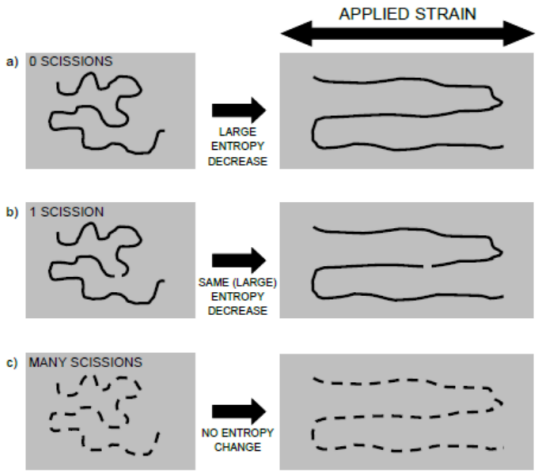

Fig. 3.15. Schematic diagram describing the entropy theory for biodegradable polymers introduced by Wang et al. (2010). A polymer chain (black line) embedded in a matrix of other amorphous polymer chains (grey box) straightens out during elongation of the overall polymer. A chain is shown with a) 0 scissions, b) 1 scission and c) many scissions. There is little effect of a single scission on entropy change during deformation, whereas many scissions can result in entropy no longer reducing during deformation. Reproduced from Gleadall (2015).

A scission model was implemented in MATLAB® (R2014a, The MathWorks, Inc., MA, U.S.A.), which took an initial representative polymer chain distribution and simulated end- and mid-chain scissions at random on the chains. The ratio of mid- to end-chain scissions was kept constant throughout the simulation. The resulting chain lengths were tracked and, implementing the two modifications to the entropy-spring theory mentioned above, provided predictions for N and, consequently, E as degradation takes place, resulting in a non-linear decrease in Young's modulus.

3.2.6.3 Coupling of models

The molecular weight model and mechanical properties model outlined above were coupled, allowing simultaneous predictions for the evolution of both properties during degradation. The molecular weight model provided predictions for changes in the ester bond concentration, C_e, which was related to M_e using Eq. (3.13), as a function of time. Meanwhile, the mechanical properties model offered insight into the evolution of Young's modulus as a function of the number average molecular weight, M_n. By assuming M_e and M_n were equivalent, predictions for Young's modulus were obtained as a function of degradation duration (Fig. 3.16). This approach enabled PLGA films and scaffolds to be modelled under mechanical loading.

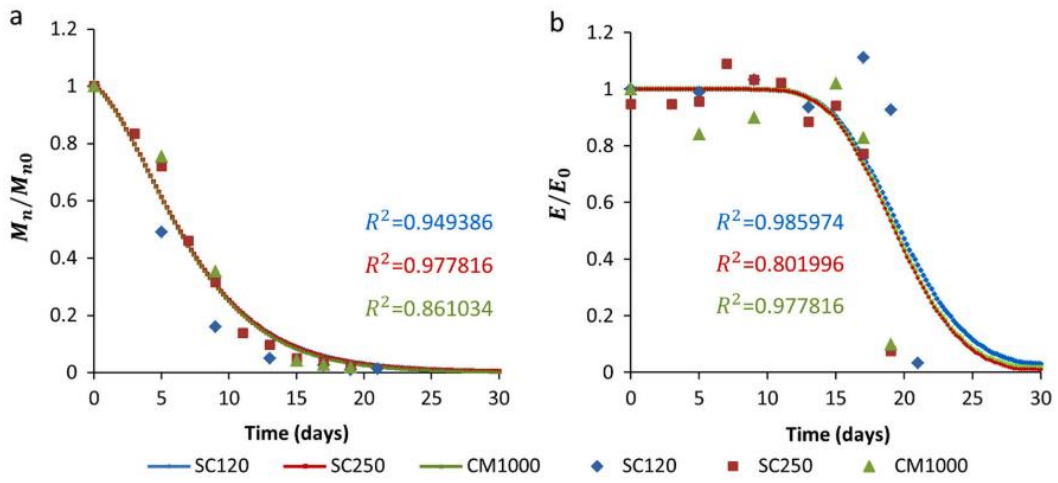

Fig. 3.16. Comparison between model predictions (lines) and experimental data (symbols) for PLGA of various thicknesses for evolution of normalised (a) number average molecular weight and (b) Young's modulus. Reproduced with permission from Shirazi et al. (2016a). Copyright © 2016, Springer Nature.

3.2.7 Finite chain extensibility

While the finite extensibility of polymer chains has often been neglected in modelling techniques, several publications have considered the effect of this on the deformation

behaviour. Edward and Vilgis (1986) extended the theory of rubber-like elasticity to include the finite extensibility of chains within the network, moving away from the Gaussian distribution function for chain end-to-end lengths, instead using a Langevin function. Arruda and Boyce (1993) developed the eight-chain model, with chains linked at the centre of a cube and extending to the corners. Chains were prescribed an initial length $r_0 = l\sqrt{n}$ (Eq. (2.25)) and a fully extended length of $r_{max} = nl$. Each chain in the system undergoes a stretch equivalent to that in every other network chain, with the contributions of a single chain averaged over eight spatial orientations.

An alternative approach was introduced by Stepto and Taylor (1995a, 1995b), where elastic properties were related to network chain end-to-end distance distributions and were assumed to arise solely as a result of conformational changes in the network chains. To begin, a network of polymer chains was generated, with the molecular conformational states of chains considered using rotational isomeric state statistics; chains were built bond-by-bond using a Monte Carlo approach and resulted in an end-to-end distribution of polymer chains constructed as a histogram. One end of each chain was assumed fixed at an origin, with the coordinates of the free ends randomly assigned according to the end-to-end distance distribution. The network of chains was subjected to a simulated uniaxial stretch, with updated coordinates and end-to-end lengths calculated. The free energy was determined from simulated changes in the end-to-end distance distributions as the network was stretched using the steps detailed in Sections 2.3.4-2.3.5, albeit using the simulated distributions in Eq. (2.26) rather than for the Gaussian example detailed. Hence, for an individual polymer chain in a network of N chains, the Helmholtz free energy change, ΔA, upon deformation at an absolute temperature T, is assumed to arise solely from the equivalent entropic change:

$$\Delta A = kT \ln\left(\frac{p_{def}\left(r_{def}\right)}{p_0(r_0)}\right) \tag{3.15}$$

where p_0 and p_{def} are the simulated undeformed and deformed probability density distributions. Once chains reached full extension, they were prevented from further stretching alongside any additional extension of the bulk material and, consequently, they no longer contributed to the change in entropy of the system. This restriction allowed non-affine deformation to be considered.

Their results showed a small but significant proportion of chains reached full extension at relatively low macroscopic strains (Fig. 3.17a). An increase in the proportion of fully extended

chains with increasing macroscopic strain resulted in a steady decrease in the rate of network free energy change, causing a reduction in the network modulus at moderate macroscopic strains, reflecting further deviation from Gaussian, affine behaviour (Fig. 3.17b). Their approach was innovative in that the elastic force was calculated from the total deformation of the end-to-end vectors of individual network chains, rather than from the deformation of an average chain. Their focus was restricted to polymers such as polydimethylsiloxane and polyethylene, which do not undergo degradation under typical conditions. Computational restrictions limited the focus to uniform systems of polymer chains containing up to 150 bonds, i.e., all chains in a network had the same molecular weight, analogous to an average molecular weight.

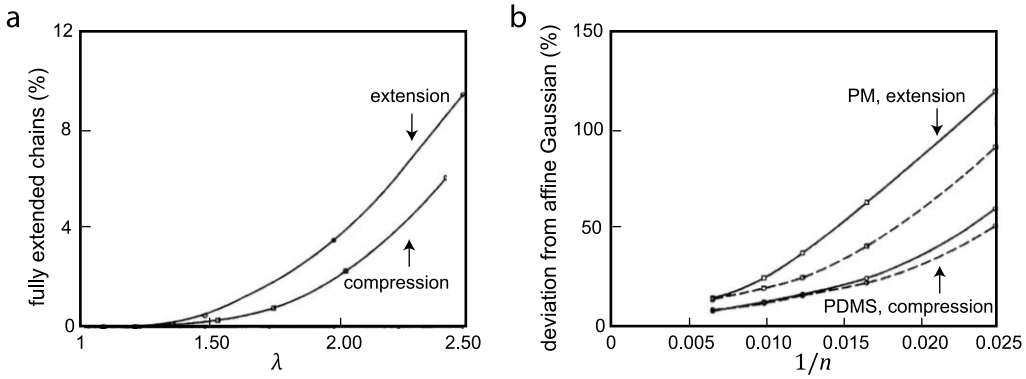

Fig. 3.17. Select results obtained by Stepto and Taylor (1995a) on simulating deformation on a network of polymer chains. (a) A small but significant proportion of chains reached full extension at relatively low macroscopic strains for 150-bond PM chains. (b) The percentage deviation from affine Gaussian network behaviour was reported as a function of reciprocal number of network-chain skeletal bonds, $1/n$, with more pronounced deviations from affine behaviour for shorter chains, accredited to an increased number of fully extended chains in those networks.

Molecular network models, such as those described in this section, can provide much insight into the network behaviour and are considered to be more insightful than phenomenological models, particularly at the exploratory phase (Ward and Sweeney, 2013).

3.3 Conclusion

This chapter provides an overview of the experimentally observed evolution of biodegradable polymers during degradation and summarises modelling techniques introduced to date.

Section 3.1 suggests many factors affect the evolution of biodegradable polymer materials during degradation, including polymer composition and structure, changes in molecular weight distribution, degradation type, and relationships between molecular weight and

mechanical properties. Each of these are given consideration at some point in the research that follows. Model validation is carried out using existing experimental data for each subsequent chapter. In Chapter 4, the experimental study of Shirazi et al. (2014) is quantitatively compared with simulated molecular weight distributions, average molecular weights and Young's modulus predictions. A quantitative comparison of predicted evolving failure strain as functions of both molecular weight and time with the observations of Tsuji (2002) (Fig. 3.4) is carried out in Chapter 5, alongside the experimental data detailed in Table 3.1. Finally, Chapter 6 considers a qualitative comparison of predicted stress-strain curves with those obtained by Vieira et al. (2011) (Fig. 3.5).

In terms of modelling techniques, Chapter 4 takes its motivation from the integrated modelling framework for molecular weight and mechanical properties presented by Shirazi et al. (2016b) and detailed in Section 3.2.6. Rather than coupling the kinetic (molecular weight) and scission (mechanical properties) models, updated kinetics are introduced and incorporated directly into the scission model. A framework which combines hydrolysis and autocatalysis due to carboxylic acid chain ends into a single model, which includes both mid- and end-chain scissions for both degradation mechanisms, will offer greater insight into how the molecular weight distribution changes as degradation takes place. Chapter 5 seeks a relationship between evolving molecular weight and ductility; an understanding of both the polymer structure and deformation mechanics are utilised for this. Finally, Chapter 6 considers the effects of finite polymer chain extensibility on mechanical properties. Stepto and Taylor's (1995a, 1995b) approach (Section 3.2.7), which motivates the work, is extended to consider an evolving molecular weight distribution.

References

Agrawal, C.M., McKinney, J.S., Lanctot, D.R., Athanasiou, K.A., 2000. Effects of fluid flow on the in vitro degradation kinetics of biodegradable scaffolds for tissue engineering. Biomaterials 21, 2443–2452. https://doi.org/10.1016/S0142-9612(00)00112-5

Antheunis, H., van der Meer, J.C., de Geus, M., Kingma, W., Koning, C.E., 2009. Improved Mathematical Model for the Hydrolytic Degradation of Aliphatic Polyesters. Macromolecules 42, 2462–2471. https://doi.org/10.1021/ma802222m

Arruda, E.M., Boyce, M.C., 1993. A three-dimensional constitutive model for the large stretch behavior of rubber elastic materials. J. Mech. Phys. Solids 41, 389–412. https://doi.org/10.1016/0022-5096(93)90013-6

ASTM F1635-16, Standard Test Method for in vitro Degradation Testing of Hydrolytically Degradable Polymer Resins and Fabricated Forms for Surgical Implants, 2016. https://doi.org/10.1520/F1635-16

Breche, Q., Chagnon, G., Machado, G., Girard, E., Nottelet, B., Garric, X., Favier, D., 2016. Mechanical behaviour's evolution of a PLA-b-PEG-b-PLA triblock copolymer during hydrolytic degradation. J. Mech. Behav. Biomed. Mater. 60, 288–300. https://doi.org/10.1016/j.jmbbm.2016.02.015

Buchanan, F.J. (Ed.), 2008. Degradation rate of bioresorbable materials: prediction and evaluation. Woodhead Publishing Limited/CRC Press LLC, Cambridge, England/Boca Raton, FL.

Busatto, C., Pesoa, J., Helbling, I., Luna, J., Estenoz, D., 2017. Heterogeneous hydrolytic degradation of poly (lactic-co-glycolic acid) microspheres: Mathematical modeling. J. Appl. Polym. Sci. 134, 45464. https://doi.org/10.1002/app.45464

Deng, M., Zhou, J., Chen, G., Burkley, D., Xu, Y., Jamiolkowski, D., Barbolt, T., 2005. Effect of load and temperature on in vitro degradation of poly(glycolide-co-L-lactide) multifilament braids. Biomaterials 26, 4327–4336. https://doi.org/10.1016/j.biomaterials.2004.09.067

Deroiné, M., Le Duigou, A., Corre, Y.-M., Le Gac, P.-Y., Davies, P., César, G., Bruzaud, S., 2014. Accelerated ageing and lifetime prediction of poly(3-hydroxybutyrate-co-3- hydroxyvalerate) in distilled water. Polym. Test. 39, 70–78. https://doi.org/10.1016/j.polymertesting.2014.07.018

Ding, L., Davidchack, R.L., Pan, J., 2012. A molecular dynamics study of Young's modulus change of semi-crystalline polymers during degradation by chain scissions. J. Mech. Behav. Biomed. Mater. 5, 224–230. https://doi.org/10.1016/j.jmbbm.2011.09.002

Duek, E.A.R., Zavaglia, C.A.C., Belangero, W.D., 1999. In vitro study of poly(lactic acid) pin degradation. Polymer 40, 6465–6473. https://doi.org/10.1016/S0032-3861(98)00846-5

Duval, C., Rahouadj, R., Nouvel, C., Six, J.L., 2018. PLGA with less than 1 month of half-life time: Tensile properties in dry and wet states and hydrolytic degradation. Int. J. Polym. Mater. Polym. Biomater. 67, 509–516. https://doi.org/10.1080/00914037.2017.1354197

Edwards, S.F., Vilgis, T., 1986. The effect of entanglements in rubber elasticity. Polymer 27, 483–492. https://doi.org/10.1016/0032-3861(86)90231-4

Farrar, D.F., 2008. Modelling of the degradation process for bioresorbable polymers, in: Degradation Rate of Bioresorbable Materials - Prediction and Evalutaion. pp. 183–206.

Farrar, D.F., Gillson, R.K., 2002. Hydrolytic degradation of polyglyconate B: The relationship between degradation time, strength and molecular weight. Biomaterials 23, 3905–3912. https://doi.org/10.1016/S0142-9612(02)00140-0

Flory, P.J., 1945. Tensile Strength in Relation to Molecular Weight of High Polymers. J. Am. Chem. Soc. 67, 2048–2050. https://doi.org/10.1021/ja01227a506

Gleadall, A., 2015. Mechanical properties of biodegradable polymers for medical applications, in: Pan, J. (Ed.), Modelling Degradation of Bioresorbable Polymeric Medical Devices. Woodhead Publishing, pp. 163–199.

Gleadall, A., Pan, J., 2013. Computer Simulation of Polymer Chain Scission in Biodegradable Polymers. J. Biotechnol. Biomater. 3, 154. https://doi.org/10.4172/2155-952X.1000154

Gleadall, A., Pan, J., Kruft, M.A., 2015. An atomic finite element model for biodegradable polymers. Part 2. A model for change in Young's modulus due to polymer chain scission. J. Mech. Behav. Biomed. Mater. 51, 237–247. https://doi.org/10.1016/j.jmbbm.2015.07.010

Gleadall, A., Pan, J., Kruft, M.A., Kellomäki, M., 2014a. Degradation mechanisms of bioresorbable polyesters. Part 1. Effects of random scission, end scission and autocatalysis. Acta Biomater. 10, 2223–2232. https://doi.org/10.1016/j.actbio.2013.12.039

Gleadall, A., Pan, J., Kruft, M.A., Kellomäki, M., 2014b. Degradation mechanisms of bioresorbable polyesters. Part 2. Effects of initial molecular weight and residual monomer. Acta Biomater. 10, 2233–2240. https://doi.org/10.1016/j.actbio.2014.01.017

Gleadall, A.C., 2015. Modelling Degradation of Biodegradable Polymers and their Mechanical Properties.

Göpferich, A., 1997. Polymer Bulk Erosion. Macromolecules 30, 2598–2604. https://doi.org/10.1021/ma961627y

Göpferich, A., Langer, R., 1993. Modeling of Polymer Erosion. Macromolecules 26, 4105–4112. https://doi.org/10.1021/ma00068a006

Grizzi, I., Garreau, H., Li, S., Vert, M., 1995. Hydrolytic degradation of devices based on poly(DL-lactic acid) size-dependence. Biomaterials 16, 305–311. https://doi.org/10.1016/0142-9612(95)93258-F

Han, X., Pan, J., 2011. Polymer chain scission, oligomer production and diffusion: A two-scale model for degradation of bioresorbable polyesters. Acta Biomater. 7, 538–547. https://doi.org/10.1016/j.actbio.2010.09.005

Han, X., Pan, J., 2009. A model for simultaneous crystallisation and biodegradation of biodegradable polymers. Biomaterials 30, 423–430. https://doi.org/10.1016/j.biomaterials.2008.10.001

Han, X., Pan, J., Buchanan, F., Weir, N.A., Farrar, D., 2010. Analysis of degradation data of poly(L-lactide-co-L,D-lactide) and poly(L-lactide) obtained at elevated and physiological temperatures using mathematical models. Acta Biomater. 6, 3882–3889.

https://doi.org/10.1016/j.actbio.2010.05.015
Hayman, D., Bergerson, C., Miller, S., Moreno, M., Moore, J.E., 2014. The Effect of Static and Dynamic Loading on Degradation of PLLA Stent Fibers. J. Biomech. Eng. 136, 1–9. https://doi.org/10.1115/1.4027614
Helder, J., Dijkstra, P.J., Feijen, J., 1990. In vitro degradation of glycine/DL-lactic acid copolymers. J. Biomed. Mater. Res. 24, 1005–1020.
Hiljanen-Vainio, M., Karjalainen, T., Seppälä, J., 1996. Biodegradable Lactone Copolymers. I. Characterization and Mechanical Behavior of ε-Caprolactone and Lactide Copolymers. J. Appl. Polym. Sci. 59, 1281–1288. https://doi.org/10.1002/(sici)1097-4628(19960222)59:8<1281::aid-app11>3.3.co;2-e
Houchin, M.L., Topp, E.M., 2008. Chemical Degradation of Peptides and Proteins in PLGA: A Review of Reactions and Mechanisms. J. Pharm. Sci. 97, 2395–2404. https://doi.org/10.1002/jps.21176
Karjalainen, T., Hiljanen-Vainio, M., Malin, M., Seppälä, J., 1996. Biodegradable Lactone Copolymers. III. Mechanical Properties of ε-Caprolactone and Lactide Copolymers After Hydrolysis in Vitro. J. Appl. Polym. Sci. 59, 1299–1304. https://doi.org/10.1002/(SICI)1097-4628(19960222)59:8<1299::AID-APP13>3.0.CO;2-1
Kasperczyk, J., Li, S., Jaworska, J., Dobrzyński, P., Vert, M., 2008. Degradation of copolymers obtained by ring-opening polymerization of glycolide and ε-caprolactone: A high resolution NMR and ESI-MS study. Polym. Degrad. Stab. 93, 990–999. https://doi.org/10.1016/j.polymdegradstab.2008.01.019
Kranz, H., Ubrich, N., Maincent, P., Bodmeier, R., 2000. Physicomechanical Properties of Biodegradable Poly(D,L-lactide) and Poly(D,L-lactide-co-glycolide) Films in the Dry and Wet States. J. Pharm. Sci. 89, 1558–1566. https://doi.org/10.1002/1520-6017(200012)89:12<1558::AID-JPS6>3.0.CO;2-8
Laycock, B., Nikolić, M., Colwell, J.M., Gauthier, E., Halley, P., Bottle, S., George, G., 2017. Lifetime prediction of biodegradable polymers. Prog. Polym. Sci. 71, 144–189. https://doi.org/10.1016/j.progpolymsci.2017.02.004
Li, S.M., Garreau, H., Vert, M., 1990a. Structure-property relationships in the case of the degradation of massive poly(α-hydroxy acids) in aqueous media, Part 2: Degradation of lactide-glycolide copolymers: PLA37.5GA25 and PLA75GA25. J. Mater. Sci. Mater. Med. 1, 131–139. https://doi.org/10.1007/bf00700872
Li, S.M., Garreau, H., Vert, M., 1990b. Structure-property relationships in the case of the degradation of massive aliphatic poly-(α-hydroxy acids) in aqueous media - Part 1: Poly(DL-lactic acid). J. Mater. Sci. Mater. Med. 1, 123–130. https://doi.org/10.1007/BF00700871
Limbert, G., Omar, R., Krynauw, H., Bezuidenhout, D., Franz, T., 2016. The anisotropic mechanical behaviour of electro-spun biodegradable polymer scaffolds: Experimental characterisation and constitutive formulation. J. Mech. Behav. Biomed. Mater. 53, 21–39. https://doi.org/10.1016/j.jmbbm.2015.07.014
Luo, Q., Liu, X., Li, Z., Huang, C., Zhang, W., Meng, J., Chang, Z., Hua, Z., 2014. Degradation model of bioabsorbable cardiovascular stents. PLoS One 9, 1–9. https://doi.org/10.1371/journal.pone.0110278
Lyu, S.P., Schley, J., Loy, B., Lind, D., Hobot, C., Sparer, R., Untereker, D., 2007. Kinetics and time-temperature equivalence of polymer degradation. Biomacromolecules 8, 2301–2310. https://doi.org/10.1021/bm070313n
Mai, V.Q., Vo, T.T., Meere, M., 2018. Modelling hyaluronan degradation by streptococcus pneumoniae hyaluronate lyase. Math. Biosci. 303, 126–138. https://doi.org/10.1016/j.mbs.2018.07.002
Mainil-Varlet, P., Curtis, R., Gogolewski, S., 1997. Effect of in vivo and in vitro degradation on molecular and mechanical properties of various low-molecular-weight polylactides. J. Biomed. Mater. Res. 36, 360–380. https://doi.org/10.1002/(SICI)1097-4636(19970905)36:3<360::AID-JBM11>3.0.CO;2-I
Malin, M., Hiljanen-Vainio, M., Karjalainen, T., Seppala, J., 1996. Biodegradable Lactone Copolymers. II. Hydrolytic Study of ε-Caprolactone and Lactide Copolymers. J. Appl. Polym. Sci. 59, 1289–1298. https://doi.org/10.1002/(SICI)1097-4628(19960222)59:8<1289::AID-APP12>3.0.CO;2-1
McGinty, S., 2014. A decade of modelling drug release from arterial stents. Math. Biosci. 257, 80–90. https://doi.org/10.1016/j.mbs.2014.06.016
McGinty, S., McKee, S., Wadsworth, R.M., McCormick, C., 2011. Modelling drug-eluting stents. Math. Med. Biol. 28, 1–29. https://doi.org/10.1093/imammb/dqq003

Messmer, D., Bertran, O., Kissner, R., Alemán, C., Schlüter, A.D., 2019. Main-chain scission of individual macromolecules induced by solvent swelling. Chem. Sci. 10, 6125–6139. https://doi.org/10.1039/c9sc01639b

Monnier, X., Delpouve, N., Basson, N., Guinault, A., Domenek, S., Saiter, A., 2015. Molecular dynamics in electrospun amorphous plasticized polylactide fibers. Polymer 73, 68–78. https://doi.org/10.1016/j.polymer.2015.07.047

Phong, L., Han, E.S.C., Xiong, S., Pan, J., Loo, S.C.J., 2010. Properties and hydrolysis of PLGA and PLLA cross-linked with electron beam radiation. Polym. Degrad. Stab. 95, 771–777. https://doi.org/10.1016/j.polymdegradstab.2010.02.012

Pickett, J.E., Coyle, D.J., 2013. Hydrolysis kinetics of condensation polymers under humidity aging conditions. Polym. Degrad. Stab. 98, 1311–1320. https://doi.org/10.1016/J.POLYMDEGRADSTAB.2013.04.001

Pitt, C.G., Gu, Z.-W., 1987. Modification of the rates of chain cleavage of poly(ε-caprolactone) and related polyesters in the solid state. J. Control. Release 4, 283–292. https://doi.org/10.1016/0168-3659(87)90020-4

Polak-Kraśna, K., Abaei, A.R., Shirazi, R.N., Parle, E., Carroll, O., Ronan, W., Vaughan, T.J., 2021. Physical and mechanical degradation behaviour of semi-crystalline PLLA for bioresorbable stent applications. J. Mech. Behav. Biomed. Mater. 118, 1–11. https://doi.org/10.1016/j.jmbbm.2021.104409

Ramchandani, M., Pankaskie, M., Robinson, D., 1997. The influence of manufacturing procedure on the degradation of poly(lactide-co-glycolide) 85:15 and 50:50 implants, Journal of Controlled Release.

Rapport, D.C., 2004. The Art of Molecular Dynamics Simulation, 2nd ed. Cambridge University Press.

Renouf-Glauser, A.C., Rose, J., Farrar, D.F., Cameron, R.E., 2005. The effect of crystallinity on the deformation mechanism and bulk mechanical properties of PLLA. Biomaterials 26, 5771–5782. https://doi.org/10.1016/j.biomaterials.2005.03.002

Schmitt, E.A., Flanagan, D.R., Linhardt, R.J., 1994. Importance of Distinct Water Environments in the Hydrolysis of Poly(DL-lactide-co-glycolide). Macromolecules 27, 743–748. https://doi.org/10.1021/ma00081a019

Shine, R., Neghabat Shirazi, R., Ronan, W., Sweeney, C.A., Kelly, N., Rochev, Y.A., McHugh, P.E., 2017. Modeling of Biodegradable Polyesters With Applications to Coronary Stents. J. Med. Device. 11, 1–12. https://doi.org/10.1115/1.4035723

Shirazi, R.N., Aldabbagh, F., Erxleben, A., Rochev, Y., McHugh, P., 2014. Nanomechanical properties of poly(lactic-co-glycolic) acid film during degradation. Acta Biomater. 10, 4695–4703. https://doi.org/10.1016/j.actbio.2014.08.004

Shirazi, R.N., Aldabbagh, F., Ronan, W., Erxleben, A., Rochev, Y., McHugh, P., 2016a. Effects of material thickness and processing method on poly(lactic-co-glycolic acid) degradation and mechanical performance. J. Mater. Sci. Mater. Med. 27, 1–12. https://doi.org/10.1007/s10856-016-5760-z

Shirazi, R.N., Ronan, W., Rochev, Y., McHugh, P., 2016b. Modelling the degradation and elastic properties of poly(lactic-co-glycolic acid) films and regular open-cell tissue engineering scaffolds. J. Mech. Behav. Biomed. Mater. 54, 48–59. https://doi.org/10.1016/j.jmbbm.2015.08.030

Simha, R., 1941. Kinetics of Degradation and Size Distribution of Long Chain Polymers. J. Appl. Phys. 12, 569–578. https://doi.org/10.1063/1.1712939

Siparsky, G.L., Voorhees, K.J., Miao, F., 1998. Hydrolysis of Polylactic Acid (PLA) and Polycaprolactone (PCL) in Aqueous Acetonitrile Solutions: Autocatalysis. J. Environ. Polym. Degrad. 6, 31–41. https://doi.org/1064-7546/98/0100-0031

Soares, J.S., Moore, J.E., Rajagopal, K.R., 2010. Modeling of Deformation-Accelerated Breakdown of Polylactic Acid Biodegradable Stents. J. Med. Device. 4, 1–10. https://doi.org/10.1115/1.4002759

Stepto, R.F.T., Taylor, D.J.R., 1995a. Molecular Modelling of the Elastic Behaviour of Polymer Chains in Networks: Comparison of Polymethylene and Poly(dimethylsiloxane). J. Chem. Soc. Faraday Trans. 91, 2639–2647. https://doi.org/10.1039/FT9959102639

Stepto, R.F.T., Taylor, D.J.R., 1995b. Modelling the elastic behaviour of real chains in polymer networks. Macromol. Symp. 93, 261–268. https://doi.org/10.1002/masy.19950930131

Thomas, D.P., Hagan, R.S., 1969. The Influence of Molecular Weight Distribution on Melt Viscosity, Melt Elasticity, Processing Behaviour and Properties of Polystyrene. Polym. Eng. Sci. 9, 164–171. https://doi.org/10.1002/pen.760090304

Tracy, M.A., Ward, K.L., Firouzabadian, L., Wang, Y., Dong, N., Qian, R., Zhang, Y., 1999. Factors affecting the degradation rate of poly(lactide-co-glycolide) microspheres in vivo and in vitro. Biomaterials 20, 1057–1062. https://doi.org/10.1016/S0142-9612(99)00002-2

Tsuji, H., 2002. Autocatalytic hydrolysis of amorphous-made polylactides: effects of L-lactide content, tacticity, and enantiomeric polymer blending. Polymer 43, 1789–1796. https://doi.org/10.1016/S0032-3861(01)00752-2

Tsuji, H., Del Carpio, C.A., 2003. In vitro hydrolysis of blends from enantiomeric poly(lactide)s. 3. Homocrystallized and amorphous blend films. Biomacromolecules 4, 7–11. https://doi.org/10.1021/bm020090v

Tsuji, H., Mizuno, A., Ikada, Y., 2000. Properties and morphology of poly(L-lactide). III. Effects of initial crystallinity on long-term in vitro hydrolysis of high molecular weight poly(L-lactide) film in phosphate-buffered solution. J. Appl. Polym. Sci. 77, 1452–1464. https://doi.org/10.1002/1097-4628(20000815)77:7<1452::AID-APP7>3.0.CO;2-S

Tsuji, H., Suzuyoshi, K., 2002. Environmental degradation of biodegradable polyesters 1. Poly(ε-caprolactone), poly[(R)-3-hydroxybutyrate], and poly(L-lactide) films in controlled static seawater. Polym. Degrad. Stab. 75, 347–355.

Venkatraman, S.S., Poh, T.L., Vinalia, T., Mak, K.H., Boey, F., 2003. Collapse pressures of biodegradable stents. Biomaterials 24, 2105–2111. https://doi.org/10.1016/S0142-9612(02)00640-3

Vey, E., Roger, C., Meehan, L., Booth, J., Claybourn, M., Miller, A.F., Saiani, A., 2008. Degradation mechanism of poly(lactic-co-glycolic) acid block copolymer cast films in phosphate buffer solution. Polym. Degrad. Stab. 93, 1869–1876. https://doi.org/10.1016/j.polymdegradstab.2008.07.018

Vieira, A.C., Guedes, R.M., Tita, V., 2014. Constitutive modeling of biodegradable polymers: Hydrolytic degradation and time-dependent behavior. Int. J. Solids Struct. 51, 1164–1174. https://doi.org/10.1016/j.ijsolstr.2013.12.010

Vieira, A.C., Vieira, J.C., Ferra, J.M., Magalhães, F.D., Guedes, R.M., Marques, A.T., 2011. Mechanical study of PLA–PCL fibers during in vitro degradation. J. Mech. Behav. Biomed. Mater. 451–460. https://doi.org/10.1016/j.jmbbm.2010.12.006

Vo, T., Lee, W., Peddle, A., Meere, M., 2017. Modelling chemistry and biology after implantation of a drug-eluting stent. Part I: Drug transport. Math. Biosci. Eng. 14, 491–509. https://doi.org/10.3934/mbe.2017030

Wang, Y., Han, X., Pan, J., Sinka, C., 2010. An entropy spring model for the Young's modulus change of biodegradable polymers during biodegradation. J. Mech. Behav. Biomed. Mater. 3, 14–21. https://doi.org/10.1016/j.jmbbm.2009.02.003

Wang, Y., Pan, J., Han, X., Sinka, C., Ding, L., 2008. A phenomenological model for the degradation of biodegradable polymers. Biomaterials 29, 3393–3401. https://doi.org/10.1016/j.biomaterials.2008.04.042

Ward, I.M., 1971. Mechanical properties of solid polymers. Wiley-Interscience.

Ward, I.M., Sweeney, J., 2013. Mechanical properties of solid polymers, 3rd ed. John Wiley & Sons.

Weir, N.A., Buchanan, F.J., Orr, J.F., Dickson, G.R., 2004a. Degradation of poly-L-lactide. Part 1: In vitro and in vivo physiological temperature degradation. Proc. Inst. Mech. Eng. Part H J. Eng. Med. 218, 307–319. https://doi.org/10.1243/0954411041932782

Weir, N.A., Buchanan, F.J., Orr, J.F., Farrar, D.F., Dickson, G.R., 2004b. Degradation of poly-L-lactide. Part 2: Increased temperature accelerated degradation. Proc. Inst. Mech. Eng. Part H J. Eng. Med. 218, 321–330. https://doi.org/10.1243/0954411041932809

Woodard, L.N., Grunlan, M.A., 2018. Hydrolytic Degradation and Erosion of Polyester Biomaterials. ACS Macro Lett. 7, 976–982. https://doi.org/10.1021/acsmacrolett.8b00424

Zhang, T., Jin, G., Han, X., Gao, Y., Zeng, Q., Hou, B., Zhang, D., 2019. Multiscale modelling for the heterogeneous strength of biodegradable polyesters. J. Mech. Behav. Biomed. Mater. 90, 337–349. https://doi.org/10.1016/j.jmbbm.2018.10.018

Zhang, T., Zhou, S., Gao, X., Yang, Z., Sun, L., Zhang, D., 2017. A multi-scale method for modeling degradation of bioresorbable polyesters. Acta Biomater. 50, 462–475. https://doi.org/10.1016/j.actbio.2016.12.046

Zhang, X., Wyss, U.P., Pichora, D., Goosen, M.F. a., 1994. An Investigation of Poly(lactic acid) Degradation. J. Bioact. Compat. Polym. 9, 80–100. https://doi.org/10.1177/088391159400900105

4 A kinetic scission model for molecular weight evolution in bioresorbable polymers

The main contents of this chapter have been published in Polymer Engineering and Science by John Wiley and Sons (Hill and Ronan, 2022).

As detailed in the previous chapters, a significant body of experimental literature has suggested a relationship between the molecular weight distribution of polymers and their mechanical properties. While several models have been proposed for predicting the evolving average molecular weight of biodegradable polymers, these rarely extend to predictions for the entire evolving molecular weight distribution as a function of degradation duration. The primary aim of this chapter is to address this gap and develop a model that considers both mid- and end-chain scissions due to hydrolysis and autocatalysis. This work is motivated by the approach of Shirazi et al. (2016b) and Wang et al. (2010, 2008), described in Section 3.2.6. A kinetic scission model (KSM) is introduced alongside a new kinetic ODE model (NKOM), which both better capture the autocatalytic effect of carboxylic acid chain ends than existing models. The models introduced are validated using existing experimental data (Shirazi et al., 2014) and by comparison with existing models (Shirazi et al., 2016b; Wang et al., 2010, 2008).

4.1 Introduction

4.1.1 Motivation

Bioresorbable stents are considered attractive alternatives to permanent metal stents for the treatment of coronary artery disease (Serruys et al., 2016; Wykrzykowska et al., 2009). However, obtaining biomechanical properties to match that offered by a metal stent has proved a difficult task (Im et al., 2017). Factors affecting the biomechanical properties of bioresorbable stents include stereo copolymer ratios (Durand et al., 2012) and variations in strut thickness (Cheng et al., 2019). In contrast to well-understood metal stents, bioresorbable stents have been shown to develop discontinuities during crimping and reinflation, before chemical degradation has initiated (Wang et al., 2018). Understanding the complex behaviour of these materials is crucial for ensuring sufficient mechanical integrity for the intended purpose. As the mechanical behaviour is related to the polymer microstructure, determining how the molecular weight distribution changes as degradation takes place is essential.

4.1.2 Degradation mechanism

Biocompatible polyesters such as polylactic acid (PLA), polyglycolic acid (PGA) and their copolymers experience degradation due to a hydrolytic reaction when placed in an aqueous medium (Buchanan, 2008), chemically described as follows:

$$-\mathrm{RCOOR'}- \xrightarrow{\mathrm{H_2O}} -\mathrm{RCOOH} + \mathrm{HOR'}- \tag{4.1}$$

Ester bonds are hydrolysed throughout polymer chains, primarily in amorphous regions of the polymer, causing chains to split. Each chain scission results in a carboxylic acid end group, $-\mathrm{RCOOH}$ (Ginjupalli et al., 2017; Laycock et al., 2017). Both mid- and end-chain scissions can occur, as outlined in Fig. 4.1a, and it is unclear which is the dominant mechanism (de Jong et al., 2001; Schliecker et al., 2003; Shih, 1995). As reported by Batycky et al. (1997), the increased acid concentration at the end of each chain may be the driver behind different mid- and end-chain scission rates. Shih (1995) reported a faster rate of end-chain scission ($k' = 0.13\mathrm{h}^{-1}$) than mid-chain scission ($k' = 0.01\mathrm{h}^{-1}$) for PLA, while reporting a completely random process for PCL, attributing this difference to the larger functional groups in PCL. During processing, the initial end groups may be capped to slow degradation (Tracy et al., 1999). Acidic degradation products can build up in the material due to limited diffusion, which can further accelerate the hydrolytic degradation (i.e., autocatalysis) and lead to heterogeneous bulk degradation (Grizzi et al., 1995; Vey et al., 2008). Shirazi et al. (2016a) predicted heterogenous degradation occurs in poly(lactic-co-glycolic acid) (PLGA) samples provided the characteristic diffusion length, calculated from material parameters, exceeds 3 µm. It is expected that the above mentioned poly(α-hydroxy acids) will degrade via bulk erosion, switching to surface erosion above a critical dimension estimated to be 7.4 cm by von Burkersroda et al. (2002).

4.1.3 Molecular weight distributions

Gel permeation chromatography (GPC) (Moore, 1964) is the method regularly employed when experimentally determining the molecular weight of a polymer material; separating the polymer chains based on hydrodynamic volume using a column packed with porous beads. The chains are characterized based on the time they spend travelling through the column: smaller chains can enter the pores more readily, increasing their retention time; larger chains, unable to fit into many of the pores, have a more direct path to follow through the column, allowing them to leave more quickly (Fig. 4.1b). It is possible for some chains to be completely retained, while others may not be retained at all; GPC is unable to separate

these chains. The detection range is determined both by the column packings used and their pore diameters (Skoog et al., 2017), and the sensitivity of the equipment used (for example, a Viscotek SEC-MALS 20 (Malvern, 2019), which couples GPC with multi-angle light scattering technology, claims a molecular weight detection range of $1000\ \mathrm{Da} - 10\ \mathrm{MDa}$ or $1.66 \times 10^{-21}\mathrm{g} - 1.66 \times 10^{-17}\mathrm{g}$, which is equivalent to approximately 14 – 140000 units of PLA). Polystyrene standards are often used to calibrate GPC, meaning the molecular weight of the sample is measured with respect to polystyrene; it has been reported that in doing so, lower molecular weights of PLA may not be accurately captured (Alex et al., 2018).

Vey et al. (2008) obtained evolving molecular weight distributions for amorphous PLGA 50:50 films degraded in phosphate buffer solution at 37°C, reproduced in Fig. 4.1c. A shift to the left was observed, with distributions initially broadening and a gradual reduction in peak height, before the opposite trend (taller and narrower distributions) was captured at later stages. The truncated tails in curves for Day 8.8 and onwards, denoted by the vertical dashed line, indicate that low molecular weight chains have either been removed through diffusion or that they are not accurately captured by this technique.

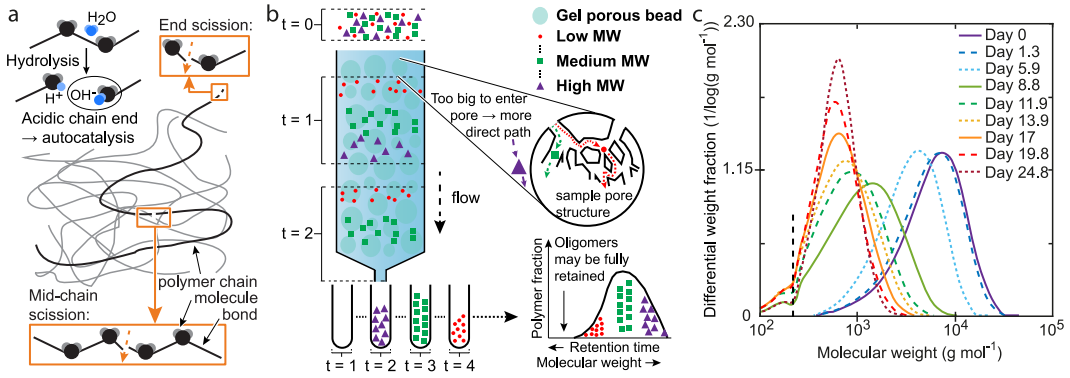

Fig. 4.1. (a) When placed in an aqueous medium, hydrolysis causes bonds to break, resulting in an acid chain end and an alcohol chain end; in turn, the former can accelerate the process. End scissions break the final bond in a polymer chain, resulting in the separation of a monomer, while mid-chain scissions cut some random bond along the chain, causing two shorter chains. (b) Schematic diagram of gel permeation chromatography. At time zero (t = 0), a polymer sample is prepared and enters the column. The sample gradually progresses, with chains characterized based on the time they spend travelling through the column. For example, the high MW chains are too big to enter the narrow pore structures and have exited at t = 2, while the medium and low MW chains follow less direct paths and are still permeating through the column. Based on their retention time, a molecular weight distribution is obtained. (c) Example of evolving molecular weight distributions for PLGA 50:50 as degradation takes place. Adapted from Vey et al. (2008). The vertical dashed line draws attention to the truncated tails at low molecular weights.

4.1.4 Evolution of amorphous polymers

Polymer composition plays a significant role in the degradation behaviour observed (Durand et al., 2012; Middleton and Tipton, 2000); this enables the optimisation of polymer properties for specific applications to be obtained through tailoring of the copolymer ratios. Certain copolymers, such as poly(DL-lactic-glycolic acid) 50:50 (50% PLA, 50% PGA), poly(DL-lactic-glycolic acid) 75:25 (37.5% PLLA, 37.5% PDLA, 25% PGA) and poly(DL-lactic acid) (50% PLLA, 50% PDLA), remain amorphous throughout degradation (Li et al., 1990a, 1990b; Shirazi et al., 2016a, 2014). This can be advantageous, resulting in a more predictable degradation profile than that seen with semi-crystalline polymers. Additionally, amorphous regions are typically the weak link in semi-crystalline polymers, degrading more quickly than crystalline regions. Consequently, the focus here is on accurately modelling amorphous polymers with the findings also relevant to the prediction of degradation in semi-crystalline polymers.

As chains break due to the hydrolytic reaction, the material transitions from having a high molecular weight to a low molecular weight (Tsuji, 2002; Tsuji and Del Carpio, 2003). A surface-centre differential has been observed in many cases as degradation proceeds, with degradation occurring more quickly at the centre (Li et al., 1990b, 1990a; Vey et al., 2008). The evolution of mechanical properties has been seen to be largely dependent on this molecular weight degradation. Experimental studies have found that changes in the mechanical behaviour of the polymer as degradation proceeds can vary substantially between different polymer compositions (Tsuji, 2002; Tsuji and Del Carpio, 2003). Shirazi et al. (2016a, 2014) observed that although the molecular weight of degrading PLGA declines rapidly, the Young's modulus remained relatively constant until a significant number of polymer chains had been removed from the system. The size of the sample is also seen to affect degradation, with thick samples degrading more quickly than thin ones, accredited to the build-up of accelerative degradation products in thicker samples as diffusion is not fast enough and autocatalysis occurs (Grizzi et al., 1995). Therefore, when modelling the evolution of these materials during degradation, important factors to consider include polymer type, changes in molecular weight distribution, degradation mechanism, and relationships between molecular weight and mechanical properties.

4.1.5 Modelling changes in molecular weight

Several models have been proposed to describe the degradation of biodegradable polymers using various approaches. Kinetic models have been developed to provide predictions for changes in average molecular weight as a function of degradation time (Antheunis et al.,

2010, 2009; Han and Pan, 2009; Lyu et al., 2007; Pitt and Gu, 1987; Siparsky et al., 1998; Wang et al., 2008). Gleadall et al (2014b) explored the effects of different hydrolysis mechanisms, determining both mid- and end-chain scissions are necessary to result in mass loss and molecular weight reduction, respectively. Scission models have been proposed to describe how chain cleavages affect the molecular weight distribution of a polymer, with both mid- and end-chain scissions considered (Batycky et al., 1997; Gleadall and Pan, 2013), but these have failed to incorporate the effect of autocatalysis on the degradation behaviour. Kinetic Monte Carlo approaches have been developed, providing predictions for the temporal evolution of the molecular weight distribution (Han and Pan, 2011; Zhang et al., 2017). The autocatalytic effect of acid chain ends created via mid-chain scission has typically been neglected, with only those of water-soluble oligomers and monomers considered (Gleadall et al., 2014b; Han and Pan, 2011, 2009; Wang et al., 2008; Zhang et al., 2017). A framework combining hydrolysis and autocatalysis due to carboxylic acid chain ends into a single model, while accounting for both mid- and end-chain scissions caused by both degradation mechanisms, will offer greater insight into how the molecular weight distribution changes as degradation takes place.

4.1.6 Modelling mechanical properties

In contrast to the many models focused on describing the degradation kinetics, few studies have focused on the time taken for the mechanical properties of a biodegradable polymer to break down. Recent models have suggested methods which couple a kinetic model with a scission model to gain insight into the evolution of Young's modulus (Shirazi et al., 2016b; Wang et al., 2010), building on the model by Wang et al. (2008) that predicts molecular weight changes and linking this to changes in Young's modulus. The effect of chain scissions on Young's modulus has also been considered, suggesting localised reduced stiffness (Gleadall et al., 2015). Zhang et al. (2019) further developed the Kinetic Monte Carlo approach (Han and Pan, 2011; Zhang et al., 2017) to consider the evolution of polymer tensile strength during degradation. A small number of studies have utilised finite element techniques to determine the mechanical responses to degradation, allowing for devices of any shape to be considered (Shine et al., 2017; Shirazi et al., 2016b; Soares et al., 2010; Wang et al., 2010). A full description of the polymer material, and, thus, the molecular weight distribution and its evolution during degradation, is likely necessary for more rigorous predictions of the mechanical properties.

4.1.7 A chronology of the models to date

Following the original kinetic phenomenological model of Wang et al. (2008), a variety of developments have been proposed. In the initial work, a reaction-diffusion model was developed to describe the degradation of amorphous biodegradable polymers; this was extended by Han and Pan (2009) to consider crystalline regions using a modified version of Avrami's theory to account for degradation-induced crystallisation. A further extension accounted for the production and diffusion of oligomers (Han et al., 2010). Gleadall et al. (2014b) updated the kinetic model by differentiating between mid-chain and end-chain scissions in new rate equations; although, comprehensive experimental data to separate the kinetics of these processes is lacking. A more detailed comparison between the model developments is provided in Table 3.4.

Despite the success of this family of models in capturing experimental trends, some key issues persist in the model assumptions and formulation. First, it is assumed that only monomers (and oligomers in later publications) could catalyse the hydrolysis reaction. The polymer end group plays an important role in degradation, with uncapped PLGA degrading faster than ester capped (Tracy et al., 1999), suggesting all carboxylic acid ends should be considered catalysts and not only those of short chains. Second, simplified molecular weight distributions were assumed, characterised by the ester bond concentration, C_e, and the oligomer (or monomer, C_m) concentration, C_{ol}. This assumed distribution is unable to consider the effect of the overall molecular weight distribution on mechanical properties; this may be important, with reports that a narrow distribution of polystyrene had improved tensile strength, elongation at break and tensile creep properties compared to broader samples with the same value of weight average molecular weight, M_w (Thomas and Hagan, 1969). Third, although Han et al. (2010) improved the equations of Wang et al. (2008) to more correctly account for mid-chain scissions and thus prevent all scissions from affecting C_{ol} (i.e., not all scissions create oligomers), the effect of mid-chain scissions on C_e has not been accounted for (i.e., the updated rate equations do not account for the reduction of ester bonds due to mid-chain scissions). Fourth, it was assumed in earlier studies that average molecular weight was proportional to C_e and although later studies (Gleadall et al., 2014b; Han et al., 2010) calculated an average molecular weight based on C_e and other parameters, this quantity was not computed from a chain distribution and thus limited the understanding of consequential changes in molar mass dispersity (M_w/M_n).

In parallel to these models of degradation kinetics, Wang et al. (2010) introduced an entropy spring model to predict the mechanical behaviour, relating the Young's modulus to the average molecular weight, again focusing on amorphous polymers. That work was motivated by the rubber-like elasticity theory detailed by Ward and co-workers (1971; 2013) and further details are provided in Section 2.3 and Section 3.2.6. An initial MWD was prescribed and subjected to numerically simulated mid-chain and end-chain scissions; however, as this did not consider the reaction kinetics, the formulation was combined with the original kinetic model (Wang et al., 2008), where the reaction-diffusion equations were solved to describe the evolution of C_e, and it was assumed that this was equivalent to M_n of the simulated MWD, thus neglecting the effect of the formation and removal of chains from the system and not accounting for changes in molar mass dispersity. Although the entropy spring model was derived using the theory of rubber elasticity, degradation data for both amorphous PLA and PLGA below their glass transition temperature have been captured (Shirazi et al., 2016b; Wang et al., 2010). While further developments to these models have been proposed (Han and Pan, 2011), the key issues identified above persist and form the motivation for our study.

4.1.8 Current study

In the current study, a kinetic scission model (KSM) was developed, motivated by previous work by Shirazi et al. (2016b) and Pan and co-workers (Gleadall et al., 2014b; Wang et al., 2010, 2008), to predict how the polymer properties evolve as degradation proceeds. Five key limitations are addressed: (i) the kinetics are updated to account for autocatalysis due to acidic chain ends created via all chain cleavages, rather than monomers alone as done previously; (ii) complete molecular weight distributions are considered and tracked as chains are randomly cleaved; (iii) mid-chain scissions reduce the ester bond concentration; (iv) average molecular weights are calculated using the distributions; and (v) the kinetics are directly calculated within the scission model, providing a direct time-dependence and preventing the need for coupling of models.

Amorphous polyesters and their evolution caused by simple hydrolysis and autocatalysis via both mid- and end-chain scissions are considered. It is assumed that the material experiences heterogenous bulk degradation and is instantly saturated with water; as such, the water concentration is not considered in the kinetics. This is a reasonable assumption given that the polymers considered do not proceed with surface erosion, indicating that degradation initiates within the sample, with the rate of diffusion of water greater than the rate of

hydrolysis, as is generally the case for the polymers and respective sample sizes considered (Shirazi et al., 2016b; von Burkersroda et al., 2002).

The chapter is structured as follows: an existing chain scission model is first described and subsequently modified to include reaction kinetics (Kinetic Scission Model, KSM). The included kinetics are based upon an existing model where ester bonds concentrations are predicted by solving coupled ordinary differential equations (ODEs), referred to as the Kinetic ODE Model (KOM). This KSM enables the number of mid- and end-chain scissions to be calculated and performed discretely on an ensemble of polymer chains and predicts the evolution of the molecular weight distribution with time. Based on the learnings from the KSM, improvements to the KOM are proposed and comparisons are made with this New Kinetic ODE Model (NKOM). The results obtained are quantitatively compared to and calibrated with existing experimental data for amorphous PLGA films (Shirazi et al., 2014). The effects of excluding various lengths of oligomers from calculations of molecular weight and varying the initial acid end concentration are explored. Finally, by incorporating the entropy-spring theory proposed by Wang et al. (2010) into the scission model, Young's modulus is estimated from the molecular weight distributions obtained.

4.2 Kinetic Scission Model (KSM)

4.2.1 Previous scission model

In the current section, the chain scission model, as proposed by Wang et al. (2010), is described together with the numerical implementation by Shirazi et al. (2016b). In order to model the effect of ester bond cleavages on the molecular weight distribution caused by hydrolysis, a microscale model of polymer chain scissions was developed and implemented in MATLAB® (R2019a, The MathWorks, Inc., MA, USA). Scissions were performed at random on the polymer chains, with both mid- and end-chain scissions considered. End scissions reflected the final ester bond in a chain being broken, with a monomer being formed, while a mid-chain scission broke a bond selected at random, resulting in two shorter chains (Fig. 4.1a). This process was carried out as follows and as summarised in the flowchart in Fig. 4.2:

1. To begin, GPC data obtained by Shirazi et al. (2014) for PLGA 50:50 was used to generate an initial representative polymer system and each of the initial chain lengths were stored in an array.
2. The molar number of scissions to be performed in a step, S_{tot}, was calculated as

$$S_{tot} = S_{end} + S_{mid} \tag{4.2}$$

where S_{end} $(\mathrm{mol\ m^{-3}})$ and S_{mid} $(\mathrm{mol\ m^{-3}})$ are the molar number of end- and mid-chain scissions in a step, respectively, described below, and used to determine the total number of scissions to perform in a step throughout the system.

3. The i^{th} type of scission to be performed was chosen by first selecting a randomly generated number, r_i, on the interval (0,1); when $r_i \leq \frac{S_{end}}{S_{tot}}$, an end scission was performed. Otherwise, a mid-chain scission was executed.

4. Based on the outcome of Step 3, bond scissions were simulated. Chains were indexed from 1 to N_c, where N_c is the total number of chains. Before each end-chain scission, a chain index was chosen at random. An end scission was performed on the chosen chain, reducing the chain length by 1, with a monomer removed from the chain and stored separately. For a mid-chain scission, a bond was chosen at random from the total number of mid-chain bonds in the system. The index of the chain containing this bond was determined and the chosen bond was removed, with the two resulting chain lengths stored in the array.

5. Steps 3 – 4 were repeated until S_{tot} scissions had been performed. The simulation then returned to Step 2, continuing until the system of chains had been broken down completely.

It should be emphasised that for the mid-chain scission process described in Step 4, a bond was randomly chosen from all those available in the system, as opposed to randomly choosing a chain first, and then selecting a bond from that chain. For the former method, all bonds have an equal chance of being chosen; without experimental evidence to suggest that chains of a certain length are favoured by the scission mechanism, this is assumed to be correct. In contrast, for the latter method, all chains would have an equal chance of being selected, with a bond in a short chain having a greater chance of being chosen than a bond in a long chain, e.g., a chain of length 100 has the same chance of being selected as a chain of length 1000, but there are 10 times more bonds available to break in the longer one. Previous scission models kept S_{end} and S_{mid} fixed throughout the simulation (Gleadall and Pan, 2013; Shirazi et al., 2016b; Wang et al., 2010), making it difficult to relate results to time, with degradation being a non-linear process. To overcome this, we update the model to allow S_{end} and S_{mid} to vary during the simulation, as described in the following section.

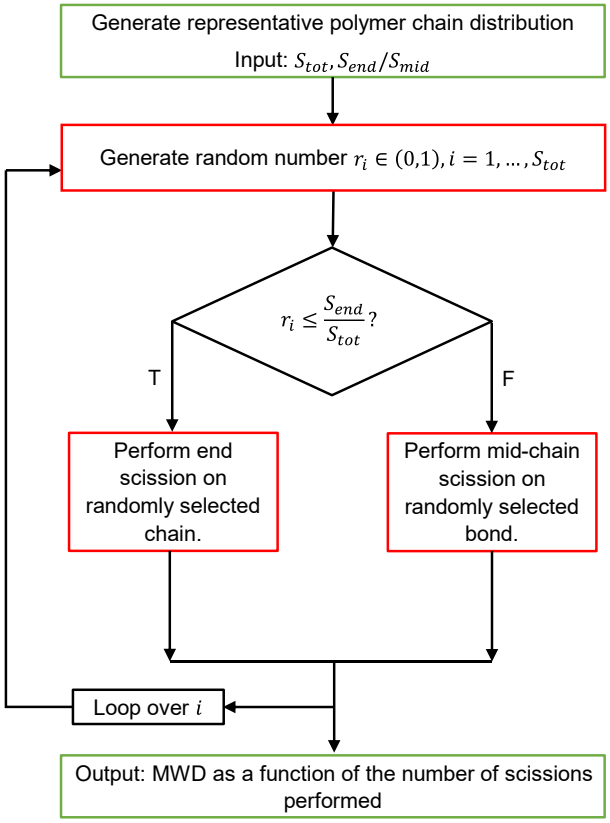

Fig. 4.2. Flowchart detailing the scission model implementation of Shirazi et al. (2016b). S_{tot} is the total number of scissions to be performed and S_{end}/S_{mid} is the proportion of end to mid-chain scissions.

4.2.2 Proposed time-dependent model

Here, the previous scission model is combined with a modified version of the kinetic phenomenological model of Wang et al. (2008) to determine the rates of mid- and end-chain scission. This development provides the following advantages: (i) the kinetics are updated to account for autocatalysis due to acidic chain ends created via all chain cleavages, rather than monomers alone as done previously; (ii) complete molecular weight distributions are considered and tracked as chains are randomly cleaved; (iii) mid-chain scissions reduce the ester bond concentration; (iv) average molecular weights are calculated using the distributions; and (v) the kinetics are directly calculated within the scission model, providing a direct time-dependence and preventing the need for coupling of models.

Wang et al. (2008) proposed the following system of reaction-diffusion equations, referred to as the kinetic ODE model (KOM) in this work, to model the degradation kinetics of bioresorbable polyesters due to both simple hydrolysis and autocatalysis:

$$\frac{\partial C_e}{dt} = -(k_h C_e + k_a C_e C_m^n) \tag{4.3}$$

$$\frac{\partial C_m}{dt} = k_h C_e + k_a C_e C_m^n + \nabla \cdot (D \nabla C_m) \tag{4.4}$$

where C_e $(\mathrm{mol\ m^{-3}})$ is the concentration of ester bonds, C_m $(\mathrm{mol\ m^{-3}})$ is the concentration of monomers, k_h $(\mathrm{day^{-1}})$ and k_a $((\mathrm{m^3 mol^{-1}})^n\ \mathrm{day^{-1}})$ are reaction rate constants for simple hydrolysis and autocatalysis respectively, and n is an acid dissociation constant, often taken to be 0.5 (Lyu et al., 2007; Siparsky et al., 1998). The last term in Eq. (4.4) takes the diffusion of monomers in the system into account; in the current work, we restrict our focus to the reaction mechanism and the implications of this are discussed below. As water is assumed to be abundant, its concentration does not appear in Eqs. (4.3)-(4.4); this assumption remains throughout this work.

For a system experiencing degradation via both mid- and end-chain scissions, each ester bond cleavage reduces the ester bond concentration and simultaneously increases the concentration of acid ends, with each scission resulting in an additional carboxylic acid end (Ginjupalli et al., 2017). However, Eqs. (4.3)-(4.4) are representative of a system where each ester bond cleavage increases the monomer concentration in the system; i.e., all scissions are, in effect, end scissions. Our proposed model expands on this by replacing C_m with C_a $(\mathrm{mol\ m^{-3}})$, the concentration of carboxylic acid ends, in Eqs. (4.3)-(4.4). Incorporating this dependence ensures all acid ends contribute to autocatalysis within the system, rather than monomers alone.

Eqs. (4.3)-(4.4) are redefined in terms of the molar number of mid-chain scission, S_{mid}, and end scission, S_{end}, with each scission reducing C_e and simultaneously increasing C_a in the system:

$$\frac{dC_e}{dt} = -\left(\frac{dS_{mid}}{dt} + \frac{dS_{end}}{dt}\right) \tag{4.5}$$

$$\frac{dC_a}{dt} = \frac{dS_{mid}}{dt} + \frac{dS_{end}}{dt} \tag{4.6}$$

The diffusive flux of monomers through the system captured in Eq. (4.4) is not included in Eq. (4.6). This flux can be included in the future, however, Eq. (4.6) would need to be modified to consider mobile acid ends, C_m, separately from acid ends attached to long chains that cannot readily diffuse; the alternative description of the updated kinetics presented in

Section 4.5 ensures this can be achieved. Assuming there is no such diffusive flux is reasonable for larger samples that experience heterogeneous bulk degradation, where autocatalysis is the dominant mechanism and monomers initially remain trapped in the system (Vey et al., 2008); see a detailed explanation by Shirazi et al. (2016b). Both the size of the sample and the surface area will affect the impact of diffusion of monomers and subsequent degradation. However, without detailed experimental data to inform what the diffusion coefficient is throughout degradation for the materials of interest here, this would be an additional parameter to calibrate and thus add uncertainty; as a result, it was excluded from the current focus. This reformulation and simplification removes the spatial gradient included in Eqs. (4.3)-(4.4); thus, the method proposed cannot readily describe differences in degradation throughout a sample according to its spatial location (e.g., at the centre, near the surface, etc.) and effectively considers a representative volume element (RVE). Going forward, several RVEs could be considered in parallel using a modified KSM that includes a spatial element to incorporate size effects.

A further modification distinguishes between the concentration of ester bonds at the end of chains, $C_{e,end}$ $(\mathrm{mol\ m^{-3}})$, and that of the remaining, mid-chain bonds, $C_{e,mid}$ $(\mathrm{mol\ m^{-3}})$, somewhat similarly to that done by Gleadall et al. (2014b). This allows the rates of mid- and end-chain scission to be calculated as follows:

$$\frac{dS_{mid}}{dt} = k_{hm}C_{e,mid} + k_{am}C_{e,mid}C_a^n \tag{4.7}$$

$$\frac{dS_{end}}{dt} = k_{he}C_{e,end} + k_{ae}C_{e,end}C_a^n \tag{4.8}$$

The simple hydrolytic reaction generates mid- and end-chain scissions according to k_{hm} $(\mathrm{day^{-1}})$ and k_{he} $(\mathrm{day^{-1}})$, respectively. Similarly, the autocatalytic reaction rates, k_{am} $((\mathrm{m^3 mol^{-1}})^n\ \mathrm{day^{-1}})$ and k_{ae} $((\mathrm{m^3 mol^{-1}})^n\ \mathrm{day^{-1}})$, govern the rate at which mid- and end-chain scissions, respectively, occur due to autocatalysis.

Returning to Step 2 of the scission model outlined in Section 4.2.1, at the beginning of each step, the molar number of scissions to be performed in that time-step, split between mid-chain scissions and end-chain scissions can be calculated as

$$S_{mid} = \left(k_{hm}C_{e,mid} + k_{am}C_{e,mid}C_a^n\right)\Delta t \tag{4.9}$$

$$S_{end} = \left(k_{he}C_{e,end} + k_{ae}C_{e,end}C_a^n\right)\Delta t \tag{4.10}$$

where the values of $C_{e,mid}$, $C_{e,end}$ and C_a are updated at the start of each step, and Δt is the time increment. In practice, $\Delta t \approx 0.04\ \mathrm{day}^{-1}$ (24 steps per day) was found to provide good precision (see Fig. 4A. 1, Fig. 4A. 2). Applying the KSM until the polymer chains have broken down completely results in evolving molecular weight distributions (MWDs) as a function of degradation time. This significant contribution ensures a more complete prediction of the polymer microstructure as degradation takes places, providing details of a representative distribution of polymer chain lengths and their evolution throughout degradation.

4.2.3 Calculating average molecular weights

To calculate values of the average molecular weight using Eqs. (4.3)-(4.4) alone, Wang et al. (2008) assumed the ester bond concentration, C_e, and an average molecular weight, M_e, could be related as follows:

$$\frac{M_e}{M_{e0}} = \frac{C_e}{C_{e0}} \tag{4.11}$$

where M_{e0} and C_{e0} are the initial values of average molecular weight and ester bond concentration, respectively. Here, we refer to this average value as M_e to avoid confusion between alternative average values. Monomers are too small to be detected experimentally using standard measuring methods, and as such are excluded from the calculation in Eq. (4.11). Average molecular weights are hugely dependent on the number of chains in the system, which this relationship fails to capture; as such, Eq. (4.11) should be used with caution, as seen in Section 4.3.

As the scission model provides insight on the overall MWD as degradation proceeds, more conventional predictions for the average molecular weight can be obtained. For example, the number average molecular weight, M_n $(\mathrm{g\ mol}^{-1})$, can be calculated as

$$M_n = \frac{\sum_{i=1}^{N_c} N_i M_i}{\sum_{i=1}^{N_c} N_i} \tag{4.12}$$

where N_c is the total number of chains and N_i is the number of polymer chains of weight M_i $(\mathrm{g\ mol}^{-1})$. Additionally, the weight average molecular weight, M_w $(\mathrm{g\ mol}^{-1})$, can be calculated as

$$M_w = \frac{\sum_{i=1}^{N_c} N_i M_i^2}{\sum_{i=1}^{N_c} N_i M_i} \tag{4.13}$$

As short, water-soluble chains or oligomers may be immeasurable by standard experimental methods, removing these from calculations may provide more meaningful comparison of results with experimental data. To account for this, chains of length L_{ol} and below were excluded from the calculations of M_n and M_w, where various values of L_{ol} were chosen to encompass those suggested in literature (Buchanan, 2008; Vey et al., 2008).

4.2.4 Solution approach

The solution approach is carried out as follows, with the main steps summarised in the flowchart in Fig. 4.3:

- An array of chains was considered, representative of amorphous PLGA 50:50 prior to degradation based on experimental data obtained by Shirazi et al. (2014).
- A step-size for the KSM was chosen (24 steps per day, $\Delta t \approx 0.04\ \mathrm{day}^{-1}$), with temporal convergence checked (see Fig. 4A. 1, Fig. 4A. 2).
- The molar reaction rates ($k_{hm}, k_{am}, k_{he}, k_{ae}$), initial molar concentration of ester bonds ($C_{e0} = 17300\ \mathrm{mol\ m^{-3}}$ (Wang et al., 2008)) and acid dissociation constant ($n = 0.5$ (Siparsky et al., 1998)) were input. The size of the system, φ, was calculated by scaling the total number of ester bonds in the generated chain array, N_{e0}, with C_{e0}: $\varphi = N_{e0}/C_{e0}$. Then, the initial molar concentration of ester bonds at the end of chains $C_{e0,end} = 2N_c/\varphi$, and that of mid-chain bonds $C_{e,mid} = (N_{e0} - 2N_c)/\varphi$, where N_c is the number of generated chains. The initial molar carboxylic acid concentration was either input (e.g., $C_{a0} = 0\ \mathrm{mol\ m^{-3}}$) or calculated (e.g., $C_{a0} = N_c/\varphi$).
- In each step, the number of mid- and end-chain scissions to be performed was calculated using Eqs. (4.9)-(4.10) and scaled to account for the size of the system, and scissions were then carried out as described in Section 4.2.1. The array was set-up to track the evolution of each individual chain during the scission process, and stored information on all chain lengths; this provided the molecular weight distributions, from which average molecular weights were obtained. Fig. 4.4 shows a random sample of 25 initial chains at various stages of the simulation, with each section of a stacked bar representative of a fragmented piece of that parent chain created via scission.
- Various reaction rates were explored by choosing incremental values and the coefficient of determination, r^2, was calculated for each iteration using an

orthogonal regression following the approach of Shirazi et al. (2016b); see Section 2.4.1 for more details. The reaction rates were first calibrated to fit predictions for M_e to the experimental data of Shirazi et al. (2014) for M_n (Section 4.3), determining the values that maximised r^2; these were then recalibrated when predictions for M_n were considered (Section 4.4), highlighting the discrepancy between these properties.

- These results were explored further and compared to experimental data (Shirazi et al., 2014) in the context of examining the effect of L_{ol} on M_n and M_w. In these simulations, a scission resulting in a chain of length i, where $i \leq L_{ol}$, was assumed to instantly dissolve to form i monomers and was updated in the array accordingly.
- The initial carboxylic acid end concentration, C_{a0}, was varied to examine the effect end-capping has on M_n and M_w during degradation (Section 4.5).
- Finally, the previously calibrated values were used when examining changes in Young's modulus during degradation, described in Section 4.6.

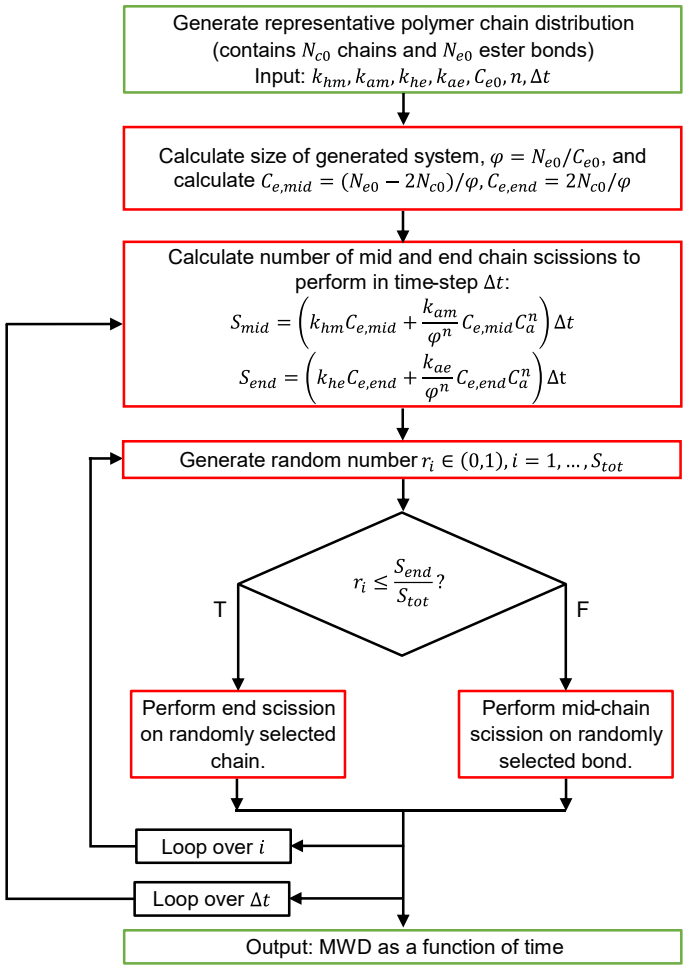

Fig. 4.3. Flowchart outlining the main processes of the kinetic scission model.

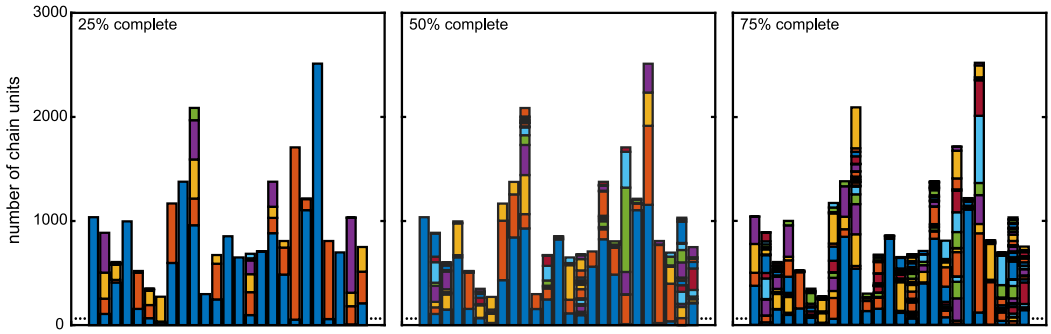

Fig. 4.4. A sample of 25 initial chains (from ~24000) at various stages of the simulation. Each bar corresponds to one initial chain, with each coloured section representative of a fragmented piece of the chain created via scission. Chains are initially coloured arbitrarily; however, the colouring of specific chain fragments remain fixed throughout the figure with the larger of the child fragments retaining the parent colour.

4.2.5 Calibration of model

For all simulations, the acid dissociation constant, n, was taken to be 0.5, based on that described in literature (Lyu et al., 2007; Siparsky et al., 1998). The reaction rate constants, k_{he}, k_{ae}, k_{hm} and k_{am}, were calibrated to fit the experimental data of Shirazi et al. (2014), which examined the evolution of molecular weight and Young's modulus for amorphous PLGA (50:50) films (with a thickness of 250 μm) degraded in a phosphate buffer solution, pH 7.4, at 37°C. This calibration was carried out by calculating the coefficient of determination, r^2, for a range of reaction rates and parameters that maximised r^2 were chosen. In Section 4.3, it was assumed that end scissions were dominant, with $k_{hm} = k_{am} = 0$, to compare different average molecular weight calculations using assumptions from previous models (Shirazi et al., 2016b; Wang et al., 2010, 2008). From Section 4.4 onwards, without comprehensive experimental evidence to suggest either scission mechanism is dominant for this material (or in what proportion), it was assumed that both mid- and end-chain scissions were equally likely, with $k_{hm} = k_{he}$ and $k_{am} = k_{ae}$. The reaction rates are taken to be constants, as in previous work (Shirazi et al., 2016b; Wang et al., 2008), with changes in the rate of degradation instead captured by the evolution of C_e and C_a. It should be noted that the calibrated parameters indicate the predictive capability of the model but may not uniquely optimise r^2 and a more robust material characterisation would be necessary for further analysis. Finally, the calibration assumed that the maximum length of short chains $L_{ol} = 1$, and the initial carboxylic acid end concentration $C_{a0} = 0$, representative of an ester-capped system, as outlined in the Discussion; the effect of varying these is explored.

4.3 Comparison between the previous Kinetic ODE Model (KOM) & the newly proposed KSM

This section explores how the newly proposed kinetic scission model (KSM) compares with solutions obtained using the previous kinetic ODE model (KOM) alone. This is completed in three steps, as summarised in Fig. 4.5:

1. The KSM is first calibrated to fit predictions for M_e to experimental data for M_n (Shirazi et al., 2014).
2. Then, predictions obtained using the KOM outlined in Eqs. (4.3)-(4.4) are compared with those of the KSM.
3. Finally, alternative methods of calculating average molecular weight are compared using the KSM.

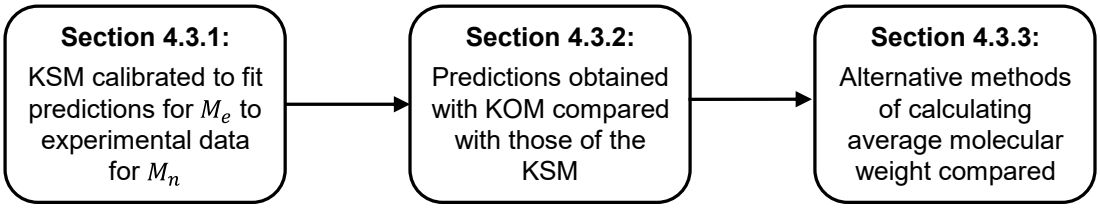

Fig. 4.5. Overview of the steps carried out in this section.

4.3.1 KSM: degradation via end scissions and simplified molecular weight predictions

To begin, the KSM was calibrated to fit predictions for M_e to experimental data for M_n (Shirazi et al., 2014). The KSM was used to track the evolution of an ensemble of polymer chains, as described. In order to compare the KSM with the KOM, rate constants were chosen such that only end scissions were permitted ($k_{hm} = k_{am} = 0$), with each scission increasing the monomer concentration. Additionally, the KOM calculates M_e, which effectively only considers a reduction in molecular weight caused by end scissions.

The remaining reaction rates, k_{he} and k_{ae}, were chosen to optimise r^2 for M_e with experimental data for M_n (Shirazi et al., 2014). A good fit was found when $k_{he} = 7.20\ \mathrm{day}^{-1}$ and $k_{ae} = 8.84 \times 10^{-1}\ (\mathrm{m^3 mol^{-1}})^{1/2}\ \mathrm{day}^{-1}$, giving $r^2 = 0.9695$ (Fig. 4.6a, dashed line). Additionally, the maximum oligomer length $L_{ol} = 1$, again chosen for comparison with previous assumptions, where only monomers were excluded from calculations.

4.3.2 KOM: degradation via end scissions and simplified molecular weight predictions

Next, predictions obtained using the KOM outlined in Eqs. (4.3)-(4.4) are compared with those of the KSM. Predictions for M_e, as described by the ODEs of Wang et al. (2008), were obtained by solving Eqs. (4.3)-(4.4) using the in-built ode45 solver in MATLAB® (R2019a, The MathWorks, Inc., MA, USA), a single step-solver based on an explicit Runge-Kutta (4,5) formula with an adaptive step-size (outlined in Section 2.4.1). The initial concentrations matched that of the initial chain array used for the KSM, with $C_{e0} = 17300\ \mathrm{mol\ m^{-3}}$ (Wang et al., 2008) and $C_{m0} = 0$. The solution obtained provided predictions of how the ester bond concentration, C_e, within the polymer system evolved with time, which could then be related to M_e using Eq. (4.11) (Fig. 4.6a, solid line). The parameters were held consistent with those calibrated above, with the reaction rates scaled as follows:

$$k_h = \frac{k_{he} C_{e,end0}}{C_{e0}}, k_a = \frac{k_{ae} C_{e,end0}}{C_{e0}} \tag{4.14}$$

to factor in the modification in the KSM that distinguishes between the concentration of ester bonds at the end of chains. As seen in Fig. 4.6a, the KOM solution agreed with that of the KSM initially but departed from it by Day 3. At this point, chains containing one remaining bond that are broken in the KSM result in the addition of two new acid ends and can further accelerate the reaction. This cannot be captured by the KOM, resulting in a slower decline in C_e for that method. Thus, while the KOM can capture some changes, it is less reliable when short chains are present.

4.3.3 KSM: degradation via end scissions and conventional molecular weight predictions

Alternative methods of calculating average molecular weight are now compared using the KSM. With the KSM, we also obtain evolving MWDs (Fig. 4.6b), displayed as a function of the number of chains here. The initial distribution was generated based on the experimental study of Shirazi et al. (2014). After 5 days, the distribution had broadened, with chains gradually shortening. As shorter chains were broken down completely through the unzipping of chain ends, the number of chains remaining in the system declined, and the peak height reduced. The right-hand limits of the distributions experienced minimal change during this period. The corresponding values of M_e, M_n and M_w, obtained using Eqs. (4.11)-(4.13)

respectively, are highlighted on each MWD in Fig. 4.6b, where M_{n0} was used to initialise M_e. While M_e gradually declined, both M_n and M_w increased.

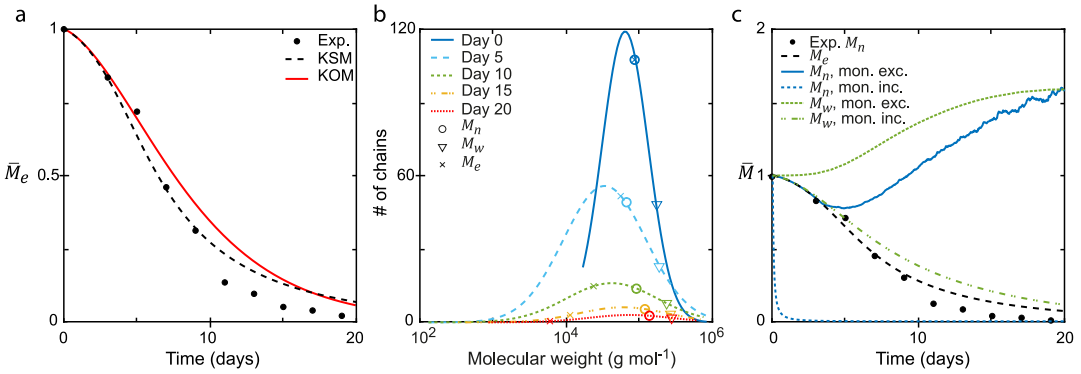

Fig. 4.6. (a) Comparison of predictions obtained for M_e (normalised as in Eq. (4.11)) by the KSM (only end scissions, $k_{hm} = k_{am} = 0$, dashed line) and by the numerical KOM (solid line) using consistent rate constants with experimental data for M_n (Shirazi et al., 2014). Predictions appear poorer towards the final timepoints due to the optimisation approach used, r^2 via orthogonal regression; by instead considering the relative error when comparing predictions with experimental data, the optimal parameters may give an improved fit at the later stages, at the expense of the earlier timepoints. This tail off in the strength of the prediction at later timepoints may also be due to the effects of diffusion and mass loss that are not included in the framework. (b) Evolving molecular weight distributions (lines), indicating the number of chains as degradation occurs as predicted by the KSM, showing the average molecular weight as calculated using the number average, M_n (○), weight average, M_w (▽), and as by Wang et al. (2008), M_e (×). (c) Although, using the KSM, the average molecular weight, M_e, (dashed black line) agrees approximately with experimental data, an increase is observed for both the number average molecular weight, M_n, (solid blue line) and weight average molecular weight, M_w, (dashed green line) when monomers are excluded from calculations, in disagreement with experimental observations (Shirazi et al., 2014) (which are shown for M_n; a similar trend is seen for M_w (see Fig. 4.7c)). Including monomers in the calculations results in a rapid decline for M_n (dashed blue line), while predictions for M_w (dash-dotted green line) are now similar to that seen experimentally. All molecular weight quantities are normalised by their initial values, denoted by the overbar.

Predictions for the various average molecular weights, as obtained previously, are presented in Fig. 4.6c as a function of degradation time. Initially, M_n followed the same trend as seen for M_e when monomers were excluded from calculations. However, after approximately 3 days an unphysical shift was seen, where the predicted value increased; again, this coincided with the complete depolymerisation of some of the initially shorter chains. A similar increase was predicted for M_w, despite the similar decreasing trend observed for both experimentally. Additionally, we see that including monomers in the calculations resulted in an instant significant decline for M_n as monomers quickly built up due to end scissions, while M_w now appears similar to the experimental data. Although the average molecular weight

described by Wang et al. (2008), M_e, captures both data approximately, M_n and M_w are not representative of the data when explored using the KSM for end scissions only. Thus, while M_e quantifies some changes in the MWD, the conventional predictions provided by the KSM provide a more in-depth description and mimic the approach of experimental calculations. In the following section, the KSM is recalibrated against experimental data for degradation (Shirazi et al., 2014) via both mid- and end-chain scissions.

4.4 Mid- and end-chain scission model

Building from the previous section, mid-chain scissions are now included in the KSM; this is accounted for by removing the restriction in the previous section that set $k_{hm} = k_{am} = 0$. Evolving MWDs are presented and the effect of varying the maximum length of water-soluble chains, L_{ol}, is explored. Without consistent experimental evidence to suggest either scission mechanism is dominant for this material, it was assumed that both mid- and end-chain scissions are equally likely, with $k_{hm} = k_{he}$ and $k_{am} = k_{ae}$.

4.4.1 Evolving molecular weight distributions

The KSM was recalibrated when both mid- and end-chain scissions were performed, with the coefficient of determination optimised for predictions for M_n with experimental data (Shirazi et al., 2014). Resulting predictions for the evolving MWDs are shown in Fig. 4.7a ($L_{ol} = 1$). The distributions gradually shift to the left, with minimal change to the broadness. When the distributions were normalised to peak height and compared with experimental data (Shirazi et al., 2014), similar trends were seen (Fig. 4.7b). However, by Day 19 the experimental distribution had broadened, which is not well captured by the predictions here. Removing oligomers below some critical length from the calculations, representing those undetected experimentally, varies the distributions obtained, resulting in a more accelerated degradation profile (Fig. 4.7b). When $L_{ol} = 15$, the later stages of degradation are better captured.

4.4.2 Predictions for average molecular weights

Using the MWDs obtained, predictions for the evolution of the number average molecular weight, M_n, and the weight average molecular weight, M_w, were found using Eqs. (4.12)-(4.13). In contrast to the increase seen previously for end scissions only, a good fit was found between the predicted values and experimental data when $L_{ol} = 1, k_{he} = k_{hm} = 1 \times 10^{-7}\ \text{day}^{-1}$ and $k_{ae} = k_{am} = 9.2 \times 10^{-5}\ \left(\text{m}^3\text{mol}^{-1}\right)^{1/2}\text{day}^{-1}$ ($r^2 = 0.9075$) (Fig. 4.7c); these are several orders of magnitude smaller than the previously calibrated values in

Section 4.3 ($k_{he} = 7.20\ \text{day}^{-1}$ and $k_{ae} = 8.84 \times 10^{-1}\ (\text{m}^3\text{mol}^{-1})^{1/2}\ \text{day}^{-1}$), where higher reaction rates were necessary due to only end scissions taking place, with individual end scissions having minimal impact on the molecular weight. Now that mid-chain scissions are also incorporated in the scission model, the gradual decline in these properties seen experimentally is successfully captured. Results are shown for various values of L_{ol} (Fig. 4.7c), with increasing values further accelerating the decline in $M_n$and M_w due to their contribution towards the concentration of acid ends, C_a, as it was assumed that they instantly broke down into their monomeric form.

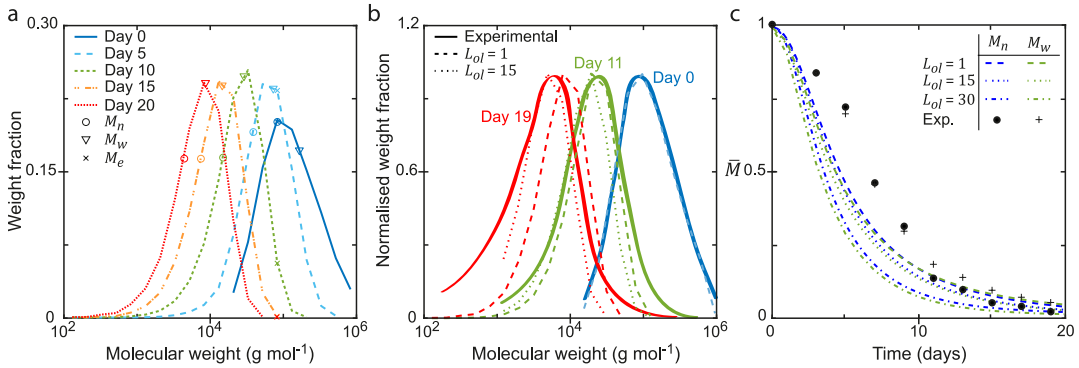

Fig. 4.7. (a) Evolving molecular weight distributions (lines) as degradation occurs showing M_n (○), M_w (▽) and M_e (×) (where M_{e0} is taken to be M_{n0}) when $k_{he} = k_{hm} = 1.0 \times 10^{-7}\ \text{day}^{-1}$, $k_{ae} = k_{am} = 9.2 \times 10^{-5}\ \left(\text{m}^3\text{mol}^{-1}\right)^{1/2}\text{day}^{-1}$ and $L_{ol} = 1$. (b) Normalised molecular weight distributions compared with experimental data (Shirazi et al., 2014) for varied values of L_{ol}. (c) Comparison of M_n and M_w (normalised by their initial values) to experimental data (Shirazi et al., 2014) for various values of L_{ol}.

4.5 New Kinetic ODE Model (NKOM) and effect of initial carboxylic acid concentration

The previous sections have shown that deviations exist between predictions obtained from the KSM and KOM. Furthermore, the KOM is unable to capture the effect of mid-chain scissions. Thus, an updated, new kinetic ODE model (NKOM) is now presented that captures the same mechanisms as the KSM. While the KSM simulates degradation on a complete representative molecular weight distribution, the NKOM predicts the evolution of C_e and C_a based on initial concentrations and reaction rates and can be used to calculate M_n.

The NKOM is described by the following ODEs:

$$\frac{dC_{e,mid}}{dt} = -3\frac{dS_{mid}}{dt} - \frac{dS_{end}}{dt} \tag{4.15}$$

$$\frac{dC_{e,end}}{dt} = 2\frac{dS_{mid}}{dt} \tag{4.16}$$

$$\frac{dC_a}{dt} = \frac{dS_{mid}}{dt} + \frac{dS_{end}}{dt} \tag{4.17}$$

where $\frac{dS_{mid}}{dt}$ and $\frac{dS_{end}}{dt}$ are described by Eqs. (4.7)-(4.8), respectively. Eqs. (4.15)-(4.16) describe each mid-chain scission removing one ester bond from the middle of a chain and transforming the two adjacent bonds to end bonds, and each end scission removing an end bond and simultaneously transforming the adjacent bond to an end bond (Fig. 4.8). Note that these equations are only valid for long chains; this is one of the disadvantages of using a kinetic model alone.

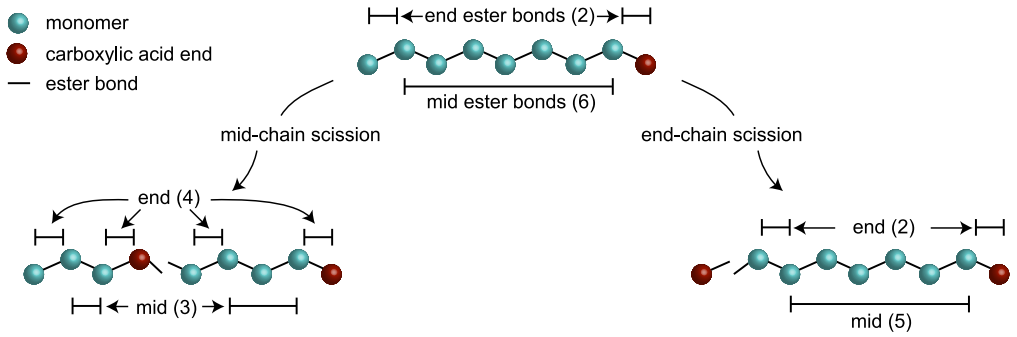

Fig. 4.8. Schematic detailing the form of Eqs. (4.15)-(4.17). Each mid-chain scission removes one ester bond from the middle of a chain, transforms the two adjacent bonds to end bonds, and creates a carboxylic acid end. Each end scission removes an end bond and simultaneously transforms the adjacent bond to an end bond, while creating a carboxylic acid end.

Solving the ODEs (4.15)-(4.17) provides predictions for the evolution of C_e and C_a, whereas simulating degradation on an ensemble of polymer chains using the KSM offers greater insight into the evolution of the polymer molecular weight distribution. However, predictions for number average molecular weight can be obtained as follows:

$$M_N = \frac{\left(C_{e,mid} + C_{e,end}\right)M_0}{C_{e,end}/2} \tag{4.18}$$

where M_0 $(\mathrm{g\ mol^{-1}})$ is the molar mass of a single repeat unit, and the subscript is capitalised to differentiate between the calculation in Eq. (4.12). However, Eq. (4.18) assumes only monomers are not captured using GPC; oligomers cannot be excluded from calculations, with no information on evolving chain lengths. While the KSM remains more robust, the NKOM is

more readily solved and can explore, for example, the effect of reaction rates or initial concentrations on M_N, prior to a more in-depth exploration using the KSM.

4.5.1 Varying the initial carboxylic acid end concentration

The KSM and NKOM are now used to explore the effect of varying the initial acid end concentration, C_{a0}, providing a comparison between the solutions for both. The initial conditions for the NKOM are held consistent with the polymer chain ensemble used in the KSM.

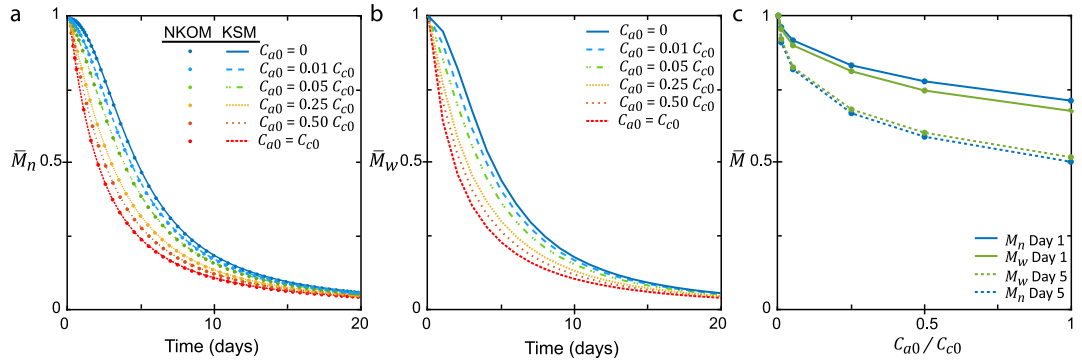

Fig. 4.9. (a) Predictions obtained using the KSM (lines) for M_n (Eq. (4.12)) and the NKOM (markers) for M_N (Eq. (4.18)), normalised by initial value, as a function of degradation time for various values of initial carboxylic acid end concentration, C_{a0}, ranging from 0 to C_{c0}, the initial molar concentration of chains in the system, when $k_{he} = k_{hm} = 1.0 \times 10^{-7}$ day^{-1}, $k_{ae} = k_{am} = 9.2 \times 10^{-5}$ $\left(\text{m}^3\text{mol}^{-1}\right)^{1/2}$day^{-1} and $L_{ol} = 1$. As C_{a0} increases, the predictions gradually change from an S-shaped curve, with the initial days of degradation showing a more abrupt decline due to the increased number of carboxylic acid ends available to catalyse the reaction. (b) The effect of varying the initial carboxylic acid end concentration on M_w, obtained using the KSM. (c) Predictions for M_n and M_w at Days 1 and 5, normalised by the corresponding values when $C_{a0} = 0$, as a function of C_{a0}/C_{c0}, highlighting the impact this property has on the initial days of degradation. The dots represent simulated predictions.

As the experimental data (Shirazi et al., 2014) considered here did not specify the initial end group of the polymer used, an ester capped system was assumed up to now ($C_{a0} = 0$), with reports that these are more appropriate for medical devices (Sigma-Aldrich, n.d.). Keeping all other parameters constant, the effect of various values of C_{a0} on the degradation behaviour was explored. Values ranging from 0, representative of a system where each chain was initially capped, to C_{c0}, the initial molar concentration of chains in the system where each chain was initially acid terminated, were considered. For increasing values of C_{a0} both M_n and M_w declined more abruptly in the initial days of degradation due to the increased number of carboxylic acid ends available to catalyse the reaction (Fig. 4.9). After Day 1, M_n had reduced by more than 25% for a system where all chains were initially acid terminated

($C_{a0} = C_{c0}$) compared to that where $C_{a0} = 0$, and this had jumped to an almost 50% difference after Day 5 of the simulation (Fig. 4.9c). This effect reduced over time, with predictions converging as degradation progressed. The lines in Fig. 4.9a were obtained using the KSM, while the solutions obtained using the NKOM are denoted with markers, highlighting the agreement between these two methods. However, unlike the KSM, the NKOM is unable to offer insight into M_w.

4.6 Young's modulus

The KSM described above can be extended to estimate Young's modulus of the system. Wang et al. (2010) developed an entropy-spring theory for amorphous bioresorbable polymers based on the relationship between Young's modulus and the number of polymer chains per unit volume. They proposed that the entropic elasticity of the system is not significantly altered by isolated chain scissions; rather, it is suggested that a critical molecular weight exists for a chain, below which the chain has deteriorated to the point of no longer contributing to the entropy and thus the Young's modulus of the material. Thus, Young's modulus ($\bar{E}$), normalised at $t = 0$, can be calculated as follows:

1. Each initial chain and its resulting sub-chains created by scissions form one of N_{c0} groups, where N_{c0} is the initial number of chains in the system; M_w is calculated for each individual group. (Each bar in Fig. 4.10 is representative of a group and corresponds to a row in the sample array.)
2. Once $M_w < M_w^{crit}$ for a group, where M_w^{crit} is a specified critical molecular weight, the group no longer contributes to the calculation of $\bar{E}$ and is excluded from $N_{c>M_w^{crit}}$, the number of chain groups above the molecular weight threshold (Fig. 4.10).
3. Then, Young's modulus can be related to $N_{c>M_w^{crit}}$ as follows:

$$\bar{E} = \frac{N_{c>M_w^{crit}}}{N_{c0}} \tag{4.19}$$

The weight average molecular weight, M_w, is chosen here to better capture any remaining longer chains that may have a more pronounced effect on stiffness. Scissions were performed until sufficient degradation had taken place ($\bar{E} < 0.05$).

The temporal evolution of E is obtained directly from the KSM using this approach due to the time-dependence introduced in the model. In contrast, the previous work (Shirazi et al., 2016b; Wang et al., 2010) obtained E as a function of M_n ($E = f(M_n)$) using a scission model

and coupled this with temporal predictions of M_e ($M_e = g(t)$) obtained using a kinetic model to provide E as a function of time. However, M_e and M_n are different properties, with the former being a measure of bonds remaining in the system and the latter the mean mass of polymer chains. Thus, this proposed approach provides more physically based predictions.

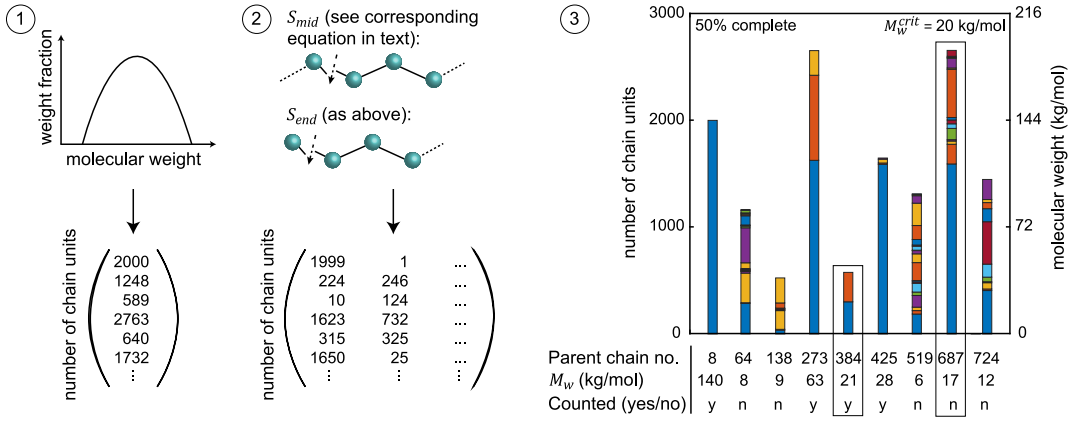

Fig. 4.10. Schematic illustration of kinetic scission model and calculation of $N_{c>M_w^{crit}}$. As detailed in the text, a representative polymer chain distribution is considered in the form of an array of chains with a distribution of lengths. Scissions are simulated on the array of chains according to Eq. (4.9) for mid-chain scissions and Eq. (4.10) for end-chain scissions. The updated chain lengths are stored in the array, with each row representing an initial chain and its resulting sub-chains. A sample of 9 initial representative polymer chains (from approximately 24000) are shown halfway through simulated degradation, where each bar represents an initial chain and each coloured fragment represents a sub-chain created via simulated scission. To calculate $N_{c>M_w^{crit}}$, the number of chain groups above a critical molecular weight, M_w^{crit}, each initial chain and resulting sub-chains are taken as an individual group. Once $M_w < M_w^{crit}$ for a group, that group is excluded from the calculation of $N_{c>M_w^{crit}}$; otherwise, the group contributes to the count of $N_{c>M_w^{crit}}$. Note that despite Chain 384 appearing short compared with Chain 687 (and its largest fragment), it is included in the count of $N_{c>M_w^{crit}}$ as it has experienced few scissions and thus has a higher value of M_w than the highly degraded Chain 687.

4.6.1 Results

Using the previously calibrated parameters, where $L_{ol} = 1$, $k_{he} = k_{hm} = 1.0 \times 10^{-7}$ day^{-1}, $k_{ae} = k_{am} = 9.2 \times 10^{-5}$ $\left(\text{m}^3\text{mol}^{-1}\right)^{1/2}$day^{-1} and $C_{a0} = 0$, the effect of various critical molecular weights, M_w^{crit}, on the predictions for Young's modulus was explored. Fig. 4.11a shows the evolution of $\bar{E}$ as a function of degradation time. It is evident that the choice of M_w^{crit} significantly alters the results, with this parameter controlling the point of initial decline in $\bar{E}$.

The relationship between Young's modulus and average molecular weights obtained by the KSM are compared to experimental data in Fig. 4.11b-c. Higher values of M_w^{crit} result in

accelerated decline in $\bar{E}$. These relationships are well captured provided a suitable choice of M_w^{crit} is made.

The model formulation and specifically the "no-rise rule" introduced by Wang et al. (2010) prevents increases in E to be captured. Although increases in E during degradation are typically attributed to changes in crystallinity (Tsuji and Ikada, 1995), the initially amorphous PLGA samples remained amorphous throughout degradation (Shirazi et al., 2014). This increase in stiffness may instead be explained by a more stable chain packing with the introduction of water molecules (Tsuji and Suzuyoshi, 2002). A molecular scale focus would be necessary to consider this level of behaviour; however, as previously mentioned, the computational expense of molecular dynamics prevents the necessary timescales to be explored at present.

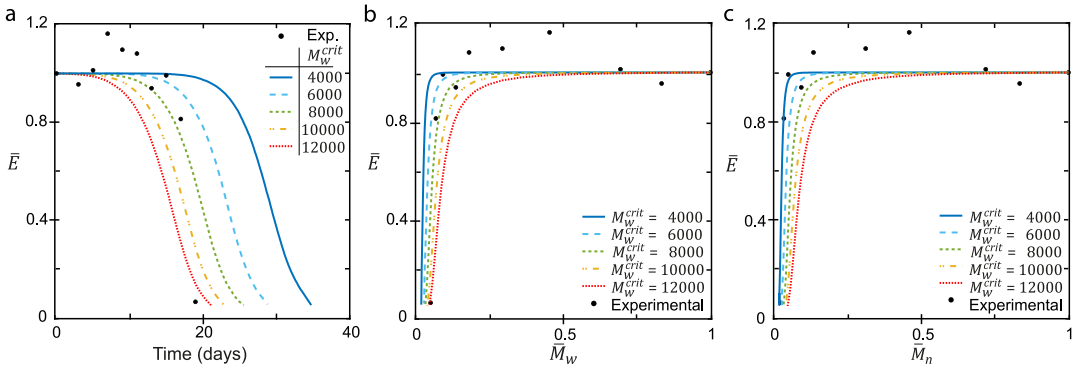

Fig. 4.11. Young's modulus predictions, normalised by its initial value, obtained using the KSM, as a function of (a) degradation duration, (b) M_w and (c) M_n for various values of M_w^{crit} compared with the experimental data of Shirazi et al. (2014). Units for M_w^{crit} are g mol^{-1}.

4.7 Discussion

The current study presents a kinetic scission model (KSM), providing predictions for the evolution of the molecular weight distribution and Young's modulus of amorphous bioresorbable polyesters. This study is motivated by previous work by Pan and co-workers (Gleadall et al., 2014b; Wang et al., 2010, 2008) and Shirazi et al. (2016b). The key modifications presented are as follows: (i) the kinetics are updated to account for autocatalysis due to acidic chain ends created via all chain cleavages, rather than monomers alone as done previously; (ii) complete molecular weight distributions are considered and tracked as chains are randomly cleaved; (iii) mid-chain scissions reduce the ester bond concentration; (iv) average molecular weights are calculated using the full distributions; and (v) the kinetics are directly calculated within the scission model, providing a direct time-dependence and preventing the need for coupling of models.

Results showed that despite assuming no diffusive flux of oligomers from the system existed, the KSM could be suitably calibrated to capture the behaviour seen experimentally. Shirazi et al. (2014) reported no significant mass loss had occurred after approximately 90% reduction in molecular weight, observing a gradual mass loss after this point, reaching 15% after 19 days. This suggests that oligomers created via chain scissions remained trapped in the system for much of the degradation, only slowly diffusing away during the later stages. Based on the analysis provided by Shirazi et al. (2016b), it is expected that a polymer film of this geometry would experience heterogenous bulk degradation, with the effects of autocatalysis dominating any diffusive flux from the system. However, the addition of a diffusive term in Eqs. (4.6) and (4.17) should better reflect the degradation kinetics and be more appropriate for a wider range of geometries.

The incorporation of Eqs. (4.9)-(4.10) into the scission model offers a suitable time-dependence, provided a reasonable time-step is taken and temporal convergence is checked (see Fig. 4A. 1, Fig. 4A. 2). A comparison between the kinetic ODE model (KOM) of Wang et al. (2008) and the KSM revealed agreement in predictions for M_e initially, but a departure from one another by Day 3 of degradation, with this discrepancy due to the inability of the KOM to consider individual chains, and, in particular, short chains (Fig. 4.6a). An updated, new kinetic ODE model (NKOM) is introduced in Section 4.5, describing the kinetics of both mid- and end-chain scissions via hydrolysis and autocatalysis and considering all carboxylic acid ends in the system. Results obtained for M_n from the NKOM and KSM were highly similar (provided end scissions are not the dominant mechanism), where the ode45 solver in MATLAB® (R2019a, The MathWorks, Inc., MA, USA) automatically adapts the step-size when solving the ODEs for the NKOM, and the chosen step-size of 1 hour for the KSM captured this very well (Fig. 4.9a). The NKOM provides predictions for M_n and can offer insight into the effect of varying parameters such as the initial carboxylic acid end concentration, C_{a0}, while the KSM is more rigorous and tracks the entire MWD. The KSM simulation corresponding to the main calibration completed in approximately 3 h on an Intel(R) Core(TM) i7-8565U CPU @ 1.80GHz 1.99 GHz computer with 16GB RAM and a 64-bit operating system (with a stopping criterion when $\bar{E} < 0.05$). In contrast, the NKOM completes in approximately 0.1 s.

The kinetic reaction rates were calibrated for experimental data at 37°C; a fast degradation profile was seen, with samples fully degraded after 19 days. The temperature dependent kinetics for polymers undergoing hydrolysis and autocatalysis is discussed by Han et al. (2010) and Lyu et al. (2007). The calibrated parameters here primarily suggest autocatalytic degradation, accompanied by some non-catalytic degradation, in agreement with the

analysis of temporal average molecular weight curves by Gleadall et al. (2014b). In order to determine constants, we have followed the same procedure as Pan and co-workers (Gleadall et al., 2014b; Han et al., 2010; Han and Pan, 2011; Wang et al., 2008) but note that a more detailed examination of the material at each time point would be necessary for a more in-depth analysis. The chosen parameters assume both mid- and end-chain scissions are equally likely; if experimental studies suggested otherwise, the parameters could easily be adjusted. Additional reaction rates would allow various copolymers to be considered, with a unique set of reaction rates expected for each different polymer; this would allow the effect of copolymer ratio on the degradation rate to be considered, as described by Han and Pan (2011).

Assuming the average molecular weight, M_e, was directly proportional to the concentration of ester bonds, as suggested previously (Shirazi et al., 2016b; Wang et al., 2010, 2008), provided good predictions compared with experimental data for M_n ($r^2 = 0.9695$) when it was assumed that only end scissions occurred in the KSM (Fig. 4.6c). In contrast, for the same simulation, the results for M_n and M_w showed an unexpected increase as degradation occurred (Fig. 4.6c). The increases observed were due to shorter chains being removed from the system through the unzipping of chain ends (Fig. 4.12). This resulted in a decrease in the number of chains in the system (Fig. 4.6b), with longer chains then contributing more to M_n and M_w. This is not generally seen experimentally as mid-chain scissions throughout the system cause chains to split, counteracting this reduction in chains. It is well accepted that both mid- and end-chain scissions can occur during degradation (de Jong et al., 2001; Shih, 1995; van Nostrum et al., 2004) and this highlights the importance of considering both within a degradation model, in addition to both hydrolytic mechanisms. Including the additional reaction rates defined in Eqs. (4.7)-(4.8) ensures that their occurrence can be altered as necessary. Once both scission mechanisms were considered, the MWD gradually shifted to the left (Fig. 4.7), similarly to what has been reported experimentally (Shirazi et al., 2014). As the molecular weight characterises the average number of repeat polymer units in a chain, it is important to take the total chain distribution into account when measuring this quantity. Thus, while M_e quantifies changes in the MWD in some instances, the conventional predictions provided by the KSM provide a more in-depth description and mimic the approach of experimental calculations.

Short, water-soluble oligomers may not be captured using standard experimental techniques, such as GPC (Antheunis et al., 2010). When this happens, these chains will not feature in experimental MWDs and, consequently, will not contribute to calculations of

average molecular weight. The maximum length of these chains, i.e., the longest chain which remains water-soluble, L_{ol}, varies for different polymers. We found that considering this effect by excluding short chains from our calculations impacted results (Fig. 4.7). It was assumed that once an oligomer was formed via chain scission, it immediately dissolved into its monomeric form. In doing so, it then contributed to the carboxylic acid end concentration, with an oligomer of length i instantly transforming to create $i - 1$ additional acid ends. Vey et al. (2008) reported the length of oligomers to be between three and five units for PLGA 50:50 based on the appearance of a truncated tail in the MWD as degradation proceeded (Fig. 4.1c), accrediting this phenomenon to oligomers which had diffused from the medium. In contrast, Antheunis et al. (2010) reported a value of 13 units for PLGA 53:47. Experimental determination of L_{ol} would provide a useful input parameter, minimising the number which need calibrated and providing more accurate predictions.

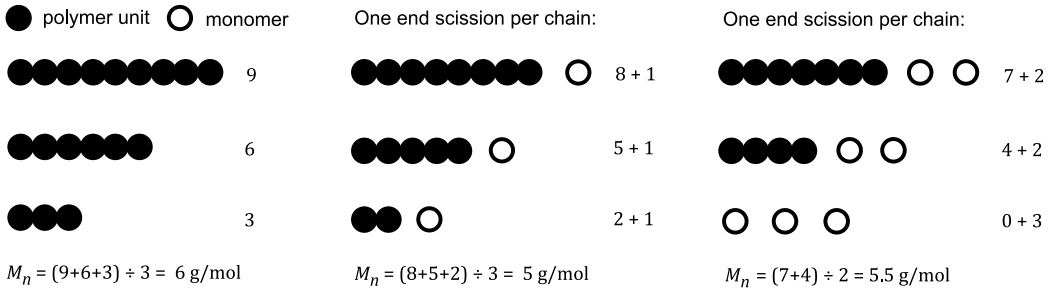

Fig. 4.12. When end scissions are the dominant mechanism, unzipping monomers from the end of chains one by one, the complete depolymerisation of chains may occur, reducing the overall number of chains in the network and, consequently, possibly contributing to an increase in M_n.

Predictions for Young's modulus were found to capture experimental data reasonably well (when $M_w^{crit} = 8000\ \mathrm{g\,mol^{-1}}$, $r^2 \approx 0.93$ for the relationship between E vs M_n but $r^2 \approx 0.6367$ for the relationship between E vs time), remaining unchanged initially, before a rapid decline at the later stages of degradation (Fig. 4.11). This further supports the use of the entropy-spring theory of Wang et al. (2010). However, in the experimental study (Shirazi et al., 2014), an increase in Young's modulus was observed in the early days, which this method is unable to capture. It should be noted that no crystallinity was reported during degradation and so this is not responsible for the increase seen. This suggests that a molecular weight threshold, with a binary inclusion of chain groups depending on their current status, may not be sufficient to predict this property. A more rigorous consideration of entropy, and free energy, may be necessary to explore the effects of polymer chain length on Young's modulus to provide a more thorough understanding of how this evolves during polymer degradation. Furthermore, the free energy, including contributions from entropy, should account for the

effect of temperature correctly, including changes in chain mobility at the glass transition temperature, T_g (Lyu et al., 2007). Although the entropy-spring theory (Wang et al., 2010) was developed for polymers above T_g, it has captured trends for polymers below T_g previously (Shirazi et al., 2016b; Wang et al., 2010). In many experimental studies, the degradation medium temperature is close to T_g (Shirazi et al., 2014; Vey et al., 2008) and it is also worth noting that T_g has been observed to change during degradation (Li et al., 1990b; Vey et al., 2008). Other approaches, such as molecular dynamics simulations on polyethylene (Ding et al., 2012) have captured changes in modulus near T_g, but the timescales associated with degradation pose challenges for this approach.

Depending on the polymer used and the processing technique, carboxylic acid ends may be present initially, or they may only be formed during degradation. The experimental study of Shirazi et al. (2014) found an S-shaped curve for M_n, suggesting a low value of the initial carboxylic acid end concentration, C_{a0} (Antheunis et al., 2009). Here, we first assumed chains were initially end-capped ($C_{a0} = 0$), with reports that these materials are more appropriate for medical devices (Sigma-Aldrich, n.d.). Various values were then explored, ranging from systems with a small amount, which can occur during processing (Antheunis et al., 2009), to those where all chains initially have carboxylic acid ends. As C_{a0} increases, the curves gradually change from S-shaped to experiencing a more abrupt initial decline due to the increased number of carboxylic acid ends available to catalyse the reaction (Fig. 4.9). This agrees with the observations of Antheunis et al. (2009) and Göpferich (1997). Previous models assumed that only the acid ends of oligomers and monomers could catalyse the reaction (Shirazi et al., 2016b; Wang et al., 2008). However, Tracy et al. (1999) observed uncapped PLGA degrading faster than ester-capped from the beginning of degradation, suggesting all carboxylic acid ends can act as catalysts. Consequently, every cleavage performed by the KSM results in the formation of a carboxylic acid end, which further catalyses degradation. Having knowledge of the initial acid end concentration is a useful input parameter to improve the accuracy of the model; similarly, residual monomers may be factored into this quantity (Gleadall et al., 2014a).

The modification in this work to consider acid ends of both monomers and longer chains must be carefully included in a diffusion equation as only the monomers are mobile. This can be facilitated by incorporating a diffusive flux term, similar to Wang et al. (2008), in Eq. (4.16). Grizzi et al. (1995) previously described homogenous degradation in PLA samples below 200 µm, while, in contrast, larger samples degraded heterogeneously. This was attributed to differences in the acid concentration at the core, where all carboxylic acid ends remain

trapped, versus the surface, where oligomers and associated acid ends can diffuse from the material, with only acid ends of long chains remaining. It should be noted that even homogenous degradation may see a non-linear decrease in molecular weight; this change in kinetics is indicative that simple hydrolysis is always accompanied by accelerative autocatalysis due to carboxylic acids. However, the effect of autocatalysis is dependent on the diffusion length scale compared with the sample size and the resulting competition of the carboxylic acids associated with monomers and oligomers. The changes made here, whereby acid ends (which would contribute to autocatalysis) occurring both on longer chains created by mid-chain scissions and on short, diffusible monomers are both counted, should improve the prediction of late-stage autocatalysis even in small samples where diffusion removes monomers.

In order to optimise mathematical models for use in predicting the degradation behaviour of polymers, it is important that standard experimental techniques ("ASTM F1635-16, Standard Test Method for in vitro Degradation Testing of Hydrolytically Degradable Polymer Resins and Fabricated Forms for Surgical Implants," 2016) are followed to robustly test and calibrate them. For example, Agrawal et al. (2000) found that testing in static or agitated conditions influenced degradation, with fluid flow decreasing the degradation rate of PLGA as reaction products could disperse more readily, reducing the autocatalytic effect. Heljak et al. (2014) further developed the model of Wang et al. (2008) to consider the effect of environmental conditions, such as dynamic or static degradation and the frequency of medium replacement, on degradation behaviour. Their proposed extension could be adapted for the work presented here, allowing a greater range of experimental studies to be modelled.

4.8 Conclusion

While many studies focus on modelling the degradation kinetics caused by polymer hydrolysis, few links have been made between these and the macroscopic scale of material performance. We have presented a kinetic scission model that considers in detail how the degradation kinetics of aliphatic polyesters impact the polymer at this level. Rate equations that consider simple hydrolysis and acid-accelerated autocatalysis were incorporated into a scission model, enabling the rates of mid- and end-chain scissions to be calculated and performed discretely on an ensemble of polymer chains. These developments allow for a more complete representation of the temporal evolution of the molecular weight distribution during degradation. Based on the understanding gained from the new scission model, a new kinetic model was proposed which captures many of the key features and can

be used in situations where computational cost is limited or in broader simulation frameworks.

By tracking the evolution of the polymer at this scale, we obtain insight into how Young's modulus of the polymer evolves during degradation. The entropy spring theory (Wang et al., 2010) is unable to capture increases in Young's modulus that are often seen, suggesting further consideration of entropy, and free energy, may be necessary to provide a more thorough understanding and improved predictions. To optimise these materials for use in clinical applications such as bioresorbable stents, it is important to understand how their material properties evolve as degradation occurs. Knowledge of the "end of use" time is of vital importance for biomedical applications, with any premature failure potentially having catastrophic effects. The extra information provided by the KSM presented here provides a platform for subsequent mechanical models or for inclusion in a wider framework which considers crystallinity.

Appendix 4A Choosing step-size for KSM

The kinetic scission model was first calibrated for end scissions only, with the reaction rates chosen to fit the predictions for average molecular weight, M_e, to experimental data for M_n (Shirazi et al., 2014). Various step-sizes were trialled until convergence was reached (Fig. 4A. 1a), where the initial number of chains $N_{c0} = 2995$. The converged solution with a step-size of 2 hours (12 steps per day) was used for the KSM in Section 4.3 of the main text (Fig. 4.6).

The above was appropriate when the simplified molecular weight, M_e, was used and only end scissions were considered. When more conventional average molecular weights and both end and random scissions were included, the reaction rates needed to be recalibrated. These were again chosen to optimise the coefficient of determination, r^2, for experimental data for M_n (Shirazi et al., 2014), however, predictions obtained for M_n were now considered (in contrast to M_e above). To ensure an appropriate time-step was taken, solutions for M_n and M_w were explored for various step-sizes until convergence was reached. Finding convergence depended on N_{c0}; for example, when $N_{c0} = 2995$, convergence had not been reached with a step-size of 1 minute. In contrast, a step-size of 1 hour was most efficient when $N_{c0} = 23960$, as shown in Fig. 4A. 1b-c. Predictions for the various average molecular weights considered corresponding to Day 20 are shown in Fig. 4A. 2 for various step-sizes, with convergence gradually reached for smaller time-steps.

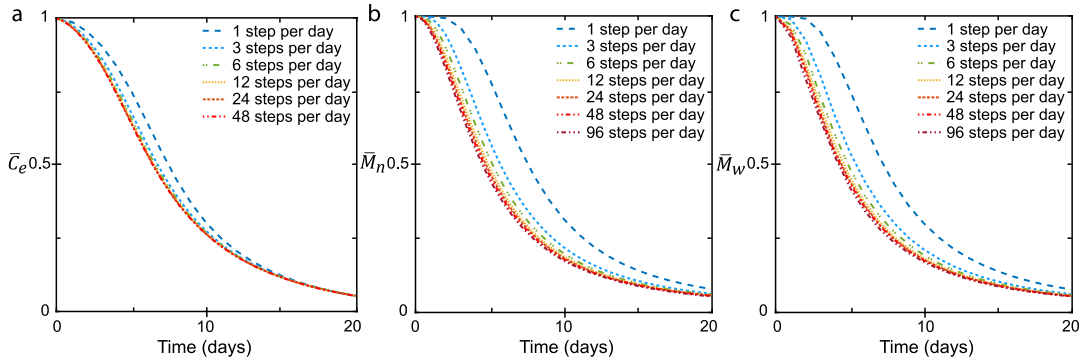

Fig. 4A. 1. Convergence of KSM solutions when (a) only end scissions are performed and both end and mid-chain scissions are considered for (b) M_n and (c) M_w.

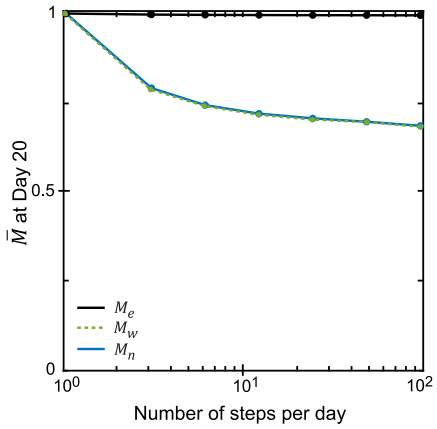

Fig. 4A. 2. Average molecular weights (normalised by peak values) as predicted by the KSM at Day 20 for various step-sizes showing gradual convergence.

Appendix 4B MATLAB live script for KSM

Kinetic Scission Model for molecular weight evolution in bioresorbable polyesters

Generate initial representative polymer chain distribution and simulate mid- and end-chain scissions according to kinetic rate equations to obtain evolving molecular weight distributions as a function of degradation duration. Extract number average molecular weight, weight average molecular weight, and Young's modulus (based on chains above a threshold molecular weight using the method of Wang et al., 2010, `10.1016/j.jmbbm.2009.02.003`) from the molecular weight distributions.

Generate representative distribution of chains

Load original chain, created using experimental molecular weight distribution data from Shirazi et al., 2014, doi.org/`10.1016/j.actbio.2014.08.004`:

```
load OrigChn.mat;
```

```
disp(size(OrigChn))
```

```
     1       23960
```

Extract initial values:

```
OrigTotChn = length(OrigChn); % number of initial chains
OrigMon = 0;    % monomers
OrigUnits = sum(OrigChn);     % total units in all chains
OrigEst = OrigUnits - OrigTotChn;    % ester bonds
```

Set parameters

```
OrigAE = 0; % original number of acid ends
StepsPD = 24; % number of steps to perform in a day
MCrit = 2000; % molecular weight threshold
OlLen = 1; % maximum length of water soluble oligomers
n = 0.5; % acid dissociation constant
MolarMass = 65;    % molar mass of a single unit of PLGA
```

Set the molar reaction rates for hydrolysis and autocatalysis via mid- and end-chain scissions:

```
k_he = 1e-7; % reaction rate for simple hydrolytic end scissions
k_hm = 1e-7; % reaction rate for simple hydrolytic mid-chain
scissions
k_ae = 9.2e-5; % reaction rate for autocatalytic end scissions
k_am = 9.2e-5; % reaction rate for autocatalytic mid-chain scissions
```

Convert molar reaction rates to system reaction rates:

```
C_e0 = 17300; % original molar conc. of esters (from Shirazi et al.,
2016, doi.org/10.1016/j.jmbbm.2015.08.030)
sys_size = OrigEst / C_e0; % size of system
C_emid0 = (OrigEst - 2*OrigTotChn) / sys_size; % orig. middle ester
conc.
C_eend0 = (2*OrigTotChn) / sys_size; % orig. end ester conc.
C_a0 = OrigAE / sys_size; % orig. acid end conc.

kae = k_ae / (sys_size)^(1/2);
kam = k_am / (sys_size)^(1/2);
khe = k_he;
khm = k_hm;
```

Set stopping criteria

```
TotScis = round(OrigEst * 1);   % maximum number of scissions to
perform
ScisSteps = 20*StepsPD;         % X days, stopping criteria
```

Initialise arrays

```
Nsubchns = ones(OrigTotChn, 1);  % number of subchains
ChnArray = sparse(OrigTotChn,round(max(OrigChn)/6)); % sparse chain
array
ChnArray(:,1) = OrigChn.'; % input initial chains in array
```

Track units in chains, ester bonds, monomers, acid ends and number of chains at each step:

```
NumUnits = zeros(1, ScisSteps + 1); NumUnits(1) = OrigUnits;
NumEst = zeros(1, ScisSteps + 1); NumEst(1) = OrigEst;
NumMon = zeros(1, ScisSteps+1); NumMon(1) = OrigMon;
NumAE = zeros(1, ScisSteps+1); NumAE(1) = OrigAE;
NumChns = zeros(1, ScisSteps+1); NumChns(1) = OrigTotChn;
```

Track which chains monomers belong to:

```
MonPerChn = zeros(OrigTotChn, ScisSteps+1);
```

Track scissions per step:

```
ScDone = zeros(1,ScisSteps + 1);
EndCuts = zeros(1, ScisSteps + 1);
MidCuts = zeros(1, ScisSteps + 1);
ScInStep = zeros(1,ScisSteps + 1);
MSinStep = zeros(1, ScisSteps + 1);
ESinStep = zeros(1, ScisSteps + 1);
```

Store chain array at various points for MWDs:

```
struct(1).ChnArray = OrigChn;
```

Calculate number & weight average MWs:

```
Mn = zeros(1, ScisSteps+1);
Mn(1) = OrigUnits/OrigTotChn*MolarMass;
Mw = zeros(1, ScisSteps+1);
Mw(1) = sum(OrigChn.^2)/OrigUnits*MolarMass;
```

Calculate weight average molecular weight for each group, where each initial chain and its resulting sub-chains created via scissions are tracked as an individual group:

```
molwMW = zeros(OrigTotChn, ScisSteps+1);
molwMW(:,1) = OrigChn.*MolarMass;
```

Track number of chain groups above a threshold molecular weight, where `molwMW>MCrit`:

```
ChnsAboveThresh = zeros(1, ScisSteps+1);
```

```
ChnsAboveThresh(1) = sum(molwMW(:,1)>=MCrit);
```

Calculate normalised Young's modulus:

```
normmod = zeros(1, ScisSteps+1);
normmod(1) = ChnsAboveThresh(1)/OrigTotChn;
```

Initialise values:

```
cutablechns = OrigTotChn; % number of cutable chains
unitsinchns = OrigUnits; % number of units in chains
bonds = OrigEst;
monomers = OrigMon;
AcidEnds = OrigAE;
StepsDone = 0;
MidCutsDone = 0;
EndCutsDone = 0;
CutsDone = 0;
```

Perform scissions

```
for i = 2:ScisSteps+1
```

Stopping criteria:

```
    if normmod(i-1) < 0.05 || cutablechns == 0
       break
    end
```

Update number of monomers per chain from previous step:

```
    MonPerChn(:,i) = MonPerChn(:,i-1);
```

Calculate number of end and mid-chain cuts to do in time-step:

```
    EndCuts(i) = ceil((khe*2*cutablechns +
kae*2*cutablechns*(AcidEnds^n))/StepsPD);
    MidCuts(i) = ceil((khm*(bonds-2*cutablechns) + kam*(bonds-
2*cutablechns)*(AcidEnds^n))/StepsPD);
```

Perform `EndCuts(i)+MidCuts(i)` scissions:

```
    for j = 1:(EndCuts(i)+MidCuts(i))
        if cutablechns == 0
            break
        end
```

Determine the proportion of end cuts, `PropEndCuts`. Choose a random number, R. If R > `PropEndCuts`, perform a mid-chain scission. Otherwise, perform an end-chain scission.

```
        PropEndCuts = EndCuts(i)/(EndCuts(i)+MidCuts(i));
        R = rand;
        if R > PropEndCuts
```

Perform mid-chain scission

Randomly choose a bond to cut:

```
            ToCut = randi(bonds);
```

Determine which chain bond belongs to:

```
            temp = cumsum(ChnArray(ChnArray>0)-1);
            idx = find(temp > ToCut, 1);
            idxx = find(ChnArray>0, idx, 'first');
            ChnToCut = idxx(end);
```

Eliminate possibility of monomer being formed:

```
            while ChnArray(ChnToCut)<=3
                ToCut = randi(bonds);
                idx = find(temp > ToCut, 1);
                idxx = find(ChnArray>0, idx, 'first');
                ChnToCut = idxx(end);
            end
            BondToCut = temp(idx) - ToCut;
            while BondToCut == 1 || BondToCut == ChnArray(ChnToCut)
                ToCut = randi(bonds);
                idx = find(temp > ToCut, 1);
                idxx = find(ChnArray>0, idx, 'first');
                ChnToCut = idxx(end);
                while ChnArray(ChnToCut)<=3
                    ToCut = randi(bonds);
                    idx = find(temp > ToCut, 1);
                    idxx = find(ChnArray>0, idx, 'first');
                    ChnToCut = idxx(end);
                end
                BondToCut = temp(idx) - ToCut;
            end
```

Find which row of array chain belongs to:

```
            row = mod(ChnToCut,OrigTotChn);
            if row == 0
                row = OrigTotChn;
            end
```

Split chain in two and add new chain to end of row. If monomers/oligomers are formed, remove from ChnArray.

```
            if ChnArray(ChnToCut)-BondToCut <= OlLen && BondToCut <=
OlLen
                Nsubchns(row) = Nsubchns(row) - 1;
                monomers = monomers + ChnArray(ChnToCut);
                AcidEnds = AcidEnds + ChnArray(ChnToCut) - 1;
                unitsinchns = unitsinchns - ChnArray(ChnToCut);
                bonds = bonds - (ChnArray(ChnToCut) - 1);
                MonPerChn(row,i) = MonPerChn(row,i) +
ChnArray(ChnToCut);
                ChnArray(ChnToCut) = 0;
                cutablechns = cutablechns - 1;
            elseif BondToCut <= OlLen
                monomers = monomers + BondToCut;
                AcidEnds = AcidEnds + BondToCut;
                unitsinchns = unitsinchns - BondToCut;
                bonds = bonds - BondToCut;
                MonPerChn(row,i) = MonPerChn(row,i) + BondToCut;
                ChnArray(ChnToCut) = ChnArray(ChnToCut) - BondToCut;
            elseif ChnArray(ChnToCut) - BondToCut <= OlLen
                monomers = monomers + ChnArray(ChnToCut) - BondToCut;
                AcidEnds = AcidEnds + ChnArray(ChnToCut) - BondToCut;
                unitsinchns = unitsinchns - ChnArray(ChnToCut) +
BondToCut;
                bonds = bonds - ChnArray(ChnToCut) + BondToCut;
                MonPerChn(row,i) = MonPerChn(row,i) ...
                    + ChnArray(ChnToCut) - BondToCut;
                ChnArray(ChnToCut) = BondToCut;
            else % split chain in two and place both in array
                ChnArray(row,find(ChnArray(row,:)==0, 1, 'first'))
...
                    = ChnArray(ChnToCut) - BondToCut;
                ChnArray(ChnToCut) = BondToCut;
                Nsubchns(row) = Nsubchns(row) + 1;
                cutablechns = cutablechns + 1;
                bonds = bonds - 1;
                AcidEnds = AcidEnds + 1;
            end
            MidCutsDone = MidCutsDone + 1;
            MSinStep(i) = MSinStep(i) + 1;
            CutsDone = CutsDone + 1;
            ScInStep(i) = ScInStep(i) + 1;
        else
```

Perform end-chain scission

Choose a chain index at random:

```
            idx = find(ChnArray>0, randi(cutablechns), 'first');
            ChnToCut = idx(end);
```

Find which row of array chain belongs to:

```
            row = mod(ChnToCut,OrigTotChn);
            if row == 0
                row = OrigTotChn;
            end
            if ChnArray(ChnToCut) <= OlLen + 1
```

If the cut results in oligomer, remove from ChnArray:

```
                Nsubchns(row) = Nsubchns(row) - 1;
                monomers = monomers + ChnArray(ChnToCut);
                AcidEnds = AcidEnds + ChnArray(ChnToCut) - 1;
                unitsinchns = unitsinchns - ChnArray(ChnToCut);
                bonds = bonds - (ChnArray(ChnToCut) - 1);
                MonPerChn(row,i) = MonPerChn(row,i) +
ChnArray(ChnToCut);
                ChnArray(ChnToCut) = 0;
                cutablechns = cutablechns - 1;
            else
```

Remove one monomer from end of chain:

```
                ChnArray(ChnToCut) = ChnArray(ChnToCut) - 1;
                monomers = monomers + 1;
                AcidEnds = AcidEnds + 1;
                unitsinchns = unitsinchns - 1;
                bonds = bonds - 1;
                MonPerChn(row,i) = MonPerChn(row,i) + 1;
            end
            EndCutsDone = EndCutsDone + 1;
            ESinStep(i) = ESinStep(i) + 1;
            CutsDone = CutsDone + 1;
            ScInStep(i) = ScInStep(i) + 1;
        end
    end
```

Update arrays

```
    NumUnits(i) = unitsinchns;
    NumEst(i) = bonds;
    NumMon(i) = monomers;
    NumAE(i) = AcidEnds;
    NumChns(i) = sum(Nsubchns);
    ScDone(i) = CutsDone;
    StepsDone = StepsDone + 1;
```

Calculate polymer properties

Calculate number average molecular weight, Mn, weight average molecular weight, Mw, and Young's modulus, E:

```
    Mn(i) = (unitsinchns)/sum(Nsubchns)*MolarMass;
    if mod(i-1, StepsPD)==0
        idx = ChnArray > 0;
        struct(max(size(struct)+1)).ChnArray=ChnArray(idx);
        Mw(i) =
(sum(struct(max(size(struct))).ChnArray.^2)/unitsinchns)*MolarMass;
    end
    molwMW(:,i) = sum((ChnArray.^2),2)./sum(ChnArray,2)*MolarMass;
    ChnsAboveThresh(i) = sum(molwMW(:,i)>=MCrit);
    if ChnsAboveThresh(i) > ChnsAboveThresh(i-1)
        ChnsAboveThresh(i) = ChnsAboveThresh(i-1);
    end
    normmod(i) = ChnsAboveThresh(i)/OrigTotChn;
end
```

References

Agrawal, C.M., McKinney, J.S., Lanctot, D.R., Athanasiou, K.A., 2000. Effects of fluid flow on the in vitro degradation kinetics of biodegradable scaffolds for tissue engineering. Biomaterials 21, 2443–2452. https://doi.org/10.1016/S0142-9612(00)00112-5

Alex, A., Ilango, N.K., Ghosh, P., 2018. Comparative Role of Chain Scission and Solvation in the Biodegradation of Polylactic Acid (PLA). J. Phys. Chem. B 122, 9516–9526. https://doi.org/10.1021/acs.jpcb.8b07930

Antheunis, H., van der Meer, J.C., de Geus, M., Heise, A., Koning, C.E., 2010. Autocatalytic Equation Describing the Change in Molecular Weight during Hydrolytic Degradation of Aliphatic Polyesters. Biomacromolecules 11, 1118–1124. https://doi.org/10.1021/bm100125b

Antheunis, H., van der Meer, J.C., de Geus, M., Kingma, W., Koning, C.E., 2009. Improved Mathematical Model for the Hydrolytic Degradation of Aliphatic Polyesters. Macromolecules 42, 2462–2471. https://doi.org/10.1021/ma802222m

ASTM F1635-16, Standard Test Method for in vitro Degradation Testing of Hydrolytically Degradable Polymer Resins and Fabricated Forms for Surgical Implants, 2016. https://doi.org/10.1520/F1635-16

Batycky, R.P., Hanes, J., Langer, R., Edwards, D.A., 1997. A Theoretical Model of Erosion and Macromolecular Drug Release from Biodegrading Microspheres. J. Pharm. Sci. 86, 1464–1477. https://doi.org/10.1021/js9604117

Buchanan, F.J. (Ed.), 2008. Degradation rate of bioresorbable materials: prediction and evaluation. Woodhead Publishing Limited/CRC Press LLC, Cambridge, England/Boca Raton, FL.

Cheng, Y., Gasior, P., Ramzipoor, K., Lee, C., McGregor, J.C., Conditt, G.B., McAndrew, T., Kaluza, G.L., Granada, J.F., 2019. In vitro mechanical behavior and in vivo healing response of a novel thin-strut ultrahigh molecular weight poly-L-lactic acid sirolimus-eluting bioresorbable coronary scaffold in normal swine. Int. J. Cardiol. 286, 21–28. https://doi.org/10.1016/j.ijcard.2019.04.012

de Jong, S.J., Arias, E.R., Rijkers, D.T.S., van Nostrum, C.F., Kettenes-van den Bosch, J.J., Hennink, W.E., 2001. New insights into the hydrolytic degradation of poly(lactic acid): participation of the alcohol terminus. Polymer 42, 2795–2802. https://doi.org/10.1016/S0032-3861(00)00646-7

Ding, L., Davidchack, R.L., Pan, J., 2012. A molecular dynamics study of Young's modulus change of semi-crystalline polymers during degradation by chain scissions. J. Mech. Behav. Biomed. Mater. 5, 224–230. https://doi.org/10.1016/j.jmbbm.2011.09.002

Durand, E., Lemitre, M., Couty, L., Sharkawi, T., Brasselet, C., Vert, M., Lafont, A., 2012. Adjusting a polymer formulation for an optimal bioresorbable stent: a 6-month follow-up study. EuroIntervention 8, 242–249. https://doi.org/10.4244/EIJV8I2A38

Ginjupalli, K., Shavi, G.V., Averineni, R.K., Bhat, M., Udupa, N., Nagaraja Upadhya, P., 2017. Poly(α-hydroxy acid) based polymers: A review on material and degradation aspects. Polym. Degrad. Stab. 144, 520–535. https://doi.org/10.1016/j.polymdegradstab.2017.08.024

Gleadall, A., Pan, J., 2013. Computer Simulation of Polymer Chain Scission in Biodegradable Polymers. J. Biotechnol. Biomater. 3, 154. https://doi.org/10.4172/2155-952X.1000154

Gleadall, A., Pan, J., Kruft, M.A., 2015. An atomic finite element model for biodegradable polymers. Part 2. A model for change in Young's modulus due to polymer chain scission. J. Mech. Behav. Biomed. Mater. 51, 237–247. https://doi.org/10.1016/j.jmbbm.2015.07.010

Gleadall, A., Pan, J., Kruft, M.A., Kellomäki, M., 2014a. Degradation mechanisms of bioresorbable polyesters. Part 1. Effects of random scission, end scission and autocatalysis. Acta Biomater. 10, 2223–2232. https://doi.org/10.1016/j.actbio.2013.12.039

Gleadall, A., Pan, J., Kruft, M.A., Kellomäki, M., 2014b. Degradation mechanisms of bioresorbable polyesters. Part 2. Effects of initial molecular weight and residual monomer. Acta Biomater. 10, 2233–2240. https://doi.org/10.1016/j.actbio.2014.01.017

Göpferich, A., 1997. Polymer Bulk Erosion. Macromolecules 30, 2598–2604. https://doi.org/10.1021/ma961627y

Grizzi, I., Garreau, H., Li, S., Vert, M., 1995. Hydrolytic degradation of devices based on poly(DL-lactic acid) size-dependence. Biomaterials 16, 305–311. https://doi.org/10.1016/0142-9612(95)93258-F

Han, X., Pan, J., 2011. Polymer chain scission, oligomer production and diffusion: A two-scale model for degradation of bioresorbable polyesters. Acta Biomater. 7, 538–547. https://doi.org/10.1016/j.actbio.2010.09.005

Han, X., Pan, J., 2009. A model for simultaneous crystallisation and biodegradation of biodegradable polymers. Biomaterials 30, 423–430. https://doi.org/10.1016/j.biomaterials.2008.10.001

Han, X., Pan, J., Buchanan, F., Weir, N.A., Farrar, D., 2010. Analysis of degradation data of poly(L-lactide-co-L,D-lactide) and poly(L-lactide) obtained at elevated and physiological temperatures using mathematical models. Acta Biomater. 6, 3882–3889. https://doi.org/10.1016/j.actbio.2010.05.015

Heljak, M.K., Swieszkowski, W., Kurzydlowski, K.J., 2014. Modeling of the degradation kinetics of biodegradable scaffolds: The effects of the environmental conditions. J. Appl. Polym. Sci. 131, 40280:1–7. https://doi.org/10.1002/app.40280

Hill, A., Ronan, W., 2022. A kinetic scission model for molecular weight evolution in bioresorbable polymers. Polym. Eng. Sci. 1–20. https://doi.org/10.1002/pen.26131

Im, S.H., Jung, Y., Kim, S.H., 2017. Current status and future direction of biodegradable metallic and polymeric vascular scaffolds for next-generation stents. Acta Biomater. 60, 3–22. https://doi.org/10.1016/J.ACTBIO.2017.07.019

Laycock, B., Nikolić, M., Colwell, J.M., Gauthier, E., Halley, P., Bottle, S., George, G., 2017. Lifetime prediction of biodegradable polymers. Prog. Polym. Sci. 71, 144–189. https://doi.org/10.1016/j.progpolymsci.2017.02.004

Li, S.M., Garreau, H., Vert, M., 1990a. Structure-property relationships in the case of the degradation of massive aliphatic poly-(α-hydroxy acids) in aqueous media - Part 1: Poly(DL-lactic acid). J. Mater. Sci. Mater. Med. 1, 123–130. https://doi.org/10.1007/BF00700871

Li, S.M., Garreau, H., Vert, M., 1990b. Structure-property relationships in the case of the degradation of massive poly(α-hydroxy acids) in aqueous media, Part 2: Degradation of lactide-glycolide copolymers: PLA37.5GA25 and PLA75GA25. J. Mater. Sci. Mater. Med. 1, 131–139. https://doi.org/10.1007/bf00700872

Lyu, S.P., Schley, J., Loy, B., Lind, D., Hobot, C., Sparer, R., Untereker, D., 2007. Kinetics and time-temperature equivalence of polymer degradation. Biomacromolecules 8, 2301–2310. https://doi.org/10.1021/bm070313n

Malvern, 2019. Viscotek SEC-MALS 20 MRK1920-04-EN-00 [WWW Document]. URL https://www.malvernpanalytical.com/en/assets/MRK1920-04_tcm50-17235.pdf (accessed 2.23.21).

Middleton, J.C., Tipton, A.J., 2000. Synthetic biodegradable polymers as orthopedic devices. Biomaterials 21, 2335–2346. https://doi.org/10.1016/S0142-9612(00)00101-0

Moore, J.C., 1964. Gel Permeation Chromatography. I. A New Method for Molecular Weight Distribution of High Polymers. J. Polym. Sci. Part A 2, 835–843. https://doi.org/10.1002/pola.1996.842

Pitt, C.G., Gu, Z.-W., 1987. Modification of the rates of chain cleavage of poly(ε-caprolactone) and related polyesters in the solid state. J. Control. Release 4, 283–292. https://doi.org/10.1016/0168-3659(87)90020-4

Schliecker, G., Schmidt, C., Fuchs, S., Kissel, T., 2003. Characterization of a homologous series of D,L-lactic acid oligomers; a mechanistic study on the degradation kinetics in vitro. Biomaterials 24, 3835–3844. https://doi.org/10.1016/S0142-9612(03)00243-6

Serruys, P.W., Chevalier, B., Sotomi, Y., Cequier, A., Carrié, D., Piek, J.J., Van Boven, A.J., Dominici, M., Dudek, D., McClean, D., Helqvist, S., Haude, M., Reith, S., de Sousa Almeida, M., Campo, G., Iñiguez, A., Sabaté, M., Windecker, S., Onuma, Y., 2016. Comparison of an everolimus-eluting bioresorbable scaffold with an everolimus-eluting metallic stent for the treatment of coronary artery stenosis (ABSORB II): a 3 year, randomised, controlled, single-blind, multicentre clinical trial. Lancet 388, 2479–2491. https://doi.org/10.1016/S0140-6736(16)32050-5

Shih, C., 1995. Chain-end scission in acid catalyzed hydrolysis of poly(D,L- lactide) in solution. J. Control. Release 34, 9–15. https://doi.org/10.1016/0168-3659(94)00100-9

Shine, R., Neghabat Shirazi, R., Ronan, W., Sweeney, C.A., Kelly, N., Rochev, Y.A., McHugh, P.E., 2017. Modeling of Biodegradable Polyesters With Applications to Coronary Stents. J. Med. Device. 11, 1–12. https://doi.org/10.1115/1.4035723

Shirazi, R.N., Aldabbagh, F., Erxleben, A., Rochev, Y., McHugh, P., 2014. Nanomechanical properties of poly(lactic-co-glycolic) acid film during degradation. Acta Biomater. 10, 4695–4703. https://doi.org/10.1016/j.actbio.2014.08.004

Shirazi, R.N., Aldabbagh, F., Ronan, W., Erxleben, A., Rochev, Y., McHugh, P., 2016a. Effects of material thickness and processing method on poly(lactic-co-glycolic acid) degradation and mechanical performance. J. Mater. Sci. Mater. Med. 27, 1–12. https://doi.org/10.1007/s10856-016-5760-z

Shirazi, R.N., Ronan, W., Rochev, Y., McHugh, P., 2016b. Modelling the degradation and elastic properties of poly(lactic-co-glycolic acid) films and regular open-cell tissue engineering scaffolds. J. Mech. Behav. Biomed. Mater. 54, 48–59. https://doi.org/10.1016/j.jmbbm.2015.08.030

Sigma-Aldrich, n.d. RESOMER® Biodegradable Polymers for Medical Device Applications Research [WWW Document]. URL https://www.sigmaaldrich.com/IE/en/technical-documents/technical-article/materials-science-and-engineering/drug-delivery/resomer (accessed 6.8.22).

Siparsky, G.L., Voorhees, K.J., Miao, F., 1998. Hydrolysis of Polylactic Acid (PLA) and Polycaprolactone (PCL) in Aqueous Acetonitrile Solutions: Autocatalysis. J. Environ. Polym. Degrad. 6, 31–41. https://doi.org/1064-7546/98/0100-0031

Skoog, D.A., Holler, F.J., Crouch, S.R., 2017. Separation Methods, in: Principles of Instrumental Analysis. Cengage Learning, pp. 746–781.

Soares, J.S., Moore, J.E., Rajagopal, K.R., 2010. Modeling of Deformation-Accelerated Breakdown of Polylactic Acid Biodegradable Stents. J. Med. Device. 4, 1–10. https://doi.org/10.1115/1.4002759

Thomas, D.P., Hagan, R.S., 1969. The Influence of Molecular Weight Distribution on Melt Viscosity, Melt Elasticity, Processing Behaviour and Properties of Polystyrene. Polym. Eng. Sci. 9, 164–171. https://doi.org/10.1002/pen.760090304

Tracy, M.A., Ward, K.L., Firouzabadian, L., Wang, Y., Dong, N., Qian, R., Zhang, Y., 1999. Factors affecting the degradation rate of poly(lactide-co-glycolide) microspheres in vivo and in vitro. Biomaterials 20, 1057–1062. https://doi.org/10.1016/S0142-9612(99)00002-2

Tsuji, H., 2002. Autocatalytic hydrolysis of amorphous-made polylactides: effects of L-lactide content, tacticity, and enantiomeric polymer blending. Polymer 43, 1789–1796. https://doi.org/10.1016/S0032-3861(01)00752-2

Tsuji, H., Del Carpio, C.A., 2003. In vitro hydrolysis of blends from enantiomeric poly(lactide)s. 3. Homocrystallized and amorphous blend films. Biomacromolecules 4, 7–11. https://doi.org/10.1021/bm020090v

Tsuji, H., Ikada, Y., 1995. Properties and morphologies of poly(L-lactide): 1. Annealing condition effects on properties and morphologies of poly(L-lactide). Polymer 36, 2709–2716. https://doi.org/10.1016/0032-3861(95)93647-5

Tsuji, H., Suzuyoshi, K., 2002. Environmental degradation of biodegradable polyesters 1. Poly(ε-caprolactone), poly[(R)-3-hydroxybutyrate], and poly(L-lactide) films in controlled static

seawater. Polym. Degrad. Stab. 75, 347–355.
van Nostrum, C.F., Veldhuis, T.F.J., Bos, G.W., Hennink, W.E., 2004. Hydrolytic degradation of oligo(lactic acid): a kinetic and mechanistic study. Polymer 45, 6779–6787. https://doi.org/10.1016/j.polymer.2004.08.001
Vey, E., Roger, C., Meehan, L., Booth, J., Claybourn, M., Miller, A.F., Saiani, A., 2008. Degradation mechanism of poly(lactic-co-glycolic) acid block copolymer cast films in phosphate buffer solution. Polym. Degrad. Stab. 93, 1869–1876. https://doi.org/10.1016/j.polymdegradstab.2008.07.018
von Burkersroda, F., Schedl, L., Göpferich, A., 2002. Why degradable polymers undergo surface erosion or bulk erosion. Biomaterials 23, 4221–4231. https://doi.org/10.1016/S0142-9612(02)00170-9
Wang, P.-J., Ferralis, N., Conway, C., Grossman, J.C., Edelman, E.R., 2018. Strain-induced accelerated asymmetric spatial degradation of polymeric vascular scaffolds. Proc. Natl. Acad. Sci. 115, 2640–2645. https://doi.org/10.1073/pnas.1716420115
Wang, Y., Han, X., Pan, J., Sinka, C., 2010. An entropy spring model for the Young's modulus change of biodegradable polymers during biodegradation. J. Mech. Behav. Biomed. Mater. 3, 14–21. https://doi.org/10.1016/j.jmbbm.2009.02.003
Wang, Y., Pan, J., Han, X., Sinka, C., Ding, L., 2008. A phenomenological model for the degradation of biodegradable polymers. Biomaterials 29, 3393–3401. https://doi.org/10.1016/j.biomaterials.2008.04.042
Ward, I.M., 1971. Mechanical properties of solid polymers. Wiley-Interscience.
Ward, I.M., Sweeney, J., 2013. Mechanical properties of solid polymers, 3rd ed. John Wiley & Sons.
Wykrzykowska, J.J., Onuma, Y., Serruys, P.W., 2009. Advances in stent drug delivery: the future is in bioabsorbable stents. Expert Opin. Drug Deliv. 6, 113–126. https://doi.org/10.1517/17425240802668495
Zhang, T., Jin, G., Han, X., Gao, Y., Zeng, Q., Hou, B., Zhang, D., 2019. Multiscale modelling for the heterogeneous strength of biodegradable polyesters. J. Mech. Behav. Biomed. Mater. 90, 337–349. https://doi.org/10.1016/j.jmbbm.2018.10.018
Zhang, T., Zhou, S., Gao, X., Yang, Z., Sun, L., Zhang, D., 2017. A multi-scale method for modeling degradation of bioresorbable polyesters. Acta Biomater. 50, 462–475. https://doi.org/10.1016/j.actbio.2016.12.046

5 Relationship between failure strain, molecular weight, and chain extensibility in biodegradable polymers

Prior to degradation, biocompatible polymers exhibit ductile behaviour and yield stress offers a suitable design approach. However, as degradation proceeds the material transitions to a brittle failure mode, suggesting a more conservative design approach is necessary. The current chapter predicts the evolving ductility of biodegrading polymers, concentrating on the relationship between molecular weight, MW, and failure strain, ε_f, in poly(lactic acid) (PLA). Several datasets are chosen from literature to explore the relationship, with all hydrolytic experimental studies carried out on PLA and copolymers in phosphate buffer solution that report evolving molecular weight and failure strain that could be found included; Table 5.1 presents details of the datasets considered. Failure criteria are proposed and examined alongside these datasets: the first (Section 5.3.1) assumes ε_f is related to the finite chain extensibility of an average chain; the second (Section 5.3.2) introduces an exponential empirical trend; and the third (Section 5.3.3) proposes a modified extensibility criterion (based on Section 5.3.1) that considers the entire molecular weight distribution. The kinetic scission model (KSM) introduced in Chapter 4 can provide predictions for the molecular weight distribution (MWD) for the third criterion and may also be used to obtain results as a function of degradation duration (Section 5.4). The predictions obtained can offer insight into material failure, particularly at advanced stages of degradation.

5.1 Introduction

5.1.1 Motivation

To optimise biodegradable materials for use in a wider range of applications, it is important to understand how their properties evolve as degradation occurs. A device needs to have sufficient mechanical integrity to withstand the initial loading and support healing, and a suitable degradation rate is desired to minimize risks associated with some long-term implants. Prior to degradation, biocompatible polymers of interest are typically ductile, suggesting determination of yield stress would offer a suitable design approach. However, as degradation proceeds the material transitions to a brittle failure mode (Polak-Kraśna et al., 2021) (Fig. 5.1), indicating a more conservative design approach is necessary.

A link between mechanical properties and molecular weight has been observed, often suggesting a critical molecular weight coincident with a ductile to brittle transition (Fayolle et al., 2007, 2004; Gardner and Martin, 1979; Golden et al., 1964). For example, Golden et

al. (1964) studied the effect of molecular weight (by using irradiation to induce scissions and decrease molecular weight) on flexural modulus, strength and strain for polycarbonate, reproduced in Fig. 5.2a. Below a critical molecular weight, rapid declines in flexural strength and strain were detected, while above this, mechanical properties were less sensitive to molecular weight. Fayolle et al. (2004) also found a critical molecular weight separating the ductile-brittle transition for thermally oxidised polypropylene (Fig. 5.2b). Thomas and Hagan (1969) reported MWD affecting mechanical properties, with a polystyrene sample with dispersity $Đ_M$ = 1.06 having improved tensile strength, elongation at break and tensile creep properties compared with a sample with equal M_w and $Đ_M$ = 2.6, suggesting that a broader distribution reduces the mechanical performance. Venkatraman et al. (2003) observed a transition from ductile to brittle failure for PLLA with reducing molecular weight (Fig. 5.2c). While hydrolysis is not always the degradation mechanism at play in many of the above-mentioned studies, it is likely that the overall effect of molecular weight on mechanical properties is similar for the materials of interest in this thesis.

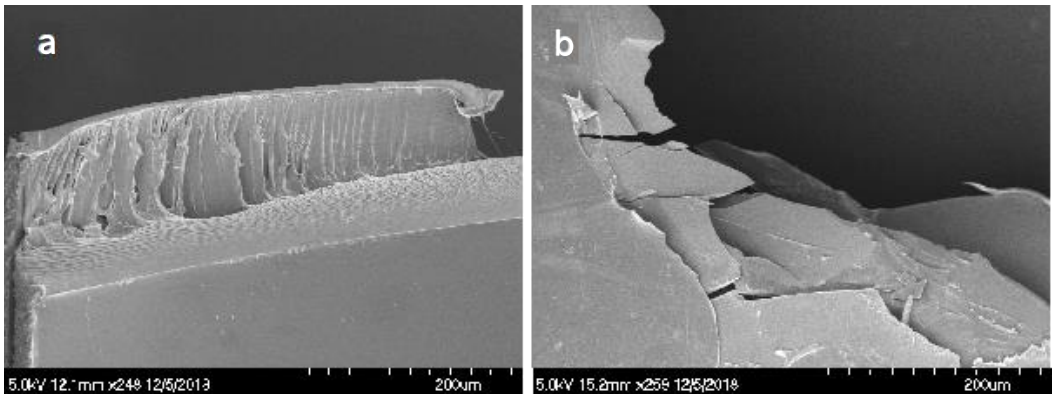

Fig. 5.1. Microscopic images of PLA samples (approximately ×250 magnification) (a) before degradation, exhibiting ductile failure on tensile testing, and (b) after 112 days degradation, showing brittle fracture on gentle handling. Reproduced from Polak-Kraśna et al. (2021), licensed under CC BY 4.0.

5.1.2 Existing models

A vast number of predictive tools for the evolution of polymer molecular weight have been developed using a variety of techniques, typically focused on average values such as number average, M_n, or weight average, M_w (Antheunis et al., 2009; Busatto et al., 2017; Gleadall et al., 2014b; Lyu et al., 2007; Pitt and Gu, 1987; Siparsky et al., 1998; Wang et al., 2008). Despite the importance of the evolving mechanical properties in the context of material performance, there have been fewer studies focusing on the time taken for the mechanical properties of a polymer to break down. Attempts have been made to uncover a relationship

between evolving mechanical properties and molecular weight (Deng et al., 2005; Flory, 1945; Shirazi et al., 2016b; Wang et al., 2010), often taking advantage of the existing models for the latter. Such a relationship may allow for tailoring of the mechanical properties via the initial molecular weight of the material.

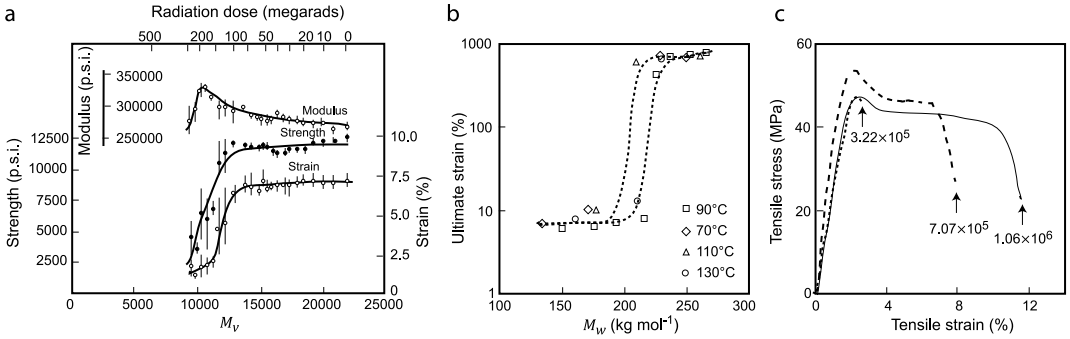

Fig. 5.2. (a) Flexural properties vs viscometric-average molecular weight for polycarbonate bars undergoing irradiation. (b) Ultimate strain vs weight average molecular weight for thermally oxidised polypropylene. (c) PLLA stress-strain curves showing a transition from ductile when $MW = 1.06 \times 10^6$ g mol^{-1} to brittle when $MW = 3.22 \times 10^5$ g mol^{-1} (average molecular weight measured not specified). Adapted from: (a) (Golden et al., 1964), (b) (Fayolle et al., 2004), (c) (Venkatraman et al., 2003).

One of the earliest such models is that proposed by Flory (1945), albeit not in relation to biodegradable polymers specifically. Tensile strength, σ, was related to number average molecular weight, M_n, as follows:

$$\sigma = \sigma_\infty - \frac{B_F}{M_n} \tag{5.1}$$

where σ_∞ is the fracture strength at infinite molecular weight and B_F is a constant. As Eq. (5.1) is an empirical relationship, both σ_∞ and B_F must be determined using experimental data. Focusing on biodegradable polymers, Weir et al. (2004b) found an almost linear relationship existed between the two properties (Fig. 5.3a), while Deng et al. (2005) found the following relationship between breaking strength retention, BSR, i.e., ultimate tensile strength as a percentage of its original value, and average molecular weight, MW, for the degradation of PLGA braids (Fig. 5.3b):

$$BSR = a + b \ln MW \tag{5.2}$$

where MW was taken to be either number average, M_n, or weight average, M_w, and a and b are constants. Eq. (5.2) successfully captured the behaviour of PLGA at various increased temperatures, suggesting its practicality in accelerated degradation studies. The different

trends observed by Weir et al. (2004b) and Deng et al. (2005) may be due to the large difference in initial molecular weight ($M_{n0} \approx 160,000$ and $19,000$ g/mol, respectively). Both studies did determine a clear relationship between M_n and nominal stress, σ, over a range of testing conditions; however, this relationship must be further explored using a wider range of experimental data.

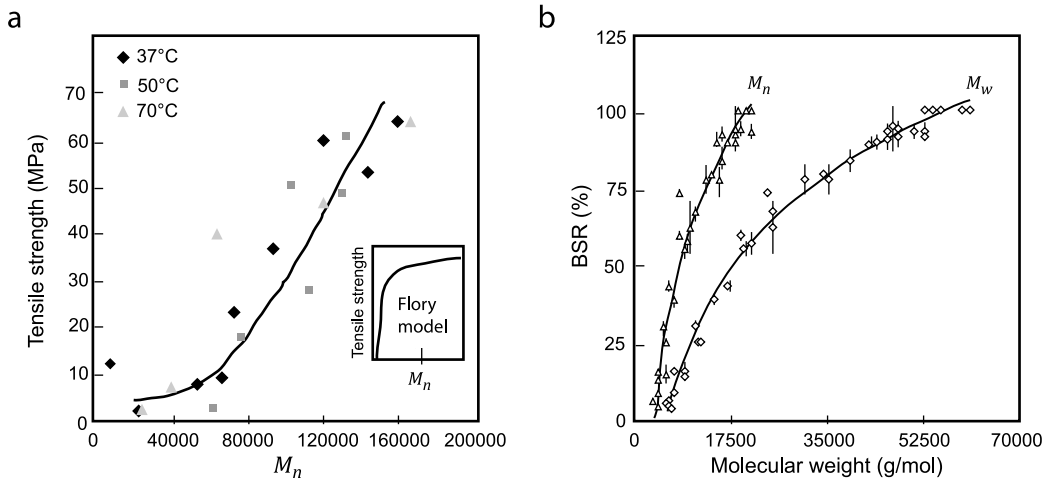

Fig. 5.3. (a) Adapted from Weir et al. (2004b), where an almost linear relationship between tensile strength and M_n was observed in contrast to Flory's relationship (Eq. (5.1)). (b) The relationship between breaking strength retention, BSR, i.e., ultimate tensile strength as a percentage of its original value, and average molecular weight, MW, described by Eq. (5.2). Adapted from Deng et al. (2005).

Models concerned with relating polymer stiffness to average molecular weight have also previously been introduced. Wang et al. (2010) developed a theory for amorphous bioresorbable polymers based on the relationship between Young's modulus and the number of polymer chains per unit volume according to a molecular weight threshold, successfully capturing PLLA degradation data (Tsuji, 2002). Shirazi et al. (2016b) expanded on that approach, combining a scission model (Wang et al., 2010) to capture the relationship between stiffness and M_n and then coupling that with a kinetic model (Wang et al., 2008) that predicts changes in average molecular weight as a function of degradation duration, finding agreement with experimental trends for PLGA films (Shirazi et al., 2014). In Chapter 4, this was further developed, updating the kinetic model and including a time dependence within the scission model, accounting for hydrolysis and autocatalysis via mid- and end-chain scissions, providing a framework which directly predicts the temporal evolution of both the molecular weight distribution and Young's modulus during degradation.

Although it is unlikely for any property to depend solely on molecular weight, it has been shown that when most properties are held constant and degradation conditions are minorly

varied (for example, increased temperature leading to accelerated testing), relationships can be found between M_n and properties ranging from tensile strength to Young's modulus to strain retention/ductility (Deng et al., 2005; Weir et al., 2004b). While these are typically empirical relationships, they nevertheless prove insightful for designing improved devices, with accelerated testing used to determine parameters, reducing development time.

Damage and constitutive models have also been developed to describe the evolution of mechanical properties in degrading polymers. Towards this, Vieira et al. (2014, 2011) presented a model that combined a relationship between fracture strength and molecular weight with hyperelastic material models to obtain evolving stress-strain curves for PLA–PCL fibres during degradation. Soares et al. (2010) considered the effect of deformation on degradation behaviour; they considered PLLA stent fibres under tensile loading conditions with a deformation-dependent rate of degradation and obtained qualitative evolving stress-strain curves. Hayman et al. (2014) proceeded by expanding on this model in conjunction with an experimental study investigating the effect of different loads at different stages of degradation on PLLA fibres. Their model captured the increased reduction in mechanical properties with increased loading observed experimentally. As the material parameters are functions of degradation damage instead of material constants in those constitutive models, extensive experimental data is needed for that approach.

Despite the multiple efforts that have been given to modelling these materials, the evolution of the ductility has not been focused on. Although experimental data has suggested a relationship exists between ductility and molecular weight independent of temperature (Deng et al., 2005; Weir et al., 2004b), this does not appear to have been translated into a predictive tool. Deroiné et al. (2014) suggested as little as 20% reduction in failure strain could correspond to end-of-use, with abrupt declines often seen after an induction period, while mechanical failure of polymers is often assessed by a 95% reduction in elongation at break (Laycock et al., 2017), thus highlighting the importance of understanding the mechanisms behind failure strain evolution during degradation.

5.1.3 Polymer ductility

A substantial reduction in failure strain indicates that the polymer can no longer yield and will fail in a brittle mode on the application of force (Laycock et al., 2017). Wang et al. (2018) investigated microstructural heterogeneities within polymeric scaffolds and determined that the stress generated from crimping and inflation caused loss of structural integrity before

chemical degradation was initiated. When assessing failure in polymer materials, elongation at break can provide valuable insight.

As degradation proceeds in PLA, large declines in ductility have been observed (Duek et al., 1999; Kranz et al., 2000; Tsuji, 2002). In an experimental degradation study carried out by Tsuji (2002), various forms of PLA were investigated in vitro (some emerging results are reproduced in Fig. 5.4). A substantial increase in ductility was observed for PLLA as degradation proceeded, while the elongation at break of PL/DLA declined rapidly. Both the copolymer (PDLLA, $\varepsilon_{f0} = 21.0\%$) and the polymer blend (PL/DLA, $\varepsilon_{f0} = 14.5\%$) demonstrated larger initial values of elongation at break compared with the homopolymers (PLLA, $\varepsilon_{f0} = 6.5\%$ and PDLA, $\varepsilon_{f0} = 5.3\%$). At the next observation point, the elongation at break of both the copolymer and polymer blend had decreased, while both homopolymers showed increases, although to a lesser extent for PDLA. Nevertheless, this may suggest that different mechanisms are at play for homopolymers and heteropolymers. It was reported that the initially amorphous films remained so throughout degradation, therefore excluding the influence of crystallinity.

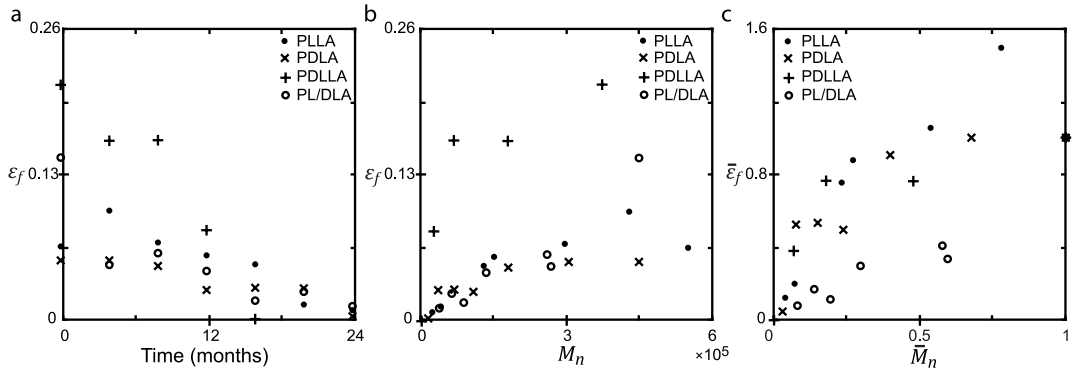

Fig. 5.4. Experimental degradation data adapted from Tsuji (2002) for amorphous PLA. (a) Evolving elongation at break, ε_f ($\varepsilon_f = \frac{L_f - L_0}{L_0}$, where L_f is the final length and L_0 is the initial length of the sample tested). Various trends emerge, ranging from an initial increase (PLLA) to a rapid decline (PL/DLA). For PDLLA, $\varepsilon_f = 0$ after 16 months degradation, while for the other three polymers, $\varepsilon_f \to 0$ after 24 months degradation. (b) Relationship between ε_f and number average molecular weight, M_n. PLLA, PDLA and PL/DLA appear to follow a similar pathway after variances in initial values of ε_f and M_n. (c) Alternative version of (b), where both properties are normalised by their respective initial values. Two trends emerge: (i) PLLA, PDLA and PDLLA experience a lagged reduction in ε_f, with minimal decline until M_n has reduced by >50%; (ii) the polymer blend, PL/DLA, experiences a more rapid decline.

With minimal variances in the study of Tsuji (2002) between the four polymer types, the relationship between evolving ε_f and M_n is explored (Fig. 5.4b-c). When absolute values are

considered (Fig. 5.4b), PLLA, PDLA and PL/DLA appear to follow a similar pathway after variances in initial values of ε_f and M_n. In contrast, when both properties are normalised by their respective initial values, different relationships are evident (Fig. 5.4c). In that case, two trends emerge: (i) PLLA, PDLA and PDLLA experience a lagged reduction in ε_f, with minimal decline until M_n has reduced by >50%; and (ii) the polymer blend, PL/DLA, experiences a more rapid decline, no longer appearing to exhibit similar behaviour to the homopolymers. The factors contributing to these two trends should be further explored in the context of a wider set of experimental data to determine the underlying causes.

5.1.4 Objectives

The current study aims to predict the evolving ductility of biodegrading polymers, concentrating specifically on PLA and its copolymers. While factors such as crystallinity and molecular orientation impact ductility (Wang et al., 2018), here the focus is restricted to the relationship between molecular weight and failure strain. To begin, a literature survey is carried out, providing a more thorough investigation of observed relationships between elongation at break, ε_f, and average molecular weight, MW. Based on details given in the experimental studies considered, detailed in Table 5.1, factors which may contribute to the trends observed are explored. Mathematical models describing these relationships are introduced as three failure criteria and their predictive capability is explored for a wide range of data. The first of these is physically based and considers chain extension using a freely jointed chain approach (Ward, 1971) and relates this to average molecular weight. The second criterion describes an empirical relationship based on observed trends, following a similar approach to Flory (1945) and Deng et al. (2005) for tensile strength. Finally, the third model considers a relationship between ductility and a molecular threshold, similar to the approach of Wang et al. (2010) when modelling stiffness. These criteria are then used in conjunction with the kinetic scission model of Chapter 4 to obtain predictions for the temporal evolution of ductility.

5.2 Experimental relationship between failure strain and average molecular weight

From Fig. 5.4 and the experimental study of Tsuji (2002), it appears as though a single trend may not exist between ε_f and M_n. To further explore this, a larger dataset was examined. Focusing solely on PLA and its copolymers, 27 datasets from 9 publications that measured the evolution of molecular weight and mechanical properties were considered (Deng et al., 2005; Duek et al., 1999; Kranz et al., 2000; Polak-Kraśna et al., 2021; Tsuji, 2002; Tsuji et al.,

2000; Tsuji and Del Carpio, 2003; Weir et al., 2004a, 2004b). Several variances exist in those studies, encompassing polymers which are either amorphous or crystalline, prepared using different techniques, having varying geometries, and tested with different equipment, with details outlined in Table 5.1. While some of these studies reported both M_n and M_w, others restricted their focus to one of those. Absolute data is presented in Fig. 5.5a, while both properties have been normalised by their respective initial values in Fig. 5.5b. Focusing first on the absolute data, it is challenging to determine a unique relationship between these properties due to the large variance in initial values. The normalised data also spans a wide range; while often a lag in the decline in ε_f was evident, other data suggested an exponential-like decline. Separating the data based on these two observations, two trends emerge: (i) Trend 1 typically experiences no decline in ductility initially (or even increases), with a lagged decline compared with the reduction in MW (Fig. 5.5c); while (ii) for Trend 2, ε_f has declined by >50% with a 20% reduction in MW and no initial increase in ε_f was observed (Fig. 5.5d).

To understand what may contribute to these differing trends, Table 5.1 indicates many features of the experimental parameters and polymers considered. Interestingly, many of the features present spanned both trends. Most surprisingly may be the lack of distinction between amorphous and semi-crystalline materials. It has typically been accepted that when the polymer undergoes loading, chains in amorphous regions unwind and adopt extended configurations, allowing for relatively large, typically reversible deformations, while in contrast, the rigid structure exhibited by crystalline regions prevents those regions from responding in the same way (Bartczak, 2017; Callister Jr and Rethwisch, 2018a). Despite this, instances of both polymer types were seen to follow both identified trends. While glass transition temperature also plays a role in the loading response, little variance is expected for the polymers considered here. Based on the data provided in each of the experimental studies considered, no distinction could be made between trends.

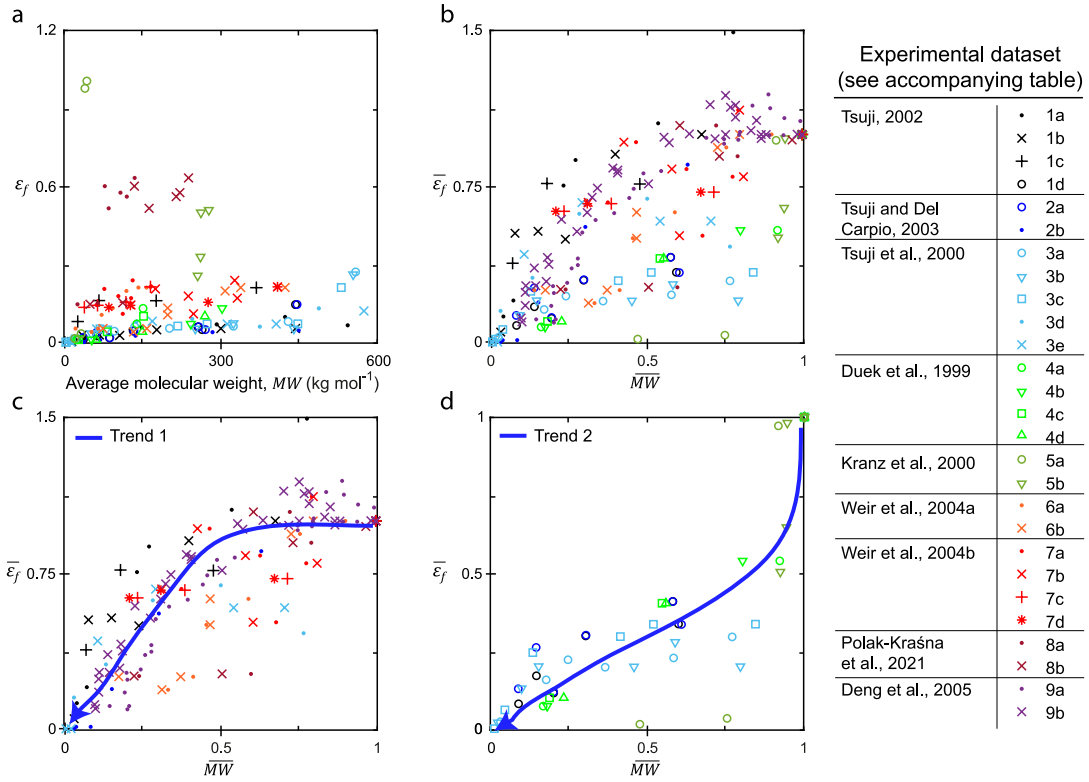

Fig. 5.5. Experimental datasets from literature (Deng et al., 2005; Duek et al., 1999; Kranz et al., 2000; Polak-Kraśna et al., 2021; Tsuji, 2002; Tsuji et al., 2000; Tsuji and Del Carpio, 2003; Weir et al., 2004a, 2004b) showing the relationship between elongation at break, ε_f, and average molecular weight, MW. Details on each dataset is given in Table 5.1. Each unique colour corresponds to a different publication. (a) Absolute data for publications 1 – 8 covers a wide range, with large variances in initial values of both properties. Differences between M_n and M_w data are not evident. (b) Normalised data for all 9 publications, where both properties are normalised by their initial values. No single trend emerges. (c) Normalised data for a subset of the overall datasets where a lag in the decline of ε_f is observed, subsequently referred to as Trend 1. (d) The remaining normalised datasets not shown in (c), where ε_f has declined by >50% with a 20% reduction in MW (Trend 2). Closed symbols correspond to Trend 1, while open symbols represent datasets following Trend 2.

Table 5.1. Details on each dataset considered are given based on that provided in literature, indicating the corresponding publication (Ref.), identification number and symbol assigned in this study (ID), polymer type, trend observed in the relationship between ε_f and MW (see Fig. 5.5), polymer structure (homopolymer (H), copolymer (C), or polymer blend (B), and amorphous (Am.) or semi-crystalline (SC)), average molecular weight, MW, provided in experimental study (number, M_n, or weight average, M_w) and the corresponding initial value ($\times 10^5$ g/mol), the testing temperature, sample geometry, and methods of preparation, degradation protocol, molecular weight determination and mechanical properties testing. Where information was not provided, the cell is left unfilled.

Ref.	ID	Polymer	Trend	Structure		MW	MW_0	Temp.	Geometry	Preparation	Degradation protocol	MW det.	Mechanical properties test method
(Tsuji, 2002)	• 1a	PLLA	1	H	Am.	M_n	3.7	37°C	Films – 3 mm x 30 mm x 50-150 μm	Solvent-cast – evaporation at room temperature for ~1 day. Films dried in vacuum for 1 week.	10mL PBS (pH 7.4±0.1) containing 0.02 wt% sodium azide exchanging buffered solution once a month.	GPC	Washed and dried under reduced pressure for >2 weeks. Measured at 25°C using a tensile tester at a crosshead speed of 100%/min (20 mm/min). Gauge length: 20 mm.
	× 1b	PDLA	1	H			4.4						
	+ 1c	PDLLA	1	C			5.4						
	o 1d	PL/DLA	2	B			4.4						
(Tsuji and Del Carpio, 2003)	o 2a	PL/DLA	2	B	Am.	M_n	4.4	37°C	As above	As above.	As above.	GPC	As above.
	• 2b		1		SC		4.5						
(Tsuji et al., 2000)	o 3a	PLLA	2	H	SC	M_n	5.4	37°C	Films – 18 mm x 30 mm x 50 μm	PLLA films melted at 200°C for 3 min and annealed at 140°C for (3a) 0, (3b) 15, (3c) 30, (3d) 45, (3e) 60 min prior to being quenched at 0°C.	As above; 0.15M PBS.	GPC	As above.
	▽ 3b		2				5.5						
	□ 3c		2				5.1						
	• 3d		1				5.0						
	× 3e		1				5.8						
(Duek et al., 1999)	o 4a	PLLA	2	H	Am.	M_n	1.5	38°C	Rods – 30mm x 3mm	Injection-moulded (190°C) and quenched (20°C).	Samples sterilized with ethylene oxide and immersed in tubes containing PBS (pH 7.4) in a thermally- controlled bath.	GPC	Three-point bending of a 19 mm segment were made at 15°C using an MTS-810.
	▽ 4b		2		→ SC	M_w	3.0						
	□ 4c		2		SC	M_n	1.5		Rods – 30mm x 2mm	Injection-moulded (190°C); cooled at room temperature for 30 min.			
	Δ 4d		2			M_w	2.7						
(Kranz et al., 2000)	o 5a	PDLLGA	2	C	-	M_w	2.7	37°C	Films – 40 mm x 40 mm x 100 μm	Solvent-cast – dried for 12h at room temperature and for 12h at 40°C.	200 mL of PBS (pH 7.4).	SEC	Instron 4466, 500 N load, 10 mm/min, wet condition.
	▽ 5b	PDLLA	2				0.57						
(Weir et al., 2004a)	• 6a	PLLA	1	H	SC	M_n	1.6	37°C	Plates (0.8mm thick) – type V tensile samples	Compression moulded and annealed at 120°C for 4 hours.	28 ml screw-top glass bottles, fully immersed in PBS (pH 7.4 – monitored throughout) (ISO 15814:1999). Placed in air circulating oven. PBS (mm):polymer mass (g) > 30:1.	GPC	JJ Lloyd EZ 50 tensile testing machine equipped with a 1 kN load cell and tested at 10 mm/min while wet. Gauge length: 7.62 mm.
	× 6b		1			M_w	4.2						
(Weir et al., 2004b)	• 7a	PLLA	1	H	SC	M_n	1.7	50°C	As above	As above.		GPC	
	× 7b		1			M_w	4.1						
	+ 7c		1			M_n	1.7	70°C					
	* 7d		1			M_w	4.1						
(Polak-Kraśna et al., 2021)	• 8a	PLLA	1	H	SC	M_n	0.98	50°C	1.5 mm diameter tubes cut into curved dog-bones for mechanical testing	Pre-processed.	PBS (pH 7.4±0.2) changed every 3-4 weeks to maintain pH.	GPC	Zwick mechanical test machine with 100 N load cell tested at 10 mm/min while wet. Gauge length: 5mm.
	× 8b		1			M_w	2.2						
(Deng et al., 2005)	• 9a	PLLGA	1	C	SC	M_n	0.19	27.5 – 47.5°C	Multifilament braids, diameter: 0.304 mm	Pre-processed.	0.1M PBS (pH 7.4) changed at least once a week.	GPC	Instron 4501, 500-N load at 127 mm/min. Room temperature, wet. Gauge length: 80mm.
	× 9b		1			M_w	0.57						

5.3 Failure strain criteria

In the following sections, three criteria are considered: first, a model which accounts for the finite extension of a polymer chain with a representative length taken from the average molecular weight; second, an empirical relationship is explored for the experimental data not captured by the first model; and finally, a model which accounts for the extension of all chains in a molecular weight distribution.

5.3.1 Finite chain extensibility criterion

A physically based failure criterion is introduced and explored. The finite chain extensibility of a single polymer chain is first considered. The failure strain is then related to the finite extensibility of an average chain in the system using an average molecular weight.

With gradual declines observed in both molecular weight and failure strain throughout degradation in experimental studies (Fig. 5.5), the existence of a relationship between these properties is explored. To begin, polymer chains are idealised as freely jointed chains, with chains containing equal links randomly jointed. This is a fundamental approach taken in many polymer models (Ward, 1971; Ward and Sweeney, 2013), and has previously proved successful when modelling polymers below their glass transition temperature (Shirazi et al., 2016b; Wang et al., 2010). It is assumed that a chain begins at some most-probable length, $L_0 = \sqrt{N}L_m$ (Fig. 5.6), where N is the number of polymer units (related to the weight of an individual chain) or degree of polymerisation, and L_m is the length of each link (Ward and Sweeney, 2013). A chain is assumed to reach full extension during stretching, with a final length $L_f = NL_m$ at failure, resulting in chain breakage (Fig. 5.6).

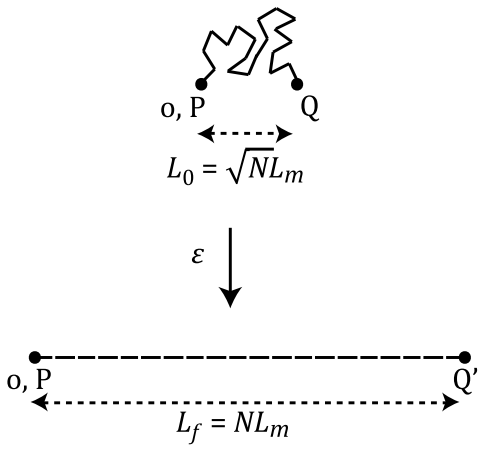

Fig. 5.6. A polymer chain, modelled as a freely-jointed chain, is assumed to begin at some most-probable length, $L_0 = \sqrt{N}L_m$, where N is the number of polymer units and L_m is the length of each link (Ward and Sweeney, 2013). On extension, the chain may reach its final length, $L_f = NL_m$, with any further extension causing chain breakage.

The nominal failure strain, ε_f, of such a chain is then given as

$$\varepsilon_f = \frac{L_f - L_0}{L_0} = \frac{NL_m - \sqrt{N}L_m}{\sqrt{N}L_m} = \sqrt{N} - 1 \tag{5.3}$$

dependent on the number of polymer units, N, which is typically on the order of approximately 10 – 200000, suggesting unrealistically large values of ε_f for the materials of interest. To overcome this, a scaling parameter, A, is introduced to provide more realistic predictions, giving the following:

$$\varepsilon_f = A\left(\sqrt{N} - 1\right) \tag{5.4}$$

As presented, Eq. (5.4) considers just one individual chain. To extend this approach to consider the failure strain for the complete system, an average material characterisation such as average molecular weight, MW, which characterises the average number of repeat polymer units in all chains in the system, may be useful. Thus, by equating N with MW the failure strain may be related to the molecular basis of the polymer. This provides the following failure criteria:

$$\varepsilon_f^{MW} = A_1\left(\sqrt{MW} - 1\right) \approx A_1\sqrt{MW} \tag{5.5}$$

where MW is taken to be an average molecular weight, such as number average, M_n, or weight average, M_w, both of which are typically on the order of 10^5 g mol^{-1} initially (Table 5.1). A parameter, A_1, is again included as a scaling parameter.

5.3.1.1 Results

Using the experimental data shown in Fig. 5.5, the accuracy of Eq. (5.5) was explored. Firstly considering normalised data (Fig. 5.5b), it is evident that Eq. (5.5) captures the relationship between these two properties reasonably well in the case of Trend 1 (Fig. 5.7a). A gradual reduction is seen, with ε_f lagging behind MW. However, it is unable to capture the more rapid decline exhibited by Trend 2 (Fig. 5.7a, open symbols). Turning the focus to absolute data (Fig. 5.5a), Fig. 5.7b investigates various values of A_1 ranging from $5 \times 10^{-3} - 1 \times 10^{-4}$ alongside absolute experimental data. While some data is captured reasonably well provided a suitable choice of A_1 is made (e.g., 1b, 6a), it is observed that some data cannot be described by Eq. (5.5) (e.g., 3b, 5b).

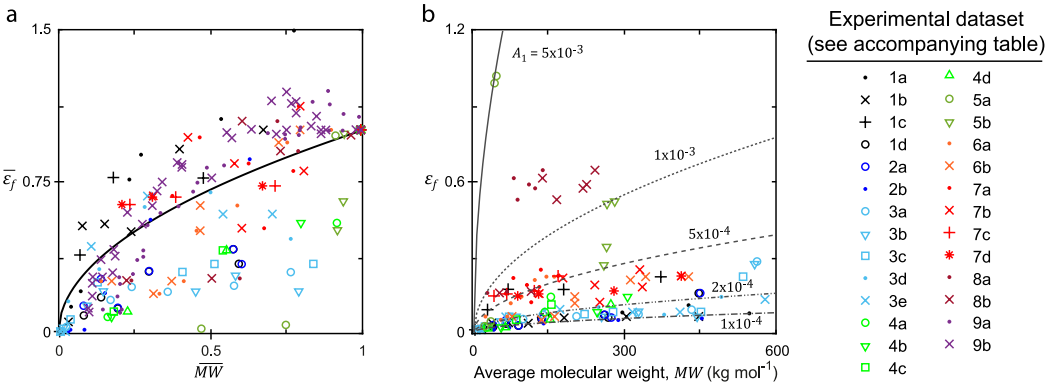

Fig. 5.7. (a) Prediction obtained for the relationship between elongation at break, ε_f, and average molecular weight, MW, using Eq. (5.5) (solid line) alongside normalised experimental data from literature (Table 5.1). Data following Trend 1 (solid filled symbols) are captured reasonably well, while the more rapid declining data categorised as Trend 2 (unfilled symbols) are not well described. (b) Various values of A_1 are explored using Eq. (5.5) alongside absolute data. Again, some datasets are reasonably captured (e.g., 1b, 6a), while others are not (e.g., 3b, 5b). For decreasing values of A_1, lower initial values of ε_f are predicted alongside a more gradual decline in this property.

5.3.2 Exponential empirical criterion

Although we have not yet determined the cause behind these two differing trends, now that Trend 1 can be reasonably predicted, our focus turns to predicting the more rapid declining failure strain with decreasing molecular weight exhibited by Trend 2. Re-examining Fig. 5.5d, an exponential-like relationship is seen between these two properties. An empirical relationship of this form may be described as follows:

$$\varepsilon_f^{exp} = A_2\, exp(A_3 MW) \tag{5.6}$$

where A_2 and A_3 are empirical constants.

5.3.2.1 Results

Eq. (5.6) was fit to each experimental dataset in Trend 2 (Table 5.1) for MW (Fig. 5.8), where values for A_2 and A_3 were chosen to maximise r^2 using the Curve Fitting Tool in MATLAB® (R2019a, The MathWorks, Inc., MA, USA). It was determined that Eq. (5.6) had good predictive capability for Trend 2, resulting in $r^2 > 0.90$ in many cases. Dataset 5b appears as an outlier, with $r^2 = 0.695$; however, that degradation study ended prior to MW having declined to the extent of the other studies considered here. As Eq. (5.6) is empirical in nature, experimental calibration is required to obtain values for both A_2 and A_3, thus reducing its predictive capability in a wider setting. Additionally, this is not valid for describing Trend 1.

Therefore, finding an underlying cause for these two trends would first be necessary for Eq. (5.5) and Eq. (5.6) to be practical in a wide setting.

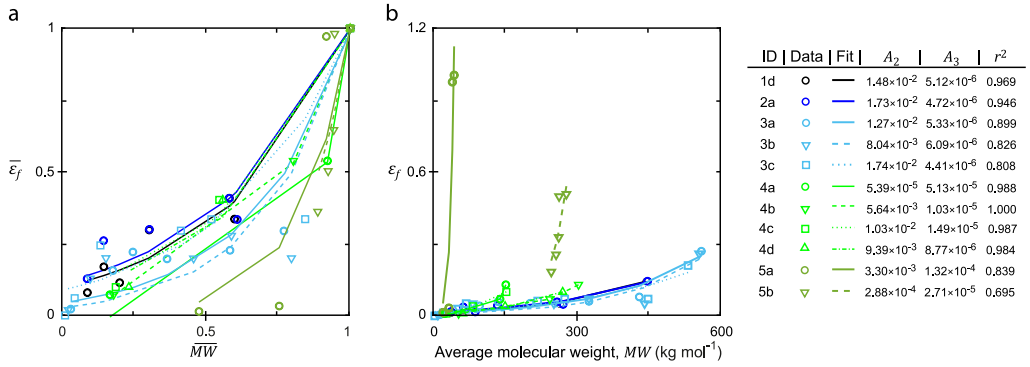

Fig. 5.8. Eq. (5.6) was explored for predicting each dataset in Trend 2 (Table 5.1), with the plotted lines corresponding to the predictions and the discrete symbols representing the data being predicted for (a) data normalised by their initial value and (b) absolute data. The empirical constants, A_2 and A_3, were chosen to maximise r^2 as described in the text.

5.3.3 Modified finite chain extensibility criterion to consider molecular weight distribution

While Eq. (5.5) and Eq. (5.6) were both found to capture certain trends, a priori knowledge of which one is appropriate for the polymer being studied is necessary before widespread use. Alternatively, as polymer ductility is likely to be controlled by various aspects of the molecular weight distribution (MWD) rather than an average value solely, considering the entire MWD may provide an improved, all-encompassing predictive technique. Returning to the physically based approach in Section 5.3.1, a modified finite chain extensibility criterion is now introduced, taking a more rigorous consideration of the molecular weight distribution and its evolution during degradation.

Ward (1971) described the following classic equation:

$$E = 3NkT \tag{5.7}$$

relating Young's modulus, E, to the number of polymer chains per unit volume, N, where k is the Boltzmann constant and T is temperature. As N increases due to chain scissions in a degrading polymer, an unrealistic increase is suggested by Eq. (5.7) for biodegradable polymers. To overcome this, Wang et al. (2010) further considered the changing entropy of a degrading system, reasoning that isolated scissions and very short chains are unlikely to contribute significantly to changes in polymer entropy. To this end, it was assumed that N never increases and the number of chain groups above a threshold number average

molecular weight, M_n^{crit}, denoted N_c, was introduced. It was reasoned that chains that have experienced sufficient degradation to fall below M_n^{crit} no longer contribute to the entropy and thus E in Eq. (5.7).

Here, a similar approach is followed, where a threshold molecular weight is used to consider the impact of degradation on failure strain. Returning to Eq. (5.5), which related the failure strain of a single chain to the number of polymer units, N, ($\varepsilon_f = A\left(\sqrt{N} - 1\right)$), this is extended to more rigorously consider the complete molecular weight distribution than in Section 5.3.1. It is assumed that once a system consists mostly of short chains, then the behaviour becomes brittle and this is measured by tracking N_c during simulated degradation, as previously done for Young's modulus (Wang et al., 2010), as described above. A new failure criterion based on the finite extensibility of polymer chains and a threshold molecular weight is then introduced as:

$$\varepsilon_f^N = A_4\sqrt{N_c} \tag{5.8}$$

where A_4 is a constant. N_c is found by tracking each original chain and its resulting sub-chains as the scissions proceed (see Fig. 5.9 for an illustration of this concept). An average molecular weight is calculated for each group of sub-chains and if the weight is above a critical value, M_n^{crit}, then it is included in the count of N_c. Note that M_n^{crit} is chosen here in contrast to M_w^{crit} when predicting Young's modulus in Chapter 4; M_n better captures short chains, which should be more susceptible to finite extensibility and, thus, be of importance when considering ductility, while M_w places more emphasis on long chains, which are assumed to contribute more to the stiffness of the polymer.

To use Eq. (5.8), knowledge of the entire molecular weight distribution and its evolution during degradation is necessary to obtain N_c. Predictions for this quantity may be acquired using the kinetic scission model (KSM) introduced in Chapter 4, illustrated in Fig. 5.9. This was carried out as follows:

1. An initial representative molecular weight distribution was considered in the form of an array of chains with a distribution of lengths. This was characterised based on the experimental data of Tsuji (2002) for amorphous PLA.
2. A suitable step-size was chosen ($\Delta t \approx 0.03\ \mathrm{month}^{-1}$), with temporal convergence checked by comparing results for M_n vs time with those obtained using the automatic adaptive step-size NKOM method introduced in Chapter 4. End- and mid-chain scissions

were simulated on bonds at random as previously outlined (Chapter 4) according to the following equations:

$$S_{mid} = \left(k_{hm}C_{e,mid} + k_{am}C_{e,mid}C_a^n\right)\Delta t \quad (5.9)$$

$$S_{end} = \left(k_{he}C_{e,end} + k_{ae}C_{e,end}C_a^n\right)\Delta t \quad (5.10)$$

where S_{mid} and S_{end} are the molar number of mid- and end-chain scissions, respectively, $C_{e,mid}$, $C_{e,end}$ and C_a are the molar concentrations of mid-chain ester bonds, end-chain ester bonds, and carboxylic acid ends, respectively, n is the acid dissociation constant, and Δt is the time increment. The simple hydrolytic reaction generates mid- and end-chain scissions according to k_{hm} and k_{he}, respectively. Similarly, the autocatalytic reaction rates, k_{am} and k_{ae}, govern the rate at which mid- and end-chain scissions, respectively, occur due to autocatalysis. The evolution of each individual chain was tracked during the scission process, with information on all chain lengths stored in the array; this provided the evolving molecular weight distributions, from which average molecular weights may be obtained. The reaction rates were calibrated to fit experimental predictions for MW using the method previously described (Chapter 4). The reaction rates for k_{he} and k_{hm} were assumed to be equal without clear evidence to suggest which is dominant for these materials, and similarly for k_{ae} and k_{am}. Values for n, the length of oligomers, L_{ol}, and the initial acid end concentration, C_{a0}, further discussed previously (Chapter 4), were all kept constant.

3. Values for N_c were found as follows (Chapter 4):
    a. Each initial chain and its resulting sub-chains created by scissions form one of N_{c0} groups, where N_{c0} is the initial number of chains in the system; M_n is calculated for each individual group (each bar in Fig. 5.9 corresponds to a group).
    b. Once $M_n < M_n^{crit}$ for a group, where M_n^{crit} is a specified critical molecular weight, the group falls below the threshold value and is excluded from N_c, the number of chain groups above the molecular weight threshold.
4. Finally, Eq. (5.8) was used to predict the evolution of elongation at break.

5.3.3.1 Results

Using the KSM described above provided evolving molecular weight distributions (Fig. 5.10a), with the initial distribution characterised based on PLLA data from Tsuji (2002) (dataset 1a, see Table 5.1). Fig. 5.10b shows the resulting trends for values of M_n^{crit} in the range $[50\ \mathrm{kg/mol}, 5000\ \mathrm{kg/mol}]$ (obtained using the KSM and Eq. (5.8)) alongside dataset 1a. For

$M_n^{crit} \leq 50$ kg/mol, a pronounced lagging behaviour is observed, with an 80% reduction in MW before ε_f declines (with $M_n^{crit} = 50$ kg/mol shown in Fig. 5.10 and similar trends seen for smaller values of M_n^{crit} simulated). The next interval of values explored, $M_n^{crit} = (50\text{ kg/mol}, 500\text{ kg/mol})$, results in a less pronounced lag, similar to that exhibited by Trend 1. Finally, for $M_n^{crit} \geq 500$ kg/mol, an instant decline in ε_f is observed alongside reductions in MW, similar to the behaviour displayed by Trend 2. In terms of the temporal evolution, which is directly obtained from the method already outlined, Fig. 5.10c indicates the wide range of behaviour captured depending on the choice of M_n^{crit}. For the dataset considered here, $M_n^{crit} = 100$ kg/mol reasonably captures both the relationship between $\overline{\varepsilon_f}$ vs $\overline{MW}$ and the temporal evolution of $\overline{\varepsilon_f}$, where properties are normalised by their initial values.

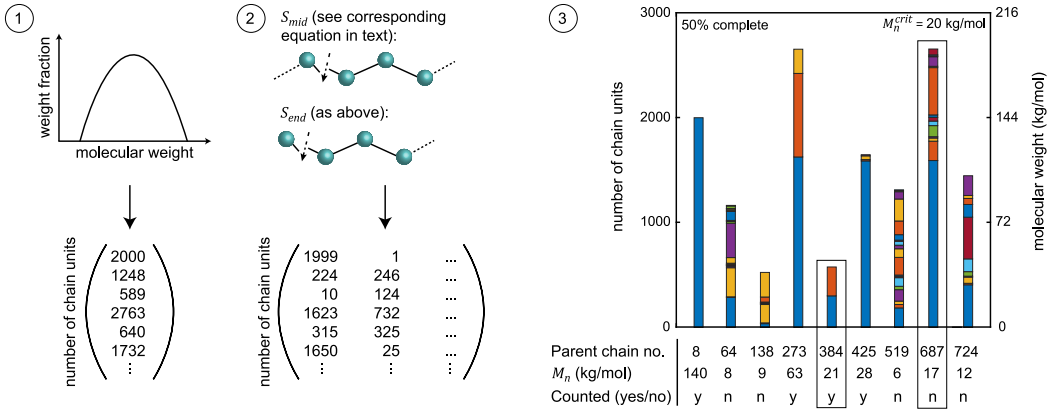

Fig. 5.9. Schematic illustration of kinetic scission model introduced in Chapter 4. Step 1 takes a representative polymer chain distribution in the form of an array of chains with a distribution of lengths. Step 2 simulates scissions on the array of chains according to Eq. (5.9) for mid-chain scissions and Eq. (5.10) for end-chain scissions. The updated chain lengths are stored in the array, with each row representing an initial chain and its resulting sub-chains. A sample of 9 initial representative polymer chains (from approximately 24000) are shown halfway through simulated degradation, where each bar represents an initial chain and each coloured fragment represents a sub-chain created via simulated scission. To calculate N_c, the number of chain groups above a critical molecular weight, M_n^{crit}, in Step 3, each initial chain and resulting sub-chains are taken as an individual group. Once $M_n < M_n^{crit}$ for a group, that group is excluded from the calculation of N_c; otherwise, the group contributes to the count of N_c. Note that despite Chain 384 appearing short compared with Chain 687 (and its largest fragment), it is included in the count of N_c as it has experienced few scissions and thus has a higher value of M_n than the highly degraded Chain 687.

For the normalised relationship being explored, $\overline{\varepsilon_f}$ vs $\overline{MW}$, Eq. (5.8) describes unique relationships dependent only on N_c. The evolution of N_c depends on the initial molecular weight distribution and how this evolves for each specific polymer, with the kinetic scission model requiring information on this initial distribution as input prior to the simulation.

However, this is not provided in many of the experimental studies surveyed here. Nevertheless, it is evident that many trends are captured by varying M_n^{crit}, ranging from lagged to abrupt declines in ε_f with reducing MW. Thus, Eq. (5.8) and the corresponding method described above offers an all-inclusive tool for predicting the relationship between ε_f and MW. By considering the entire MWD when predicting these properties, as done here, insight into the physicochemical mechanisms responsible for this behaviour may be obtained on further investigation.

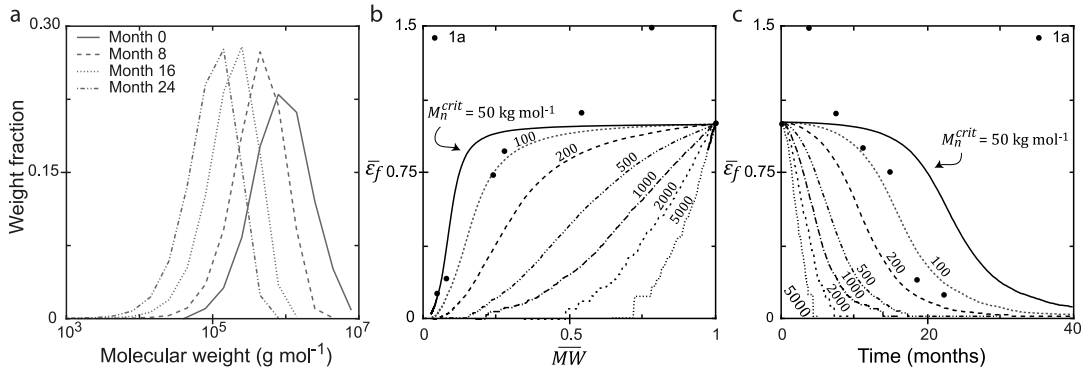

Fig. 5.10. (a) The KSM (Chapter 4) outlined in the text was used to obtain predictions for evolving molecular weight distributions. The initial distribution matches the experimental distribution of Tsuji (2002) for PLLA (dataset 1a). These distributions were then used to obtain values for N_c as described in Fig. 5.9. (b) Predictions for the relationship between ε_f and MW were obtained using Eq. (5.8) for ε_f^N. Both quantities were normalised by their initial values. Values for the molecular weight threshold were varied from 50 kg/mol to 5000 kg/mol. This resulted in predictions varying from a large lag, with $MW < 0.2MW_0$ before a decline in ε_f ($M_n^{crit} = 50$ kg/mol), to gradually more rapid declines in ε_f for larger values of M_n^{crit}. Experimental data corresponding to the initial MWD used is also shown. While increases in ε_f were not predicted, appropriate choice of M_n^{crit} allows for reasonable predictions. Alternatively, a failure envelope may be estimated using two threshold values, providing an upper and lower prediction. (c) The temporal evolution of ε_f is also found using the KSM. Increasing values of M_n^{crit} again result in more rapid declines in ε_f.

5.4 Temporal evolution of failure strain

Returning our focus to the experimental study of Tsuji (2002) and the temporal evolution of failure strain found for various forms of amorphous PLA (reproduced in Fig. 5.4a), the three failure criteria described by Eq. (5.5), Eq. (5.6) and Eq. (5.8) are explored in this context. Both Eq. (5.5) and Eq. (5.6) simply require parameter determination to best fit the relevant experimental data, while for Eq. (5.8) it is necessary to model the entire molecular weight distribution and its evolution during simulated degradation. This was carried out as outlined above for each of the four forms of PLA, with the corresponding initial MWD described by

Tsuji (2002) used as input for Step 1 of the KSM. Each of the parameters were calibrated as described in Steps 2 – 3 of the previous section and are outlined in Table 5.2.

To begin, the kinetic scission model (KSM) was calibrated as described in Chapter 4 for each set of experimental data in the study of Tsuji (2002), providing the temporal evolution of M_n and Young's modulus, E. From Fig. 5.11a-d, it is seen that the previously described KSM captured each dataset well. In addition to these properties, predictions for the evolution of the molecular weight distribution during degradation were obtained. This then provides information on N_c, the number of chain groups above the molecular weight threshold. With this information, it is now possible to consider each of the failure criteria.

Fig. 5.11e-h shows each of the three failure criteria for the various forms of PLA in the context of the relationship between ε_f and M_n, while Fig. 5.11i-l shows the temporal evolution of ε_f. Normalised properties are considered, reducing the number of parameters to be calibrated. Starting first with ε_f^{MW}, obtained using Eq. (5.5), a gradual decline in ε_f is observed, lagging the reduction in M_n. However, the decline in ε_f occurs more abruptly than that seen for PLLA, PDLA and PDLLA, while it is too gradual for PL/DLA. This is also seen with the temporal evolution, with ε_f^{MW} predicting a more rapid decline for all data except PL/DLA.

Next, ε_f^{exp} was considered, obtained using Eq. (5.6). With many of these polymers clearly not experiencing an exponential decline with M_n, A_3 was inversely chosen to ensure the first and final data points were captured, provided in Table 5.3. While PLLA, PDLA and PDLLA were poorly captured by this technique, good predictions were found for PL/DLA.

Finally, predictions were found for ε_f^N using Eq. (5.8) and details on the evolution of N_c obtained from the KSM. Various values of molecular weight threshold, M_n^{crit}, were explored to best fit the data, with r^2 maximised for the values given in Table 5.3. The relationship between ε_f and M_n is reasonably predicted for each of the polymers, with ε_f^N capable of predicting both lagged and more rapid declines. The predictions for the temporal evolution also capture the experimental trends reasonably well. Thus, Eq. (5.8) and the corresponding failure criterion, ε_f^N, appears to be suitable for predicting the temporal evolution of ε_f when used in conjunction with the KSM (Chapter 4), irrespective of the experimental trend.

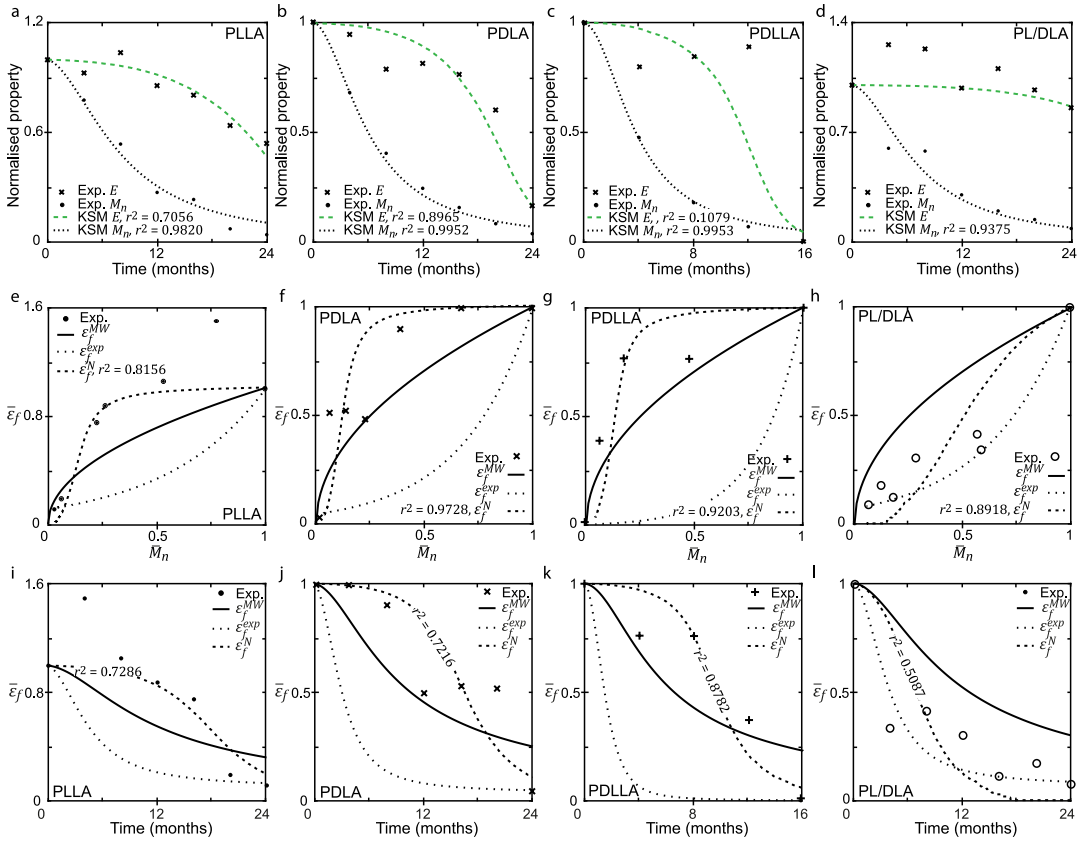

Fig. 5.11. (a-d) Temporal evolution of M_n and E as obtained in the degradation study of Tsuji (2002) (discrete symbols) alongside predictions obtained using the KSM (Chapter 4) (lines). The KSM successfully captured the trends using the parameters detailed in Table 5.2. (e-h) Relationship between ε_f and M_n for each failure criteria, where ε_f^{MW} depends on average molecular weight (Eq. (5.5)), ε_f^{exp} describes an exponential delince (Eq. (5.6)), and ε_f^N depends on a molecular weight threshold (Eq. (5.8)). While ε_f^{MW} and ε_f^{exp} poorly capture some of the experimental trends of Tsuji (2002), ε_f^N reasonably captures both the lagged decline of ε_f for PLLA, PDLA and PDLLA and the more rapid decline of ε_f for PL/DLA. (i-l) Temporal evolution of ε_f for each failure criteria, again indicating the predicitive capability of ε_f^N. Properites are normalised by initial values.

Table 5.2. Input parameters used for the kinetic scission model for each of the polymers modelled. The simple hydrolytic reaction generates mid- and end-chain scissions according to k_{hm} and k_{he}, respectively. Similarly, the autocatalytic reaction rates, k_{am} and k_{ae}, govern the rate at which mid- and end-chain scissions, respectively, occur due to autocatalysis. Additionally, n is the acid dissociation constant, L_{ol} is the oligomer length, C_{a0} is the initial carboxylic acid end concentration and C_{e0} is the initial ester bond concentration. Finally, M_w^{crit} is the weight average molecular weight threshold, the parameter used when predicting Young's modulus, E.

Polymer	k_{he} (month^{-1})	k_{hm} (month^{-1})	k_{ae} $\left(\left(\text{m}^3\text{mol}^{-1}\right)^{1/2}\text{month}^{-1}\right)$	k_{am} $\left(\left(\text{m}^3\text{mol}^{-1}\right)^{1/2}\text{month}^{-1}\right)$	n	L_{ol}	C_{a0} (mol m^{-3})	C_{e0} (mol m^{-3})	M_w^{crit} (kg mol^{-1})
PLLA	1×10^{-6}	1×10^{-6}	2×10^{-5}	2×10^{-5}	0.5	1	0	17300	100
PDLA	1×10^{-6}	1×10^{-6}	3×10^{-5}	3×10^{-5}	0.5	1	0	17300	70
PDLLA	1×10^{-6}	1×10^{-6}	7×10^{-5}	7×10^{-5}	0.5	1	0	17300	40
PL/DLA	1×10^{-6}	1×10^{-6}	2.5×10^{-5}	2.5×10^{-5}	0.5	1	0	17300	40

Table 5.3. Parameters used for each of the failure criteria in obtaining the predictions for the four forms of PLA studied by Tsuji (2002) shown in Fig. 5.11. As normalised trends are considered, parameters A_1, A_2 and A_4 are not required.

Failure criteria	ε_f^{MW}	ε_f^{exp}	ε_f^{N}
Parameter	–	A_3	M_n^{crit} (kg mol^{-1})
PLLA	–	4.02×10^{-6}	100
PDLA	–	7.10×10^{-6}	70
PDLLA	–	2.08×10^{-5}	40
PL/DLA	–	6.23×10^{-6}	500

5.5 Discussion

Following a detailed literature survey of 27 datasets from 9 publications (Deng et al., 2005; Duek et al., 1999; Kranz et al., 2000; Polak-Kraśna et al., 2021; Tsuji, 2002; Tsuji et al., 2000; Tsuji and Del Carpio, 2003; Weir et al., 2004a, 2004b), two trends were identified for the relationship between failure strain, ε_f, and average molecular weight, MW: (i) Trend 1 typically experiences no decline in ductility initially (or even increases), with a lagged decline compared with the reduction in MW (Fig. 5.5c); while (ii) for Trend 2, ε_f has declined by >50% with a 20% reduction in MW and no initial increase in ε_f is observed (Fig. 5.5d). However, the underlying cause behind these two differing trends is not obviously evident from the information provided in experimental studies (Table 5.1).

Further investigation into the causes behind the two identified trends may provide valuable insight into the physicochemical degradation mechanisms and the impact of these on the mechanical behaviour. While it is expected that amorphous and semi-crystalline polymers would vary in terms of ductility, with the chains within the more rigid structure of semi-crystalline polymers assumed to be more restricted during stretching, neither structure type was uniquely defined by either trend. Furthermore, strain is higher in the amorphous phase and the ductility of this phase should set the overall ductility (Callister Jr and Rethwisch, 2018). In the study by Tsuji et al. (2000) where PLLA with various degrees of crystallinity, X_c, were investigated, those with lower values of X_c were found to lose their ductility more abruptly, following Trend 2. However, it should be noted that each of the datasets identified as Trend 2 from that study had a higher initial value of ε_f and they also experienced a larger increase in X_c during degradation, both of which may impact the trends seen.

Amongst the studies considered, several reported number average molecular weight, M_n, others reported weight average molecular weight, M_w, and some reported both, as detailed in Table 5.1. Flory (1945) previously discussed the importance of the number of ends of molecules, and consequently M_n, when considering failure in polymers, albeit primarily focused on cellulose, ultimately leading to a relationship between tensile strength and M_n. However, no difference was evident for the relationship between ε_f and either M_n or M_w in the experimental data considered here, suggesting that a more general relationship between ε_f and an average molecular weight, MW, may exist, where MW is either M_n or M_w.

While differences in technique may be expected between experimental studies, uniformity is expected between different datasets within isolated publications. However, several of the publications considered here contain data spanning both trends (Tsuji, 2002; Tsuji et al.,

2000; Tsuji and Del Carpio, 2003). For example, in a study carried out by Tsuji (2002), various forms of amorphous PLA (PLLA, PDLA, PDLLA, PL/DLA) were subjected to the same degradation conditions, with all except PL/DLA found to exhibit the behaviour described by Trend 1. While this lends the question as to potential differences exhibited by polymer blends, nothing concrete can be determined from this small dataset. It should also be noted that large error margins for ε_f were reported in several studies, most notably being >40% reported by Tsuji (2002).

All the studies surveyed had similarities in degradation protocol, with each study carried out in phosphate buffer solution (pH 7.4) and many at 37 °C. However, from the details provided, large variances in solution volume were evident (Kranz et al., 2000; Tsuji, 2002). Additionally, some reported changing the solution every week (Deng et al., 2005), some once a month (Polak-Kraśna et al., 2021), while others did not mention this at all. Furthermore, no information was provided on the initial acid end concentration of the polymers and whether they were end capped, which has been shown previously to influence degradation (Tracy et al., 1999). While the glass transition temperature should begin at a similar value for each of the polymers considered here, its evolution during degradation may vary between datasets. The effect of processing may also influence this behaviour, particularly in terms of the resulting molecular weight distribution generated. Each of these factors could influence the degradation behaviour, potentially contributing to differences observed.

Despite the uncertainty in why such variances are evident in the data, several failure criteria were introduced, and their predictive capabilities were explored in the context of both trends. The first criterion, ε_f^{MW} (Eq. (5.5)), defines a physical relationship between evolving molecular weight and failure strain by considering the finite extensibility of an average polymer chain. This was successful in capturing the lagged decline in ε_f seen for reducing MW exhibited by most of the data, i.e., Trend 1 (Fig. 5.7). In contrast, an empirical relationship was necessary to capture the exponential-like decline of Trend 2 (Fig. 5.8), leading to the introduction of the second criterion, ε_f^{exp} (Eq. (5.6)). However, without proper understanding of the mechanism behind these trends, use of these criteria require caution. While much of the data is predicted by ε_f^{MW}, it is not appropriate for polymers exhibiting Trend 2 behaviour, predicting much later failure than that observed for these polymers. In contrast, using ε_f^{exp} for all polymers may have the opposite effect, possibly resulting in over-engineered materials with longer lifetimes than necessary in many cases, potentially leading to undesirable long-term effects.

The third failure criterion introduced, ε_f^N (Eq. (5.8)), introduces a modification to the previous chain extensibility criterion (Eq. (5.5)). This criterion captures the reduction in long chains during degradation and connects it with the ability of the polymer to undergo ductile deformation. Once the network consists mostly of short chains, then the behaviour becomes brittle. This is factored in using a molecular weight threshold, which requires a detailed description of the evolving molecular weight distribution. Predictions for this were obtained using the kinetic scission model (KSM) (Fig. 5.10) proposed in Chapter 4, which was described for amorphous polymers experiencing heterogenous bulk degradation. In this chapter, the KSM was used to obtain evolving molecular weight distributions for a sample case in Section 5.3.3 (based on an initial distribution from Tsuji (2002), dataset 1a) and for each of the polymers studied by Tsuji (2002) in Section 5.4 (datasets 1a-1d). Little mass loss was reported for PLLA, PDLA and PL/DLA after 24 months degradation and for PDLLA up to 12 months degradation, and each of the initially amorphous films remained so throughout degradation (Tsuji, 2002). It is also expected that PLA films with dimension 3 mm x 30 mm x 50-150 μm undergo heterogenous bulk degradation (Shirazi et al., 2016a; von Burkersroda et al., 2002). As such, the KSM is deemed appropriate for modelling that set of data and was suitably calibrated to describe changes in M_n and E in agreement with experimental data. Additionally, it was found that ε_f^N reasonably predicted the data of Tsuji (2002) (Fig. 5.11). Going forward, this approach may be used to explore the influence of the initial molecular weight distribution to determine if the brittle transition can be delayed during processing. A modified KSM would be necessary to consider factors such as crystallinity and mass loss.

The first two criteria introduced, ε_f^{MW} and ε_f^{exp}, both consider an average molecular weight of a polymer network and showed success in capturing Trend 1 and Trend 2, respectively. In contrast, ε_f^N considers the entire polymer molecular weight distribution and links ductility to the portion of short chains in the network using a critical molecular weight threshold. It was observed that ε_f^N could capture a wide range of trends, spanning both Trend 1 and Trend 2 behaviour. This may suggest that short chains play an important role in ductility, with short chains readily reaching their finite extensibility during stretching. Changes in the molecular weight distribution during degradation and any preferential degradation towards chain ends that result in a build-up of short chains may explain the different trends observed. Many of the studies considered in Table 5.1 do not provide details on molecular weight distribution, making a detailed investigation into this challenging at present; a more in-depth experimental exploration of the effect of the width of the molecular weight distribution on the ductility of these materials may provide valuable insight into the underlying behaviour.

Alternatively, the datasets categorised as Trend 2 may have formed local imperfections during processing that could explain the rapid declines in ductility observed; the large error margins reported in studies would support this.

The failure criteria introduced here assume nominal strain, with several of the literature studies surveyed specifying that this quantity was considered in the data presented (Deng et al., 2005; Polak-Kraśna et al., 2021). A simple adjustment to each criterion would offer predictions for the incremental failure strain. The criteria presented offer predictions for the decline in ductility as degradation takes place in PLA and can likely be extended to other biocompatible polymers that experience similar degradation behaviour. Several of the experimental studies surveyed reported an initial increase in ε_f (Fig. 5.5). Deng et al. (2005) suggested that this increase may be due to fibre relaxation caused by water absorption, leading to swelling and plasticization and a decrease in molecular chain orientation. While these effects are not considered herein, early failure and, thus, the decline in ε_f is of primary concern here.

Predictions for the temporal evolution of ε_f obtained using the kinetic scission model was found to agree reasonably with experimental data provided appropriate selection of criteria (Fig. 5.11). This can be used to predict the time taken for half ductility, for example, and provide an estimated timeline for end-of-use. While each of the criterion introduced has provided good predictions in certain settings, prior knowledge of which is most appropriate may be challenging without further insight into why the two identified trends emerge. Thus, the immediate priority should be experimental in nature and explore the effects of factors discussed above on these trends, for example, acid concentration, changes in crystallinity, width of the MWD, etc. In the meantime, multiple failure criteria may be used in parallel with one another, offering a failure envelope. Such predictions can be visualised in Fig. 5.11, where a selection of two or more criteria provides predictions for an upper and lower value of ε_f.

5.6 Conclusion

Analysis of published data for the relationship between ε_f and MW in degrading PLA revealed two distinct trends. The first (Trend 1) typically experiences no decline in ductility initially with a subsequent lagged decline compared with the reduction in MW, while the second (Trend 2) showed a rapid decline in ε_f, declining by >50% with a 20% reduction in MW. No underlying cause for these differing trends could be identified from the details provided in the respective experimental studies.

Nevertheless, several failure criteria were introduced, and their predictive capability was explored in the context of both trends: (i) ε_f^{MW}, which considers the finite extensibility of an average polymer chain based on MW, is appropriate for modelling the datasets characterised as Trend 1; (ii) an exponential empirical criterion, ε_f^{exp}, captures Trend 2; while (iii) ε_f^{N}, a modification of ε_f^{MW} that considers the entire molecular weight distribution and places more emphasis on short, degraded chains, successfully captures both trends, but requires knowledge of initial molecular weight distributions.

Each criterion provides good predictions when used in the right setting; however, clarification of why the two degradation trends identified emerge should be explored as this may provide greater insight into the degradation mechanism and in turn allow for improved predictions of these materials. The framework developed here can be combined with detailed experimental characterisation (to include fully describing the molecular weight distribution and measuring the initial acid concentration and end capping) to further explore the onset of brittle behaviour in degrading polymers.

References

Antheunis, H., van der Meer, J.C., de Geus, M., Kingma, W., Koning, C.E., 2009. Improved Mathematical Model for the Hydrolytic Degradation of Aliphatic Polyesters. Macromolecules 42, 2462–2471. https://doi.org/10.1021/ma802222m

Bartczak, Z., 2017. Deformation of semicrystalline polymers – the contribution of crystalline and amorphous phases. Polimery 62, 787–799. https://doi.org/10.14314/polimery.2017.787

Busatto, C., Pesoa, J., Helbling, I., Luna, J., Estenoz, D., 2017. Heterogeneous hydrolytic degradation of poly (lactic-co-glycolic acid) microspheres: Mathematical modeling. J. Appl. Polym. Sci. 134, 45464. https://doi.org/10.1002/app.45464

Callister Jr, W.D., Rethwisch, D.G., 2018a. Materials Science and Engineering - An Introduction, 10th ed. John Wiley & Sons.

Callister Jr, W.D., Rethwisch, D.G., 2018b. Deformation of semicrystalline polymers, in: Materials Science and Engineering - An Introduction. John Wiley & Sons, pp. 522–525.

Deng, M., Zhou, J., Chen, G., Burkley, D., Xu, Y., Jamiolkowski, D., Barbolt, T., 2005. Effect of load and temperature on in vitro degradation of poly(glycolide-co-L-lactide) multifilament braids. Biomaterials 26, 4327–4336. https://doi.org/10.1016/j.biomaterials.2004.09.067

Deroiné, M., Le Duigou, A., Corre, Y.-M., Le Gac, P.-Y., Davies, P., César, G., Bruzaud, S., 2014. Accelerated ageing and lifetime prediction of poly(3-hydroxybutyrate-co-3- hydroxyvalerate) in distilled water. Polym. Test. 39, 70–78. https://doi.org/10.1016/j.polymertesting.2014.07.018

Duek, E.A.R., Zavaglia, C.A.C., Belangero, W.D., 1999. In vitro study of poly(lactic acid) pin degradation. Polymer 40, 6465–6473. https://doi.org/10.1016/S0032-3861(98)00846-5

Fayolle, B., Audouin, L., Verdu, J., 2004. A critical molar mass separating the ductile and brittle regimes as revealed by thermal oxidation in polypropylene. Polymer 45, 4324–4330. https://doi.org/10.1016/j.polymer.2004.03.069

Fayolle, B., Colin, X., Audouin, L., Verdu, J., 2007. Mechanism of degradation induced embrittlement in polyethylene. Polym. Degrad. Stab. 92, 231–238. https://doi.org/10.1016/j.polymdegradstab.2006.11.012

Flory, P.J., 1945. Tensile Strength in Relation to Molecular Weight of High Polymers. J. Am. Chem. Soc. 67, 2048–2050. https://doi.org/10.1021/ja01227a506

Gardner, R.J., Martin, J.R., 1979. Humid aging of plastics: Effect of molecular weight on mechanical properties and fracture morphology of polycarbonate. J. Appl. Polym. Sci. 24, 1269–1280.

https://doi.org/10.1002/app.1979.070240512
Gleadall, A., Pan, J., Kruft, M.A., Kellomäki, M., 2014. Degradation mechanisms of bioresorbable polyesters. Part 1. Effects of random scission, end scission and autocatalysis. Acta Biomater. 10, 2223–2232. https://doi.org/10.1016/j.actbio.2013.12.039
Golden, J.H., Hammant, B.L., Hazell, E.A., 1964. Degradation of polycarbonates. IV. Effect of molecular weight on flexural properties. J. Polym. Sci. Part A Gen. Pap. 2, 4787–4794. https://doi.org/10.1002/pol.1964.100021109
Hayman, D., Bergerson, C., Miller, S., Moreno, M., Moore, J.E., 2014. The Effect of Static and Dynamic Loading on Degradation of PLLA Stent Fibers. J. Biomech. Eng. 136, 1–9. https://doi.org/10.1115/1.4027614
Kranz, H., Ubrich, N., Maincent, P., Bodmeier, R., 2000. Physicomechanical Properties of Biodegradable Poly(D,L-lactide) and Poly(D,L-lactide-co-glycolide) Films in the Dry and Wet States. J. Pharm. Sci. 89, 1558–1566. https://doi.org/10.1002/1520-6017(200012)89:12<1558::AID-JPS6>3.0.CO;2-8
Laycock, B., Nikolić, M., Colwell, J.M., Gauthier, E., Halley, P., Bottle, S., George, G., 2017. Lifetime prediction of biodegradable polymers. Prog. Polym. Sci. 71, 144–189. https://doi.org/10.1016/j.progpolymsci.2017.02.004
Lyu, S.P., Schley, J., Loy, B., Lind, D., Hobot, C., Sparer, R., Untereker, D., 2007. Kinetics and time-temperature equivalence of polymer degradation. Biomacromolecules 8, 2301–2310. https://doi.org/10.1021/bm070313n
Pitt, C.G., Gu, Z.-W., 1987. Modification of the rates of chain cleavage of poly(ε-caprolactone) and related polyesters in the solid state. J. Control. Release 4, 283–292. https://doi.org/10.1016/0168-3659(87)90020-4
Polak-Kraśna, K., Abaei, A.R., Shirazi, R.N., Parle, E., Carroll, O., Ronan, W., Vaughan, T.J., 2021. Physical and mechanical degradation behaviour of semi-crystalline PLLA for bioresorbable stent applications. J. Mech. Behav. Biomed. Mater. 118, 1–11. https://doi.org/10.1016/j.jmbbm.2021.104409
Shirazi, R.N., Aldabbagh, F., Erxleben, A., Rochev, Y., McHugh, P., 2014. Nanomechanical properties of poly(lactic-co-glycolic) acid film during degradation. Acta Biomater. 10, 4695–4703. https://doi.org/10.1016/j.actbio.2014.08.004
Shirazi, R.N., Aldabbagh, F., Ronan, W., Erxleben, A., Rochev, Y., McHugh, P., 2016a. Effects of material thickness and processing method on poly(lactic-co-glycolic acid) degradation and mechanical performance. J. Mater. Sci. Mater. Med. 27, 1–12. https://doi.org/10.1007/s10856-016-5760-z
Shirazi, R.N., Ronan, W., Rochev, Y., McHugh, P., 2016b. Modelling the degradation and elastic properties of poly(lactic-co-glycolic acid) films and regular open-cell tissue engineering scaffolds. J. Mech. Behav. Biomed. Mater. 54, 48–59. https://doi.org/10.1016/j.jmbbm.2015.08.030
Siparsky, G.L., Voorhees, K.J., Miao, F., 1998. Hydrolysis of Polylactic Acid (PLA) and Polycaprolactone (PCL) in Aqueous Acetonitrile Solutions: Autocatalysis. J. Environ. Polym. Degrad. 6, 31–41. https://doi.org/1064-7546/98/0100-0031
Soares, J.S., Moore, J.E., Rajagopal, K.R., 2010. Modeling of Deformation-Accelerated Breakdown of Polylactic Acid Biodegradable Stents. J. Med. Device. 4, 1–10. https://doi.org/10.1115/1.4002759
Thomas, D.P., Hagan, R.S., 1969. The Influence of Molecular Weight Distribution on Melt Viscosity, Melt Elasticity, Processing Behaviour and Properties of Polystyrene. Polym. Eng. Sci. 9, 164–171. https://doi.org/10.1002/pen.760090304
Tracy, M.A., Ward, K.L., Firouzabadian, L., Wang, Y., Dong, N., Qian, R., Zhang, Y., 1999. Factors affecting the degradation rate of poly(lactide-co-glycolide) microspheres in vivo and in vitro. Biomaterials 20, 1057–1062. https://doi.org/10.1016/S0142-9612(99)00002-2
Tsuji, H., 2002. Autocatalytic hydrolysis of amorphous-made polylactides: effects of L-lactide content, tacticity, and enantiomeric polymer blending. Polymer 43, 1789–1796. https://doi.org/10.1016/S0032-3861(01)00752-2
Tsuji, H., Del Carpio, C.A., 2003. In vitro hydrolysis of blends from enantiomeric poly(lactide)s. 3. Homocrystallized and amorphous blend films. Biomacromolecules 4, 7–11. https://doi.org/10.1021/bm020090v
Tsuji, H., Mizuno, A., Ikada, Y., 2000. Properties and morphology of poly(L-lactide). III. Effects of initial crystallinity on long-term in vitro hydrolysis of high molecular weight poly(L-lactide) film in phosphate-buffered solution. J. Appl. Polym. Sci. 77, 1452–1464. https://doi.org/10.1002/1097-

4628(20000815)77:7<1452::AID-APP7>3.0.CO;2-S

Venkatraman, S.S., Poh, T.L., Vinalia, T., Mak, K.H., Boey, F., 2003. Collapse pressures of biodegradable stents. Biomaterials 24, 2105–2111. https://doi.org/10.1016/S0142-9612(02)00640-3

Vieira, A.C., Guedes, R.M., Tita, V., 2014. Constitutive modeling of biodegradable polymers: Hydrolytic degradation and time-dependent behavior. Int. J. Solids Struct. 51, 1164–1174. https://doi.org/10.1016/j.ijsolstr.2013.12.010

Vieira, A.C., Vieira, J.C., Ferra, J.M., Magalhães, F.D., Guedes, R.M., Marques, A.T., 2011. Mechanical study of PLA–PCL fibers during in vitro degradation. J. Mech. Behav. Biomed. Mater. 451–460. https://doi.org/10.1016/j.jmbbm.2010.12.006

von Burkersroda, F., Schedl, L., Göpferich, A., 2002. Why degradable polymers undergo surface erosion or bulk erosion. Biomaterials 23, 4221–4231. https://doi.org/10.1016/S0142-9612(02)00170-9

Wang, P.-J., Ferralis, N., Conway, C., Grossman, J.C., Edelman, E.R., 2018. Strain-induced accelerated asymmetric spatial degradation of polymeric vascular scaffolds. Proc. Natl. Acad. Sci. 115, 2640–2645. https://doi.org/10.1073/pnas.1716420115

Wang, Y., Han, X., Pan, J., Sinka, C., 2010. An entropy spring model for the Young's modulus change of biodegradable polymers during biodegradation. J. Mech. Behav. Biomed. Mater. 3, 14–21. https://doi.org/10.1016/j.jmbbm.2009.02.003

Wang, Y., Pan, J., Han, X., Sinka, C., Ding, L., 2008. A phenomenological model for the degradation of biodegradable polymers. Biomaterials 29, 3393–3401. https://doi.org/10.1016/j.biomaterials.2008.04.042

Ward, I.M., 1971. Mechanical properties of solid polymers. Wiley-Interscience.

Ward, I.M., Sweeney, J., 2013. Mechanical properties of solid polymers, 3rd ed. John Wiley & Sons.

Weir, N.A., Buchanan, F.J., Orr, J.F., Dickson, G.R., 2004a. Degradation of poly-L-lactide. Part 1: In vitro and in vivo physiological temperature degradation. Proc. Inst. Mech. Eng. Part H J. Eng. Med. 218, 307–319. https://doi.org/10.1243/0954411041932782

Weir, N.A., Buchanan, F.J., Orr, J.F., Farrar, D.F., Dickson, G.R., 2004b. Degradation of poly-L-lactide. Part 2: Increased temperature accelerated degradation. Proc. Inst. Mech. Eng. Part H J. Eng. Med. 218, 321–330. https://doi.org/10.1243/0954411041932809

6 Modelling finite chain extensibility in a degrading polymer network

Although Chapter 5 saw the introduction of failure criteria that reasonably capture the failure strain of polymers such as PLA, it did not shed sufficient light onto the physical mechanisms behind this evolution. Up to this point of the thesis, the models introduced have considered entropy in a simplistic way, with a binary count of chain groups depending on their molecular weight with respect to a molecular weight threshold parameter. We now turn our focus to a more rigorous consideration of entropy.

Upon deformation of a polymer network, chains change from a coiled to an extended configuration, with a gradual reduction in entropy. Short chains may fully extend at modest strains, contributing nothing more to the change in entropy on further extension of the material. Using statistical mechanics methods for rubber-like materials, we investigate how finite chain extensibility contributes to elasticity changes during degradation. Here, elastic properties are related to network chain end-to-end distance distributions and are assumed to arise solely as a result of conformational changes in the network chains.

Following an overview of the motivation for this work in Section 6.1, Section 6.2 provides an overview of theory and some initial explorations. Predictions for the mechanical behaviour are first investigated using an average molecular weight (Section 6.3), similar to the approach of Stepto and Taylor (1995a) for non-degrading polymers. The solution approach is detailed in Section 6.3.1 by way of a flowchart. Subsequently, molecular weight distributions and proper treatment of fully extended chains are considered for more accurate predictions of the mechanical properties (Section 6.4); a comparison between the approaches of Section 6.3 and Section 6.4 is presented in Fig. 6.13. The kinetic scission model developed in Chapter 4 is used to generate a full evolving molecular weight distribution to represent degrading PLA-PCL (90:10) for the input to model the material studied by Vieira et al. (2011), who only report M_n for each timepoint alongside evolving stress-strain curves. Considering the stress response, the method is validated using a qualitative comparison with the stress-strain curves of Vieira et al. (2011) reproduced in Fig. 6.1a, with similar mechanical behaviour observed between the experimental study and the simulated system (Section 6.5). In Section 6.6, the failure criteria introduced in Chapter 5 are used to overlay predictions for failure strain on the stress-strain predictions obtained in this chapter. Section 6.7 briefly explores extending the method introduced for uniaxial tension to alternative modes of deformation, prior to a discussion of the findings in Section 6.8. A sensitivity analysis, pseudocode and

MATLAB® (R2020b, The MathWorks, Inc., MA, USA) code may be found in the Appendices at the close of this chapter.

6.1 Motivation

6.1.1 Degradation behaviour

As previously described (Section 2.1), biodegradable polymers contain many long macromolecular chains with a distribution of chain lengths containing repeat units bonded together chemically. Biocompatible materials such as polylactic acid (PLA) and polycaprolactone (PCL) experience degradation due to a hydrolytic reaction when placed in an aqueous medium, with bonds being broken throughout polymer chains (Buchanan, 2008). As chains break, the molecular weight distribution transitions, resulting in a lower molecular weight for the material. A simultaneous reduction in the mechanical properties is observed.

On mechanically testing PLA-PCL (90:10) fibres during degradation, Vieira et al. (2011) found that while the stress-strain behaviour was initially characteristic of ductile polymer behaviour, this transitioned during degradation, with a progressive loss in strength and ultimate strain (reproduced in Fig. 6.1). A simultaneous reduction in number average molecular weight, M_n, was observed, with little mass loss up to 8 weeks degradation. Polak-Kraśna et al. (2021) detected similar for degrading PLLA, observing an almost immediate post-yield fracture as degradation progressed.

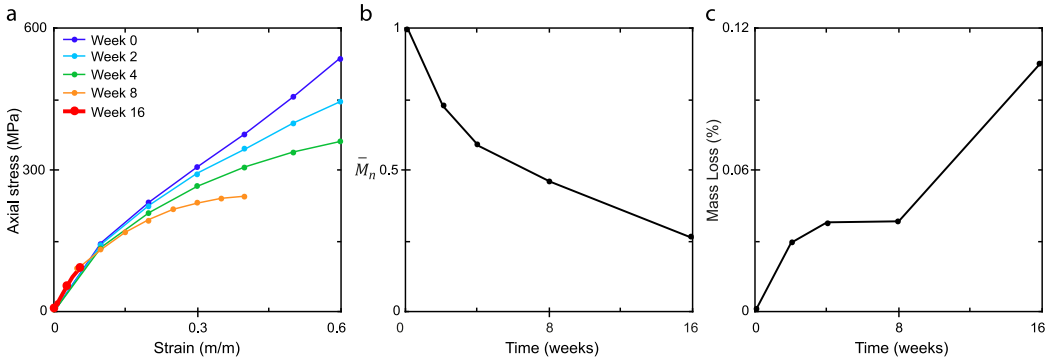

Fig. 6.1. Experimental mechanical testing and degradation study of PLA-PCL (90:10) fibres show the (a) stress-strain response transitions from ductile to brittle behaviour during degradation, (b) the normalised number average molecular weight, $\overline{M_n}$, simultaneously declines, and this is accompanied by (c) mass loss of the material. Adapted from Vieira et al. (2011).

6.1.2 Existing models for biodegradable polymers

Several studies have developed material constitutive models to describe the evolution of mechanical properties in degrading polymers, as further outlined in Section 3.2.4. Efforts

from Vieira et al. (2014, 2011), Soares et al. (2010), and Hayman et al. (2014) have contributed significantly to this area in recent years, including (i) the development of a model combining the relationship between fracture strength and molecular weight with hyperelastic material models, resulting in evolving stress-strain curves for PLA-PCL fibres during degradation (Vieira et al., 2014, 2011); (ii) a thermodynamic approach that considered the effect of deformation on degradation behaviour, providing evolving stress-strain curves for PLLA stent fibres under tensile loading conditions (Soares et al., 2010); and (iii) an investigation into the effect of different loads at different stages of degradation on PLLA fibres, capturing the increased reduction in mechanical properties with increased loading observed experimentally (Hayman et al., 2014). Nevertheless, these constitutive models require extensive experimental data as the material parameters are material functions of degradation damage instead of material constants. This poses a challenge, with small changes to these materials often resulting in significantly different behaviour. Further understanding of the physicochemical response during deformation may allow for an improved modelling framework throughout degradation that requires less sensitive experimentally determined parameters. To obtain this understanding, a model that considers the elastic response of all individual chains rather than an average chain may be instrumental.

6.1.3 Finite chain extensibility

Towards this understanding, the effect of short chains and their finite extensibility on the mechanical response is considered. As the evolution of the molecular weight distribution during degradation is accompanied by the evolution of mechanical properties, an investigation into how these interrelate should be carried out. In particular, considering how the introduction of shorter chains into the molecular weight distribution contributes to the elastic properties of the material may be valuable in understanding the overall behaviour.

While the finite extensibility of polymer chains has often been neglected in modelling techniques, several publications have considered this effect on the deformation behaviour, with focus restricted to non-degrading polymers. Edward and Vilgis (1986) extended the theory of rubber-like elasticity to include the finite extensibility of chains within the network using a phenomenological approach with a Langevin probability function for chain end-to-end lengths (Kuhn and Grün, 1946). Arruda and Boyce (1993) introduced the eight-chain model, with chains linked at the centre of a cube and extending to the corners. Each chain in the system undergoes a stretch equivalent to that in every other network chain, with the

contributions of a single chain averaged over eight spatial orientations. Stepto and Taylor (1995a) extended that approach by calculating the elastic force from the total deformation of the end-to-end vectors of individual network chains, rather than from the deformation of average chains. They implemented a statistical mechanics approach, taking a sample of $\sim 10^6$ chain conformations and accounting for the gradual change in entropy caused by chains moving from a coiled to an extended configuration on deformation. It was observed that short chains could fully extend at physically relevant strains, at which point they contributed nothing more to the change in entropy on further deformation, resulting in a steady decrease in the rate of network free energy change. Experimentally observed deviations from affine, Gaussian network-chain behaviour were reproduced. Computational limitations prevented non-uniform polymers from being modelled in their studies, with each chain in the simulated network having the same length, consistent with an average molecular weight. Further details of their approach are presented in Section 3.2.7.

6.1.4 Objectives

The current chapter aims to address the limitations outlined above in the context of biodegradable polymers with an evolving molecular weight distribution. We propose a physically based approach, taking a representative polymer chain distribution subjected to incremental degradation, as outlined in Chapter 4, applying an end-to-end distance distribution for the network, and subjecting the chain ensemble to an incremental stretch at each timepoint. Motivated by Stepto and Taylor (1995a), a statistical mechanics model is implemented, allowing for more rigorous considerations of both (i) entropy changes within the polymer network and (ii) the finite extensibility of polymer chains than that offered by current models for biodegradable polymers. A comparison between Stepto and Taylor's (1995a) method and the proposed method is provided in Table 6.3 in the Discussion.

The novel work presented herein, when coupled with previous chapters, allows for (i) an evolving molecular weight distribution of chains to be considered, as opposed to an average molecular weight, (ii) with predictions obtained for evolving stress-strain curves throughout degradation, (iii) alongside predictions for failure strain that may be overlayed on the curves. A qualitative comparison between the simulated system and both the experimental study of Vieira et al. (2011) and the neo-Hookean model helps validate the model. The solution approach is detailed in Section 6.3.1.

6.2 Statistical mechanics of polymeric chains – rubber-like elasticity

In this section, the statistical mechanics theory for rubber-like deformation of materials is outlined, with further details presented in Section 2.3; also see the textbooks of Ward and co-workers (1971; 1993; 2013) and Mark and co-workers (2007; 2007). This section summarises "entropy springs" (Section 6.2.1), polymer chain models (Section 6.2.2), the end-to-end distance distribution for polymer chains (Section 6.2.3), the change in entropy of a polymer system as it is subjected to an external force (Section 6.2.4), and the resulting strain-energy potential of a Gaussian system (Section 6.2.5).

Although polymers such as PLA ($T_g = 49 - 69°\mathrm{C}$) (Hiljanen-Vainio et al., 1996; Weir et al., 2004a) and PGA ($T_g = 35 - 45°\mathrm{C}$) (Buchanan, 2008; Reed and Gilding, 1981) are typically below T_g initially and therefore not in their rubber-like state at typical operable temperatures, models that assume rubber-like behaviour have previously sufficiently captured their behaviour (Shirazi et al., 2016b; Wang et al., 2010). Throughout degradation, variations in T_g exist, often declining below the testing temperature (Malin et al., 1996; Vey et al., 2008). Additionally, the deformation of glassy polymers is not well understood. Consequently, we restrict our focus to the generally accepted rubber-like theories.

6.2.1 "Entropy springs"

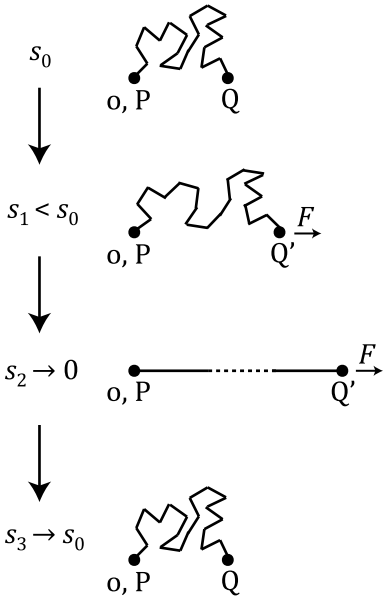

Fig. 6.2. Prior to deformation, a chain is attracted to a maximum state of entropy, s_0. On deformation, F, the entropy reduces ($s_1 < s_0$), with fewer possible configurations, gradually reaching its fully extended state ($s_2 \to 0$), for which only one configuration exists. On removal of the external force, the chain is once again attracted to a maximum state of entropy ($s_3 \to s_0$), provided no irreversible deformation has taken place.

In contrast to materials known as “energy springs”, where extension causes an increase in internal energy, the terms “probability or entropy springs” are sometimes used to refer to rubber-like materials. This is because all chain configurations have approximately the same internal energy and it is instead the entropy primarily controlling the deformation. When subjected to an external force, chains, forced from their state of maximum entropy, extend in the direction of the force, reducing the entropy and resulting in a state of strain (Fig. 6.2); on the removal of an external stress, an extended chain returns to its most probable state (assuming no irreversible deformation has taken place). By first calculating the entropy of a single chain in the polymer network and then relating this to the change in entropy of a network of chains as a function of strain, one can gain insight into the stress-strain characteristics of the material; subsequent sections describe how to approach this.

6.2.2 Equivalent freely jointed chain

The idealised equivalent freely jointed chain model (Kuhn and Grün, 1946) is considered in this work; further details on alternative polymer chain models are presented in Section 2.3.2. As well described by Fetters et al. (2007), aliphatic backbone polymers have n monomers, each with n_b backbone bonds, with a well-defined average backbone bond length l, and known average backbone bond angle θ. An alternative idealisation to the freely rotating chain, which contains n links of length l and fixed valence bond angle $\pi - \theta$ (Fig. 6.3a), the equivalent freely jointed chain contains n_K equivalent Kuhn links of length l_K, referred to as the Kuhn length. The Kuhn length holds information on short scale interactions and stiffness and each of the n_K Kuhn links contains n/n_K physical links (Fig. 6.3b). The advantage of the equivalent freely jointed chain over the freely rotating chain lies with the characteristic ratio, C_n, included in the former. Defined as the ratio of the mean-square end-to-end vectors of a real chain, $\langle r^2 \rangle_0$, with that of a freely jointed chain (i.e., with no restriction on bond angles) containing the same number of bonds, nl^2, $C_n = \langle r^2 \rangle_0 / nl^2$, it is a measure of chain flexibility and contains information on both θ and other short scale interactions. For flexible chains, $C_n \approx 1$, while this increases for more rigid polymers. For large n, $C_n \to C_\infty$, a polymer specific constant.

While the focus here is primarily restricted to the equivalent freely jointed chain case, a brief comparison is made between that and the freely jointed chain (Section 6.2.3.2). In the case of freely jointed chains, where valence bond angles are ignored, i.e., there is no restriction on θ, the maximum end-to-end length of a chain, r_{max}, is a completely straightened chain: $r_{max} = nl$ (Fig. 6.3c). In contrast, r_{max} is limited for equivalent freely jointed chains by θ,

giving $r_{max} = nl\cos(\theta/2)$ in the all-trans conformation (Fig. 6.3c). A comparison between the three main chain idealisations is given in Table 6.1.

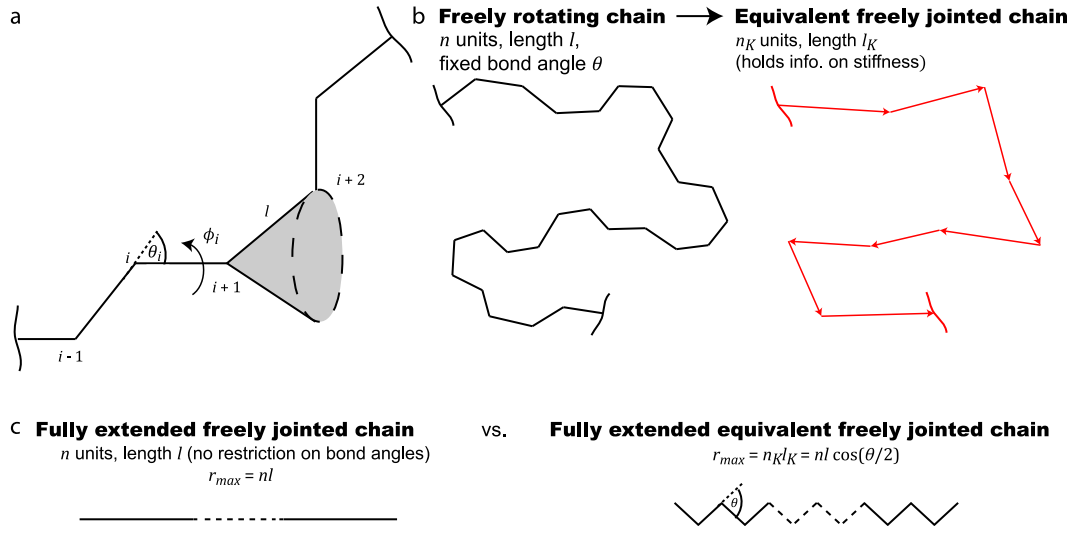

Fig. 6.3. (a) In the freely rotating polymer chain model, a chain contains bonds of average length l, while the valence bond angle between two neighbouring bonds at the ith backbone atom is $\pi - \theta_i$, where θ_i is the angle between consecutive bond vectors. The torsional rotation about bonds i and $i+1$ is denoted as ϕ_i. If the positions of $i-1$, i and $i+1$ are fixed, and rotation is allowed about the bonds i and $i+1$, then the position of backbone atom $i+2$ is shown by the dashed circle. Adapted from Mark and Erman (2007). (b) The chain is reconsidered as having equivalent links of length l_K, referred to as the Kuhn gth, where l_K holds information on short scale interactions and stiffness (i.e., more than just fixed θ_i). The number of links scales with this to give n_K Kuhn links, where each of these contains n/n_K physical links. (c) The maximum end-to-end length $r_{max} = nl$ for a freely jointed chain (where there is no restriction on bond angles), while for an equivalent freely jointed chain this is limited by the enforced bond angle θ, with $r_{max} = nl\cos(\theta/2)$.

Table 6.1. Comparison between the freely jointed, freely rotating, and equivalent freely jointed chain models in terms of their (undeformed) mean-square end-to-end distance, $\langle r^2\rangle_0$, and their maximum physical extension, r_{max}. Where a link contains multiple backbone bonds, n_b, average bond lengths and bond angles may be taken, with $n = nn_b$ below; see example in Section 6.2.2.2.

	Number of links	Bond length	$\langle r^2\rangle_0$	r_{max}
Freely jointed chain	n	l	nl^2	nl
Freely rotating chain	n	l	$nl^2\dfrac{1+\cos\theta}{1-\cos\theta}$	$nl\cos\left(\dfrac{\theta}{2}\right)$
Equivalent freely jointed chain	$n_K = \dfrac{n\cos^2\left(\frac{\theta}{2}\right)}{C_\infty}$	$l_K = \dfrac{C_\infty l}{\cos\left(\frac{\theta}{2}\right)}$	$n_K l_K^2 = nl^2 C_\infty$	$n_K l_K = nl\cos\left(\dfrac{\theta}{2}\right)$

6.2.2.1 Comparison between equivalent freely jointed PLA and PCL chains

The finite chain extensibility of a polymer is influenced by its respective chemical structure. Here, we investigate how the chemical structure of PLA and PCL chains compare and how

this effects finite chain extensibility. As just detailed, a chain may be well described with knowledge of n, n_b, l, θ and C_∞. Several studies have described these conformational properties of PLA, PGA and PCL (Anderson and Hillmyer, 2004; Blomqvist, 2001; Hamidi et al., 2018; Tonelli and Flory, 1969); see Table 6.2. For example, Blomqvist (2001) calculated C_∞ for poly(L-lactic), poly(L,D-lactic) and polyglycolic acids using the RIS Metropolis Monte Carlo method (outlined in Section 2.3.2).

Table 6.2. Polymer structure characteristics for PLA, PCL and PGA, detailing (i) the number of backbone bonds in a monomeric unit, n_b; (ii) the average angle θ between consecutive bond vectors (Fig. 6.4a), where θ is taken to be the average of all backbone bond angles in a repeat unit (i.e., $\theta = (\theta_1 + \cdots + \theta_{n_b})/n_b$ for a unit with n_b backbone bond angles); (iii) the average backbone bond length, l ($l = (l_1 + \cdots + l_{n_b+1})/(n_b + 1)$); and (iv) the characteristic ratio, C_∞, offering a measure of chain flexibility, obtained from the corresponding references. The corresponding valence bond angles are $\pi - \theta$.

	n_b	Average θ	Average l (nm)	C_∞	Ref.
PLA	3	68°	0.143	7.68	(Blomqvist, 2001; Brant et al., 1969)
PCL	7	71°	0.149	4.9	(Hamidi et al., 2018)
PGA	3	68°	0.142	7.53	(Blomqvist, 2001)

For PLA, the average backbone bond angle is $\theta = 68°$, the average length of these bonds is 0.143 nm, and there are three backbone bonds, n_b, per monomeric unit (Fig. 6.4b) (Brant et al., 1969). Note that this is valid for both PLLA and PDLA, with the differences in the structure of these isomeric states occurring solely in the side-groups. Thus, for an equivalent freely jointed chain (Table 6.1) with $n = 100$ PLA units, $r_{max} = n_b n l \cos(\theta/2) \approx 35.57$ nm, while the corresponding root-mean-square end-to-end length $r_{rms} = \sqrt{\langle r^2 \rangle} = \sqrt{C_\infty n_b n l^2} \approx 6.86$ nm. On the other hand, a chain of PCL containing $n = 100$ units, with $n_b = 7$ (Fig. 6.4c), has $r_{max} \approx 84.91$ nm and $r_{rms} \approx 8.73$ nm. This suggests that PLA is much more likely to reach r_{max} on extension than a chain of PCL with equal values of n.

Alternatively, a more insightful comparison would consider PLA and PCL with equal molecular mass. Again considering a chain of PLA with $n = 100$ repeat units, the mass is $M = nM_0 = 7200$ g mol^{-1}, where the molar mass $M_0 = 72$ g mol^{-1}. As above, $r_{max} \approx 35.57$ nm, while $r_{rms} \approx 6.86$ nm. Now considering a chain of PCL with $M = 7200$ g mol^{-1}, $n \approx 63$, giving $r_{max} \approx 53.49$ nm and $r_{rms} \approx 6.93$ nm. Fig. 6.4d looks at the relationship between both r_{max} and r_{rms} and molecular weight for PLA and PCL. Again, we see that PLA is more likely to reach r_{max} on extension than a chain of PCL of equal mass, with r_{rms} similar for both and r_{max} for PLA approximately 2/3 of that for PCL. Thus, this suggests that the chemical structure of PLA may enable short chains to reach full extension at lower strains than for an equivalent chain of PCL, with this finite extensibility possibly impacting mechanical properties such as

ductility. This general observation is in agreement with the experimental study of Målberg et al. (2011) wherein PCL was extended twice as much as PLA prior to failure (reproduced in Fig. 6.4e). It should be noted that in that study both polymers had the same geometry and similar initial M_n (within $\sim 13\%$), but M_n for PLA did decline more rapidly; a further experimental investigation may provide valuable insight.

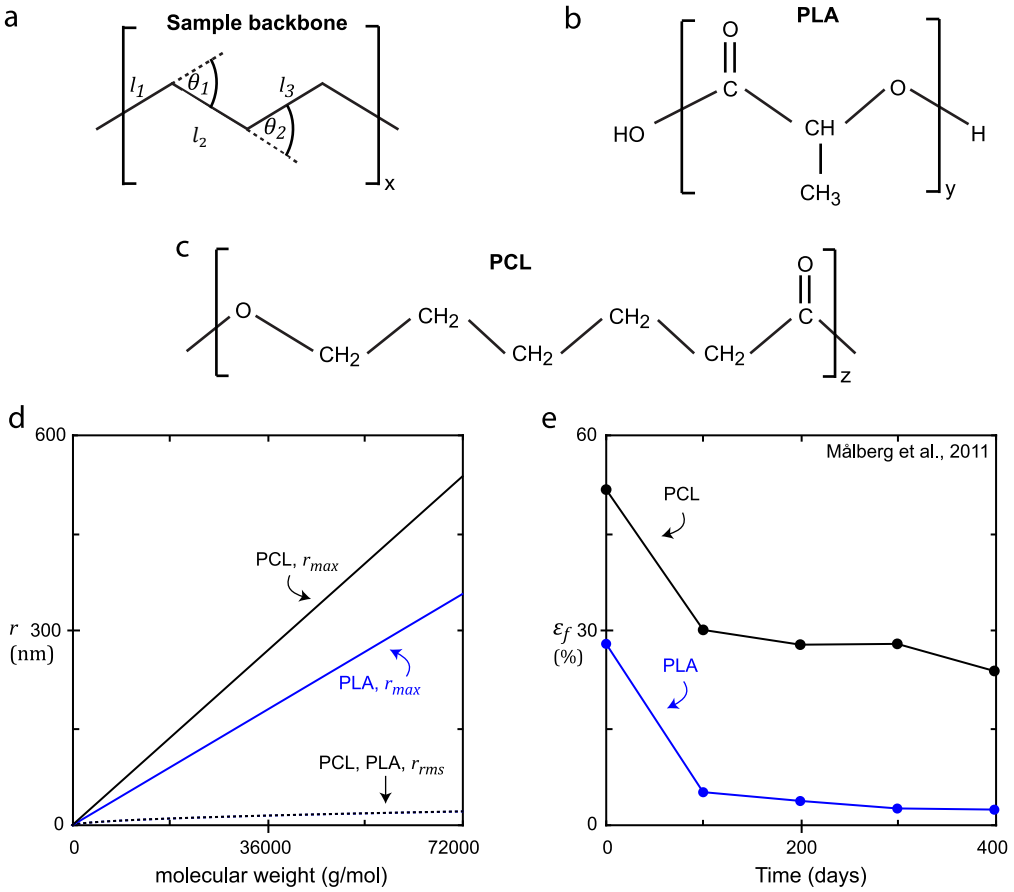

Fig. 6.4. (a) A sample backbone is shown containing three backbone bonds, n_b, of lengths l_1, l_2, l_3 and backbone bond angles θ_1, θ_2. (b) Chemical structure of PLA ($n_b = 3$). (c) Chemical structure of PCL ($n_b = 7$). (d) The relationship between molecular weight and both the maximum end-to-end distance, r_{max}, and the root mean-squared end-to-end distance, r_{rms}, for PLA and PCL, obtained using Table 6.1 and Table 6.2 as outlined in the text. Both polymers have similar r_{rms}, while r_{max} for PLA is approximately 2/3 of that for PCL. This suggests that PLA may be more likely to reach r_{max} on extension than a chain of PCL with equivalent molecular weight. (e) Evolving failure strain, ε_f, for PLA and PCL during an experimental degradation study by Målberg et al. (2011). The higher ε_f for PCL supports the findings of (d).

6.2.2.2 Determining parameters for copolymers

To obtain parameters for copolymers, Fischel et al. (1997) determined that a homopolymer approximation that preserved the contour length and the mean-square end-to-end distance of the original copolymer provided the best results when compared with the exact solution

for a block copolymer. Thus, for an equivalent freely jointed copolymer chain containing α segments made up of $n_{K,\alpha}$ units of length $l_{K,\alpha}$, an approximate homopolymer chain with n'_K bonds of length l'_K can be defined by $\sum_\alpha n_{K,\alpha} l_{K,\alpha} = n'_K l_K{}'$, analogous with r_{max}, and $\sum_\alpha n_{K,\alpha} l^2_{K,\alpha} = n'_K (l'_K)^2$, analogous with $\langle r^2 \rangle$.

For example, consider a block copolymer containing two distinct monomer units, say lactic acid (LA) and caprolactone (CL), ordered as follows: LA-LA-LA-LA-LA-CL-CL-CL-CL-CL-LA-LA-LA-LA-LA, i.e., alternating five-unit strings of lactic acid and caprolactone. Each segment can be considered individually, i.e., three segments each containing five units, or like segments can be considered together, i.e., ten units of lactic acid and five units of caprolactone. Thus, the lactic acid units would contribute $r_{max,LA} = n_{K,LA} l_{K,LA} = n_{b,LA} n_{LA} l_{LA} \cos(\theta_{LA}/2) \approx 3.56\ \text{nm}$, $\langle r^2 \rangle_{LA} = n_{K,LA} \left(l_{K,LA}\right)^2 = C_{\infty,LA} n_{b,LA} n_{LA} l^2_{LA} \approx 4.71\ \text{nm}$, while the caprolactone units have $r_{max,CL} = n_{K,CL} l_{K,CL} = n_{b,CL} n_{CL} l_{CL} \cos(\theta_{CL}/2) \approx 4.25\ \text{nm}$, $\langle r^2 \rangle_{CL} = n_{K,CL} \left(l_{K,CL}\right)^2 = C_{\infty,CL} n_{b,CL} n_{CL} l^2_{CL} \approx 3.81\ \text{nm}$, where the subscripts represent the type of monomer unit and parameters are taken from Table 6.2. To obtain parameters for an appropriate homopolymer approximation, let $n'_K l'_K = \sum_{\alpha=LA,CL} n_{K,\alpha} l_{K,\alpha} \approx 7.81\ \text{nm}$ and $n'_K (l'_K)^2 = \sum_\alpha n_{K,\alpha} l^2_{K,\alpha} \approx 8.52\ \text{nm}$. Finally, solving for n'_K and l'_K gives $n'_K \approx 7.16$ and $l'_K \approx 1.09\ \text{nm}$. Reconsidering the copolymer using these parameters for a homopolymer approximation allows for a simpler description of the end-to-end distance distribution, which is described in the following section.

6.2.3 End-to-end distance distribution

Much like a polymer has a molecular weight distribution, chains of equal weight are expected to have an end-to-end distance distribution. As we saw in Fig. 6.2, chains are typically attracted to a coiled state, with this controlled by entropy. For chains of increasing weight, i.e., containing more monomeric units, an increasing number of configurations or end-to-end distances are possible. Distributions such as the Gaussian and Langevin distributions describe these end-to-end distances well, with the latter favoured for greater accuracy when considering shorter chains.

To describe the end-to-end distance distribution, first consider an isolated idealised equivalent freely jointed polymer chain containing n_K links of length l_K. Any such chain has an end-to-end length, r, and its length at maximum physically possible extension is denoted r_{max} (Fig. 6.5a). A spherical distribution of chains is assumed, giving a surface area of $4\pi r^2$, with one end of each chain fixed at the origin, as is standard practice (Ward, 1971) (Fig. 6.5b). For a chain containing n_K links, the probability of a corresponding end-to-end length can be

described using a Langevin distribution approximation, as detailed by Kuhn and Grün (1946). Thus, the probability of a chain having a particular end-to-end distance, r, is as follows:

$$\begin{aligned} P(r)\,\mathrm{d}r &= p(r)4\pi r^2\,\mathrm{d}r \\ &= \left(\frac{3}{2n_K l_K^2 \pi}\right)^{3/2} 4\pi r^2 \exp\left(-n_K\left(\frac{3}{2}\left(\frac{r}{n_K l_K}\right)^2 + \frac{9}{20}\left(\frac{r}{n_K l_K}\right)^4\right.\right. \\ &\quad \left.\left. + \frac{99}{350}\left(\frac{r}{n_K l_K}\right)^6 + \frac{1539}{9000}\left(\frac{r}{n_K l_K}\right)^8 + \cdots\right)\right)\mathrm{d}r \end{aligned} \tag{6.1}$$

with additional terms corresponding to more accurate approximations of the Langevin distribution. The end-to-end distance distribution, $P(r)$, is thus dependent on the chain parameters (n_K, l_K). Note that $P(r)$ is a volumetric end-to-end distribution, which accounts for a spherical distribution of chains via the factor of $4\pi r^2$, while $p(r)$ is the more general probability density distribution (Treloar, 1975b; Ward, 1971).

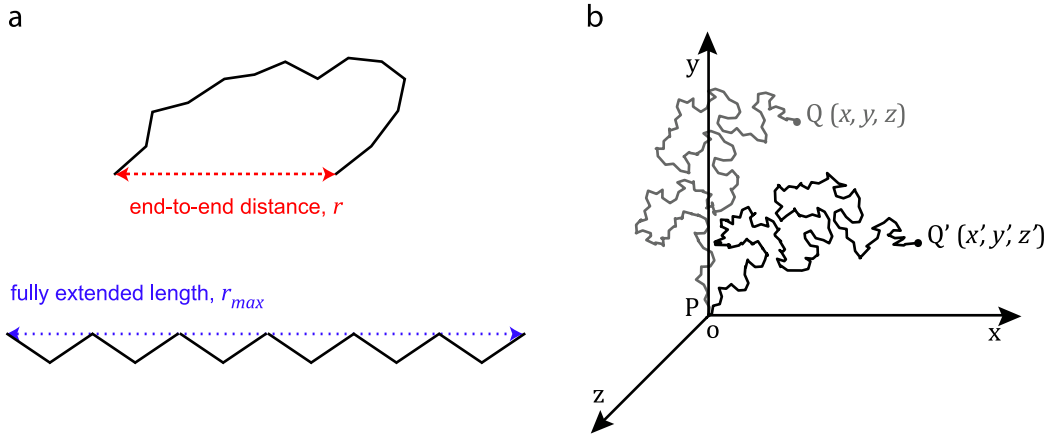

Fig. 6.5. (a) Each chain has both an end-to-end length, r, and a fully extended length, r_{max}. (b) Chains are considered to have one end, P, fixed at the origin, o, with the other end Q displaced to Q′ during deformation.

6.2.3.1 Comparison between Gaussian and Langevin approximations

The Langevin approximation shown in Eq. (6.1) is explored for variously refined approximations. Often, Gaussian distributions are considered, corresponding to the first term in Eq. (6.1). While this is sufficient provided n is large enough (typically $n > 100$) and $r \ll nl$ (James and Guth, 1943), errors in the approximation are observed in the case of short chains. In Fig. 6.6, the discrepancy between approximations using from one up to four terms are explored. As expected, in the case of long polymer chains ($n = 500$), approximations containing both one and four terms are in good agreement; however, sensitivities are visually evident for smaller values of n ($n = 20, 5$). In Fig. 6.6c, $P(r_0)$ has not tailed off prior to

reaching r_{max}. While this is partially due to the approximation in Eq. (6.1), as can be seen from the improvements with additional terms, the short length and resulting small number of possible configurations also contributes to this, i.e., short chains are more likely to conform to r_{max} in their undeformed state. Although the approximation of Eq. (6.1) may be further improved as described by, for example, Morovati et al. (2019), the discrepancy between three and four terms is deemed sufficiently small when $n = 5$ here, and so this approximation is used for the remainder of this chapter.

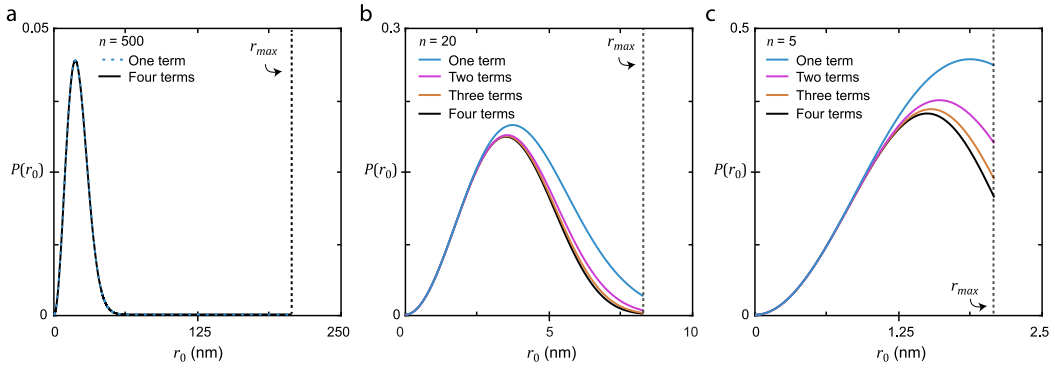

Fig. 6.6. Investigation of the convergence of the Langevin distribution approximated by Eq. (6.1) while considering from one up to four terms for different values of n, the number of bonds in the polymer. The focus is restricted only up to the maximum possible extension, r_{max}, in the case of equivalent freely jointed chains (Table 6.1), shown by the vertical dashed lines. For large values of n ($n = 500$), one term (i.e., a Gaussian approximation) sufficiently captures the behaviour, while for smaller values of n ($n = 20, 5$), four terms are deemed sufficient.

6.2.3.2 Considering the effect of bond angle restrictions

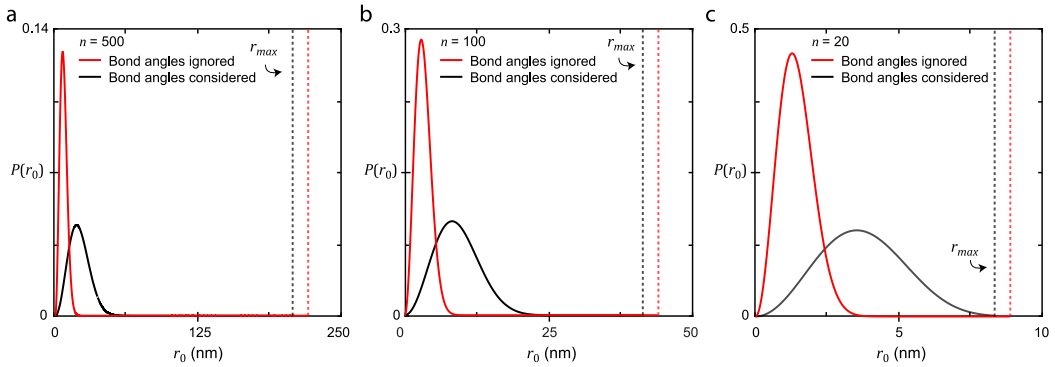

Fig. 6.7. Investigation into the difference between freely jointed chains, where bond angles are ignored, and equivalent freely jointed chains, where stiffness and fixed valence bond angles are considered according to the chemical structure of the polymer via C_∞. When bond angles are ignored, chains are free to occupy any state, and thus tend towards condensed, disordered arrangements, while r_{max} corresponds to a completely straightened chain. Once bond angles are considered, the number of possible configurations decreases and very compact chains are no longer possible, resulting in broader distributions and a decrease in r_{max} (Table 6.1, Fig. 6.3).

In Fig. 6.7, the difference between the freely jointed and equivalent freely jointed chain models are considered. Without the restriction on bond angles, Eq. (6.1) mainly describes compact chain packings that would require large stretches to reach full extension. When bond angles (and other short scale interactions, via C_∞) are considered, the number of possible chain configurations decrease, and the end-to-end distribution broadens, with compact chain packings less likely. A reduction in r_{max} is also observed, with this idealisation preventing a completely straight chain (Fig. 6.3c). It is thus evident that the more accurate equivalent freely jointed chain model will better capture the finite extensibility of polymer chains at physically relevant stretches.

6.2.4 Change in entropy of the system

The change in entropy of a single polymer chain is first considered and extended to consider the change in entropy of the entire system, as detailed by Ward and Sweeney (2013). As mentioned, polymer chains are often described as "probability or entropy springs" because all chain configurations have approximately the same internal energy and it is instead the entropy primarily controlling the deformation. When subjected to an external force, chains, forced from their state of maximum entropy, extend in the direction of the force, reducing the entropy and resulting in a state of strain (Fig. 6.2).

The entropy of a single chain, s, is proportional to the logarithm of the probability per unit volume, $p(r)$:

$$s = k \ln p(r) \tag{6.2}$$

where k is the Boltzmann constant. Thus, in the case of a Gaussian distribution of freely jointed chains, which the Langevin distribution (Eq. (6.1)) reduces to for large n (Fig. 6.6), the number of configurations available to a chain is given as

$$s = c - k\beta^2 r^2 = c - k\beta^2(x^2 + y^2 + z^2) \tag{6.3}$$

where $\beta^2 = 3/2nl^2$, $r^2 = x^2 + y^2 + z^2$ and c is a constant. While Eq. (6.2) is the general form used as we proceed, Eq. (6.3) is used to derive the following equations, which are subsequently used in this chapter to compare the predicted stretch behaviour with that of the general assumption of a freely jointed Gaussian distribution in existing theories (Mark and Erman, 2007; Ward, 1971).

As the network is subjected to a stretch, the entropy of a single Gaussian chain becomes

$$s' = c - k\beta^2(\lambda_x^2 x^2 + \lambda_y^2 y^2 + \lambda_z^2 z^2) \tag{6.4}$$

where affine deformation is assumed, i.e., a stretch λ changes components of the vector length of each chain in the same ratio as the corresponding dimensions of the bulk material. The updated coordinates of Q → Q′ (Fig. 6.5b) are given by $x' = \lambda_x x, y' = \lambda_y y, z' = \lambda_z z$, where $\lambda_x, \lambda_y, \lambda_z$ are the principal extension ratios chosen parallel to the x, y, z axes, respectively, without loss of generality. Thus, the change in entropy for that chain is found to be

$$\Delta s = s' - s = -k\beta^2\left((\lambda_x^2 - 1)x^2 + \left(\lambda_y^2 - 1\right)y^2 + (\lambda_z^2 - 1)z^2\right) \tag{6.5}$$

Summing over all N chains in the network provides the overall change in entropy for the system. Provided the system is isotropic, i.e., $\sum_1^N x^2 = \sum_1^N y^2 = \sum_1^N z^2 = \frac{1}{3}\sum_1^N r^2$, and using $\langle r^2 \rangle = nl^2 = 3/2\beta^2$ (Table 6.1), this is given by

$$\Delta S = \sum_1^N \Delta s = -\frac{1}{2}Nk\left(\lambda_x^2 + \lambda_y^2 + \lambda_z^2 - 3\right) \tag{6.6}$$

In the case of non-Gaussian chains, the same procedure is followed, albeit for a different end-to-end distribution, $p(r)$, i.e., Eqs. (6.3)-(6.6) are not valid.

6.2.5 Resulting strain-energy potential of a Gaussian system

Following on from the previous section, the resulting strain energy potential of a Gaussian system is calculated following the techniques outlined by Ward (1971) and further detailed in Section 2.3.5. This is later used to investigate the level of stretch required to result in a departure from this behaviour for an equivalent freely jointed Langevin distribution of chains tending towards its limit of finite extensibility. The same technique is used to determine the strain-energy potential of the Langevin distribution of polymer chains, as outlined in the following section.

Assuming no change in internal energy on deformation, the change in Helmholtz free energy is as follows:

$$\Delta A = -T\Delta S = \frac{1}{2}NkT\left(\lambda_x^2 + \lambda_y^2 + \lambda_z^2 - 3\right) \tag{6.7}$$

The Helmholtz free energy suggests an isothermal change of state at constant volume. It is considered, as is standard practice (Ward, 1971), as it can easily be calculated theoretically

for a polymer in rubbery state from statistical mechanical considerations in terms of strains existing in the material.

Provided the strain-energy function, U, is zero in the undeformed state,

$$U = \Delta A = \frac{1}{2} NkT\left(\lambda_x^2 + \lambda_y^2 + \lambda_z^2 - 3\right) \tag{6.8}$$

Here, Eq. (6.8) has been presented as a consequence of molecular theories of a rubber network; however, it is equivalent to the phenomenological neo-Hookean relationship proposed by Rivlin (1948) for finite deformation of an isotropic, incompressible solid (further details are given in Section 2.2.4). While this captures the initial response to stress, polymer chains have a finite extensibility (which this model fails to consider) and is typically accurate for strains less than 20% (Vieira et al., 2011).

6.3 Simulated stretching using average molecular weight

Next, we return to the concept of a Langevin distribution of chains and describe how to simulate a uniaxial stretch on the polymer chain ensemble. A uniform system of polymer chains is considered, i.e., all chains have the same molecular weight, consistent with an average molecular weight. The elastic properties are calculated from the total deformation of the end-to-end vectors of individual network chains and are assumed to arise solely from conformational changes in the network.

The uniform polymer systems considered in this section are consistent with the polymer systems considered by Stepto and Taylor (1995a), where all chains in the network had equal values of n. On simulating these systems, a stretch is applied to the polymer network, similarly to the technique of Stepto and Taylor (1995a), however, expanded to consider incremental points of degradation. The finite extensibility of polymer chains is not enforced in this section, in contrast to Stepto and Taylor's (1995a) method; this will be investigated in the following section in order to compare results from both sections and determine its effect.

We consider the case where an average molecular weight is used to describe the entire polymer network. That is, a uniform polymer system is assumed, containing N equivalent freely jointed chains each with a maximum end-to-end length proportional to the number average molecular weight, M_n, i.e., $r_{max} \propto M_n$. The end-to-end lengths of these chains are described by the distribution in Eq. (6.1), where $n_K \propto M_n$ and l_K is a polymer specific constant (see Table 6.2 for more details on the polymer specific constants considered); a restriction is applied to ensure no chains are generated with $r_0 > r_{max}$. One end of each

chain is taken to be fixed at the origin (Fig. 6.5b), while the coordinates for the other ends are chosen to be consistent with the initial end-to-end distance distribution, $P(r_0)$, described by Eq. (6.1) and are assumed to be isotropic. This is carried out by first generating three random Gaussian variables for each chain, $x_{0,i}, y_{0,i}, z_{0,i}$, $i = 1, \dots, N$, on $(-1,1)$ and scaling each one as follows:

$$x_{0,i} = \frac{x_{0,i}}{\sqrt{x_{0,i}^2 + y_{0,i}^2 + z_{0,i}^2}} r_0 \tag{6.9}$$

and similarly for $y_{0,i}$ and $z_{0,i}$. Using the generated polymer system, an incremental simulated stretch, λ, is applied in the z-direction, with one end of each chain remaining fixed at the origin (Fig. 6.5b). Assuming affine behaviour and incompressibility ($\lambda_x \lambda_y \lambda_z = 1$), the updated coordinates of the free end of chains are given as

$$x_{def,i} = \frac{x_{0,i}}{\sqrt{\lambda}}, \qquad y_{def,i} = \frac{y_{0,i}}{\sqrt{\lambda}}, \qquad z_{def,i} = \lambda z_{0,i} \tag{6.10}$$

where $(x_{0,i}, y_{0,i}, z_{0,i})$ are the initial coordinates of chain i. The updated end-to-end length for chain i, $r_{def,i}$, is calculated as the square root of

$$r_{def,i}^2 = x_{def,i}^2 + y_{def,i}^2 + z_{def,i}^2 \tag{6.11}$$

Returning to the more general description of entropy in Eq. (6.2) and combining this with Eq. (6.6), the change in entropy for this system is

$$\Delta S = \sum_1^N \Delta s = \sum_{i=1}^N k \ln \left(\frac{P_{gen,def}(r_{def,i})}{P_{gen,0}(r_{0,i})} \frac{r_{0,i}^2}{r_{def,i}^2} \right) \tag{6.12}$$

where $p(r) = P(r)/4\pi r^2$ (Eq. (6.1)) and $P_{gen,0}$ and $P_{gen,def}$ are the generated end-to-end distance distributions in the initial and deformed state. From Eq. (6.7), the average change in Helmholtz free energy per chain is then given as

$$\frac{\Delta A}{NkT} = \frac{1}{N} \sum_{i=1}^N \ln \left(\frac{P_{gen,0}(r_{def,i})}{P_{gen,def}(r_{0,i})} \frac{r_{def,i}^2}{r_{0,i}^2} \right) \tag{6.13}$$

6.3.1 Solution approach

In order to simulate a uniaxial stretch on a network of polymer chains, the procedure outlined above was implemented in MATLAB® (R2020b, The MathWorks, Inc., MA, USA). Fig.

6.8 contains a flowchart detailing the solution method used. In the current section, the steps in blue are ignored, with a uniform network of chains considered, i.e., all chains are assumed to be of length M_n, and no restriction on the final length of chains during stretching is implemented. The blue boldfaced text accounts for modifications introduced in Section 6.4 and are included in the flowchart for completeness. A more detailed description of the method can be found in the pseudocode included in Appendix 6B Pseudocode.

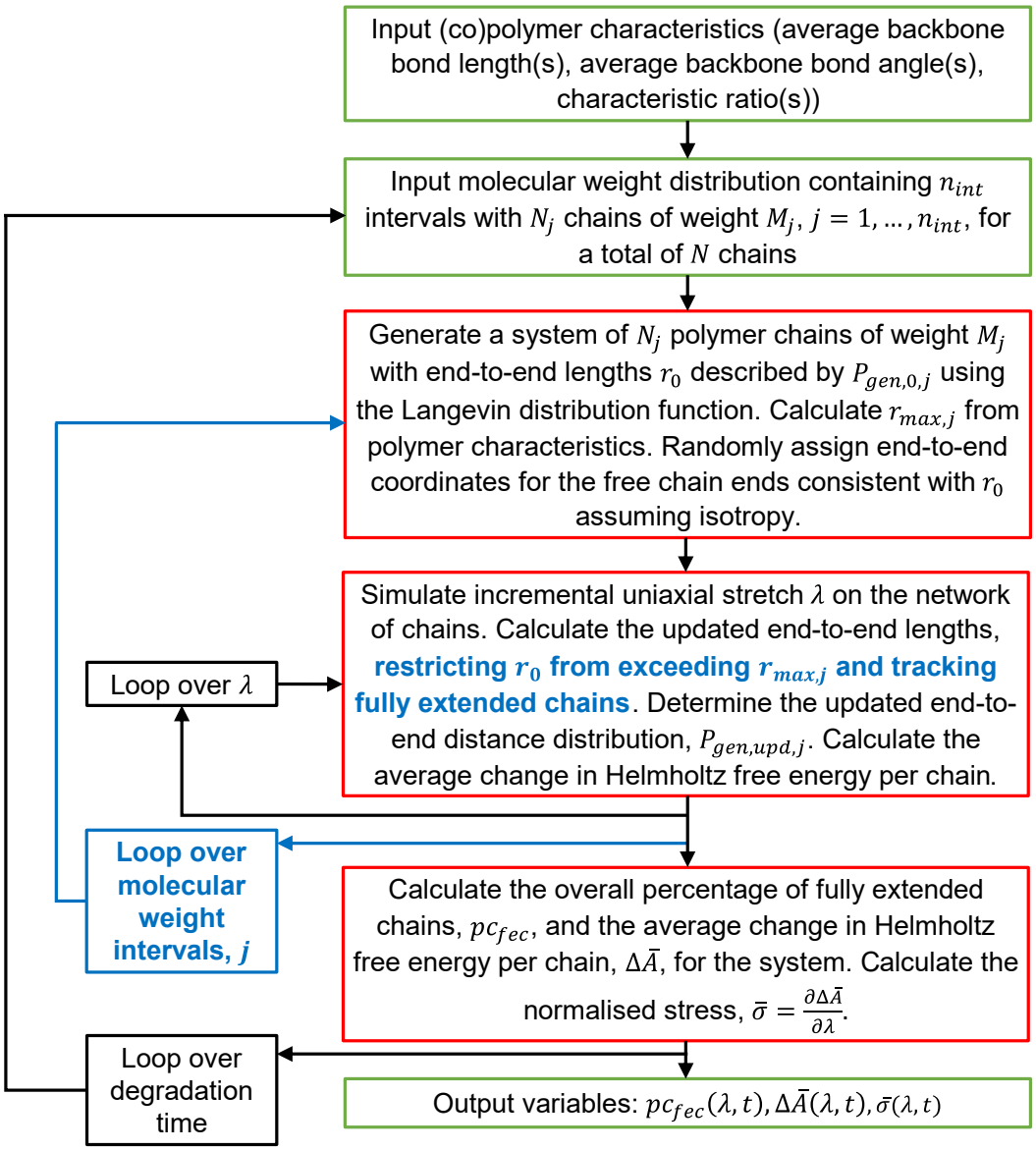

Fig. 6.8. Flowchart detailing the solution approach. The elements of the flowchart in blue relate to the further developments of the model described below in Section 6.4 and are included here for completeness. In the current section, $n_{int} = 1$.

6.3.2 Results

The experimental study of Vieira et al. (2011) was used to initialise the simulation, with the evolving M_n of PLA-PCL fibres during degradation used to investigate the simultaneous

change in mechanical properties (Fig. 6.9a). PLA and PCL chains were first described as equivalent freely jointed chains using the polymer characteristics detailed in Table 6.2. A homopolymer approximation was then obtained using the approach of Fischel et al. (1997) outlined in Section 6.2.2.2.

Each value of M_n corresponds to a specific n and, consequently, r_{max}. The simulation considered each timepoint individually, where $P(r_0)$ was calculated using Eq. (6.1) for a given value of M_n (Fig. 6.9b) and used to create a sufficiently large system ($N = 10^6$), resulting in the generated end-to-end distance distribution, $P_{gen,0}(r_0)$. An incremental stretch was then applied to the network of chains, as described above.

In this section, affine behaviour is simulated as detailed in Eq. (6.10), with no restrictions imposed on the maximum extensibility of chains. Eq. (6.13) was used to calculate the average change in Helmholtz free energy per chain at each increment of stretch. Fig. 6.9c compares the simulated results for the network of chains with a straightforward calculation of the neo-Hookean relationship using Eq. (6.8), which describes the affine, incompressible stretching of a Gaussian system of freely jointed chains. The x-axis is chosen to produce a linear neo-Hookean relationship. An initial agreement is observed, with a deviation beginning when $\lambda \approx 1.2$ ($\lambda^2 + \frac{2}{\lambda} - 3 \approx 0.1$), expected due to the removal of assumptions such as a Gaussian distribution of freely jointed chains. For smaller values of N, the simulated behaviour resulted in noisy results, while larger values of N agreed with that shown (see Appendix 6A Sensitivity analysis for a more in-depth sensitivity analysis).

As degradation progresses, chains are broken down, resulting in increasingly shorter chains in the system. It is expected that these short chains could fully extend at modest strains and consequently, no longer contribute to the changing energy in the system (Edwards and Vilgis, 1986; Stepto and Taylor, 1995a). Thus, simulations corresponding to progressive points of degradation are expected to have increasing departures from affine, neo-Hookean behaviour. On comparison of the system prior to degradation (Week 0) with degraded systems (Week 4 and Week 16 of the experimental study) this was observed, with a slight departure beginning when $\lambda \approx 2.5$ ($\lambda^2 + \frac{2}{\lambda} - 3 \approx 4$) for Week 16 and further deviating for larger strains (Fig. 6.9c).

The resulting percentage of chains with $r \geq r_{max}$ caused by the simulated stretch indicate that very large stretches are needed before this occurs when a uniform system of polymer chains, each with r_{max} proportional to M_n, is considered (Fig. 6.9d), however, to a gradually lesser extent for degraded systems. Fig. 6.7 indicates that the peak of $P(r_0)$ tends closer

towards r_{max} for decreasing values of n; thus, it is expected that short chains could reach r_{max} at much lower stretches. Hence, this indicates that simulating a system of chains where $n \propto M_n$ may fail to accurately capture the full extent of finite extensibility during stretching. Rather, the effect of the entire molecular weight distribution should be considered to fully explore the effect of finite chain extensibility at physical stretches for this material.

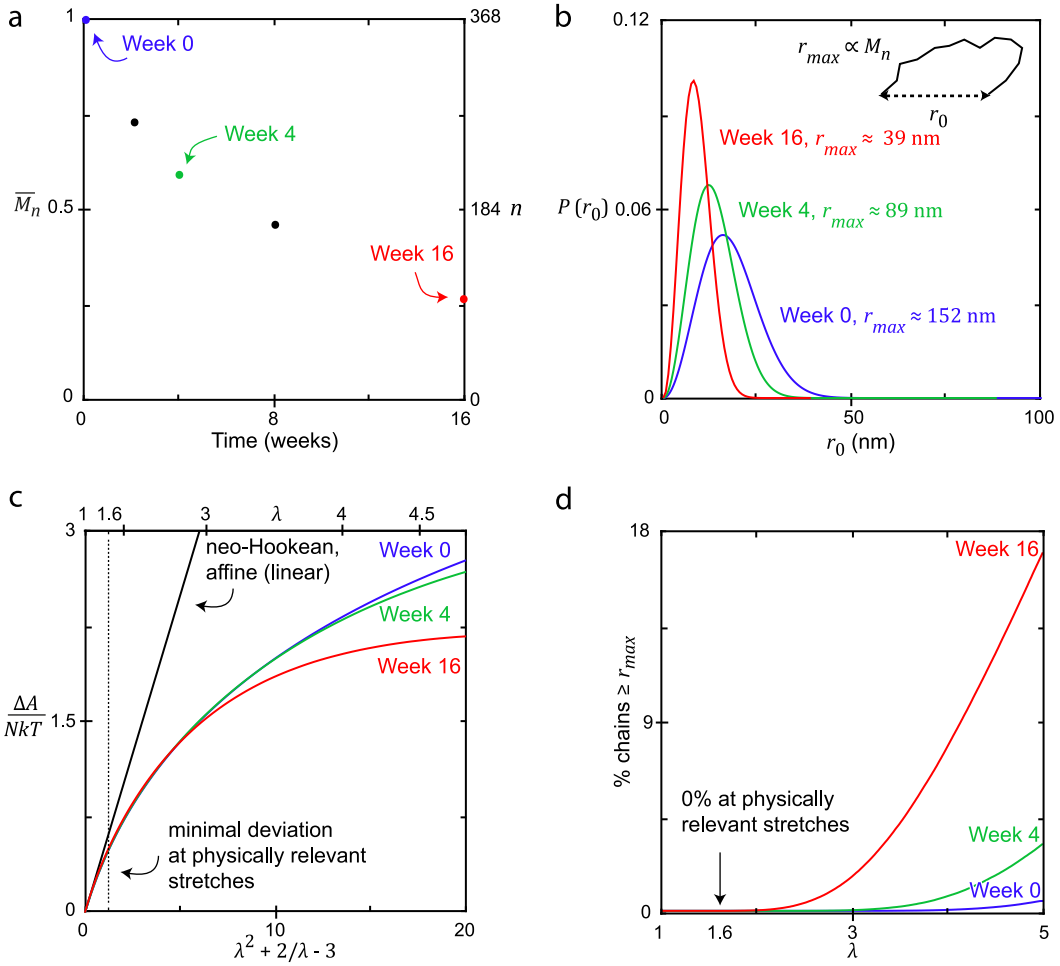

Fig. 6.9. In Section 6.3, a uniform polymer system containing N chains was generated, with each chain containing $n \propto M_n$ links. (a) Values of M_n corresponding to PLA-PCL (90:10) at Week 0, Week 4 and Week 16 of degradation were considered using experimental data of Vieira et al. (2011). (b) The end-to-end distance distributions were calculated using Eq. (6.1) for each of the systems and subsequently scaled to generate a system of N chains, each with $r_{max} \propto M_n$, with a distribution of initial end-to-end lengths, r_0. (c) Simulating a stretch on the networks of chains and determining the average change in Helmholtz free energy per chain, $\Delta A/NkT$, using Eq. (6.13) indicated a deviation from neo-Hookean behaviour (calculated using Eq. (6.8) without a simulated stretch, describing the behaviour of affine, Gaussian freely jointed chains) at modest strains. However, large simulated stretches were necessary before differences in the undegraded and degraded systems were evident. (d) The percentage of chains with $r \geq r_{max}$ were tracked during the simulation, although these were not present at physical stretches for this material ($\lambda_{max} \approx 1.6$, according to Vieira et al. (2011)).

6.4 Simulated stretching of MWD – departure from affine behaviour

The previous section suggested the possible importance of considering the entire molecular weight distribution (MWD) when modelling the mechanical response of these materials to a simulated stretch. Additionally, a departure from the affine behaviour assumption enforced by Eq. (6.11) is needed in the simulation to consider the contribution of fully extended chains in the system. Thus, the model is updated to account for both modifications. These model developments correspond to the blue elements of the solution approach shown in Fig. 6.8, with the entire flowchart now implemented.

On considering a MWD, generated using M_{n0} and M_{w0}/M_{n0} detailed by Vieira et al. (2011), it is divided into equally spaced intervals along the x-axis, with the intervals successively labelled as M_1, M_2, M_3, etc. A distribution of r_{max} now exists, in addition to the distribution of end-to-end lengths, r, with each M_j having a unique distribution $P(r)$, found using Eq. (6.1) (Fig. 6.10). For each M_j, a sufficient number of chains N are considered ($N \geq 10^6$), as before, while being held proportionally consistent with the MWD.

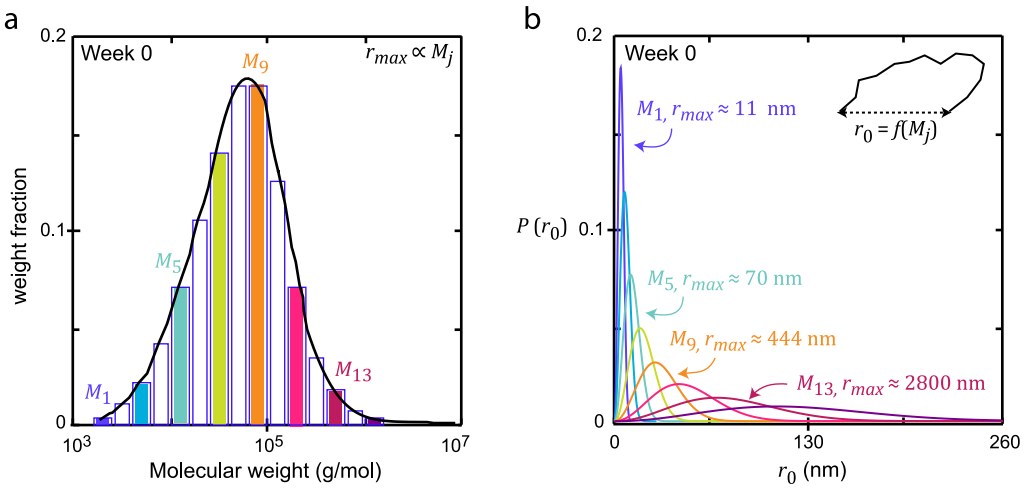

Fig. 6.10. (a) A representative polymer molecular weight distribution is considered, generated using M_{n0} and M_{w0}/M_{n0} detailed by Vieira et al. (2011). The MWD is divided into j equally spaced intervals along the x-axis, with the intervals successively labelled as M_1, M_2, M_3, etc. Each interval has a unique maximum possible extension, with $r_{max} \propto M_j$. (b) The initial end-to-end distance distributions, $P(r_0)$, corresponding to each coloured bar in (a) (i.e., every second M_j) are shown, alongside the values of r_{max} for a selection of the distributions.

Each system of chains corresponding to an M_j is then subjected to a simulated stretch, as previously described (Fig. 6.8), before the results are finally combined for the entire MWD system. A restriction is added to account for the finite extensibility of chains such that if the incremental stretch results in $r_{def,i} > r_{max,j}$, this is updated as $r_{def,i} = r_{max,j}$ (Fig. 6.11).

These chains are not permitted to lengthen further alongside any additional extension of the bulk material, thus removing the assumption of complete affine deformation imposed by Eq. (6.11). This is achieved by modifying Eq. (6.11) as follows:

$$r_{def,i}^2 = \min\left(x_{def,i}^2 + y_{def,i}^2 + z_{def,i}^2, r_{max,j}\right) \tag{6.14}$$

This modification removes the affine assumption of Eq. (6.11) once a chain reaches maximum extension and directly affects the generated deformed end-to-end distance distribution, $P_{gen,def}\left(r_{def,i}\right)$, that is used when calculating the changing entropy and energy using Eq. (6.12) and Eq. (6.13), respectively. The number of fully extended chains are simultaneously tracked based on the outcome of Eq. (6.14).

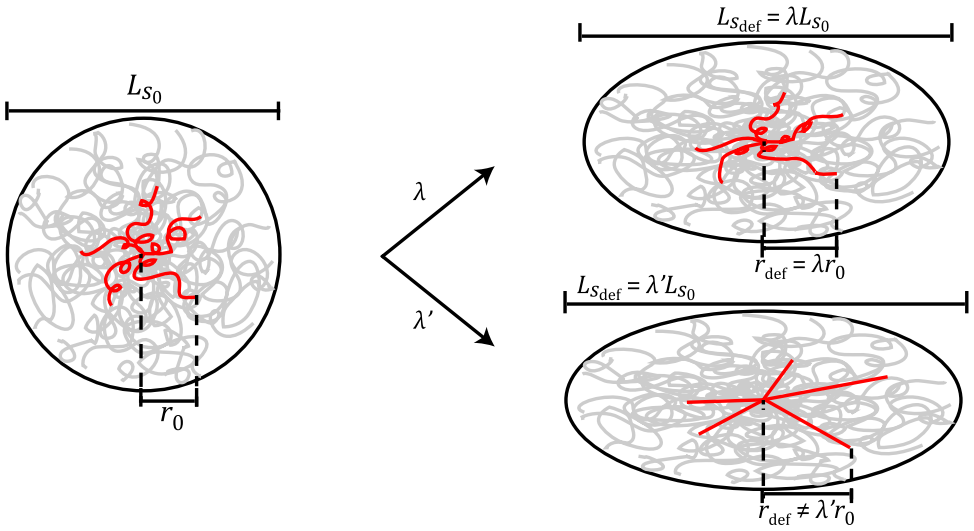

Fig. 6.11. Prior to deformation, the polymer sample, S, has length L_{S_0}, and chain i has length r_0. Originally, affine deformation is assumed, with a stretch λ changing components of the vector length of each chain in the same ratio as the corresponding dimensions of the bulk material (i.e., $L_{S_{def}} = \lambda L_{S_0}, r_{def} = \lambda r_0$). As the stretch increases, $\lambda' > \lambda$, some chains become fully extended and cannot lengthen further alongside additional extension in the bulk material, thus removing the assumption of complete affine behaviour (i.e., $L_{S_{def}} = \lambda' L_{S_0}$ but $r_{def} \neq \lambda' r_0$).

6.4.1 Results

Molecular weight distributions corresponding to various points of degradation were subjected to a simulated stretch while accounting for finite chain extensibility. The average change in Helmholtz free energy per chain and the percentage of fully extended chains were explored and compared with the results of the previous section, where an average molecular weight and affine behaviour were considered.

The experimental study of Vieira et al. (2011) did not report the MWD and, so, for the initial timepoint a MWD was generated with $M_{n0} = 28\ \mathrm{kg\ mol^{-1}}$ and $M_{w0}/M_{n0} = 3.3$, as reported in that study. Inputting this initial MWD into the kinetic scission model (introduced in Chapter 4) provided evolving MWDs for different stages of degradation (Fig. 6.12a). The KSM was calibrated such that the simulated M_n agreed with experimental observations ($r^2 > 0.99$).

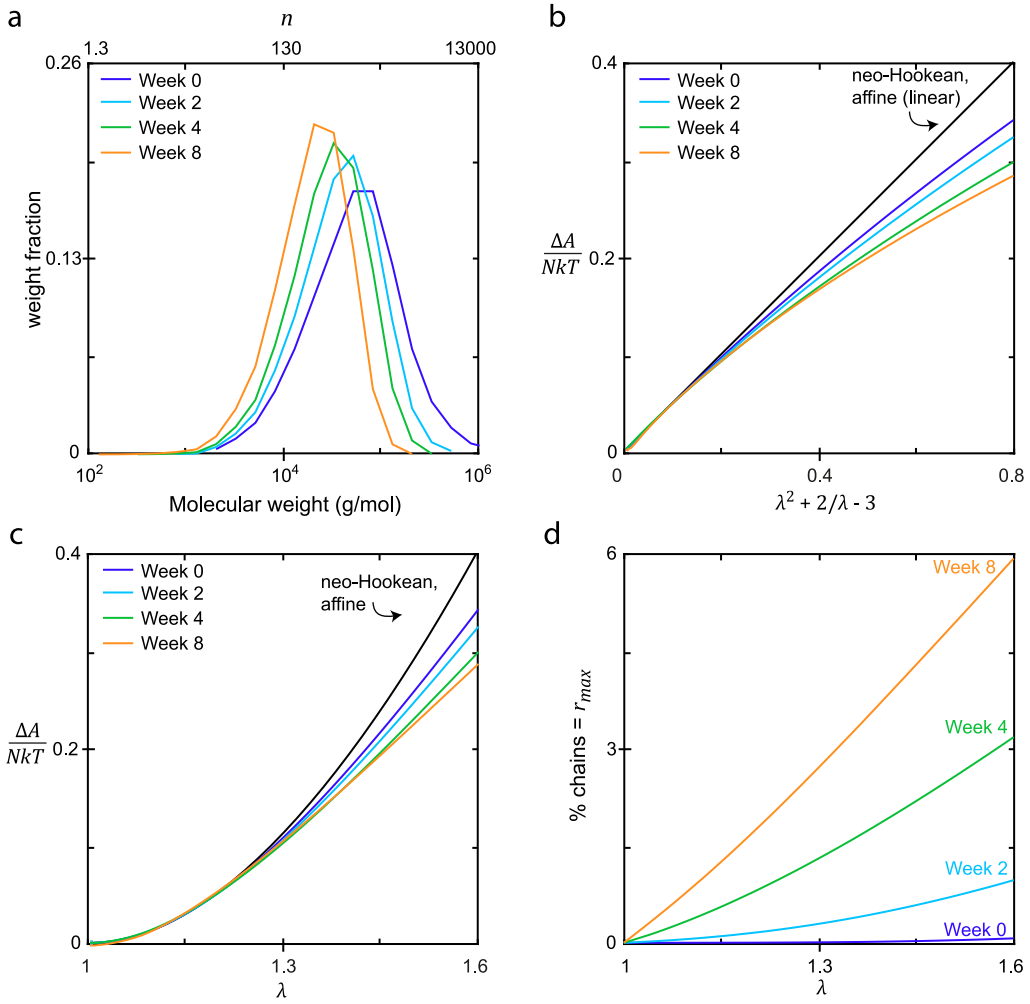

Fig. 6.12. (a) Evolving molecular weight distributions used to generate the polymer systems were obtained using the kinetic scission model (introduced in Chapter 4) using initial information on PLA-PCL (90:10) (Vieira et al., 2011). (b,c) The average change in Helmholtz free energy per chain, $\Delta A/NkT$, caused by a simulated stretch, λ, was found for each representative timepoint. A deviation from neo-Hookean behaviour (calculated using Eq. (6.8) without a simulated stretch, describing the behaviour of affine, Gaussian freely jointed chains) was observed at modest strains. Week 0 behaviour agreed with that found in the previous section for the stretch range considered here. A deviation from Week 0 was found at much lower stretches than that needed in the previous section as degradation progressed (e.g., $\lambda \approx 1.08$ vs $\lambda \approx 3.5$ for Week 4). (d) The percentage of fully extended chains were tracked during the simulation and indicated that very modest stretches could produce these, and this was increasingly evident for more degraded systems, as expected.

Beginning with the MWD representative of the material prior to degradation (Week 0), $\Delta A/NkT$ was found to agree with the previous predictions obtained for $\Delta A/NkT$ when considering M_n for this timepoint at physically relevant stretches. As degradation progressed, deviations from Week 0 behaviour were found for much lower stretches than that observed for undegraded and degraded systems in the previous section (e.g., $\lambda \approx 1.08$ vs $\lambda \approx 3.5$ for Week 4) (Fig. 6.12b,c). This coincided with increasing numbers of fully extended chains at low stretches due to the build up of shorter chains in the systems that had experienced more degradation (Fig. 6.12d). Hence, considering all chains in the system, especially short ones, suggests that finite chain extensibility has relevance at physical stretches, particularly for degraded systems. Thus, while considering this concept is less significant for a polymer system in its original state, it becomes increasingly important when considering the evolving mechanical response of these materials as they experience degradation.

Fig. 6.13 presents an overview and comparison of Section 6.3 (left of the vertical black line), where uniform systems of polymer chains were considered corresponding to M_n, with the current section, where entire MWDs of chains were simulated. Intuitively, one may question why a short chain is more likely to reach its finite extensibility at lower stretches than a long chain, with both chains subjected to the same stretch ratio, λ. From Fig. 6.13(b,d,f), it is evident that the Langevin distribution described by Eq. (6.1) suggests increasingly small distances between the peak of the distribution and r_{max} for smaller values of n. Taking three approximately equivalent points on each of the end-to-end distance distribution curves and applying a stretch λ, it is observed that the chain with the largest value of r_0 reaches r_{max} first and this occurs at lower values of λ for increasingly degraded systems, i.e., smaller values of n (Fig. 6.13(c,e,g)). Note that while these are not physical stretches, with values of λ explored in the range $[1,5]$, it illustrates the point that shorter chains are likely to reach full extension at lower values of λ than for larger n. It should also be noted that the chains chosen to illustrate this concept lie approximately parallel to the stretch direction, with $\lambda \approx r/r_0$ and hence $r_{def} > r_0$ for each chain shown. Nevertheless, the other simulations did not restrict their focus to this case, with a spherical distribution of chain ends considered. Therefore, during stretching, chains may lengthen, as indicated in Fig. 6.13(c), for example, or shorten, depending on where they lie with respect to the stretch direction.

Once the entire MWD is used to generate a system of chains, and breaking them into intervals M_j as described in Fig. 6.10, it is observed that the intervals corresponding to the smallest values of n, i.e., the lowest M_j, reach full extension when restricting the focus to

physically relevant stretches ($1 < \lambda < 1.6$) (Fig. 6.13(i-n)). Note that additional intervals M_j exist at each timepoint, with only the smallest ones shown here due to their increased likelihood of reaching full extensibility. The extension from considering a uniform system of chains corresponding to M_n to an entire MWD is necessary to capture the finite extensibility of short chains in these degrading systems at physically relevant stretches. Consequently, the restriction preventing $r_{def} > r_{max}$ is necessary to capture the subsequent effect this may have on the material.

6.5 Stress response

The results of the simulated stretch and, in particular, predictions for the change in the Helmholtz free energy, ΔA, may be related to the stress-strain behaviour, as described by Ward (1971); further details are presented in Section 2.2. Firstly, the work done per unit undeformed volume in an infinitesimal displacement from $\lambda_x, \lambda_y, \lambda_z \rightarrow \lambda_x + \mathrm{d}\lambda_x, \lambda_y + \mathrm{d}\lambda_y, \lambda_z + \mathrm{d}\lambda_z$ is related to the strain-energy potential, U, as

$$\mathrm{d}U = \sigma_{xx}\mathrm{d}\lambda_x + \sigma_{yy}\mathrm{d}\lambda_y + \sigma_{zz}\mathrm{d}\lambda_z \tag{6.15}$$

where σ_{ii} is the nominal stress, i.e., the force per unit undeformed cross-section. In the case of uniaxial stress in the z direction, $\sigma_{xx} = \sigma_{yy} = 0$. Incorporating this into Eq. (6.15), the stress $\sigma = \sigma_{zz}$ is found as follows:

$$\sigma = \frac{\partial U}{\partial \lambda} = \frac{\partial \Delta A}{\partial \lambda} \tag{6.16}$$

where $\lambda = \lambda_z$. The Lagrangian approach to strain is taken, wherein the reference state is the undeformed state of material, to enable comparison with the experimental nominal stress versus strain of Vieira et al. (2011). A transformation, where the reference state is the deformed state of material, could be facilitated as described by, for example, Belytschko et al. (2014).

In order to extract results using the output from the simulation detailed above, where the average change in Helmholtz free energy per chain, $\frac{\Delta A}{NkT}$, is obtained as a function of the stretch, λ, Eq. (6.16) is presented as follows:

$$\bar{\sigma} = \frac{\partial}{\partial \lambda}\frac{\Delta A}{NkT} \tag{6.17}$$

where $\bar{\sigma}$ is the normalised nominal stress, $\bar{\sigma} = \sigma/NkT$.

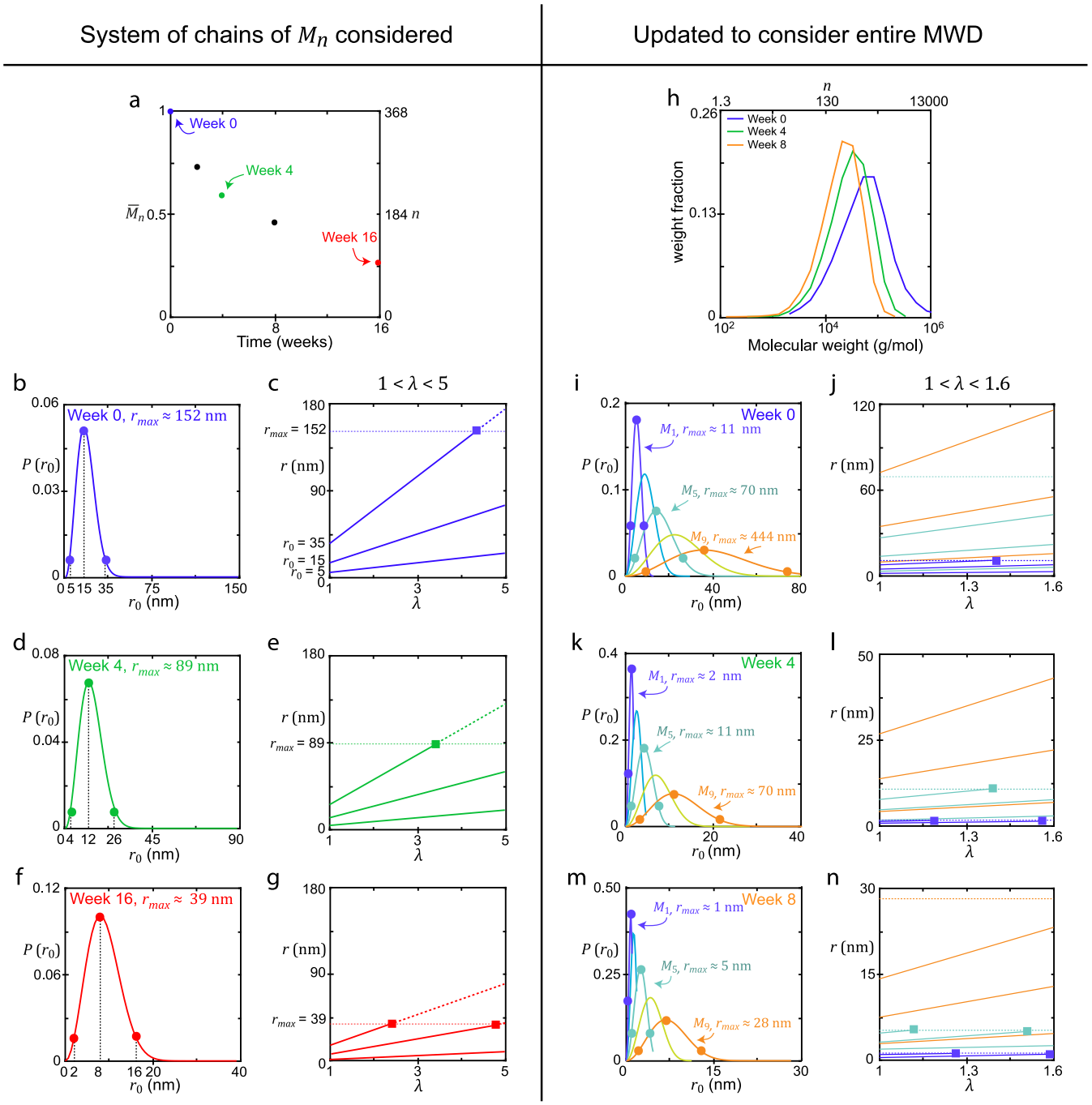

Fig. 6.13. Comparison between Section 6.3 (a-g), where all simulated chains had weight M_n, i.e., n units (a), and Section 6.4 (h-n), where molecular weight distributions (MWDs) of chains were generated, resulting in systems of chains with distributions of n units (h). An initial probability distribution of chain end-to-end lengths, $P(r_0)$ (Eq. (6.1)), and maximum end-to-end length, r_{max}, exists for each value of n. Thus, for each M_n a single $P(r_0)$ and r_{max} exist (b,d,f), while multiple $P(r_0)$ and r_{max} exist for each MWD, some of which are shown in (i,k,m). In (c), three representative chains are considered, corresponding to the three points shown in (b). Solely to illustrate this concept, it is assumed that each chain lies approximately parallel to the stretch direction, with $\lambda \approx r/r_0$. Large stretches ($\lambda > 4$) are needed before chains reach r_{max}. While smaller values of M_n (e,g) reach (and exceed) full extension for lower values of λ than in (c), it nevertheless occurs past the physical stretching limit for this material ($\lambda \approx 1.6$ (Vieira et al., 2011)). In (j,l,n), several values of r_{max} exist (many of which are beyond the limit of the y-axis shown) and due to the shorter tails of $P(r_0)$ for decreasing values of n, shorter chains, corresponding to the lowest M_j, are more likely to reach r_{max} at physically relevant stretches ($\lambda < 1.6$). The updated model prevents any additional extension of chains once they reach r_{max}, denoted by square markers. This thus validates the importance of considering the entire MWD alongside finite-extensibility for degrading polymer systems, with short chains particularly relevant and the number of these growing as degradation progresses.

Knowledge of the relationship between $\Delta A/NkT$ and λ (shown in Fig. 6.12c), which is evaluated numerically by considering the contribution of each individual chain to the elastic properties via the evolving network chain end-to-end distance distributions, as already described, allows the gradient to be calculated using a central difference operator (facilitated using the in-built gradient function in MATLAB® (R2020b, The MathWorks, Inc., MA, USA), outlined in Section 2.4.3).

6.5.1 Results

Using the predictions for $\Delta A/NkT$ obtained in the previous section (Fig. 6.12c), the normalised nominal stress, $\bar{\sigma}$, was calculated using Eq. (6.17) via the in-built gradient function in MATLAB® (R2020b, The MathWorks, Inc., MA, USA). This provided predictions for the stress-strain behaviour for different stages of degradation (accounted for with different molecular weight distributions). Fig. 6.14a-b presents the behaviour found in the experimental study of Vieira et al. (2011) for PLA:PCL (90:10) alongside the simulated behaviour for the same polymer. Without access to the experimental evolving MWD, predictions had to be made for these and thus limit the value of a quantitative comparison here. Instead, we focus on a qualitative comparison. It is observed that the simulated behaviour follows a similar trend to the experimental data, with increased timepoints of degradation having gradual reductions in gradient for larger values of stretch; however, this was more pronounced for the simulated behaviour compared with the experimental observations. The linear elastic stage remained constant for each simulated timepoint, suggesting no significant variation in Young's modulus occurred during degradation, in agreement with the experimental observations. The onset of yield was less pronounced for the simulated behaviour. Additionally, this approach cannot predict when failure occurs. Nevertheless, the simulation reasonably captures the general trend of the stress-strain behaviour during degradation of PLA-PCL fibres and may be further improved by considering experimental MWD rather than simulated ones, as done here.

Further simulations explored pure PLA and pure PCL polymers using the same MWD as in Fig. 6.12a, with the stress-strain predictions shown in Fig. 6.14c-d. While PLA followed similar behaviour to the PLA-PCL (90:10) system simulated, albeit with a slightly greater decline in $\bar{\sigma}$ for the former, PCL indicated a much less significant difference between Week 0 and Week 8 behaviour. The chemical structure of both polymers impacts this, with their respective chain dimensions resulting in $r_{max}(\mathrm{PLA}) < r_{max}(\mathrm{PCL})$ (Fig. 6.4). Thus, a more significant

loss in tensile strength as degradation proceeds was predicted for PLA compared with PCL, in agreement with experimental observations (Målberg et al., 2011).

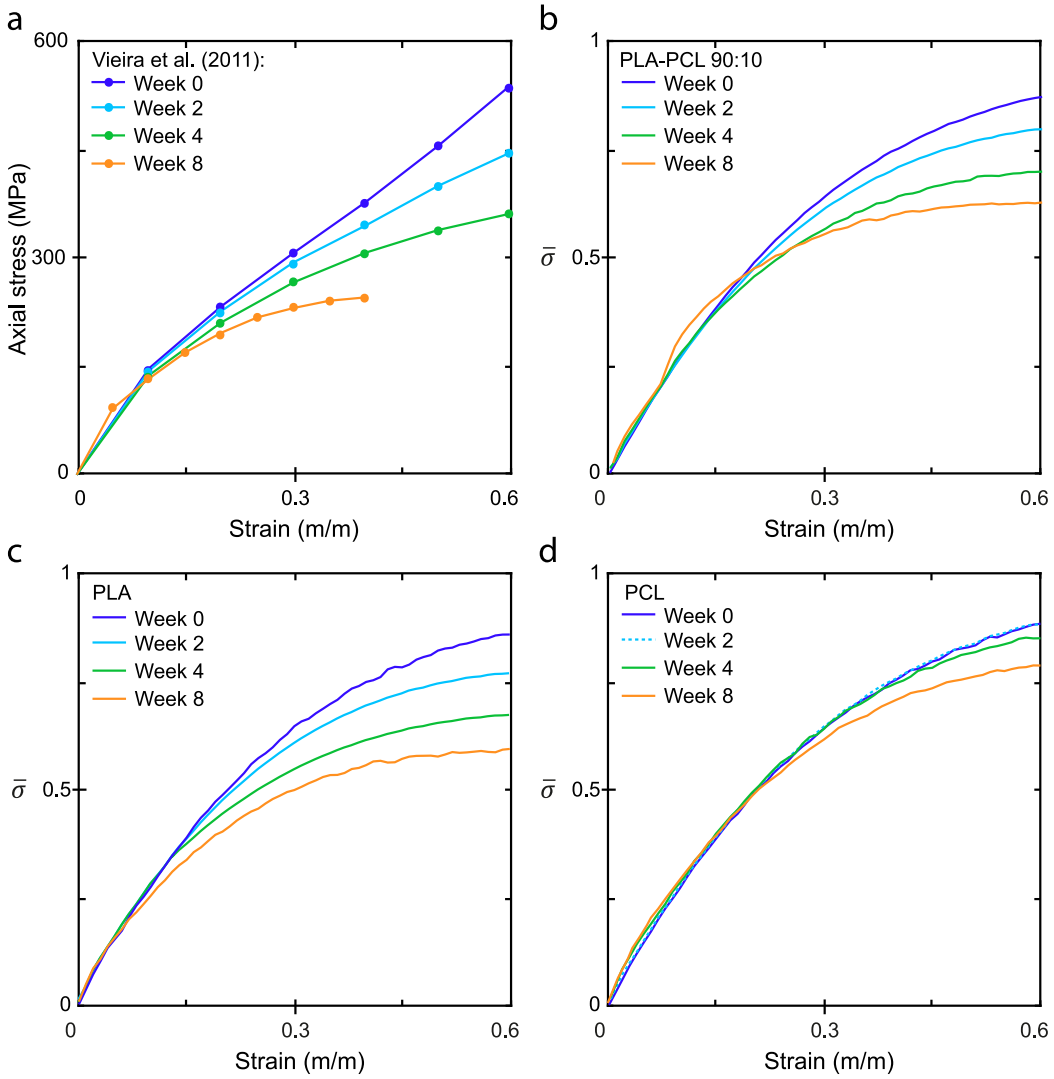

Fig. 6.14. (a) Experimental data of Vieira et al. (2011) showing stress-strain behaviour of PLA-PCL (90:10) undergoing degradation. (b) Simulated stress-strain behaviour of PLA-PCL (90:10) obtained using Eq. (6.17) for normalised stress, $\bar{\sigma} = \frac{\sigma}{NkT}$. A qualitative comparison between the experimental behaviour in (a) and simulated predictions in (b) indicates similarities, with gradual reductions in the maximum stress for increasing degradation for both, albeit comparatively to a greater extent for the predicted behaviour. The onset of yield is less prominent for the simulated behaviour and the onset of failure is not estimated using this technique. (c) Simulated stress-strain behaviour of pure PLA using the same MWD shown in Fig. 6.12. A slightly larger decline in $\bar{\sigma}$ is observed than in (b), with PLA reaching r_{max} more readily than PCL due to their respective chemical structures. (d) The simulated stress-strain behaviour of pure PCL indicates that finite extensibility is less evident for this material at moderate strains, with less difference observed between Week 0 and Week 8 than previous simulations, as expected (Fig. 6.4).

6.6 Coupling model for finite chain extensibility with failure criteria

Several failure criteria to describe the relationship between average molecular weight, MW, and failure strain, ε_f, were previously introduced (Chapter 5). These criteria are now used alongside the predictions for the stress-strain behaviour shown in Fig. 6.14 to estimate the onset of failure.

As an exponential decline in ε_f was not seen in the experimental study of Vieira et al. (2011), ε_f^{exp} has not been considered here. Thus, focus is restricted to the remaining two criteria previously introduced, $\varepsilon_f^{MW} = A_1\sqrt{MW}$, where MW is an average molecular weight, and $\varepsilon_f^{N} = A_4\sqrt{N_c}$, where N_c is the number of chain groups above a threshold molecular weight, M_n^{crit}. The parameters A_1 and A_4 were selected to ensure the initial failure strain agreed with the experimental observations, $\varepsilon_{f0} = 0.6$, (i.e., $A_1 = 0.6/\sqrt{M_{n0}}$, $A_4 = 0.6/\sqrt{N_{c0}}$) while M_n^{crit} was selected to ensure ε_f at Week 8 agreed by trialling several values. The results are presented in Fig. 6.15 for both failure criteria alongside comparison with the experimental findings (Vieira et al., 2011).

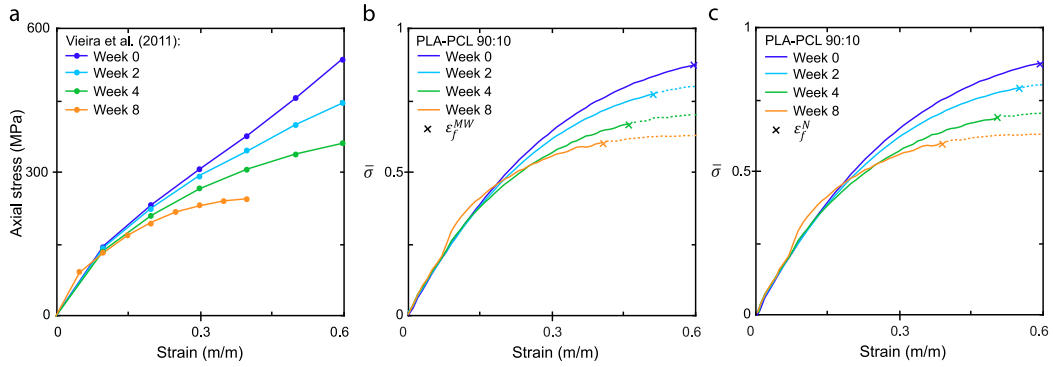

Fig. 6.15. Using the failure criteria introduced in Chapter 5, the points corresponding to failure strain, ε_f, are denoted (×) on the simulated stress-strain curves for PLA-PCL (90:10) from Fig. 6.14b. In (a), the experimental data of Vieira et al. (2011) is reproduced for comparison, where little change in ε_f was observed from Week 0 to Week 4 and $\varepsilon_f \approx 0.4$ at Week 8. (b) The failure criterion related to average molecular weight, $\varepsilon_f^{MW} = A_1\sqrt{MW}$, is shown where experimental values of M_n have been used for MW and A_1 was chosen to give $\varepsilon_{f0} = 0.6$. Week 2 and Week 4 predictions suggest a decline in ε_f that was not observed experimentally, while the Week 8 prediction is not pronounced enough. (c) The failure criterion that considers the entire molecular weight distribution via a threshold parameter, $\varepsilon_f^{N} = A_4\sqrt{N_c}$, is shown, where A_4 was chosen such that $\varepsilon_{f0} = 0.6$ and M_n^{crit} was selected to give $\varepsilon_f = 0.4$ at Week 8. Again, a decline in ε_f is seen for Week 2 and Week 4, but to a lesser extent than for ε_f^{MW}.

Both criteria suggested gradual declines in ε_f that were not apparent in the initial four weeks of the experimental study, with this decline more pronounced for ε_f^{MW}. Despite this, ε_f^{MW}

predicted a slightly more modest decline in ε_f by Week 8 than observed experimentally. Although ε_f^N relies on additional parameter calibration for M_n^{crit}, it does allow for improved predictions throughout the degradation scale considered. Coupling the models in this way allows for more robust predictions, providing insight into the point of failure alongside the evolution of the stress-strain behaviour. As detailed in Chapter 5, while these criteria can offer a reasonable prediction, further investigation into the mechanisms behind failure should be carried out.

6.7 Extending to alternative modes of deformation

The above implementation of the incremental uniaxial stretch of a network of polymer chains can readily be extended to consider alternative forms of mechanical testing. Here, we explore equibiaxial tension and pure shear.

To simulate equibiaxial tension $\sigma_y = \sigma_z = \sigma, \sigma_x = 0$, the extension ratios in the y- and z-directions are $\lambda_y = \lambda_z = \lambda$. Continuing the assumption of incompressibility, $\lambda_x = \frac{1}{\lambda^2}$. Eq. (6.10) is updated as

$$x_{def,i} = \frac{x_{0,i}}{\lambda^2}, \qquad y_{def,i} = \lambda y_{0,i}, \qquad z_{def,i} = \lambda z_{0,i} \tag{6.18}$$

and the rest of the simulation is carried out as before. From Eqs. (6.15) and (6.16), the nominal stress is found to be

$$\sigma = \frac{1}{2}\frac{\partial \Delta A}{\partial \lambda} \tag{6.19}$$

which is half of the relation for the uniaxial case in Eq. (6.16) and evaluated numerically as before.

Similarly, simple shear may be simulated by setting $\lambda_z = \lambda$, $\lambda_y = 1$ and $\lambda_x = 1/\lambda$, which gives a purely deviatoric stretch, i.e., with no volume change ($\lambda_x \lambda_y \lambda_z = 1$) (Treloar, 1975a). Consequently, Eq. (6.10) becomes

$$x_{def,i} = \frac{x_{0,i}}{\lambda}, \qquad y_{def,i} = y_{0,i}, \qquad z_{def,i} = \lambda z_{0,i} \tag{6.20}$$

with the simulation otherwise proceeding as before. Assuming the work done on the body is due entirely to the shear stress $\tau = \tau_{yz}$, it follows that

$$\mathrm{d}U = \tau \mathrm{d}\gamma \tag{6.21}$$

where $\gamma = \gamma_{yz}$ is the shear strain and here γ may be related to the principal extension ratios as follows (Love, 1944):

$$\gamma = \lambda - \frac{1}{\lambda} \tag{6.22}$$

Thus, combining Eqs. (6.21) and (6.22),

$$\tau = \frac{\partial U}{\partial \gamma} = \frac{\partial \Delta A}{\partial \lambda}\frac{\partial \lambda}{\partial \gamma} = \frac{\partial \Delta A}{\partial \lambda}\frac{\lambda^2}{\lambda^2 + 1} \tag{6.23}$$

which provides the relationship between τ and γ in a form that can easily be extracted from the results of the simulation using the same numerical techniques as before. Comparing to the purely affine case for simple shear, the equivalent shear response for the neo-Hookean (Eq. (6.8)) is of the following form:

$$U = \Delta A = \frac{1}{2}NkT\left(\lambda^2 + \frac{1}{\lambda^2} - 2\right) = \frac{1}{2}NkT\gamma^2 \tag{6.24}$$

and from Eq.(6.21),

$$\tau = NkT\gamma \tag{6.25}$$

with the shear stress proportional to the shear strain.

Continuing in this way, alternative modes of deformation can be simulated by appropriately altering Eq. (6.10) and determining the relevant stresses. The correct form for these may be obtained from Treloar (1975a), where an outline of the principal extension ratios and the general stress relationship for some additional classic modes of deformation is provided. Once these are updated, the simulation may proceed as previously detailed.

6.7.1 Results

The finite extensibility of polymer chains during simulated equibiaxial tension and simple shear and the effect of this on the stress-strain behaviour was considered as outlined above. Fig. 6.16 presents the stress-strain predictions for both cases alongside the uniaxial behaviour found above in Fig. 6.14b. The corresponding neo-Hookean affine behaviour, determined as the gradient of Eq. (6.8) with respect to λ for the uniaxial and equibiaxial cases and as Eq. (6.25) in the case of simple shear, is also shown in each case. For each mode of testing, a gradual departure from Week 0 behaviour is observed for increasing points of degradation. An initial agreement with neo-Hookean behaviour is observed in each case,

with equibiaxial tension showing the greatest departure by approximately a multiple of two greater than the other deformations at the final strain considered. Simulating deformation in this way captures increasing declines in the rate of change of free energy and, consequently, lower stresses are observed for increasing macroscopic strain in all cases, as expected. As in previous sections, σ and τ are normalised as in Eq. (6.17). Due to a lack of experimental data to compare with, these simulations are exploratory in nature.

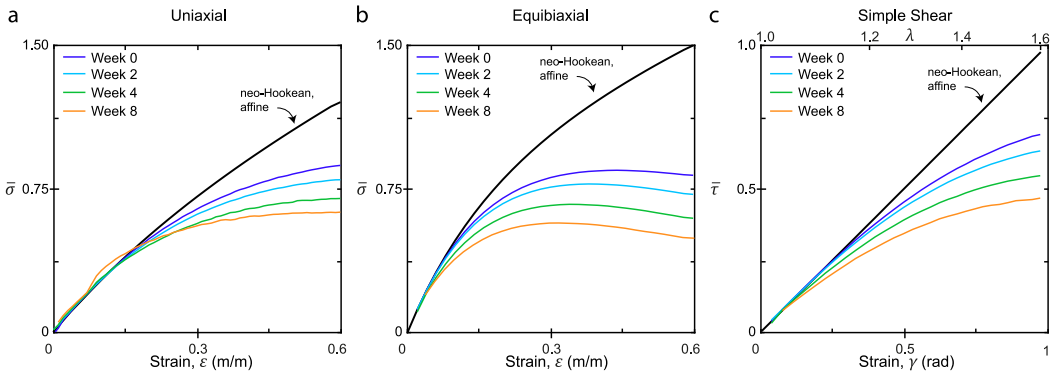

Fig. 6.16. Simulated stress-strain curves are obtained for various points of degradation using the same MWD as throughout this study for different modes of deformation. In (a), the uniaxial tension results from Fig. 6.14b are reproduced for comparison with (b) equibiaxial tension and (c) simple shear. In (a) and (b), affine Gaussian behaviour (black line) is plotted by taking the gradient of Eq. (6.8) with respect to λ, while in (c) Eq. (6.25) is used. Similar trends are seen for each mode of deformation, with increasing departures from both affine and Week 0 behaviour for more advanced points of degradation and increasing strain. At the final strain considered for Week 0, the equibiaxial case shows a departure from affine behaviour approximately twice that of the other modes of deformation.

6.8 Discussion

A finite chain extensibility model has been developed for degrading polymers to predict the evolution of the stress-strain response during degradation. While this concept has ordinarily not been considered when modelling biodegradable polymers (Hayman et al., 2014; Soares et al., 2010; Vieira et al., 2014), it has been explored when modelling non-degrading polymers (under typical conditions) (Arruda and Boyce, 1993; Edwards and Vilgis, 1986; Stepto and Taylor, 1995b). In particular, Stepto and Taylor (1995b) considered the effect of finite chain extensibility on the mechanical behaviour of polydimethylsiloxane by first generating a large network of chain conformations (5×10^6) and then simulating a uniaxial stretch on those chains, which reproduced experimentally observed deviations from affine Gaussian network behaviour. Motivated by that work, we explore the effect of finite chain extensibility in a degrading PLA-PCL (90:10) copolymer. While the same general approach is taken, the main modifications chosen here are detailed in Table 6.3.

A Langevin distribution of chain end-to-end lengths was chosen in this work. A simpler alternative often used, the Gaussian distribution, an approximation of the Langevin distribution, is appropriate for long chains (>100 units), but the solutions deviate for short chains. Here, an approximation of the Langevin distribution containing four terms was deemed acceptable (Fig. 6.6); improved approximations may be obtained using the method of, for example, Morovati et al. (2019). Alternatively, the rotational isomeric state statistics method may be used in conjunction with a Monte Carlo method to build chain conformations bond-by-bond, as was done by Stepto and Taylor (1995b); ultimately, this was deemed to be too computationally expensive in the current study, with each length of chain in the molecular weight distribution having to be considered individually.

Table 6.3. With this work following a similar approach to Stepto and Taylor (1995b), the main modifications are listed below.

Current model	Stepto and Taylor (1995b)	Comments
Langevin chain end-to-end distributions used to generate system of chains	Rotational isomeric state (RIS) statistics combined with Monte Carlo method to generate system of chains	The RIS approach is more computationally expensive than using a Langevin distribution, with chain conformations built bond-by-bond for the former. While the former is more accurate, the latter allows focus to be shifted to non-uniform polymer systems and remain computationally feasible for the current work.
Molecular weight distribution considered	Uniform polymer system considered (analogous with an average molecular weight)	By considering a MWD, the effect of short chains in the system (and their finite extensibility) can be better captured than when considering a uniform polymer system.
Degrading polymer system considered at multiple timepoints	Non-degrading polymers (under typical conditions) considered at one timepoint	By running the simulation at multiple timepoints for variously degraded MWDs, the effect of the build-up of short chains during degradation on the stress-strain response may be obtained, as shown in this study.
Coupled with failure criteria	No insight into failure	Coupling the finite chain extensibility model with the failure criteria introduced in Chapter 5 allows the predicted point of failure to be noted on the simulated stress-strain curves.
Various modes of deformation considered	Uniaxial tension and compression considered	While the main results presented here are for simulated uniaxial tension, modifications to consider alternative modes of deformation have been included.

While various polymer chain models exist, the equivalent freely jointed chain model was selected here. As shown in Fig. 6.7, the benefit of this over the standard freely jointed chain model lies with the inclusion of C_∞ for the equivalent freely jointed chain model, a local stiffness parameter that considers restrictions on bond angles and other conformational properties. The chosen model ensures a broader distribution of chain end-to-end lengths, as expected, with many condensed conformations not possible due to local interactions within the chains. Additionally, the maximum end-to-end length, r_{max}, is shorter for the chosen

model, again expected, with a fully extended straight chain not feasible due to bond angle restrictions (Fig. 6.3c). Both of these factors contribute to the peak of the distribution being closer to r_{max} than with the freely jointed chain model, which consequently ensures the effect of finite chain extensibility is better captured.

As discussed in Section 3.1.3, sourcing experimental data that detailed all properties of relevance to the models introduced herein proved a difficult task. The ideal experimental study would agree with assumptions made in this thesis, i.e., be amorphous throughout the study and experience little mass loss, while reporting on the evolution of MWD and stress-strain curves for a material such as PLA or PGA. The PLA-PCL degradation study of Vieira et al. (2011) reported little mass loss over the first eight weeks of the study and provided stress-strain curves over a long degradation duration. Although MWDs were not included, M_n was reported as a function of degradation duration, alongside information on the initial dispersity, M_{w0}/M_{n0}. With this information, an initial representative polymer chain distribution can be generated and the kinetic scission model introduced in Chapter 4 can be used to estimate evolving MWDs, as was carried out here. As the kinetic scission model does not consider mass loss, this approach was restricted to the first 8 weeks of the study of Vieira et al. (2011), prior to the point of more pronounced mass loss (Fig. 6.1). Crystallinity was not measured in their study, and it is unclear as to whether it was amorphous: reports of both amorphous and semi-crystalline PLA-PCL copolymers exist (Hiljanen-Vainio et al., 1996). Nevertheless, it is assumed to be amorphous here, with any contributions from or changes in the crystalline regions not considered in the current work.

The first polymer system modelled here (Section 6.3) assumed a uniform polymer system, with all chains having equal molecular weight, analogous to an average molecular weight such as M_n. In this case, a single end-to-end distance distribution exists at each timepoint of degradation, with $r_{max} \propto M_n$. A large uniaxial stretch was required before any chains with $r \geq r_{max}$ were observed, with no such chains existing when $\lambda = 1.6$ (Fig. 6.9d), the maximum extension prior to failure in the study of Vieira et al. (2011) for the same material modelled here. Although this uniform system of chains suggests finite chain extensibility is irrelevant at physical strains, a further exploration considers a more representative system of polymer chains.

The solution approach used in Section 6.3 was updated as outlined in the flowchart presented in Fig. 6.8 for use in Section 6.4, with a molecular weight distribution of chains now considered and removal of the affine deformation assumption to ensure chains are not extended past their respective r_{max}. In doing so, the effect of shorter in the system was

explored. This time, the simulated uniaxial stretch indicated that very low strains resulted in chains becoming fully extended, with more degraded systems exhibiting more fully extended chains (Fig. 6.12d).

Despite all chains being subjected to the same stretch, λ, shorter chains reach their respective r_{max} at lower stretches than required for longer chains. This is explained by Fig. 6.13, which compares the polymer systems from both Sections 6.3 and 6.4 in terms of the relevant end-to-end distance distributions of chains and the respective r_{max}, and considers comparable points of the distribution, r_0, simulating a stretch on each of the points. The stretch considered for the purpose of illustrating this concept, $\lambda \approx r/r_0$, is simplistic and assumes that each chain lies approximately parallel to the stretch direction; in the rest of the simulations in this study, no such assumption exists. Nevertheless, it helps illustrate the point that the peak of the distribution of end-to-end lengths becomes increasingly close to r_{max} for shorter chains and consequently means less stretch is needed for such short chains to approach their respective r_{max}. Ultimately, Section 6.4 indicates that considering finite chain extensibility, in conjunction with MWDs, becomes increasingly important as polymer systems degrade and contain a higher number of short chains.

The results of Section 6.4 were used to predict the stress-strain response of the material (Section 6.5). A qualitative comparison between the experimental behaviour (Vieira et al., 2011) and simulated predictions indicates similarities, with (i) gradual reductions in the maximum stress for increasing degradation and (ii) no change to the linear elastic stage throughout degradation for both (Fig. 6.14). Focus was restricted to qualitative comparisons due to not having robust experimental data including both evolving MWDs and stress-strain curves. Consequently, molecular weight distributions had to be generated, where agreement between simulated and experimental M_n was ensured ($r^2 > 0.99$). However, as was discussed in Section 2.1.2.2, chains with low molecular weight may be poorly captured experimentally; if this is the case, the simulated MWDs should include more short chains, which would subsequently readily reach finite extensibility during the simulated stretch applied here. While this approach may be used going forward, it is advised that improved verification of the model is first carried out using a complete set of experimental data.

Nevertheless, we compare the simulated predictions with the experimental data (Vieira et al., 2011) by fitting the linear elastic phase of the experimental curves shown in Fig. 6.14a to that of the predicted linear elastic phase (Fig. 6.14b), presented in Fig. 6.17. Predictions for Weeks 0, 2 and 4 agree very well with the experimental data up to a 30% strain. After this point, the predicted behaviour shows further decline in the slope that was not observed

experimentally. Additionally, predictions for the Week 8 behaviour show a higher maximum stress than that seen experimentally. These discrepancies may be due to factors such as possible deviations in the predicted and experimental MWDs, potential crystalline effects in the experimental behaviour, or, perhaps, further extension causing rupture of the fully extended chains and subsequent retraction or reorientation of chains in the experimental study. Still, the finite extensibility model not only captures experimental behaviour up to approximately 10%, as with the neo-Hookean model, but also captures an additional 20% for the initial 4 weeks of degradation. In doing so, the results suggest that finite chain extensibility may be responsible for the stress response in that region of strain.

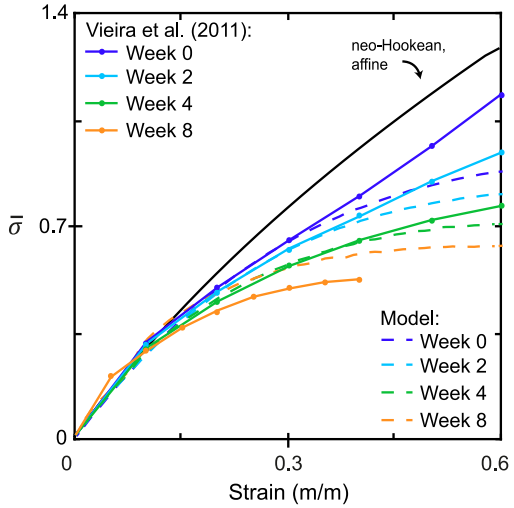

Fig. 6.17. A graphic fitting of the linear elastic phase of the experimental curves (Fig. 6.14a, (Vieira et al., 2011)) to the simulated predictions (Fig. 6.14b) for the normalised stress-strain response. Predictions for Weeks 0, 2 and 4 show good agreement with the experimental curves up to a strain of 30%, while Week 8 predictions show a higher stress than observed experimentally after approximately 10% strain. While the neo-Hookean model shows agreement with both the simulated and experimental observations initially, deviations are apparent after approximately 10% strain.

The normalised relationships considered, for example normalised nominal stress, $\bar{\sigma} = \sigma/NkT$, follows the approach of Stepto and Taylor (1995b) and allows relationships to be readily extracted from the simulation without the need for parameter calibration. Note that for progressive points of degradation the number of chains in the system, N, increases, which the normalisation fails to consider. Previous reports have suggested that an increase in N due to chain scission does not contribute to entropy in the usual way, with a "no-rise" rule suggested (Wang et al., 2010). Interestingly, for low stretches, $\bar{\sigma}$ for each timepoint was in agreement with each other, which was also observed for the non-normalised stress experimentally (Fig. 6.17). Going forward, a more complete understanding of how evolving

N contributes to entropy is needed to provide an appropriate calculation of the non-normalised behaviour.

The predicted stress-strain curves corresponding to PLA-PCL (90:10) (Fig. 6.14b) are similar to the Mooney-Rivlin predictions presented by Vieira et al. (2011). Although the Mooney-Rivlin model may be implemented more simply, it is phenomenological in nature. As detailed by Ward and Sweeney (2013), molecular network models can provide greater insight into the network behaviour and offer a more physical description and understanding than phenomenological models. To date, the relationship between deformation at macroscopic and molecular levels is not fully understood. The method implemented here allows the mechanisms behind the behaviour to be investigated. The results obtained suggest that the finite extensibility of polymer chains is an important feature that contributes to the evolving mechanical properties during degradation. Going forward, it may be possible to directly link the evolving molecular weight distribution, specifically the fraction of chains below some weight where the probability of them fully extending at physical strains is high, to changes in mechanical properties.

A comparison between PLA-PCL (90:10), pure PLA and pure PCL (Fig. 6.14) indicates chains with equal molecular weight are more likely to fully extend in PLA, with the entropy of such chains tending towards zero as they approach full extension and consequently their contribution towards free energy, and subsequently stress, minimises towards zero. This is due to the chemical structure of PLA compared with PCL, as shown in Fig. 6.4, and is supported by the experimental study of Målberg et al. (2011) wherein PCL was extended twice as much as PLA prior to failure (reproduced in Fig. 6.4e). By incorporating just 10% PCL with PLA, a slightly higher value of maximum stress was predicted at each timepoint than for pure PLA. Increasing the PCL content is expected to further reduce the degradation of mechanical properties; however, this should be verified with experimental data.

By coupling the methods detailed in this chapter (Fig. 6.8) with the preceding chapters, evolving stress-strain curves may be modelled as degradation proceeds in a polymer material (Fig. 6.15). Specifically, amorphous polymers with little mass loss have been considered herein. The input parameters for (i) the kinetic scission model were evolving M_n, initial dispersity and molar mass, (ii) the failure criteria model were ε_{f0} (for ε_f^{MW} and ε_f^N), ε_f at Week 8 (for ε_f^N) and KSM outputs, and (iii) the finite extensibility model were KSM outputs and polymer chain characteristics for PLA and PCL. While the KSM requires several parameters to be calibrated, the follow-up studies depend on those but require limited

additional calibration aside from a sensitivity analysis to ensure appropriate step-sizes have been used. As already mentioned, further investigations are needed to determine how best to obtain non-normalised solutions for this study using a physical understanding of the contribution of N where possible.

While the focus was on uniaxial tension, extending to alternative modes of deformation simply required modification of Eq. (6.10) using the correct principal stretch ratios and reanalysis of the stress response. The results (Fig. 6.16) showed agreement between predictions and neo-Hookean behaviour for uniaxial tension, equibiaxial tension and simple shear up to at least 10% strain at Week 0 prior to a decline in slope for the simulated behaviour, while additional timepoints of degradation further deviated for increasingly lower strains. This deviation is expected due to an increased number of short chains for increasingly degraded systems reaching full extension at modest strains and thus contributing to less affine behaviour. At 60% strain, the deviation between neo-Hookean and simulated behaviour at Week 0 for biaxial tension was twice that of uniaxial tension. This is expected due to the chain orientation effect, where chains in the undeformed network whose end-to-end vectors lie close to the extension axes reach full extension at relatively low strains (Stepto and Taylor, 1995b); as there are two axes of extension in the biaxial tension case and only one axis of extension for uniaxial tension, approximately twice as many chains will become fully extended in the biaxial case (Fig. 6.18).

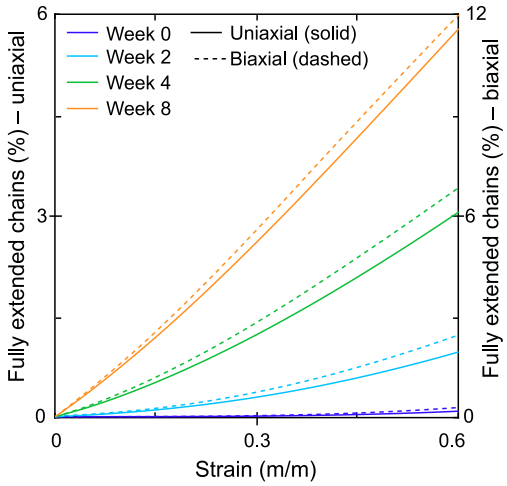

Fig. 6.18. Comparison between the percentage of fully extended chains in the case of uniaxial (left axis, solid lines) and biaxial (right axis, dashed lines), highlighting the importance of chain orientation with respect to the axes of deformation.

The finite extensibility model introduced here has been validated using both experimental data (Vieira et al., 2011) and the existing neo-Hookean model. Agreement between the neo-Hookean model and both the simulated and experimental observations was found up to

approximately 10% strain (Fig. 6.17). Additional agreement between the simulated curves and the experimental data was seen up to approximately 30% strain, halfway to the point of failure, for Weeks 0, 2 and 4. For Week 8, the simulated behaviour predicted a slightly higher stress response than the experimental data. Including additional short chains in the MWD would solve this discrepancy; however, as mentioned, further experimental verification should be carried out using a complete set of data. Furthermore, the model has been verified as shown in Appendix 6A Sensitivity analysis. Thus, from the validation and verification, it is apparent that finite chain extensibility plays a role in the deviation from affine behaviour of polymer systems up to at least 30% strain. The finite extensibility model simulation corresponding to one timepoint from the main results completed in approximately 1 h on an Intel(R) Core(TM) i7-8565U CPU @ 1.80GHz 1.99 GHz computer with 16GB RAM and a 64-bit operating system; this is a stark improvement compared to the eight-week experimental study considered here.

6.9 Conclusion

In summary, statistical mechanics methods for rubber-like materials have been applied to understand how elasticity changes during degradation in a polymer, where the molecular weight distribution is evolving. The elastic properties were related to network chain end-to-end distance distributions and assumed to arise solely as a result of conformational changes in the network chains. The total deformation of the end-to-end vectors of individual chains were considered, rather than the deformation of an average chain.

We found realistic polymer chain distributions provided improved predictions compared with average molecular weights, with deviations from affine behaviour observed at physically relevant stretches with the former. By removing the affine Gaussian assumption during stretching of a polymer network, we observed that proper treatment of fully extended chains, especially shorter chains in the distribution, is necessary to capture departures from Week 0 behaviour for degraded systems when considering the stress response.

This framework provides a foundation for further investigation of degrading materials. Other aspects to consider include plasticity, unloading behaviour, entanglements, and fracture. We see in experimental data that degraded polymers are substantially more brittle (Polak-Kraśna et al., 2021; Tsuji, 2002). This work offers insight into the evolution of mechanical properties as the system degrades. Going forward, detailed experimental testing where the MWD is known for different load deformations is needed to further validate the model. Once this has been suitably achieved, an analytical description of the behaviour in terms of the strain

invariants may be sought. Ideally, this would allow for the introduction of a new strain energy potential that takes the deviation from affine deformation into account. This may then be input into finite element software such as Abaqus, providing wide-spread usability and enabling realistic geometries to be considered.

Appendix 6A Sensitivity analysis

A sensitivity analysis was carried out for uniform polymer systems to determine a suitable value for the number of chains in the simulation, N, and increment values for the stretch, λ, and the end-to-end length, r (Fig. 6A. 1). This was investigated with respect to values of n, the number of units per chain, and the resulting stress-strain predictions obtained. Incremental values of λ, λ_{inc}, are reported as the magnitude of the stretch between incremental points of the simulation, while incremental values of r are taken as $r_{inc} = r_{max}/Cn$, for constant C for improved efficiency. The latter parameter, r_{inc}, is comparable with the width of histogram bins for the end-to-end distance distribution rather than the smooth formula distribution and this was a necessary requirement for computational reasons (i.e., having a finite sample size) to ensure the change in Helmholtz free energy could be calculated using Eq. (6.12).

For decreasing values of n, the system is more sensitive to each of the parameters investigated. A deviation from the origin $(0,0)$ is evident to varying degrees and it is seen that this is primarily controlled by both λ_{inc} (Fig. 6A. 1d-f), with larger values not capturing the initial behaviour, and r_{inc} (Fig. 6A. 1g-i), with larger values (corresponding to less refined histogram approximations) resulting in unsmooth distributions ($P_{gen,0}(r_0)$ and $P_{gen,def}(r_{def})$) and, thus, relatively large changes in ΔA as chains are stretched from one interval to the next. Further refinement of these properties, particularly at low levels of strain, would lessen this deviation further. However, uniform grids were chosen and $N = 1 \times 10^7$, $\lambda_{inc} = 0.01$, and $r_{inc} = r_{max}/5n$ were deemed sufficient to balance computational efficiency with convergence, with excellent convergence found when $\varepsilon > \lambda_{inc}$.

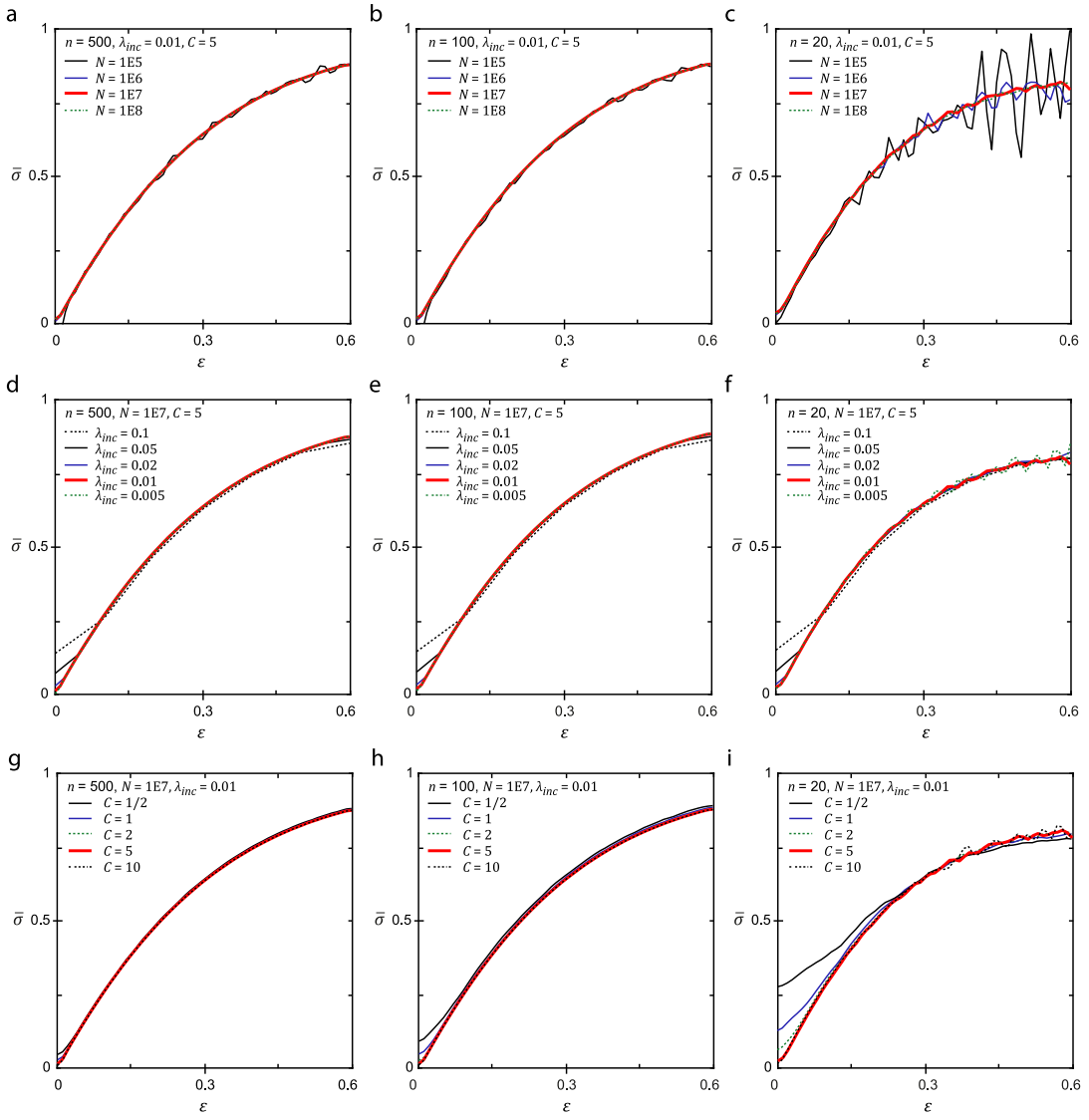

Fig. 6A. 1. A sensitivity analysis was carried out to determine optimal values for the (a-c) number of chains in the simulation, N, (d-f) increment values for the stretch, λ, λ_{inc}, and (g-i) increment values for the end-to-end length, r, defined as $r_{inc} = r_{max}/Cn$, for constant C. Refinement towards the origin (0,0) is possible for further refined parameters; however, $N = 1 \times 10^7, \lambda_{inc} = 0.01$ and $r_{inc} = r_{max}/5n$ were deemed sufficient to balance computational efficiency and provided excellent convergence when $\varepsilon > \lambda_{inc}$.

Appendix 6B Pseudocode

The pseudocode below outlines the code used to simulate stretching on a system of polymer chains in this chapter. The elements in blue correspond with the modifications introduced in Section 6.4, while without these elements, the simulations in Section 6.3 are described.

Input: (co)polymer characteristics for polymer p_k ($p_k = p_1, p_2, \ldots$ at percentage $X_1 : X_2 : \ldots$): average backbone bond lengths, l_{p_k}, average backbone bond angles, θ_{p_k}, and characteristic ratio, C_{∞,p_k}

for degradation time

Input: molecular weight distribution containing n_{int} intervals with N_j chains of weight M_j for a total of N chains

for j in 1:n_{int}

Generate system of polymer chains:

For polymer p_k, set the mean-squared end-to-end distance $\langle r^2 \rangle_{0,j,p_k} = C_{\infty,p_k} \frac{nn_b M_j}{M_{0,p_k}} l_{p_k}^2$ and the maximum end-to-end length $r_{max,j,p_k} = \frac{nn_b M_j}{M_{0,p_k}} l_{p_j} \cos\left(\frac{\theta_{p_k}}{2}\right)$ for a monomer with molar mass M_{0,p_k} containing nn_b backbone bonds

Calculate the Kuhn length as $l_{K,j} = \frac{\sum_k \frac{X_k}{100} \langle r^2 \rangle_{0,j,p_k}}{\sum_k \frac{X_k}{100} r_{max,j,p_k}}$ and the number of Kuhn monomers as $n_{K,j} = \frac{\left(\sum_k \frac{X_k}{100} r_{max,j,p_k}\right)^2}{\sum_k \frac{X_k}{100} \langle r^2 \rangle_{0,j,p_k}}$ for the homopolymer approximation

Calculate $r_{max,j} = n_{K,j} l_{K,j}$ to obtain the maximum end-to-end distance for the polymer

Using the Langevin distribution function, generate a histogram approximation of end-to-end distances, determining the number of chains to be generated in an interval of size r_{inc} for a total of N_j chains with an end-to-end length between 0 and $r_{max,j}$

for i in 1:N_j

Assign chain i an initial end-to-end length, $r_{0,i}$, at random within their interval

Randomly select coordinates for the free chain ends consistent with $r_{0,i}$ assuming isotropy

end

Set $P_{gen,0,j}$ to be the generated end-to-end distance distribution

for λ in 1:λ_{max}

Simulate incremental uniaxial stretch λ on the network with one end of each chain remaining fixed at the origin:

Calculate the updated coordinates for the free chain ends and determine the updated end-to-end length, $r_{upd,i}$, of each chain

if $r_{upd,i} > r_{max,j}$

Set $r_{upd,i} = r_{max,j}$

Track the number of fully extended chains, $n_{fec,j}$

end

Set $P_{gen,upd,j}$ as the updated end-to-end distance distribution

Calculate the normalised average change in Helmholtz free energy for each chain as $\frac{\Delta A_j}{N_j kT} = \frac{1}{N_j}\sum_{i=1}^{N_j} \log\left(\frac{P_{gen,0,j}(r_{0,i})}{r_{0,i}^2}\right) - \log\left(\frac{P_{gen,upd,j}(r_{upd,i})}{r_{upd,i}^2}\right)$ where k is the Boltzmann constant and T is temperature

end

end

Calculate the overall percentage of fully extended chains for the system, $pc_{fec} = \frac{\sum_j \frac{n_{fec,j}}{N_j}}{n_{int}} \times 100$

Calculate the overall average change in Helmholtz free energy per chain for the system, $\frac{\Delta A}{N k_B T} = \frac{\sum_j \frac{\Delta A_j}{N_j k_B T}}{n_{int}}$

Calculate the normalised stress as the gradient of the average change in Helmholtz free energy per chain for the system, $\frac{\sigma}{N k_B T} = \nabla\left(\frac{\Delta A}{N k_B T}\right)$

end

Output: $pc_{fec}(\lambda, t), \Delta\bar{A}(\lambda, t), \bar{\sigma}(\lambda, t)$

Appendix 6C MATLAB live script for simulated stretching of a network

Generation and simulated stretching of a polymer network

Stretch PLA-PCL (90:10) at various stages of degradation and compare with experimental data from Vieira et al., 2011, doi.org/10.1016/j.jmbbm.2010.12.006

Set-up

Input molecular weight distribution containing `n_int` intervals with `rep` repeat chains containing UPC units per chain. Make `rep` large enough for each value of UPC to ensure appropriate randomness as the simulation proceeds.

```
 UPC = [100,200]; rep = [1E6,1E7];  % test values - replace with
respresentative molecular weight distribution data
```

Choose number of stretching increments and maximum stretch:

```
 inc = 60;  % number of increments for lambda;
 lambda_f = 1.6;
```

Generate `struct` for storing results:

```
 for i = 1:length(UPC)
     St(i).Nm = struct('UPC', cell(1), 'chains', cell(1), 'r2',
cell(1,inc+1), 'dASys', cell(1,inc+1), 'fully_ext', cell(1,inc+1));
 end
```

Generate end-to-end distance distribution of chains

For each individual value of UPC, set-up system by generating initial chain lengths.

```
 for N = 1:length(UPC)
```

Input chain parameters for equivalent freely jointed chains. Use the method of Fischel et al., 1997, doi.org/10.1039/a705898e to obtain a homopolymer approximation from copolymer parameters. Determine the maximum possible end-to-end distance, `r_max`, for chains with a given value of UPC.

```
     n = UPC(N); % number of units
     linkL_PCL = 0.149;  % 7 skeletal bonds per unit
     theta_PCL = 71; % valence bond angle
     C_inf_PCL = 4.9; % characteristic ratio
     r_msd_PCL = C_inf_PCL*7*n*linkL_PCL^2; % mean-square end-to-end
distance
     r_max_PCL = 7*n*linkL_PCL*cosd(theta_PCL/2);
     linkL_PLA = 0.143;  % 3 skeletal bonds per unit
```

```
    theta_PLA = 68;
    C_inf_PLA = 7.68;
    r_msd_PLA = C_inf_PLA*3*n*linkL_PLA^2;
    r_max_PLA = 3*n*linkL_PLA*cosd(theta_PLA/2);
    Kuhn_l = (0.1*r_msd_PCL+0.9*r_msd_PLA)/(0.1*r_max_PCL +
0.9*r_max_PLA);
    Kuhn_n = (0.1*r_max_PCL +
0.9*r_max_PLA)^2/(0.1*r_msd_PCL+0.9*r_msd_PLA);
    r_max = Kuhn_n * Kuhn_l; % maximum end-to-end distance of
homopolymer approximation
```

End-to-end distance distributions will be created using histogram approximations. Choose increment size for r (i.e., the width of histogram bins):

```
    r_inc = r_max/(5*n);
```

Calculate volumetric Langevin probability distribution, assuming a spherical distribution of chain end-to-end lengths:

```
    LPV = zeros(1, ceil(r_max/r_inc)+1);
    for i = 0:ceil(r_max/r_inc)
        LPV(i+1) =
4*pi*(i*r_inc)^2*((3/(2*Kuhn_n*Kuhn_l^2*pi))^(3/2))*exp(-
Kuhn_n*((3/2*((i*r_inc)/(Kuhn_n*Kuhn_l))^2)+(9/20*((i*r_inc)/(Kuhn_n*K
uhn_l))^4)+(99/350*((i*r_inc)/(Kuhn_n*Kuhn_l))^6)+(1539/9000*((i*r_inc
)/(Kuhn_n*Kuhn_l))^8)));
    end
```

Generate distribution of chain end-to-end lengths using LPV:

```
    numch = LPV*rep(N)*r_inc;    % determine no. of chains of each
length
    r0 = [];
    for i = 1:ceil(r_max/r_inc)+1
        if (i-1)*r_inc > r_max
            break
        end
        for j = 1:round(numch(i))
            temp = ((i-1) + rand)*r_inc;
            if temp > r_max     % prevent chains from having r >
r_max
                continue
            end
            r0(numel(r0)+1) = temp;
        end
    end
    r02 = sum(r0.^2)/numel(r0); % mean-square end-to-end distance
```

Determine initial generated radial end-to-end distance distribution:

```
    Pgen0 = (1/r_inc)/numel(r0)*histcounts(r0,
(0:ceil(r_max/r_inc)+1)*r_inc);
```

Assuming one end of each chain is fixed at the origin, determine coordinates of the other end consistent with r0:

```
    x0 = rand(1, numel(r0))*2 - 1; % choose random number between (-
1,1)
    y0 = rand(1, numel(r0))*2 - 1;
    z0 = rand(1, numel(r0))*2 - 1;
    xyz = sqrt(x0.^2 + y0.^2 + z0.^2); % find the norm of the vector
    x0 = x0./xyz.*r0; % scale each coordinate with r0 and the vector
norm for isotropy
    y0 = y0./xyz.*r0;
    z0 = z0./xyz.*r0;
    xyz=[];
```

Simulate stretch on network of chains

Apply uniaxial stretch incrementally in z-direction, assuming incompressibility. Determine updated coordinates of chain ends (assuming one end remains fixed at the origin).

Initialise:

```
    St(N).Nm(1).UPC = n;
    St(N).Nm(1).chains = numel(r0);
    St(N).Nm(1).r2 = r02;
    St(N).Nm(1).dASys = 0;
    St(N).Nm(1).fully_ext = 0;
    it = 1; % iteration number
    for lambda = linspace(1+(lambda_f-1)/inc, lambda_f, inc)
        it = it + 1;
```

Determine updated end-to-end lengths, where chains are stretched only until they reach full extension.

```
        r_upd = min((sqrt((x0./sqrt(lambda)).^2 +
(y0./sqrt(lambda)).^2 + (z0.*lambda).^2)), r_max);
        St(N).Nm(it).r2 = sum(r_upd.^2)/numel(r_upd);
```

Determine updated end-to-end distance distribution:

```
        Pgen_upd = (1/r_inc)/numel(r0)*histcounts(r_upd,
(0:ceil(r_max/r_inc)+1)*r_inc);
        Pgen_upd(Pgen_upd==0) = eps; % prevent numerical errors as
the simulation proceeds by removing zeros from array (unnecessary for
large enough systems/well chosen parameters)
```

Calculate the change in Helmholtz free energy per chain, and the average change in Helmholtz free energy per chain for the system:

```
        dApCh = log(Pgen0(ceil(r0/r_inc))./r0.^2) -
log(Pgen_upd(ceil(r_upd/r_inc))./r_upd.^2); % per chain
        St(N).Nm(it).dASys = sum(dApCh)/numel(r0); % average change
in Helmholtz free energy per chain for the system
        St(N).Nm(it).fully_ext = sum(r_upd==r_max); % track the
number of fully extended chains
    end
end
```

Compile results

Compile results for each value of UPC to determine values for entire system.

```
lambda = linspace(1,lambda_f,inc+1);
Helm = zeros(1, inc + 1);
f_ext_pc = zeros(1, inc + 1);
for ii = 1:max(size(St))
    for i = 1:inc + 1
        Helm(i) = St(ii).Nm(i).dASys + Helm(i);
        f_ext_pc(i) = St(ii).Nm(i).fully_ext/St(ii).Nm(1).chains*100
+ f_ext_pc(i);
    end
end
Helm = Helm/max(size(St));
f_ext_pc = f_ext_pc/max(size(St));
stress = gradient(Helm, lambda(2)-lambda(1));
```

Calculate affine, Gaussian behaviour (for uniaxial stretch):

```
nH = lambda.^2 + 2./lambda - 3;
stress_aff = gradient(0.5*nH, lambda(2)-lambda(1));
```

References

Anderson, K.S., Hillmyer, M.A., 2004. Melt Chain Dimensions of Polylactide. Macromolecules 37, 1857–1862. https://doi.org/10.1021/ma0357523

Arruda, E.M., Boyce, M.C., 1993. A three-dimensional constitutive model for the large stretch behavior of rubber elastic materials. J. Mech. Phys. Solids 41, 389–412. https://doi.org/10.1016/0022-5096(93)90013-6

Belytschko, T., Liu, W.K., Moran, B., Elkhodary, K.I., 2014. Nonlinear Finite Elements for Continua and Structures, 2nd ed. John Wiley & Sons Ltd.

Blomqvist, J., 2001. RIS Metropolis Monte Carlo studies of poly(L-lactic), poly(L,D-lactic) and polyglycolic acids. Polymer 42, 3515–3521. https://doi.org/10.1016/S0032-3861(00)00704-7

Brant, D.A., Tonelli, A.E., Flory, P.J., 1969. The Configurational Statistics of Random Poly(lactic acid) Chains. II. Theory. Macromolecules 2, 228–235. https://doi.org/10.1021/ma60009a003

Buchanan, F.J. (Ed.), 2008. Degradation rate of bioresorbable materials: prediction and evaluation. Woodhead Publishing Limited/CRC Press LLC, Cambridge, England/Boca Raton, FL.

Edwards, S.F., Vilgis, T., 1986. The effect of entanglements in rubber elasticity. Polymer 27, 483–492.

https://doi.org/10.1016/0032-3861(86)90231-4
Fetters, L.J., Lohse, D.J., Colby, R.H., 2007. Chain Dimensions and Entanglement Spacings, in: Mark, J.E. (Ed.), Physical Properties of Polymers Handbook. Springer, pp. 447–454.
Fischel, L.B., Newman, J., Theodorou, D.N., 1997. Segment density of a block copolymer chain tethered at both ends. J. Chem. Soc. - Faraday Trans. 93, 4355–4370. https://doi.org/10.1039/a705898e
Hamidi, N., Edmonds, S., Frazier, V., Clemons, F., 2018. Temperature Dependence Characteristics of Biodegradable Polycaprolactone Grafted Propargyl Dehydroabietic Ester (PCL-g-DAPE). J. Macromol. Sci. Part B Phys. 57, 129–150. https://doi.org/10.1080/00222348.2018.1429750
Hayman, D., Bergerson, C., Miller, S., Moreno, M., Moore, J.E., 2014. The Effect of Static and Dynamic Loading on Degradation of PLLA Stent Fibers. J. Biomech. Eng. 136, 1–9. https://doi.org/10.1115/1.4027614
Hiljanen-Vainio, M., Karjalainen, T., Seppälä, J., 1996. Biodegradable Lactone Copolymers. I. Characterization and Mechanical Behavior of ε-Caprolactone and Lactide Copolymers. J. Appl. Polym. Sci. 59, 1281–1288. https://doi.org/10.1002/(sici)1097-4628(19960222)59:8<1281::aid-app11>3.3.co;2-e
James, H.M., Guth, E., 1943. Theory of the elastic properties of rubber. J. Chem. Phys. 11, 455–481. https://doi.org/10.1063/1.1723785
Kuhn, W., Grün, F., 1946. Statistical behavior of the single chain molecule and its relation to the statistical behavior of assemblies consisting of many chain molecules. J. Polym. Sci. 1, 183–199. https://doi.org/10.1002/pol.1946.120010306
Love, A.E.H., 1944. A Treatise on the Mathematical Theory of Elasticity, 4th ed. Dover Publications, New York.
Målberg, S., Höglund, A., Albertsson, A.C., 2011. Macromolecular design of aliphatic polyesters with maintained mechanical properties and a rapid, customized degradation profile. Biomacromolecules 12, 2382–2388. https://doi.org/10.1021/bm2004675
Malin, M., Hiljanen-Vainio, M., Karjalainen, T., Seppala, J., 1996. Biodegradable Lactone Copolymers. II. Hydrolytic Study of ε-Caprolactone and Lactide Copolymers. J. Appl. Polym. Sci. 59, 1289–1298. https://doi.org/10.1002/(SICI)1097-4628(19960222)59:8<1289::AID-APP12>3.0.CO;2-1
Mark, J.E. (Ed.), 2007. Physical Properties of Polymers Handbook, Second. ed. Springer. https://doi.org/10.1016/s0039-9140(97)80037-9
Mark, J.E., Erman, B., 2007. Rubberlike Elasticity: A Molecular Primer, 2nd ed. Cambridge University Press.
Morovati, V., Mohammadi, H., Dargazany, R., 2019. A generalized approach to generate optimized approximations of the inverse Langevin function. Math. Mech. Solids 24, 2047–2059. https://doi.org/10.1177/1081286518811876
Polak-Kraśna, K., Abaei, A.R., Shirazi, R.N., Parle, E., Carroll, O., Ronan, W., Vaughan, T.J., 2021. Physical and mechanical degradation behaviour of semi-crystalline PLLA for bioresorbable stent applications. J. Mech. Behav. Biomed. Mater. 118, 1–11. https://doi.org/10.1016/j.jmbbm.2021.104409
Reed, A.M., Gilding, D.K., 1981. Biodegradable polymers for use in surgery - poly(glycolic)/poly(lactic acid) homo and copolymers: 2. In vitro degradation. Polymer 22, 494–498. https://doi.org/10.1016/0032-3861(81)90168-3
Rivlin, R.S., 1948. Large elastic deformations of isotropic materials. I. Fundamental concepts. Philos. Trans. R. Soc. London Ser. a-Mathematical Phys. Sci. 240, 459–508.
Shirazi, R.N., Ronan, W., Rochev, Y., McHugh, P., 2016. Modelling the degradation and elastic properties of poly(lactic-co-glycolic acid) films and regular open-cell tissue engineering scaffolds. J. Mech. Behav. Biomed. Mater. 54, 48–59. https://doi.org/10.1016/j.jmbbm.2015.08.030
Soares, J.S., Moore, J.E., Rajagopal, K.R., 2010. Modeling of Deformation-Accelerated Breakdown of Polylactic Acid Biodegradable Stents. J. Med. Device. 4, 1–10. https://doi.org/10.1115/1.4002759
Stepto, R.F.T., Taylor, D.J.R., 1995a. Molecular Modelling of the Elastic Behaviour of Polymer Chains in Networks: Comparison of Polymethylene and Poly(dimethylsiloxane). J. Chem. Soc. Faraday Trans. 91, 2639–2647. https://doi.org/10.1039/FT9959102639
Stepto, R.F.T., Taylor, D.J.R., 1995b. Modelling the elastic behaviour of real chains in polymer networks. Macromol. Symp. 93, 261–268. https://doi.org/10.1002/masy.19950930131
Tonelli, A.E., Flory, P.J., 1969. The Configuration Statistics of Random Poly(lactic acid) Chains. I. Experimental Results. Macromolecules 2, 225–227. https://doi.org/10.1021/ma60009a002

Treloar, L.R.G., 1975a. The Physics of Rubber Elasticity, 3rd ed. Clarendon Press, Oxford.

Treloar, L.R.G., 1975b. Experimental examination of the statistical theory, in: The Physics of Rubber Elasticity. Clarendon Press, Oxford, pp. 80–100.

Tsuji, H., 2002. Autocatalytic hydrolysis of amorphous-made polylactides: effects of L-lactide content, tacticity, and enantiomeric polymer blending. Polymer 43, 1789–1796. https://doi.org/10.1016/S0032-3861(01)00752-2

Vey, E., Roger, C., Meehan, L., Booth, J., Claybourn, M., Miller, A.F., Saiani, A., 2008. Degradation mechanism of poly(lactic-co-glycolic) acid block copolymer cast films in phosphate buffer solution. Polym. Degrad. Stab. 93, 1869–1876. https://doi.org/10.1016/j.polymdegradstab.2008.07.018

Vieira, A.C., Guedes, R.M., Tita, V., 2014. Constitutive modeling of biodegradable polymers: Hydrolytic degradation and time-dependent behavior. Int. J. Solids Struct. 51, 1164–1174. https://doi.org/10.1016/j.ijsolstr.2013.12.010

Vieira, A.C., Vieira, J.C., Ferra, J.M., Magalhães, F.D., Guedes, R.M., Marques, A.T., 2011. Mechanical study of PLA–PCL fibers during in vitro degradation. J. Mech. Behav. Biomed. Mater. 451–460. https://doi.org/10.1016/j.jmbbm.2010.12.006

Wang, Y., Han, X., Pan, J., Sinka, C., 2010. An entropy spring model for the Young's modulus change of biodegradable polymers during biodegradation. J. Mech. Behav. Biomed. Mater. 3, 14–21. https://doi.org/10.1016/j.jmbbm.2009.02.003

Ward, I.M., 1971. Mechanical properties of solid polymers. Wiley-Interscience.

Ward, I.M., Hadley, D.W., 1993. An Introduction to the Mechanical Properties of Solid Polymers. John Wiley & Sons Ltd.

Ward, I.M., Sweeney, J., 2013. Mechanical properties of solid polymers, 3rd ed. John Wiley & Sons.

Weir, N.A., Buchanan, F.J., Orr, J.F., Dickson, G.R., 2004. Degradation of poly-L-lactide. Part 1: In vitro and in vivo physiological temperature degradation. Proc. Inst. Mech. Eng. Part H J. Eng. Med. 218, 307–319. https://doi.org/10.1243/0954411041932782

7 Discussion and conclusion

While previous chapters contain in-depth discussions and analyses directly relevant to the contents of the respective individual chapters, we now present an overview of the entire body of work. The novelty and challenges of modelling biodegradable polymers in the context of the evolving (i) molecular weight and (ii) mechanical properties are summarised. The following key findings are also discussed:

- A refined, new kinetic ODE model (NKOM) was developed, accounting for four key degradation mechanisms: mid- and end-chain scissions via both hydrolysis and autocatalysis (Fig. 7.1a). The NKOM ODEs are readily solved and may be used to calibrate parameters with experimental data; however, that model is restricted to calculating the evolving number average molecular weight as a function of time. Implementing these degradation kinetics directly into a scission model to create a kinetic scission model (KSM) provided excellent agreement with the NKOM while also offering more in-depth predictions, tracking the entire evolving molecular weight distribution as a function of degradation duration (Chapter 4).
- The development of the NKOM and, consequently, the KSM ensures carboxylic acid ends are correctly accounted for throughout degradation and allows the effect of initial polymer end group to be investigated. Simulations indicate that the polymer end group plays an important role in the degradation behaviour of polymers and particularly affects the initial evolution of average molecular weight (Chapter 4).
- A literature review indicated that rather than a unique relationship existing between average molecular weight, MW, and failure strain, ε_f, two distinct trends emerge: (i) a lagged decline in ε_f compared with the reduction in MW; and (ii) a relatively rapid decline in ε_f. Introducing failure criteria that (i) consider the finite chain extensibility of an average chain and (ii) consider exponential decline via an empirical relationship reasonably captured the respective trends. A third criterion, based on the entire evolving molecular weight distribution (MWD), was shown to successfully capture both trends (Chapter 5).
- Simulating deformation on a polymer network while considering the finite extensibility of polymer chains highlighted the importance of considering an entire MWD, rather than an average value. Taking MWD corresponding to various points of degradation indicated an increase in the proportion of fully extended chains for more degraded systems, with the short chains created by degradation more

susceptible to becoming fully extended. Good agreement was found with experimental observations (Vieira et al., 2011) up to 30% strain. This is indicative that finite chain extensibility may be responsible for deviations from affine, Gaussian behaviour at moderate strains and, thus, suggests the importance that shorter chains may have on mechanical properties (Chapter 6).

Additionally, several future directions are discussed, prior to some concluding remarks that summarise the findings and implications of the thesis.

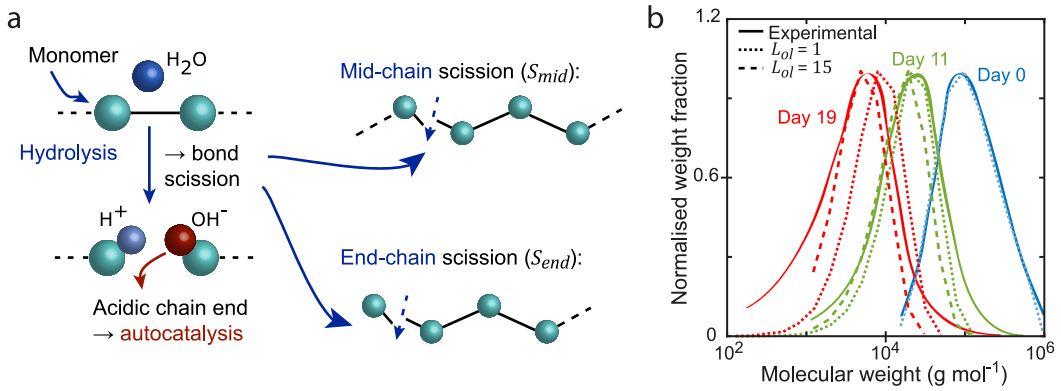

Fig. 7.1. (a) When placed in aqueous medium, hydrolysis causes bond scissions throughout polymer chains to break, creating an alcohol chain end and an acid chain end, which can then accelerate the reaction. The kinetic equations introduced in Chapter 4 describe this reaction and consider the rates of mid- and end-chain scissions via simple hydrolysis and autocatalysis, thus allowing the number of scissions to be performed in a time step in the scission model to be calculated. (b) The initial MWD of Shirazi (2014) was input into the KSM and subjected to simulated scissions according to the rate equations introduced, providing predictions for the evolving MWD. These reasonably captured experimental trends, which were further improved by removing short chains from calculations, representing those that are poorly captured experimentally.

7.1 Discussion

Many of the previous models for the molecular weight evolution of biodegradable polymers can be characterised into two groups that either considered the degradation kinetics or simulated scissions on a representative network in isolation (Gleadall and Pan, 2013; Wang et al., 2008). While a scission model provides more in-depth predictions of the evolving MWD, relating results to time had been a challenge, with the scission process typically being non-linear. Although a coupled model which integrated both approaches was previously introduced (Shirazi et al., 2016b), simplifying assumptions were made about the MWD and the concentration of carboxylic acid ends. The kinetics in the work of Shirazi et al. (2016) and related studies (Gleadall et al., 2014; Wang et al., 2008) have successfully predicted changes in properties such as number average molecular weight; however, extending this to

predictions for the entire MWD proved challenging. Gleadall et al. (2014) reported mid-chain scissions are responsible for more abrupt changes in the polymer properties, emphasizing the importance of correctly considering these in the kinetics. Where molecular weight distributions have been simulated (Han and Pan, 2011; Zhang et al., 2019, 2017), autocatalysis was assumed to arise solely from the acid ends of oligomers. Experimental observations have indicated the importance of the MWD on mechanical properties of polymers (Merz et al., 1951), with narrow MWD having improved mechanical properties compared with a sample with equal weight average molecular weight and a broader MWD (Thomas and Hagan, 1969).

Modelling of mechanical properties has typically been restricted to empirical models that relate an average molecular weight to a mechanical property (Deng et al., 2005; Wang et al., 2010). Although these can provide good agreement with experimental data, they offer limited insight into why these relationships exist in terms of physical mechanisms. Furthermore, different trends have been found for different polymers (Deng et al., 2005; Weir et al., 2004b). Damage and constitutive models have also been developed, providing predictions for evolving properties as a function of strain (Hayman et al., 2014; Soares et al., 2010; Vieira et al., 2014), but they require extensive experimental calibration throughout degradation and do not provide an understanding of the evolving physical behaviour.

In Chapter 4, a new kinetic ODE model (NKOM) was introduced, representing the change in concentration of both ester bonds and carboxylic acid ends, and incorporated into a novel kinetic scission model (KSM). Four reaction rates are included in the model, allowing the rates of end- and mid-chain scissions via both simple hydrolysis and acid accelerated autocatalysis to be varied (Fig. 7.1a). A representative initial polymer chain ensemble was generated and subjected to simulated scissions according to the rate equations providing evolving MWD as a function of degradation duration. Zhang et al. (2017) previously simulated evolving MWD using a multi-scale approach; however, the reaction kinetics described an end-chain scission degradation mechanism. Consequently, the initially monomodal distribution formed a peak at low molecular weights and had no visual change to the right-hand limit as degradation was simulated. This is in contrast to experimental observations, where a gradual shift to the left occurs throughout degradation (Tsuji, 2002; Vey et al., 2008). Simulating mid- and end-chain scissions on bonds at random using the KSM resulted in MWD that gradually shifted to lower molecular weights, retaining a relatively similar distribution shape throughout the simulation (Chapter 4). This was broadly in agreement with experimental observations (Shirazi et al., 2014), where the simulated initial

distribution matched the experimental data (Fig. 7.1b). The simulation tracks all chains, including very short ones that may not be captured experimentally due to limitations of techniques such as GPC (Alex et al., 2018). We found that by removing short chains below some set value (e.g., $L_{ol} = 15$) improved predictions. Once a better experimental understanding of where preferential degradation occurs and the sensitivity of measurement equipment is obtained this may be reflected in the parameters and will allow variances in the width of the distributions to be captured. This will also allow unique reaction rates to be calibrated for each homopolymer and provide insight into the effect of different copolymer ratios on the evolving MWD.

Once the evolving MWD predictions were obtained as a function of time, they were extended to consider Young's modulus following the method introduced by Wang et al. (2010). Previously, Young's modulus predictions were obtained as a function of molecular weight (Shirazi et al., 2016b; Wang et al., 2010). To obtain the evolution as a function of degradation duration, a coupling procedure was employed in those works; however, simplifying assumptions in the coupling framework did not utilise the valuable simulated evolving MWD. Incorporating kinetic rate equations directly into the scission model, which allows scissions to be simulated non-linearly, ensures a more complete time description is considered (Chapter 4). Taking a binary count of parent chains and their sub-chains created via scissions based on whether they lie above or below a threshold molecular weight now provides Young's modulus as a function of degradation duration. While the relationship between Young's modulus and average molecular weights was well captured, predictions for Young's modulus versus time were unable to fully capture the very abrupt decline seen experimentally (Shirazi et al., 2014). Thus, obtaining Young's modulus predictions using this simplistic consideration of entropy does not appear to sufficiently describe the behaviour.

The formulation of the NKOM describes the hydrolysis mechanism, where every bond scission splits a polymer chain, reducing the bond concentration and creating an alcohol chain end and a carboxylic acid chain end. Each carboxylic acid chain end then contributes to the accelerated autocatalytic reaction, according to reaction rates. Although this describes the well-established kinetics of ester hydrolysis (March, 1992), previous models accounted only for the acid ends of monomers (Shirazi et al., 2016b; Wang et al., 2008; Zhang et al., 2017). This is despite the findings of Tracy et al. (1999), where uncapped PLGA was observed to degrade faster than ester-capped from the beginning of degradation, suggesting all carboxylic acid ends can act as catalysts. Depending on the polymer used and the processing technique, carboxylic acid ends may be present initially, or they may only be formed during

degradation (Antheunis et al., 2009). By varying the initial acid concentration, C_{a0}, in the simulation, we found that as C_{a0} increases, the curves gradually change from S-shaped to experiencing a more abrupt initial decline due to the increased number of carboxylic acid-ends available to catalyse the reaction, in agreement with the observations of Antheunis et al. (2009) and Göpferich (1997).

The modification in this work to consider acid ends of both monomers and longer chains provides an improved picture of autocatalysis, ensuring late-stage autocatalysis may be described even when accompanied with diffusion of monomers and associated acid ends. Although diffusion is not considered in this work, it may be facilitated by incorporating a diffusive flux term, similar to Wang et al. (2008). Grizzi et al. (1995) previously described homogenous degradation in PLA samples below 200 μm, while, in contrast, larger samples degraded heterogeneously. This was attributed to differences in the acid concentration at the core, where all carboxylic acid ends remain trapped, versus the surface, where oligomers and associated acid ends can diffuse from the material, with only acid ends of long chains remaining. It should be noted that even homogenous degradation may see a non-linear decrease in molecular weight; this change in kinetics is indicative that simple hydrolysis is always accompanied by accelerative autocatalysis due to carboxylic acids. However, the effect of autocatalysis is dependent on the diffusion length scale compared with the sample size and the resulting competition of the carboxylic acids associated with monomers and oligomers. The changes made here, whereby acid ends (which would contribute to autocatalysis) occurring both on longer chains created by mid-chain scissions and on short, diffusible monomers are both counted, should improve the prediction of late-stage autocatalysis even in small samples where diffusion removes monomers.

A key issue examined in Chapter 5 is the relationship between average molecular weight, MW, and failure strain, ε_f. Golden et al. (1964) investigated the degradation of polycarbonate via irradiation and observed a rapid decline in failure strain below a critical molecular weight. Fayolle et al. (2004) observed similar behaviour for thermally oxidised polypropylene, again suggesting a critical molecular weight separates ductile and brittle behaviour. Although these degradation mechanisms vary from the hydrolysis reaction focused on in this thesis, they ultimately have the same effect on polymer materials, i.e., initiating chain scissions throughout the material. This is supported by the similar trend observed for PLA as degradation occurs, again showing a lag in the decline of failure strain with reducing molecular weight until a critical point coincides with a more rapid decline (Deng et al., 2005; Tsuji, 2002). Ultimately, this suggests that it is the molecular weight that

impacts these properties rather than being directly controlled by degradation. Thus, in theory, the initial molecular weight may be tailored to ensure the ductile-brittle transition occurs only when suitable for the intended application, designed such that the critical molecular weight is reached only after a specified degradation duration. Nevertheless, a predictive tool does not appear to have been introduced.

In Chapter 5, a wide selection of datasets from literature were examined, encompassing PLA and copolymers experiencing hydrolytic degradation, focusing on the relationship between MW and ε_f. The datasets examined exhibited two distinct trends: (i) a lagged decline in ε_f with reducing MW, similar to that mentioned above (Fig. 7.2a); and (ii) an exponential-like decline in ε_f from the onset of degradation (Fig. 7.2b). It was speculated that these differences may be due to key components of the molecular weight distribution, such as short chains, or local imperfections, but limited experimental data prevented a definitive reason from being obtained. Failure criteria were introduced and examined alongside the datasets, with varying degrees of success. The first, ε_f^{MW}, is a physically based model that assumes failure occurs when an average chain becomes fully extended. The lagged decline in ε_f with reducing MW was reasonably captured with this criterion; however, the exponential-like decline in ε_f was not. Instead, an empirical relationship, ε_f^{exp}, was introduced and successfully captured those datasets. While these two criteria capture the experimental trends, insight into which trend a material would exhibit could not be identified based on the information provided in the experimental studies considered, with overlapping features across both trends. The third failure criterion introduced, ε_f^N, describes a modified finite chain extensibility criterion and considers changes in failure strain based on the entire molecular weight distribution, with a build-up of short chains causing a reduction in ε_f^N. This is captured using a critical molecular weight parameter; varying this allows a wide range of behaviour to be described (Fig. 7.2c), reasonably qualitatively capturing each of the datasets considered. Although each criterion provides good predictions when used in the right setting, clarification of why the two degradation trends identified emerge should be explored as this may provide greater insight into the degradation mechanism and in turn allow for improved predictions of these materials. While the first two criteria use an average molecular weight in their calculation, the improved predictions provided by ε_f^N may be accredited to this criterion considering the complete molecular weight distribution, with an emphasis on the effect short chains have on ductility due to their limited extensibility compared with long chains. This was captured using a critical molecular weight threshold, with increasing values

causing more abrupt declines in ductility, with this allowing increasingly long chains to impact the ductility.

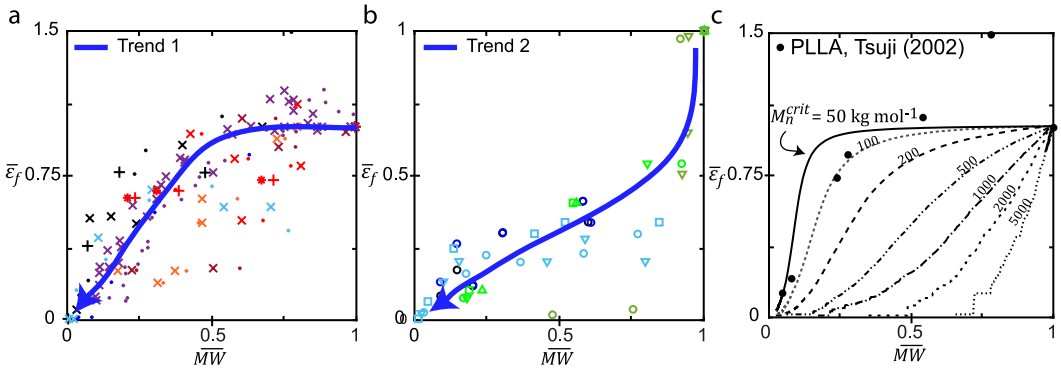

Fig. 7.2. Analysis of the experimental relationship between failure strain, ε_f, and average molecular weight, MW, for PLA and copolymers as degradation proceeded revealed two trends: (a) a lagged decline in ε_f with reducing MW (Trend 1); and (b) an exponential-like decline (Trend 2). Both quantities have been normalised by their initial values. (c) The third failure criterion introduced, ε_f^N, can capture a wide range of trends by altering the critical molecular weight parameter, M_n^{crit}, encompassing both Trend 1 and 2.

Previous reports describe polymer specific critical molecular weights to denote the transition from ductile to brittle behaviour; for example, it is reported as being 210 ± 10 kg mol^{-1} for polypropylene (Fayolle et al., 2004) and 90 kg mol^{-1} for polyethylene (Fayolle et al., 2007). Factors affecting this parameter is unclear. Thomas and Hagan (1969) considered different forms of polystyrene with equal weight average molecular weight and different molar mass dispersity. They found the width of the distribution impacted mechanical properties, with narrow distributions having improved tensile strength, elongation at break and tensile creep properties. Thus, the critical molecular weight mentioned above may be coincidental in nature, instead capturing a change in the MWD that subsequently impacts the mechanical properties. For example, as a polymer material is subjected to tension, the chains within the material respond to this and change from their default, coiled state, gradually straightening out. Chains with high molecular weight are very long and thus would require very large stretches to ever straighten fully; on the other hand, low molecular weight chains may fully extend at moderate stretches. As degradation proceeds, gradually creating a build-up of short chains in the polymer network, the effect of these short chains may eventually dominate the behaviour and cause brittle fracture if a significant proportion of fully extended chains occurs during stretching. Although many experimental studies on PLA displayed a lagged decline in failure strain with reducing molecular weight, a handful had a more rapid decline in failure strain as degradation proceeded and the molecular weight declined (Duek et al., 1999; Tsuji et al., 2000). This may be caused by a broader MWD with a higher

proportion of short chains in the initial state, or perhaps a different failure mechanism than finite extensibility; for example, local imperfections may lead to crazing, ultimately causing a crack fracture. Further experimental investigations should be carried out to explore the effect of MWD on the failure of PLA and copolymers before a more widespread predictive tool can be introduced.

Chapter 6 took a more rigorous consideration of entropy and free energy than previous chapters. A simplistic consideration of entropy was previously assumed, with a binary count of chains contributing to entropy based on whether they were above or below a critical molecular weight based on the work of Wang et al. (2010). While more rigorous considerations of entropy and free energy throughout the polymer network have been considered previously when modelling the mechanical behaviour of polymers, focus has been restricted to polymers such as polyethylene and polydimethylsiloxane that do not experience degradation under typical conditions (Stepto and Taylor, 1995b, 1995a). Computational limitations previously restricted investigations from considering MWD. Nevertheless, simulated results did suggest that a small but significant proportion of chains become fully extended during stretching and, subsequently, contribute nothing more to the change in entropy. As polymer deformation is primarily controlled by changes in entropy rather than internal energy, the rate of stress also declines with the finite extensibility of chains. Although this approach is based on the theory of rubber-like elasticity and PLA and PGA are typically below their glass transition temperature, T_g, at operable temperatures, they do exhibit ductile behaviour prior to and during the initial stages of degradation (Polak-Kraśna et al., 2021; Vieira et al., 2011). Furthermore, large changes in T_g have been observed throughout degradation (Vey et al., 2008). While molecular dynamics models can consider behaviour below T_g, the timescales associated with degradation are prohibitive for complex chemical structures like PLA. Thus, Chapter 6 expanded on the work of Stepto and Taylor (1995a, 1995b), considering an evolving MWD throughout degradation and simulating stretching on the network of chains. The finite extensibility model introduced was validated using both experimental data (Vieira et al., 2011) and the existing neo-Hookean model. Agreement between the neo-Hookean model and both the simulated and experimental observations was found up to approximately 10% strain. Additional agreement between the simulated curves and the experimental data was seen up to approximately 30% strain, halfway to the point of failure (Fig. 7.3). Going forward, detailed experimental testing where the MWD is known for different load deformations is needed to further validate the model and allow for a full quantitative comparison. Nevertheless, our results indicated that finite

chain extensibility is at least partially responsible for the deviation from affine behaviour of polymer systems up to at least 30% strain.

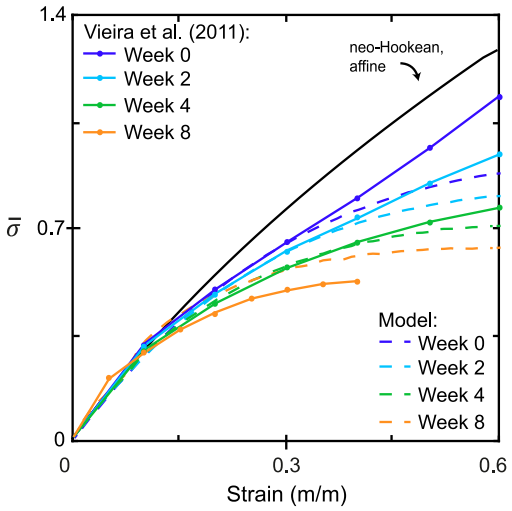

Fig. 7.3. Model predictions (dashed lines) showed excellent agreement with experimental stress-strain curves (Vieira et al., 2011) up to 30% strain. This suggests that the finite chain extensibility modelled in the simulated stretching plays an important role in the mechanical properties of the polymer.

Although in silico models do offer great benefit over both in vitro and in vivo trials for biodegradable polymer materials, reducing time and cost, a robust understanding of all aspects controlling and interfering with degradation of the material is required and needs to be captured by the model. A strong body of consistent experimental work is needed to determine the effect of aspects such as molecular weight distribution, sample size and surface area, fluid volume, fluid flow, etc., to ensure these are correctly captured by a model. However, inconsistencies in in vitro experiments (Table 5.1) and difficulties in capturing biological effects in in vivo settings (Buchanan, 2008) have made it challenging to determine the extent of the effect of various aspects on the behaviour observed. Furthermore, these materials can be sensitive to minor imperfections that occur during processing. The success of in silico models in this area is dependent on a more thorough understanding of these aspects to ensure reproducibility and translatability in the required setting.

7.2 Future directions

In the current work, a kinetic scission model was developed to predict the evolution of the molecular weight distribution of biodegradable polymers during degradation. As formulated, the model is appropriate for amorphous polymers (or amorphous regions of semi-crystalline polymers) that experience bulk degradation and have little mass loss during the degradation period modelled. Going forward, considering crystalline regions and incorporating the

diffusion of water into and oligomers from the material will allow a greater range of polymers to be considered. Some of these aspects have been previously considered (Gleadall et al., 2014b; Han and Pan, 2011) and when incorporated into the KSM, which better accounts for the accelerative effect of carboxylic acid ends and the entire MWD evolution than previous models, a more complete framework may be obtained.

Predictions for the temporal evolution of ε_f obtained using the kinetic scission model alongside the failure criteria introduced were found to agree reasonably with experimental data provided appropriate selection of criteria. This can be used to predict the time taken for half ductility, for example, and provide an estimated timeline for end-of-use. While each of the criterion introduced has shown good predictive capability in certain settings, prior knowledge of which is most appropriate may be challenging without further insight into why the two identified trends emerge. Thus, the immediate priority should be experimental in nature and explore the effects of various factors on these trends, for example, acid concentration, changes in crystallinity, width of the MWD, etc. In the meantime, multiple failure criteria may be used in parallel with one another, offering a failure envelope with predictions for an upper and lower value of ε_f.

The framework for the simulated stretching of a polymer network introduced here captures the deviation from affine, Gaussian behaviour and provides predictions for the evolving stress-strain curves of the material. A qualitative comparison between predictions and experimental data showed excellent agreement up to halfway through the simulation. Going forward, detailed experimental testing where the MWD is known for different load deformations is needed to further validate the model. Once this has been suitably achieved, an analytical description of the behaviour in terms of the strain invariants may be sought. Ideally, this would allow for the introduction of a new strain energy potential that takes the deviation from affine deformation into account. This may then be input into finite element software such as Abaqus, providing wide-spread usability and enabling realistic geometries to be considered. Other aspects to consider are viscoelasticity and plasticity, unloading behaviour, entanglements, and fracture.

While the work presented has a wide range of applications, additional factors must be considered for the chosen application. For example, in the case of biodegradable implants, the interaction between the host and the material is of great importance. Furthermore, when used as drug delivery devices, understanding how the polymer and drug interact is necessary to ensure correct drug transport into the surrounding tissue. This has been given a lot of attention in recent years, particularly in the context of drug-eluting stents (McGinty

et al., 2011; Vo et al., 2017), and further details are presented in the review by McGinty (2014). Additionally, fluid flow may affect the degradation rate, with reaction products dispersing more readily and, thus, reducing the autocatalytic effect (Agrawal et al., 2000). The effect of environmental conditions, such as dynamic or static degradation and the frequency of medium replacement, on degradation behaviour have previously been investigated with a kinetic model (Heljak et al., 2014); adapting that work to consider the updated kinetics presented herein may be valuable and allow a greater range of experimental studies to be modelled.

7.3 Conclusion

This thesis has introduced a novel kinetic scission model that simulates degradation on a representative polymer chain distribution, accounting for hydrolysis and autocatalysis via both mid- and end-chain scissions, predicting evolving molecular weight distributions. In conjunction, newly developed failure criteria and a statistical mechanics method to simulate stretching of the polymer network provide predictions for stress-strain curves.

- The new kinetic ODE model predicts the evolving number average molecular weight as degradation takes place, showing good agreement with experimental data (Shirazi et al., 2014). The effect of varying reaction rates and initial concentrations may be readily explored using this easily solved system.
- Further to this, incorporating these kinetics directly into a scission model offers predictions for evolving molecular weight distributions as a function of degradation duration. This is fundamental in a modelling framework, with the MWD linked to the mechanical properties (Merz et al., 1951; Thomas and Hagan, 1969).
- Varying the initial concentration of acid ends, C_{a0}, captured changes in the early stages of degradation. As C_{a0} increases, the curves gradually change from S-shaped to experiencing a more abrupt initial decline due to the increased number of carboxylic acid-ends available to catalyse the reaction, in agreement with experimental observations (Antheunis et al., 2009; Göpferich, 1997).
- Failure criteria have been presented, describing the relationship between failure strain and evolving molecular weight as degradation proceeds and capturing a range of experimental data (Deng et al., 2005; Duek et al., 1999; Kranz et al., 2000; Polak-Kraśna et al., 2021; Tsuji, 2002; Tsuji et al., 2000; Tsuji and Del Carpio, 2003; Weir et al., 2004a, 2004b).
- Simulated stretching of polymer networks that considered the finite extensibility of polymer chains provided excellent predictions for experimental stress-strain curves

(Vieira et al., 2011) up to 30% strain, thus indicating the important impact that short chains and, consequently, the molecular weight distribution has on mechanical properties.

The framework presented in this thesis allows the evolving mechanical properties and complete MWD to be predicted as a function of degradation duration, offering a powerful predictive tool for biodegradable materials which provides valuable insight into degradation behaviour and may be extended for a variety of applications.

References

Agrawal, C.M., McKinney, J.S., Lanctot, D.R., Athanasiou, K.A., 2000. Effects of fluid flow on the in vitro degradation kinetics of biodegradable scaffolds for tissue engineering. Biomaterials 21, 2443–2452. https://doi.org/10.1016/S0142-9612(00)00112-5

Alex, A., Ilango, N.K., Ghosh, P., 2018. Comparative Role of Chain Scission and Solvation in the Biodegradation of Polylactic Acid (PLA). J. Phys. Chem. B 122, 9516–9526. https://doi.org/10.1021/acs.jpcb.8b07930

Antheunis, H., van der Meer, J.C., de Geus, M., Kingma, W., Koning, C.E., 2009. Improved Mathematical Model for the Hydrolytic Degradation of Aliphatic Polyesters. Macromolecules 42, 2462–2471. https://doi.org/10.1021/ma802222m

Buchanan, F.J. (Ed.), 2008. Degradation rate of bioresorbable materials: prediction and evaluation. Woodhead Publishing Limited/CRC Press LLC, Cambridge, England/Boca Raton, FL.

Deng, M., Zhou, J., Chen, G., Burkley, D., Xu, Y., Jamiolkowski, D., Barbolt, T., 2005. Effect of load and temperature on in vitro degradation of poly(glycolide-co-L-lactide) multifilament braids. Biomaterials 26, 4327–4336. https://doi.org/10.1016/j.biomaterials.2004.09.067

Duek, E.A.R., Zavaglia, C.A.C., Belangero, W.D., 1999. In vitro study of poly(lactic acid) pin degradation. Polymer 40, 6465–6473. https://doi.org/10.1016/S0032-3861(98)00846-5

Fayolle, B., Audouin, L., Verdu, J., 2004. A critical molar mass separating the ductile and brittle regimes as revealed by thermal oxidation in polypropylene. Polymer 45, 4324–4330. https://doi.org/10.1016/j.polymer.2004.03.069

Fayolle, B., Colin, X., Audouin, L., Verdu, J., 2007. Mechanism of degradation induced embrittlement in polyethylene. Polym. Degrad. Stab. 92, 231–238. https://doi.org/10.1016/j.polymdegradstab.2006.11.012

Gleadall, A., Pan, J., 2013. Computer Simulation of Polymer Chain Scission in Biodegradable Polymers. J. Biotechnol. Biomater. 3, 154. https://doi.org/10.4172/2155-952X.1000154

Gleadall, A., Pan, J., Kruft, M.A., Kellomäki, M., 2014. Degradation mechanisms of bioresorbable polyesters. Part 1. Effects of random scission, end scission and autocatalysis. Acta Biomater. 10, 2223–2232. https://doi.org/10.1016/j.actbio.2013.12.039

Golden, J.H., Hammant, B.L., Hazell, E.A., 1964. Degradation of polycarbonates. IV. Effect of molecular weight on flexural properties. J. Polym. Sci. Part A Gen. Pap. 2, 4787–4794. https://doi.org/10.1002/pol.1964.100021109

Göpferich, A., 1997. Polymer Bulk Erosion. Macromolecules 30, 2598–2604. https://doi.org/10.1021/ma961627y

Grizzi, I., Garreau, H., Li, S., Vert, M., 1995. Hydrolytic degradation of devices based on poly(DL-lactic acid) size-dependence. Biomaterials 16, 305–311. https://doi.org/10.1016/0142-9612(95)93258-F

Han, X., Pan, J., 2011. Polymer chain scission, oligomer production and diffusion: A two-scale model for degradation of bioresorbable polyesters. Acta Biomater. 7, 538–547. https://doi.org/10.1016/j.actbio.2010.09.005

Hayman, D., Bergerson, C., Miller, S., Moreno, M., Moore, J.E., 2014. The Effect of Static and Dynamic Loading on Degradation of PLLA Stent Fibers. J. Biomech. Eng. 136, 1–9. https://doi.org/10.1115/1.4027614

Heljak, M.K., Swieszkowski, W., Kurzydlowski, K.J., 2014. Modeling of the degradation kinetics of

biodegradable scaffolds: The effects of the environmental conditions. J. Appl. Polym. Sci. 131, 40280:1–7. https://doi.org/10.1002/app.40280

Kranz, H., Ubrich, N., Maincent, P., Bodmeier, R., 2000. Physicomechanical Properties of Biodegradable Poly(D,L-lactide) and Poly(D,L-lactide-co-glycolide) Films in the Dry and Wet States. J. Pharm. Sci. 89, 1558–1566. https://doi.org/10.1002/1520-6017(200012)89:12<1558::AID-JPS6>3.0.CO;2-8

March, J., 1992. Advanced Organic Chemistry: Reactions, Mechanisms and Structure, 4th ed. John Wiley & Sons, New York.

McGinty, S., 2014. A decade of modelling drug release from arterial stents. Math. Biosci. 257, 80–90. https://doi.org/10.1016/j.mbs.2014.06.016

McGinty, S., McKee, S., Wadsworth, R.M., McCormick, C., 2011. Modelling drug-eluting stents. Math. Med. Biol. 28, 1–29. https://doi.org/10.1093/imammb/dqq003

Merz, E.J., Nielsen, L.E., Buchdahl, R., 1951. Influence of Molecular Weight on the Properties of Polystyrene. Ind. Eng. Chem. 43, 1396–1401. https://doi.org/10.1021/ie50498a036

Polak-Kraśna, K., Abaei, A.R., Shirazi, R.N., Parle, E., Carroll, O., Ronan, W., Vaughan, T.J., 2021. Physical and mechanical degradation behaviour of semi-crystalline PLLA for bioresorbable stent applications. J. Mech. Behav. Biomed. Mater. 118, 1–11. https://doi.org/10.1016/j.jmbbm.2021.104409

Shirazi, R.N., Aldabbagh, F., Erxleben, A., Rochev, Y., McHugh, P., 2014. Nanomechanical properties of poly(lactic-co-glycolic) acid film during degradation. Acta Biomater. 10, 4695–4703. https://doi.org/10.1016/j.actbio.2014.08.004

Shirazi, R.N., Ronan, W., Rochev, Y., McHugh, P., 2016. Modelling the degradation and elastic properties of poly(lactic-co-glycolic acid) films and regular open-cell tissue engineering scaffolds. J. Mech. Behav. Biomed. Mater. 54, 48–59. https://doi.org/10.1016/j.jmbbm.2015.08.030

Soares, J.S., Moore, J.E., Rajagopal, K.R., 2010. Modeling of Deformation-Accelerated Breakdown of Polylactic Acid Biodegradable Stents. J. Med. Device. 4, 1–10. https://doi.org/10.1115/1.4002759

Stepto, R.F.T., Taylor, D.J.R., 1995a. Modelling the elastic behaviour of real chains in polymer networks. Macromol. Symp. 93, 261–268. https://doi.org/10.1002/masy.19950930131

Stepto, R.F.T., Taylor, D.J.R., 1995b. Molecular Modelling of the Elastic Behaviour of Polymer Chains in Networks: Comparison of Polymethylene and Poly(dimethylsiloxane). J. Chem. Soc. Faraday Trans. 91, 2639–2647. https://doi.org/10.1039/FT9959102639

Thomas, D.P., Hagan, R.S., 1969. The Influence of Molecular Weight Distribution on Melt Viscosity, Melt Elasticity, Processing Behaviour and Properties of Polystyrene. Polym. Eng. Sci. 9, 164–171. https://doi.org/10.1002/pen.760090304

Tracy, M.A., Ward, K.L., Firouzabadian, L., Wang, Y., Dong, N., Qian, R., Zhang, Y., 1999. Factors affecting the degradation rate of poly(lactide-co-glycolide) microspheres in vivo and in vitro. Biomaterials 20, 1057–1062. https://doi.org/10.1016/S0142-9612(99)00002-2

Tsuji, H., 2002. Autocatalytic hydrolysis of amorphous-made polylactides: effects of L-lactide content, tacticity, and enantiomeric polymer blending. Polymer 43, 1789–1796. https://doi.org/10.1016/S0032-3861(01)00752-2

Tsuji, H., Del Carpio, C.A., 2003. In vitro hydrolysis of blends from enantiomeric poly(lactide)s. 3. Homocrystallized and amorphous blend films. Biomacromolecules 4, 7–11. https://doi.org/10.1021/bm020090v

Tsuji, H., Mizuno, A., Ikada, Y., 2000. Properties and morphology of poly(L-lactide). III. Effects of initial crystallinity on long-term in vitro hydrolysis of high molecular weight poly(L-lactide) film in phosphate-buffered solution. J. Appl. Polym. Sci. 77, 1452–1464. https://doi.org/10.1002/1097-4628(20000815)77:7<1452::AID-APP7>3.0.CO;2-S

Vey, E., Roger, C., Meehan, L., Booth, J., Claybourn, M., Miller, A.F., Saiani, A., 2008. Degradation mechanism of poly(lactic-co-glycolic) acid block copolymer cast films in phosphate buffer solution. Polym. Degrad. Stab. 93, 1869–1876. https://doi.org/10.1016/j.polymdegradstab.2008.07.018

Vieira, A.C., Guedes, R.M., Tita, V., 2014. Constitutive modeling of biodegradable polymers: Hydrolytic degradation and time-dependent behavior. Int. J. Solids Struct. 51, 1164–1174. https://doi.org/10.1016/j.ijsolstr.2013.12.010

Vieira, A.C., Vieira, J.C., Ferra, J.M., Magalhães, F.D., Guedes, R.M., Marques, A.T., 2011. Mechanical study of PLA–PCL fibers during in vitro degradation. J. Mech. Behav. Biomed. Mater. 451–460.

https://doi.org/10.1016/j.jmbbm.2010.12.006

Vo, T., Lee, W., Peddle, A., Meere, M., 2017. Modelling chemistry and biology after implantation of a drug-eluting stent. Part I: Drug transport. Math. Biosci. Eng. 14, 491–509. https://doi.org/10.3934/mbe.2017030

Wang, Y., Han, X., Pan, J., Sinka, C., 2010. An entropy spring model for the Young's modulus change of biodegradable polymers during biodegradation. J. Mech. Behav. Biomed. Mater. 3, 14–21. https://doi.org/10.1016/j.jmbbm.2009.02.003

Wang, Y., Pan, J., Han, X., Sinka, C., Ding, L., 2008. A phenomenological model for the degradation of biodegradable polymers. Biomaterials 29, 3393–3401. https://doi.org/10.1016/j.biomaterials.2008.04.042

Weir, N.A., Buchanan, F.J., Orr, J.F., Dickson, G.R., 2004a. Degradation of poly-L-lactide. Part 1: In vitro and in vivo physiological temperature degradation. Proc. Inst. Mech. Eng. Part H J. Eng. Med. 218, 307–319. https://doi.org/10.1243/0954411041932782

Weir, N.A., Buchanan, F.J., Orr, J.F., Farrar, D.F., Dickson, G.R., 2004b. Degradation of poly-L-lactide. Part 2: Increased temperature accelerated degradation. Proc. Inst. Mech. Eng. Part H J. Eng. Med. 218, 321–330. https://doi.org/10.1243/0954411041932809

Zhang, T., Jin, G., Han, X., Gao, Y., Zeng, Q., Hou, B., Zhang, D., 2019. Multiscale modelling for the heterogeneous strength of biodegradable polyesters. J. Mech. Behav. Biomed. Mater. 90, 337–349. https://doi.org/10.1016/j.jmbbm.2018.10.018

Zhang, T., Zhou, S., Gao, X., Yang, Z., Sun, L., Zhang, D., 2017. A multi-scale method for modeling degradation of bioresorbable polyesters. Acta Biomater. 50, 462–475. https://doi.org/10.1016/j.actbio.2016.12.046